Optimisation of microstructure and fatigue properties of Inconel 718 for extrusion die applications

Fabio Taina

Université de Toulouse

THÈSE

En vue de l'obtention du

DOCTORAT DE L'UNIVERSITÉ DE TOULOUSE

Délivré par :
Institut National Polytechnique de Toulouse (INP Toulouse)

Discipline ou spécialité :

Génie Mécanique, Mécanique des Matériaux

Présentée et soutenue par :
Fabio TAINA

le : mardi 18 octobre 2011

Titre :

"Optimisation of microstructure and fatigue properties of Inconel 718 for extrusion die applications"

Ecole doctorale :
Mécanique, Energétique, Génie civil et Procédés (MEGeP)

Unité de recherche :
Institut Clément Ader (ICA)-Albi- Ecole des Mines d'Albi

Directeur(s) de Thèse :
Philippe LOURS- Professeur- ICA Albi- Directeur de thèse
Denis DELAGNES- Maître Assistant- ICA Albi- Co-Directeur de thèse

Rapporteurs :
André PINEAU - Professeur - Centre des Matériaux - Ecole des Mines de Paris
Mario ROSSO - Professeur - DISMIC- Politecnico di Torino

Autre(s) membre(s) du jury

Eric ANDRIEU- Professeur - CIRIMAT- ENSIACET (Institut Carnot)-Toulouse
Jean-Luc LANFRANCHINI- Head of Technal development Center - Technal Toulouse
Marco PASQUALON- R&D Scientist - Norsk Hydro Norway - (Invité)
Vincent VELAY- Maître Assistant-ICA Albi- (Invité)

Remerciements

Apres trois années de travail intensif, mais passionnant, au sein de l'Institut Clément Ader, j'ai enfin l'occasion de remercier toutes les personnes qui ont contribué à la bonne réalisation de ce travail dans une ambiance conviviale.

Je tiens en premier lieu à remercier Philippe Lours, qui m'a encadré pendant la durée de cette thèse. Tu as su me donner suffisamment d'autonomie tout en restant présent dans les moments où j'avais besoin de tes indications sur les directions de recherche. Je te remercie également de m'avoir accueilli dans ta famille la veille de ma soutenance de thèse, ce qui a mis un peu de chaleur dans un moment aussi important.

Mes remerciements vont également à Denis Delagnes, dont je tiens à féliciter l'aboutissement de son HDR. Tu as contribué à ma formation en répondant avec patience à mes questions de jeune naïf sur les problématiques de fatigue oligocyclique. Je garderais aussi en mémoire les nombreuses discussions qu'on a pu avoir le mardi, à midi, dans les vestiaires du gymnase.

Je suis très reconnaissant au Professeur André Pineau d'avoir accepté de relire et de critiquer mes travaux de thèse. Ce fut un honneur pour moi de discuter avec vous sur ce matériau intéressant mais complexe dont vous avez contribué, de manière essentielle, au développent de la connaissance. Je ne pourrais jamais oublier notre première rencontre pendant laquelle vous avez su non seulement répondre à mes question mais aussi à celles des « dix-huit personnes » qui vous ont sollicité pendant cette entrevue.

Je réserve un remerciement chaleureux au Professeur Mario Rosso pour sa grande disponibilité lors du cursus au Politecnico de Turin et en suite pour la relecture de la thèse. J'ai sincèrement apprécié de travailler avec toi et je te suis reconnaissant pour le temps que tu m'as consacré et toutes les opportunités que tu m'as données au cours de ces années.

Mes remerciements s'adressent aussi au Professeur Eric Andrieu qui m'a fait l'honneur de présider mon jury de thèse. De même, je remercie Jean-Luc Lanfranchini, directeur du centre R&D au sein de Technal, pour avoir mobilisé un peu de son temps et de ses compétences pour participer à la soutenance.

J'adresse sincèrement mes remerciements à Marco Pasqualon, qui a été mon encadrant industriel au sein d'Hydro Aluminum. Votre investissement et votre disponibilité m'a permis d'évoluer dans les meilleures conditions : les nombreuses réflexions et discussions que nous avons échangés par mail et téléphone ont été les moteurs de ce travail.

J'ai eu la chance de travailler pendant la dernière période de ma thèse avec Vincent Velay, enseignant chercheur au sein de l'ICA, qui a encadré et orienté mes travaux de recherche portant sur la modélisation numérique et le comportement mécanique des matériaux. Son humilité et ses remarques constructives m'ont permis d'aborder un sujet complexe mais riche d'intérêt industriel et scientifique.

Une thèse focalisée sur la fatigue mécanique ne peut pas être réalisée sans la contribution d'une équipe technique à la hauteur des exigences. C'est pour cette raison que je tiens tout d'abord à remercier Thomas Papaïx d'avoir assisté à la rupture de 125 éprouvettes, de nombreux nettoyages de spires, du remplacement de 3 paires de tiges d'extensomètre (dont une cassée par ma maladresse) ainsi que pour un samedi matin passé devant la « Shenck », qui semblait complètement incontrôlable. Je ne pourrai jamais oublier les moments difficiles ainsi que ceux de joie animés par les voix de « David et Jonathan ».

Mes remerciements vont également à Monsieur Serge Tovar pour sa maitrise du MEB et celle des attaques chimiques. Si aujourd'hui, je parle aussi bien français, c'est un peu grâce à toi, Serge. Merci encore pour les nombreux surnoms que t'as su adapter à ma personnalité ; j'en cite quelques un pour qu'ils ne soient pas oubliés : « Felice !!! », « Pizzaiolo », « Ma che » !!!, « Spaghetti », « Rital », etc... Comme promis, je t'enverrai par courriel la fameuse recette de la « Pizza aux trois fromages ».

Que ce soit sur le site industriel d'Hydro ou au sein du laboratoire ICA, j'ai eu la chance tout au long de ces trois années d'être entouré par des assistantes administratives extrêmement efficaces et qui m'ont rendu la vie plus facile. Un grand merci donc à Josiane, Cathy et Esther pour votre aide et soutien.

Merci à toutes les personnes du laboratoire qui ont répondu présentes à chaque fois que je les sollicitais : Sabine pour les analyses d'images, Pascal pour l'ATD et la DRX, Vanessa pour les belles images au TEM, Didier pour les trois jours de corrélation d'images (passés devant la machine avec de la bonne musique), Florian pour le support informatique (et les discussions autour de l'Italie « Ti faccio cappuccino !!! » et le centre de documentation (Nelly, Hong et Dolores) pour le soutien constant. Enfin merci à toutes les personnes que je n'ai pas citées ici et qui se reconnaîtront dans ces quelques lignes.

Cette aventure aurait sans doute été moins agréable sans la présence des amis doctorants qui m'ont supporté pendant mon parcours. Je souhaite remercier tous les amis du bureau 1M07 qui ont toujours contribués à créer une ambiance de travail joviale même pendant les moments les plus tendus et l'ensemble des thésards avec lesquels j'ai partagé l'organisation de nombreuses initiatives liées à l'Association des doctorants (ACTA). Parmi eux, certains m'ont fait don de leur amitié. Tous ont contribué à me faire grandir tant au niveau professionnel que personnel. Bonne continuation à vous tous! Un grand merci à Cédric grâce à qui j'ai pu connaître les terres inconnus des dissolutions électrolytiques. Même en étant aussi différents en carrure qu'en caractère, on a mis en place une belle collaboration, basée sur une vraie amitié, dont je te serai toujours reconnaissant. Et dans cet esprit de convivialité, je ne pourrai jamais oublier les amis du Volley, l'équipe des « Caribous », qui a constitué ma deuxième famille sur Albi. Je me souviendrai longtemps de ces moments inoubliables, toujours avec le sourire sur les lèvres et la joie dans le cœur. Je vous remercie de m'avoir accueilli dans votre équipe dont je garderai toujours le souvenir de ce championnat cuvée 2011 en « Chantant dans le COSEC ». Un remerciement en particulier pour Thierry, pour son être humble et pour son faire « impeccable !!! » et pour JB, ou mieux « Monsieur Caribou » pour son dynamisme et pour son « clin d'œil ».

Je suis en outre tout spécialement reconnaissant à Giorgio avec lequel je partage une amitié qui dure depuis longtemps, malgré la distance qui nous sépare (1000 km). Ton soutien au quotidien et ta capacité à me faire oublier les problèmes professionnels ont été indispensables pour moi.

J'adresse toute ma gratitude à mes parents, pour leur présence et leur exemple. Pour leur capacité à accepter et supporter mes choix et mon éloignement et pour m'avoir aidé dans les différentes étapes de ma vie étudiante et le début de la vie professionnelle.

Enfin, les remerciements les plus sincères c'est pour Claire, qui représente avec son amour un repère constant et solide. Merci d'avoir accepté de partager ce studio de 16 m^2 et pour tous les week-ends et les nuits d'étude et de rédaction, ton sourire et ta joie de vivre ont effacé la fatigue et donné de la couleur à ces trois années de vie albigeoise. Je suis certain que mes encadrants ne se vexeront pas si j'écris que tu as été la découverte la plus importante de mes recherches. Bon courage pour ta nouvelle vie professionnelle, en espérant que nous pourrons réaliser, au plus tôt, nos rêves.

I Introduction

The Aluminium extrusion is a high temperature process used to produce semi-finished products in the form of bar, strip and solid sections as well as hollow sections. Extrusion processing includes a plastic deformation in which a billet, typically cylindrical, is forced by a stem to pass through a die with a cross section generating the shape of the extruded piece.

Due to the severe processing conditions and complex mechanical loading, the die is considered as the most critical element of the extrusion equipment.

The thermo-mechanical loading and the continuous contact between the tool and the aluminium enhance the risks of *wear and fatigue failures*. The alternation of tensile and compressive stresses, acting on specific zones of the die, such as sharp corners and/or section changes, represents one of the most common causes of the fatigue failure. A second significant failure is associated to friction damage on the bearing surfaces which is defined as a progressive wear of the die material.

Different researches have been performed with the objective to increase die life and reduce the connected ratio *die cost/kg extruded*. Improving die stability can also generate significant profit through process reliability and productivity increase as well as product quality stabilization (surface, dimensions).

A so-called "*Modular*" extrusion die was designed by Hydro Aluminium and prototypes were tested. For this innovative die, the part subject to strong thermo-mechanical (First module) loading was made with a ***Nickel-based Superalloy*** (Ni-SA) whereas in the bearing zone (Second Module), the insert was manufactured with a wear resistant material (such as high speed tool steel, hot working steel or precipitation hardened steel) optimised by the application of a specific coating. In particular, Inconel 718 was selected as the appropriate candidate material for the bulk structure, able to combine excellent tensile, fatigue, creep and rupture strength in the range of temperature where the die operate (almost 550° C).

The aim of this PhD work is to contribute to the development of die materials for aluminium extrusion, for a continuous improvement of the productive capabilities of Hydro Aluminium to achieve a leadership in industrial products within a global market.

Even tough the "Modular Extrusion Technology" has recently shown important benefits and good results in extrusion practice, this application is still at an early stage of its potential exploitation. The originality of the present work stands on the development of an optimized Inconel 718 alloy, with thermo-mechanical and microstructural tailored properties for a specific application, that is bulk material for extrusion die.

From this point of view, two possible research strategies can be explored:

- The investigation of the impact of the extrusion process such as extrusion speed, billet length, thermo-mechanical loading on the mechanical behaviour of the bulk material, the so called **Material Extrinsic Parameters**. The cyclic alternate tensile and compressive stresses are simulated using isothermal *Low Cycle Fatigue* (LCF)

tests giving information on the various damage mechanisms occurring in the die.

- The optimization of the Inconel 718 properties to improve its strength under extrusion loading. This second objective could be achieved by modifying the **Material Intrinsic Parameters** such as grain size, precipitates morphology through thermo-mechanical treatments in order to adapt the material to the specific conditions imposed by the extrusion process.

The manuscript is organized in five sections.

Chapter I discuss the fundamentals of the extrusion process, focusing on the die technology and presenting in detail the concept of “Modular Extrusion die”.

A literature review about Inconel 718 is reported in Chapter II to give a synthetic description of the wide variety of researches that have been previously carried out on this material. This preliminary chapter is considered as a pertinent support for the interpretation of the experimental results that will be reported in the second part of the manuscript.

Chapter III includes a detailed description of the research strategies adopted for the metallurgical optimization of the alloy. A presentation of the different experimental methods used for the metallurgical and mechanical characterisation of the alloy is reported.

The fatigue behaviour of Inconel 718 is analysed in Chapter IV under various LCF conditions. Different examples of tests are carried out in order to define a cyclic model prone to evaluate the stress-strain state in an extrusion die. In addition, a series of strain-controlled low cycle fatigue tests is conducted to investigate the impact of various parameters on the behaviour of the material. Namely, focus is placed on the influence of the *extrinsic parameters* such as the cycle frequency, the strain rate, the holding time under load and the stress relaxation. A fractographic method, based on microscopical investigations, is proposed in order to predict the crack growth rate of prevalent cracks under LCF conditions.

Alternative heat treatments, in addition to the standard procedure, are proposed in Chapter V where their mechanical properties have been assessed by tensile tests. Each modified thermal treatment is defined by a series of parameters (time, temperature, cooling rates), whose choice is related to a detailed study of the correlation between microstructure and mechanical properties. This investigation is based on the understanding and modelling of the various steps of the heat treatment process, taking into account the evolution of the so-called *material-intrinsic parameters.*

Finally, some concluding remarks are reported in order to resume the main results of the research focused on the understanding and the improvement of the mechanical behaviour of the tool bulk material (Inconel 718). Specific suggestions and additional outlooks, from a scientific and industrial point of view, are discussed in order to further increase die life, process stability and later on press productivity.

Index

Chapter I

State of the art and scope of the research work

" Una volta aver provato l'ebrezza del volo, quando sarai di nuovo coi piedi per terra, continuerai a guardare il cielo."

Leonardo da Vinci

Chapter I: State of the art and scope of the research work

II Fundamentals of Extrusion

II.1 Introduction

Aluminium extrusion is a high temperature process used to produce semi-finished products in the form of bar, strip and solid sections as well as hollow sections. The technology is based on a relatively simple concept of material forming, but it may be influenced by a series of failures that could affect the quality of the product and the efficiency of the process. For these reasons, the extrusion process is developing rapidly with the intent to lower the cost of production and simultaneously improve productivity.

During the last ten years an important research work was done regarding process control: a particular attention was given to the optimisation of the metal flow and to the development of new alloys able to show improved extrudability and secure higher mechanical properties. Today, research is also directed towards die technology: an important effort is made both to understand friction phenomena between dies and materials to extrude and test the benefit of employing alternative bulk die materials.

This first section discusses about the fundamentals of the extrusion process, focusing on the die technology and presenting a new concept of tooling that becomes a motivating challenge for this industry.

II.2 The Hot Extrusion Technology

Extrusion processing includes a plastic deformation in which a billet, typically cylindrical, is forced by a stem to pass through a die with a cross section generating the shape of the extruded piece **[Saha,2000]**. Generally, the extrusion technology can be divided into two main type:

- The *direct extrusion*: where the billet is forced to pass through a die with a defined accurate shape.
- The *indirect extrusion* (or backward extrusion) where the die is pushed through the metal in order to form the extruded product.

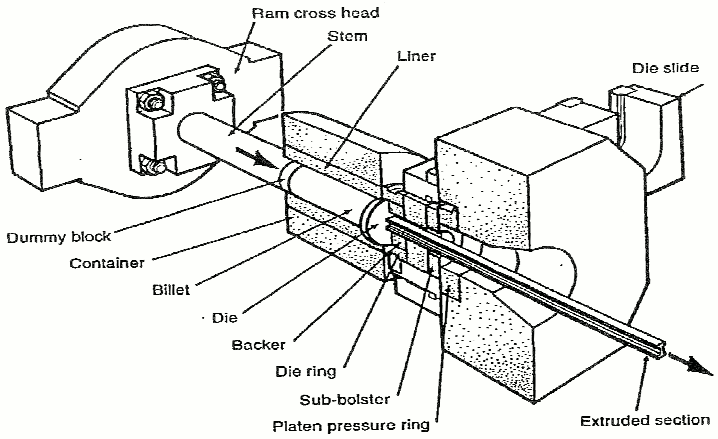

Figure I. 1 : Schematic representation of the Extrusion process. [Dwight,1999]

As described before, the stem gives the required pressure to force the metal to flow through the cavity of the die. Its movement, normal to the die surface, is controlled by a cylindrical piece of steel, the *dummy block*, which is put on the top of the ram in order to transfer the full press force to the billet. Before being formed, the material passes through heated cylinders, called *containers*, surrounded by layers of induction coils to control the billet temperature (Figure I. 1) **[Bauser et al.,2006]**.

Tooling is of primary importance for the overall quality of the extruded profile. There are two types of extrusion tooling, depending on the cross section dimensions of the final product:

- ***Flat dies***: they are employed for direct external shape extrusion concerning all extrudable metallic alloys (Figure I. 2). These dies can be equipped with a feeder plate; consisting of a solid tool put in front of the flat die and designed to produce a section larger than the billet. The extrusion process is then divided into two successive steps: in the first step, the billet is moved from the container to the feeder plate where it is expanded; in the second step the material is forced to pass through the die to achieve the final shape **[Bauser et al.,2006]**.

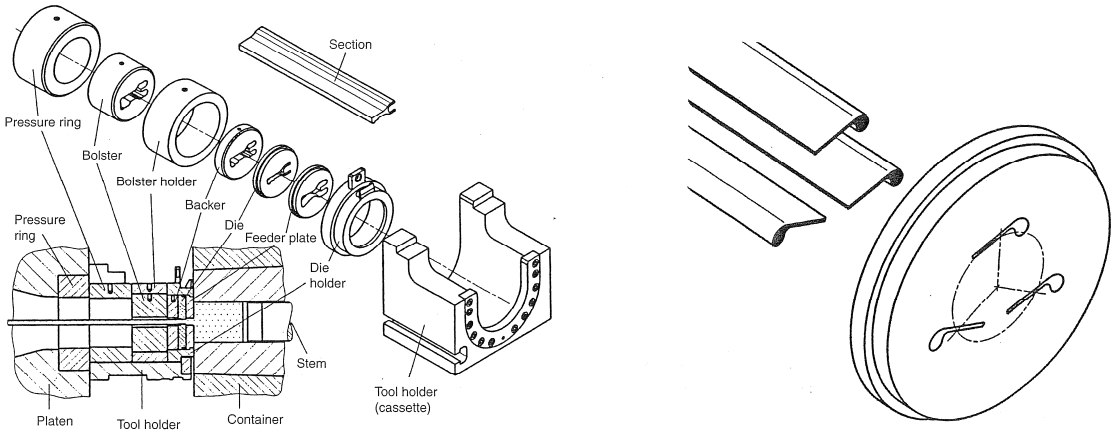

(a) **(b)**

Figure I. 2 : Assembly of the tool set (a) for the production of solid sections and example of flat extrusion die (b) with three shape forming apertures for the extrusion of aluminium alloys. [Bauser et al.,2006]

- ***Hollow dies***: they are used for the production of hollow sections and thin wall tubes characterized by long lengths (Figure I. 3). In this case, the billet is divided into several metal streams, under the application of high pressure, and then joined together in a specific part of the die surrounding the *mandrel*, called *welding chamber*. The hollow die consists of two pieces: an upper part and a lower part. The upper part (*Porthole*), characterized by the presence of a mandrel, takes part in the formation of the inner shape of the extruded section, and the lower part (*Die Plate*) serves to generate the external profile. The mandrel is joined to the porthole by bracket supports called *bridges* **[Xianghong et al.,2006]**. The die geometry is designed in order to minimize the path of the material streams to avoid any atmospheric contaminations.

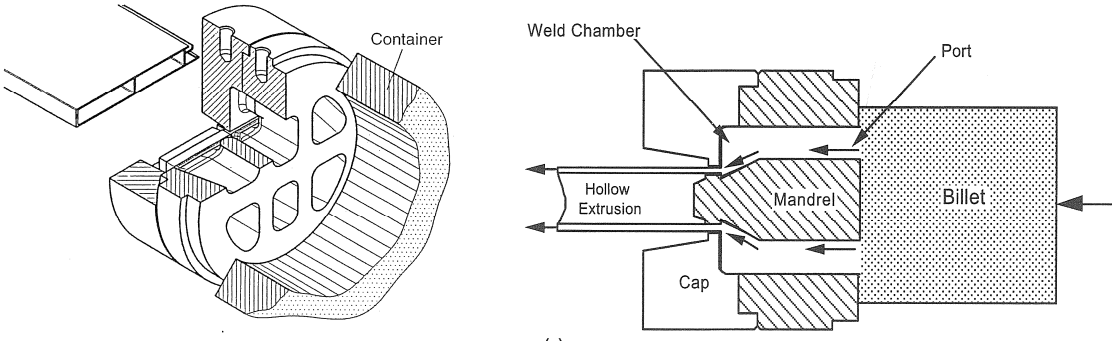

(a) **(b)**

Figure I. 3 : Single cavity two parts porthole (a) die with six ports to produce aluminium hollow sections [Bauser et al.,2006] and schematic representation (b) of the welding chamber of a hollow die [Saha,2000].

In general, the extrusion die is located in a *holder* designed with a specific diameter as a function of the die dimensions. For the production of solid shapes, it is better to employ a backer as a support tool in order to reduce the risk of fracture or collapse.

All types of dies have a bearing surface onto which the profile takes its final shape. The geometry and the surface conditions of the bearing influence significantly, together with other parameters, both product quality and extrusion productivity. It is obvious that these zones are subjected to high tribological loading those results in die loss of performances.

The extrusion parameters, such as ram speed and billet pre-heat temperature are directly dependent on the type of alloy. Saha **[Saha,2000]** gives an example of typical extrusion parameters for common aluminium alloys (Table I. 1). It is important to underline that the extrusion conditions, especially the exit speed and surface quality, are fully dependent on the complexity of the shape. A detailed control of each parameter can reduce the defects in the final product; such as blisters or cracking.

Alloy	Type	Billet temperature °F	Billet temperature °C	Exit speed ft/min	Exit speed m/min
1060	Non-heat-treatable	788	420	164–328	50–100
1100	Non-heat-treatable	806	430	164–262	50–80
3003	Non-heat-treatable	842	450	98–230	30–70
5052	Non-heat-treatable	842	450	16–33	5–10
5154, 5254, 5454	Non-heat-treatable	860	460	20–49	6–15
6061	Heat treatable	806–932	430–500	16–82	5–25
6063	Heat treatable	896–932	480–500	115–262	35–80
6066	Heat treatable	797–860	425–460	66–115	20–35
6101	Heat treatable	896–932	480–500	115–262	35–80
6463	Heat treatable	896–932	480–500	115–262	35–80
7003	Heat treatable	824–977	440–525	16–69	5–21
7005	Heat treatable	824–977	440–525	16–46	5–14

Table I. 1 : Typical values of billet temperatures and extrusion speed of extruded aluminium alloys. [Saha,2000]

Practically, the die and the tooling supports (backer and holder) must be pre- heated in specific ovens located in the vicinity of the extrusion press (Table I. 2). This practice has two main objectives: the first one is to avoid any heat loss at the beginning of the extrusion process, the second is to achieve a specific toughness to avoid early fracture. The following table reports some examples of preheating parameters employed in extrusion processing.

After pre-heating, the die is quickly transported and assembled into the holder of the extrusion press. After extrusion of a specific profile, especially for hollow dies, the tool is removed and uniformly cooled before being cleaned in a bath of hot caustic soda.

Tool size diameter, mm		Solid section: Extrusion die and backer with die holder		Hollow section: Porthole die Bridge die with die holder	
From	To	Time, h	Temperature, °C	Time, h	Temperature, °C
. . .	300	2.5–3	420–450	3–4	440–460
300	500	3–4	420–450	4–5	440–460
500	700	4–5	420–450	5–6	440–460
Over	700	5–6	420–450	6–8	440–460

Table I. 2: Preheat temperature and times for aluminium extrusion tooling. [Bauser et al.,2006]

These preliminary remarks on the fundamentals of the extrusion technology highlight the importance and the complexity relative to the choice and design of an extrusion die. A well defined hot working material and a specific heat treatment must be employed to ensure a long service life validating some specific requirements such as:

- Toughness at high temperature;
- High mechanical resistance at high temperatures (Yield strength, creep and fatigue resistance);
- Hot wear resistance;
- Thermal conductivity;
- Corrosion and oxidation resistance.

The validation of these specific requirements guarantees an optimal extrusion speed and an appropriate quality of the product based on a dimension stability and shape accuracy.

II.3 Hot work steels for extrusion dies: state of the art.

Due to severe processing conditions and complex mechanical loading, the die is considered as the most critical element of the extrusion equipment **[Reggiani et al.,2010]**. Significant focus and attention is paid in die development activities. From a material point of view, the hot work tool steel grades are still today considered to represent 90% of the total extrusion die consumption. The expression *"Hot working tool steels"* cover a large class of alloyed steels which are dedicated to different industrial applications for the hot working of metallic materials. In general, AISI H11 and H13 steels and their related grades are employed for aluminium extrusion tooling **[Gutovskaya,2003]**. These steel grades belong to the class of 5% chromium hot work steels. Chromium confers to the material good hardenability and temper resistance at the high working temperatures. The composition of the steels, traditionally employed for extrusion tooling, is reported in Table I. 3 :

Steel Designation			**Alloying Elements**						
[DIN]	W.Nr	AISI	C	Si	Mn	Cr	Mo	Ni	V
X36CrMoV5-1	1.2340	H11	0.36	0.35	0.36	5.06	1.25	0.06	0.49
X37CrMoV5-1	1.2343	H11	0.37	0.92	0.49	5.05	1.25	0.20	0.47
X40CrMoV5-1	1.2344	H13	0.40	1.0	0.4	5.3	1.3	-	1.0
X55NiCrMoV7	1.2714	L6	0.55	0.25	0.8	1.1	0.5	1.65	0.1

Table I. 3:Chemical composition of Hot Work Steels. [Delagnes,1998]

AISI H11 steels are used because they exhibit high tensile strength at elevated temperature and a good fracture toughness as well as thermal conductivity (26-29 $Wm^{-1}K^{-1}$ at 200-600°C).

X55NiCrMoV7 steel is characterised by high fracture toughness and an elevated ductility at high temperatures (mechanical shock resistance). Its application, anyway, is limited by the hardness decrease at temperature closed to 400-500°C.**[Oudin,2001]**

The alloying elements, such as Mo and V are employed to obtain the required high strength at the working temperatures, limiting softening mechanisms. In general, these elements react with the carbon to form carbides like M_7C_3, $M_{23}C_6$, M_6C and MC, where M is the metal alloying element. The distribution of carbides, especially at grain boundaries, must be carefully controlled to achieve a uniform toughness through the bulk of the tool. For this reason, the production methods for hot working steels have been improved by the use of the electro-slag remelt steel-making process (ESR) which ensure, on top of a good control of impurity levels, a fine and uniform grain structure.

The basic operations of heat treatments of hot work steels are divided into four specific stages: annealing, austenitization, quenching and tempering. The heat treatment is the most important and correlatively the most complex step in the manufacturing of an extrusion die. Whereas solid extrusion dies are commonly manufactured from heat treated steel blanks,

hollow dies can be rough-machined from annealed hot working steels.**[Bauser et al.,2006]**

For this reason, an annealing treatment is performed at a temperature prone to release residual stresses and obtain a uniform distribution of globular carbides before manufacturing starts.**[Delagnes,1998]**

Afterwards, an austenitization temperature in the range 990-1030°C is employed to ensure a complete transformation of the ferritic structure. Cooling from the austenitizing temperature must be quick enough to minimize the formation of bainite that tends to embrittle the material causing a premature cracking. After quenching, the structure is unstable and brittle: steels must be tempered to achieve the targeted mechanical properties (such as toughness). A two-stage tempering is commonly employed for the hot work steels. The first stage is run at a temperature in the range 550-600°C in order to induce a complete transformation of the residual austenite in secondary martensite and an increase in the toughness. The second tempering temperature (higher than the first one) is chosen according to the required hardness: this process guarantees the thermal stress release and the precipitation of uniformly distributed secondary carbides prone to improve the mechanical properties. Note that in the case of X55NiCrMoV7 only one tempering is performed as the material shows a continuous decrease of hardening during this final treatment.

Table I. 4 and Table I. 5 report, respectively, the heat treatment procedures selected for the traditional hot work steels and the resulting mechanical properties measured at room temperature.

Steel	***Austenitization***	***First Tempering***	***Second tempering***	***Hardness (HRC)***
X55NiCrMoV7	875°C/1h/OIL	605°C/3h/ AIR	-	42
	875°C/1h/OIL	511°C/2h/ AIR	-	47
X37CrMoV5-1	900°C/1h/AIR	550°C/2h/ AIR	625°C/2h/ AIR	42
	900°C/1h/AIR	550°C/2h/ AIR	610°C/3h/ AIR	44
	900°C/1h/AIR	550°C/2h/ AIR	601°C/3h/ AIR	47
	900°C/1h/AIR	550°C/2h/ AIR	590°C/2.4h/ AIR	50

Table I. 4 : Table: Typical heat treatment for traditional hot work steels. [Delagnes,1998; Oudin,2001]

Steel	***Rp0.2 [MPa]***	***UTS [MPa]***	***Hardness (HRC)***
X55NiCrMoV7	1100	1280	42
X37CrMoV5-1	1100	1333	42
	1200	1451	44
	1335	1584	47
	1431	1733	50

Table I. 5 : Room temperature mechanical properties of hot work steels [Delagnes,1998].

Today, all extrusion dies are subjected to surface hardening and treatment in order to obtain a more uniform bearing surfaces and reduce wear damage. Nitriding is used since

many years to increase surface hardness. It consists in a simple diffusion of nitrogen at the surface of the die: the thickness of the diffusion zone range between 130 and 160 μm depending on the composition of the alloy.

Recently, CVD or PVD coatings, with titanium and chromium carbide as well as aluminium oxide, applied on the surface of extrusion tooling, have significantly improved die life. **[Björk et al.,2001]**

II.4 The extrusion cycle and die loading

The direct extrusion is the most frequently employed extrusion process. The material is loaded as form of billet and put into the container where it is pushed, by the ram, through a stationary die.

During a typical extrusion cycle, the ram force can be split into two components:

1. The *Frictional Load (F_R):* that is consumed to overcome the container friction.
2. The *Forming Load (F_M):* governed by section shape and die design and employed to form the material.

The last one could be considered stable over the ram stroke, whereas the frictional load varies with the ram position. Depending on the billet length, the container friction force is typically 30-40% of the maximum ram force **[Oftedal,1998]**.

$$\textit{Total Extrusion Force} = F_M + F_R$$

The load displacement graph, reported in Figure I. 4, shows that a significant extrusion load is needed to start the cycle, due to the shear stress along the whole length of the billet. As the stem moves forward, the area over which the friction acts is reduced as the billet becomes shorter. The reduction of the frictional component, over the press cycle, represents the reduction of the press force, as shown in Figure I. 4 (red curve).

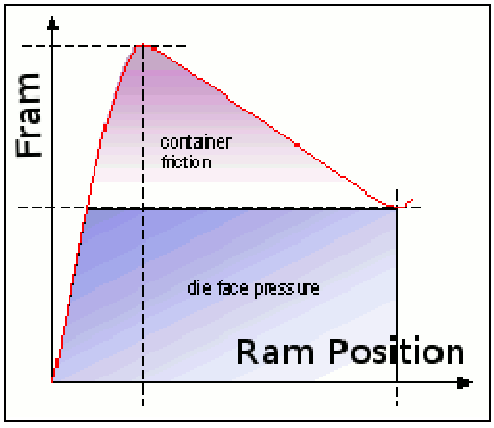

Figure I. 4 : Ram Force variation over the stroke.[Oftedal,1998]

Although the forming load is considered constant during an extrusion stroke, the stress

distribution through the tool is not uniformly distributed. For this purpose, finite element analyses of hollow dies were carried out by Hydro Aluminium in order to point out the strain and stress response of the tool. All calculations were obtained using an isotropic hardening model and considering an evolution of the cycle with time. The “Beginning of the cycle” represents the instant when the billet starts flowing through the die, the “End of the cycle” is the extrusion of the final part of the billet and the “Dead cycle” stands for the unloading process time. Figure I. 5 shows that the deformation mode, emphasized by a bending behaviour, seems to be quite similar at the beginning and at the end of the cycle. The deformation is dominated by the billet pressure exerted on the porthole: this loading predominantly acts on the portholes bridges generating a bending moment (red and black arrows) which is subsequently transferred to the die plate creating high forces in the web area (blue arrows).**[Dossin,2010]**

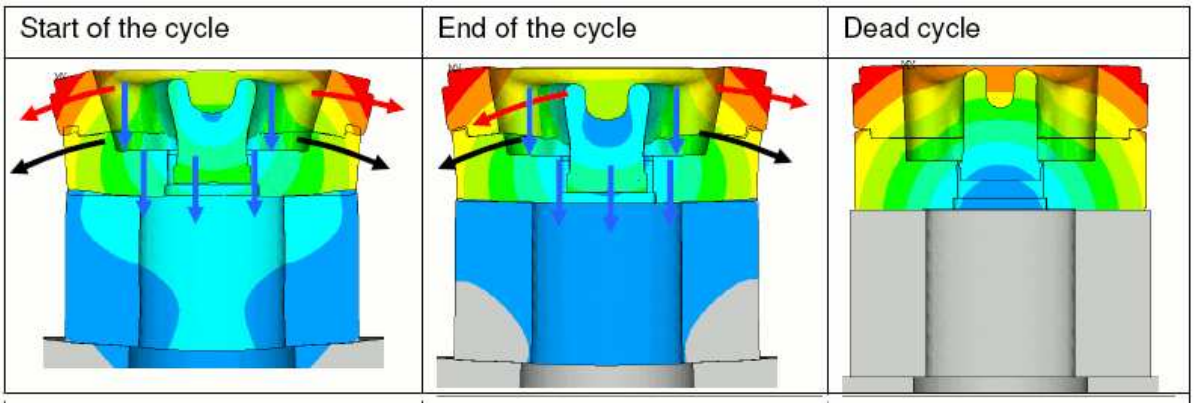

Figure I. 5 : Deformation behaviour during Extrusion cycle. [Dossin,2010]

Figure I. 6 reports some calculations experienced on the porthole at the beginning (a) and at dead cycle (b). These analyses demonstrate that during the cycle (start and end cycle), the zone of transition between the bridges and the mandrel exhibits stress concentrations well above the yield strength of the material (called “Hot Spots”) generating a plastic deformation.

During the dead cycle, Figure I. 6 (b), the plastic strained hot spots are compressed when the tool is unloaded due to the elastic energy stored in the adjacent material. **[Lange,1998]**

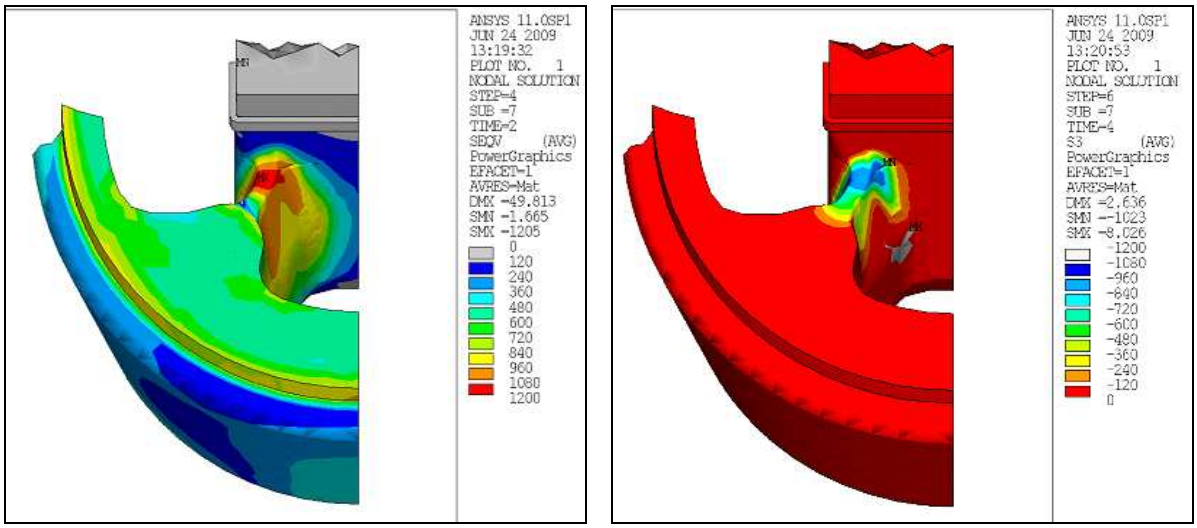

(a) **(b)**

Figure I. 6 : stress distribution in die at the "Start" of the cycle (a) and at the "Dead of the cycle" (b)

These fluctuating stresses (tension/compression) become cyclic when multiple billets are extruded. In general, the extrusion stroke corresponds to cumulative loading/unloading cycles at a frequency 1-5 billets shaped every 10 min. For these reasons, the die is submitted to a typical low-cycle fatigue regime at a temperature that remains generally stable in the range 450-580°C. The extrusion tooling is then subject to a combination of thermal and mechanical loads that enhance the occurrence of damaging processes, namely low cycle fatigue and creep **[Reggiani et al.,2010]**.

The cyclic alternate tensile and compressive stresses are simulated using Low Cycle Fatigue (LCF) tests conducted in a reversed total strain control. In such a way, the mechanisms of cyclic plasticity; enhanced by softening mechanisms at peak stress, can be evaluated in order to be close to the loading conditions of dies in service.

A trapezoidal waveform (Figure I. 7) was adopted as reference signal. The symmetric cycle is provided with an holding time (150s), at maximal strain, to assess for the extrusion loading conditions and a steady time (20s), at minimal strain, to take the unloading into consideration. The results of the experimental tests will be discussed in Chapter IV.

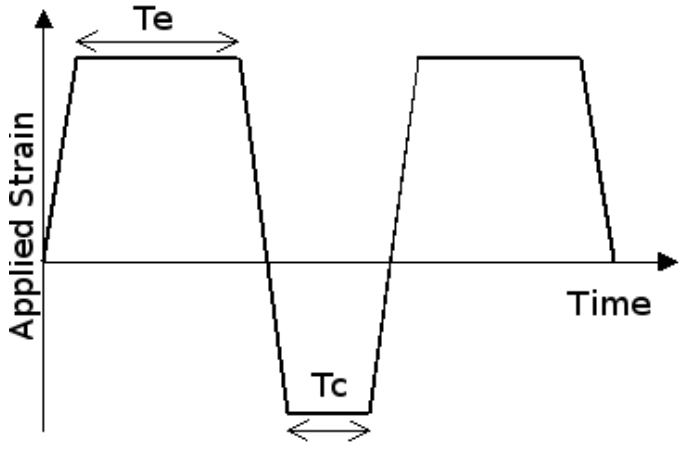

Figure I. 7 : Schematic representation of the reference cycle for LCF tests under extrusion conditions.

II.5 The failure mechanisms of the aluminium extrusion dies

Fracture is one of the principal failure modes for extrusion dies and tooling: as mentioned before, the thermo-mechanical stresses act in a cyclic way, while the aluminium friction on the die surface induces wear damage on the bearing area. For this reason, the most common modes of in-service failure are fatigue, wear and deflection.**[Qamar et al.,2008]**

A statistical study about the relationship between die profile and modes of failure, presented by Arif **[Arif et al.,2003]**, led to the conclusion that *fatigue fracture* is the main failure mode for all die shapes.

Typical fatigue failures are located at high stress concentration zones such as sharp corners, section changes or porthole bridges which are the most critical parts in the die. In this case, fracture initiation is not necessarily related to macroscopic defects in the material, but it is instantaneously followed by a rapid crack propagation. Specific microscopic investigations, reported by Hydro **[Lange,1998]**, pointed out that this kind of "in service" die fracture lead to a sudden change of the wall thickness on the last extruded profile. The hot stress cracks extend as a network under the tool surface: this crack propagation is aided by the temperature differences between the core and the surface of the die that occur during the extrusion cycle. The presence of high stresses, combined with high stress-concentrations, lead to crack propagation and failure.

The second most significant failure is associated to *friction* damage, on the bearing surfaces, which is defined as a progressive *wear* of the material. The exposure to high temperature combined with friction between the extrusion material and the die enhances the development of adhesive and abrasive wear mechanisms. The formation of an adhesive layer is due to the high tendency of the aluminium to adhere on the steel surface, especially when the temperature increases. The layer is particularly rich in magnesium, aluminium, iron and silicon: the production of Fe-Al intermetallic compounds induces a continuous dissolution of the tool and a consequent failure.**[Gutovskaya et al.,2004]**

Other kinds of extrusion die failures include the *deflection* of the tool due to an excessive plastic deformation: the bending forces, acting on the hollow die, could lead to a displacement of the mandrel pole which can induce for instance an eccentricity defect on the rounded tube profile.

III The modular extrusion die: a new concept of extrusion tool

As discussed above, there is large variety of failure modes that can strongly limit the life and the efficiency of the extrusion tools. In the last few years, different developments to improve extrusion die performance were proposed by Hydro Aluminium, addressing the damage mechanisms of the die from a material selection and surface treatment point of view. Surface treatments for die bearing address mostly wear issues employing specific CVD system in use since more than ten years. Over the last five years, different activities were ran with the objective to improve die performance considering both failure modes from a die

bulk material and surface treatment selection point of view. The main objective of these activities is to increase die life and reduce directly the connected ratio die cost/kg extruded. Improving die stability can also generate significant profit through process reliability and productivity increase, as well as product quality stabilization (surface, dimensions).

In 2004, Hydro Aluminium Automotives Structures proposed a solution to limit the frequent failures of dies employed to extrude the 7000 series aluminium alloys. This innovative approach was based on the employment of various materials, with specific tailored properties, in different parts of the die.**[Pasqualon,2010]**

A so-called "*Modular*" extrusion die was designed and prototypes were tested. For this innovative die (see Figure I. 8), the area with strong thermo-mechanical (First module) loading was made with a **Nickel-based Superalloy** (Ni-SA) whereas in the bearing zone (Second Module), the insert was manufactured with a wear resistant material (such as high speed tool steel, hot working steel or precipitation hardened steel) optimised by the application of a specific coating.

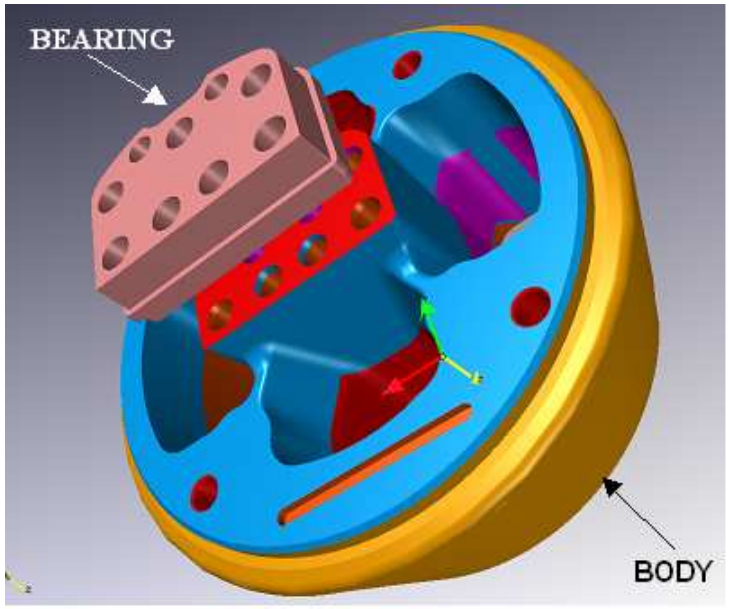

Figure I. 8 : Modular Concept of Extrusion Die.

The introduction of this new concept of die brings various industrial and technological benefits. The employment of a stronger material, in the load carrying body parts, improves the die life and allow a higher productivity for extremely complex extrusion profiles and hard to extrude alloys. The application of hard coatings on wear affected parts reduces the die maintenance actions and improves the surface quality of the extruded product, due to the low roughness of the bearing surfaces and to the improved flow characteristics. **[Kindlihagen,2008]**

For large section of 7000 series alloys *several thousands of billets* can be extruded with the same die. This result induces significant savings through die cost/kg massive reduction (die purchasing), scrap rate reduction (process capability improvement), die maintenance and cleaning cost reduction (die shop force and caustic cost) and a first contribution in productivity improvement through speed increase for all dies running.

The modular die was initially employed for the extrusion of automotive components. This industrial sector is characterised by an important volume of given sections which values long lasting extrusion dies.

In 2010, the modular die concept was employed, for the first time, in the Hydro Precision Tubing division to produce aluminium round tubes. Significant die life increase as well as process stability improvement have been achieved.**[Pasqualon,2010]**

The use of superalloys stands for a critical aspect of the Modular Die idea: these materials show high mechanical performances (creep and fatigue) at high temperature and good corrosion and oxidation resistance. For these reasons, they are known to be superior to the traditional hot work tool steels.

In particular, Inconel 718 was selected as the appropriate candidate material for the bulk structure: this alloy is the main wrought superalloy used in various industry **[Gutovskaya,2003]**. It is able to combine excellent tensile, fatigue, creep and rupture strength in the range of temperature where the die is operating (almost 550° C) **[Special Metals]**. Inconel 718 is also less expensive than different other superalloys such as Wespalloy and Udimet mostly because of its extensive worldwide usage in the Aeronautic and oil and gas fields. However some challenges are existing: manufacturing of Inconel 718 is very difficult and its thermo-chemical resistance to Al corrosion is low which forces the choice of another material for the bearing area.

The mechanical performances of this material will be investigated in this work and a particular study of the fatigue properties will be reported in Chapter IV.

III.1 Investigation of a real case of tool fracture

The service life of an extrusion die has a strong impact on the quality, efficiency and cost of a given extruded profile. The number of maintenance interventions (Die correction, Welding repair, die scrap), caused by tool defections, contributes to the commercial viability of the production. Generally, a die failure is declared when the tool has become completely inoperable or when it is unable to ensure its specific functions due to an advanced degradation: for this reason, the analysis of failure cases is a very important way for improvements in process economics and operating procedures. **[Kazanowski,1998; Akhtar et al.,2010]**

Figure I. 9 shows a detail of the fracture of an Inconel Modular extrusion die which was employed by Hydro Aluminium for the hot-extrusion of thin walled car bumpers of high strength aluminium alloys, from the A7000 series. A preliminary crack initiation was detected after the extrusion of 585 billets has been completed, the die was weld repaired and a new repair was required following the extrusion of 120 billets more, before being considered “out of service “.

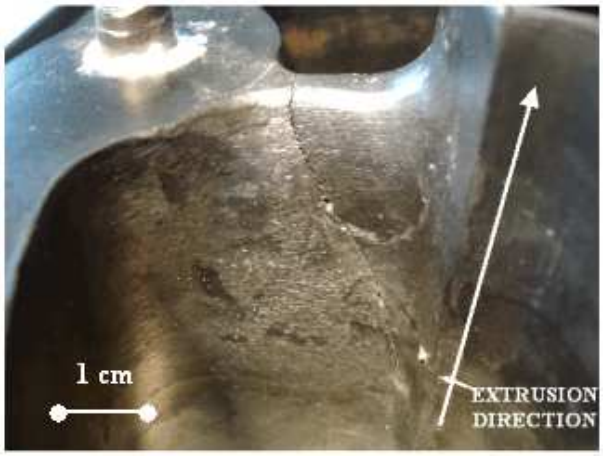

Figure I. 9 :: The fractured part of the die

The tool exhibited a large crack in the transition bridge to the mandrel, where the bulk material is subject to high stress concentration, which induces a localised plastic deformation. As reported by previous investigation **[Gutovskaya,2003]**, the crack propagated along 40 to 60 mm and it was stopped by the increased width of the bridge closed to the mandrel, where the stress concentration is lower.

The crack was opened in order to investigate the fracture surfaces. A preliminary macroscopic analysis showed a flat surface with no necking, whereas a more detailed microscopic examination, performed by SEM, revealed the presence of fatigue striations with an average spacing of about 0,3-0,5 µm **[Kazanowski,1998]**.

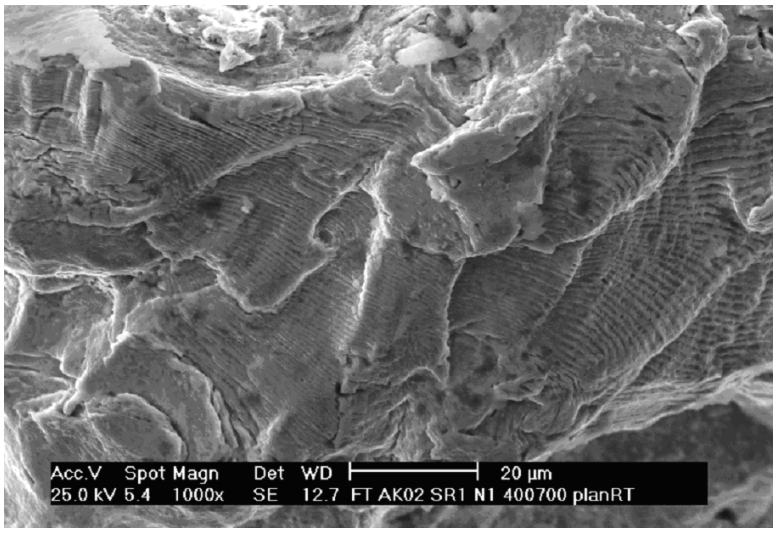

Figure I. 10 : SEM investigation of the fracture surface showing typical fatigue striations.

Considering the principal stress vectors, reported in Figure I. 11 and calculated by FEA in the die zone closed to the crack, it is assumed that the crack grew in length along a direction inclined by 45 degrees (high shear stress planes) with respect to the principal stress vector σ_1 (Red arrows S_1).

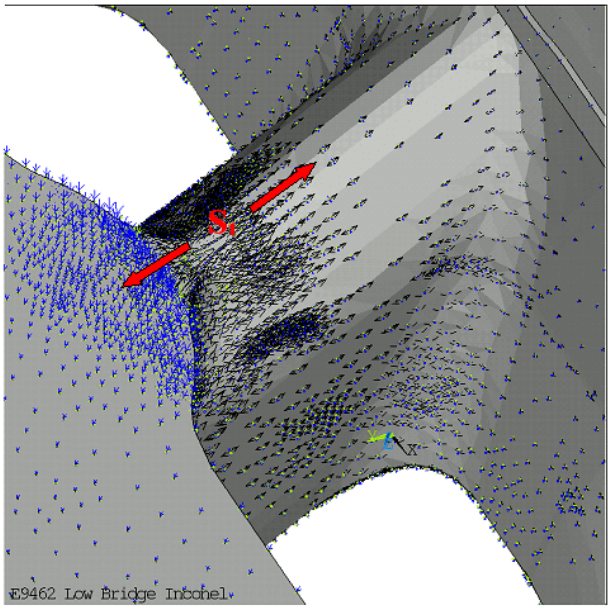

Figure I. 11 : Principal Stresses Vectors in the transition bridge of an hollow die.

This last detail confirms the hypothesis of a fatigue failure: the crack propagates long direction of fatigue propagation in Stage I. No evidence of intergranular fracture, possibly related to the coupled effects of the cyclic loading with the service environment, was detected.

The present investigation points out that fatigue is the relevant failure mode for Hollow extrusion die. The adoption of the modular concept has strongly delayed the occurrence of fatigue damage, considering that in some traditional steel dies only 25 billets were extruded before fracture initiates. However, the cyclic tensile/compressive mechanical loading is still a limiting factor for the die life.

For this reason, an important research activity, focused on the understanding and the improvement of the mechanical behaviour of the tool bulk material (Inconel 718) will be led in order to further increase die life, process stability and later on press productivity. A detailed description of the research objectives is given in the next paragraph.

IV Outlooks and Objectives of the project

In a traditional aluminium extrusion process, the tool is subject to extreme working conditions that strongly influence its service life: the variety of loading components, in terms of thermo-mechanical loading, and the continuous contact between the tool and the aluminium enhance the risks of wear and fatigue failures. The process of hot fatigue damage, during the extrusion operations is due to the alternation of tensile and compressive stresses, acting on specific zones of the die. This represents one of the most common cause of die failure, having detrimental impacts on the process efficiency especially through die cost **[Subodh,2004].**

In this economical challenge, the Modular Extrusion die is an innovative idea prone to improve die life and simultaneously reduce the directly connected costs. The application of

high performing material, Inconel 718, with thermo-mechanical and microstructural tailored properties stands for the technological step change. Even tough the technology has recently shown important benefits and good results in extrusion practice, this application is still at an early stage of its potential exploitation.

A more detailed knowledge on the mechanical behaviour of the bulk material, under extrusion conditions, might support further improvements of performances ensured by the modular die. From this point of view, two possible research options can be explored:

1. The investigation of the impact of the extrusion process such as extrusion speed, billet length, thermo-mechanical loading on the mechanical behaviour of the bulk material, the so called **Material Extrinsic Parameters**.
2. The optimization of the material properties to improve its strength under extrusion loading. This second objective could be achieved by modifying the **Material Intrinsic Parameters** such as grain size, precipitates morphology through thermo-mechanical treatments in order to adapt the material to the specific conditions imposed by the extrusion process.

The material development becomes the first step in increasing productivity and efficiency of an extrusion die. This represents the main objective of this study that will be addressed by a multidisciplinary approach including metallurgical, chemical and mechanical experiments.

In the last fifty years, considerable studies have been performed to address the cyclic behaviour of Inconel 718. This material, is employed in various industrial applications because of its high performances at elevated temperature.

The originality of the present work is based on the development of an optimized Inconel 718 alloy for specific applications, that is bulk material for extrusion die: which represents a technological jump in the employment for this superalloy in the field of tools.

From the scientific point of view, the isothermal Low Cycle Fatigue (LCF) tests are considered as the most representative testing facilities of the thermo-mechanical loading acting on the tool: various LCF conditions (strain amplitudes and strain rates) were so examined in order to address the various damage mechanisms occurring under cyclic solicitations.

The objective of this PhD work is to contribute to the development of die materials for aluminium extrusion for a continuous improvement of the productive capabilities of Hydro Aluminium to achieve a leadership in industrial products within a global market.

V References

[Akhtar et al.,2010] Akhtar, S. and Arif, A. "Fatigue Failure of Extrusion Dies: Effect of Process Parameters and Design Features on Die Life." *Journal of Failure Analysis and Prevention* 10(1): pp. 38-49, (2010).

[Arif et al.,2003] Arif, A. F. M., Sheikh, A. K. and Qamar, S. Z. "A study of die failure mechanisms in aluminum extrusion." *Journal of Materials Processing Technology* 134(3): pp. 318-328, (2003).

[Bauser et al.,2006] Bauser, M., Sauer, G. and Siegert, K. "Extrusion 2nd Ed.", ASM International, p. 592, (2006).

[Björk et al.,2001] Björk, T., Westergård, R. and Hogmark, S. "Wear of surface treated dies for aluminium extrusion -- a case study." *Wear* 249(3-4): pp. 316-323, (2001).

[Delagnes,1998] Delagnes, D. "*Comportement et tenue en fatigue isotherme d'aciers à outils Z 38 CDV5 autour de la transition fatigue oligocyclique endurance*". PhD Thesis, Ecole des Mines de Paris (1998).

[Dossin,2010] Dossin, S. "*Stress Anlaysis of Hollow die plate*". Unpublished Work Hydro Aluminium ECC (2010).

[Dwight,1999] Dwight, J. "Aluminium design and construction", E & FN Spon, p. 295, (1999).

[Gutovskaya,2003] Gutovskaya, J. "*Material development for Aluminium Hot Extrusion Dies-AISI Premium H13 Tool Steel and Nimonic 90/PK 37 Nickel-Base Superalloy*s". Phd Thesis, Norwegian University of Science and Technology (NTNU)**:** 135 (2003).

[Gutovskaya et al.,2004] Gutovskaya, J., Solberg, J. K., Lange, H. I. and Andersen, L. H. "Wear of Inconel 718 die during aluminium extrusion--a case study." *Wear* 256(1-2): pp. 126-132, (2004).

[Kazanowski,1998] Kazanowski, P. "*Die Performance Optimization through Understanding of the Surface Features of Fatigue Fractures*". ET '08: the Ninth International Aluminum Extrusion Seminar & Exposition (1998).

[Kindlihagen,2008] Kindlihagen, A. "*Modular die concepts: Cost-Benefit analyses*". Unpublished work, Hydro Aluminium ECC (2008).

[Lange,1998] Lange, H. I. "*Low Cycle Fatigue and creep testing of Hot Working Tool Steels at service temperature*". Unpublished Work SINTEF Material Technology (1998).

[Oftedal,1998] Oftedal, K. O. "*Loads acting on the tools*". Unpublished Work, Hydro Aluminium Extrusion (1998).

[Oudin,2001] Oudin, A. "*Thermo-Mechanical Fatigue of Hot Work Tool Steels* ". PhD Thesis, Ecole Nationale Superieure des Mines de Paris (2001).

[Pasqualon,2010] Pasqualon, M. "*Extrusion dies material and surface treatment developments*". Unpublished Work, Hydro Aluminium PTTC (2010).

[Qamar et al.,2008] Qamar, S. Z., Sheikh, A. K., Arif, A. F. M., Younas, M. and Pervez, T. "Monte Carlo simulation of extrusion die life." *Journal of Materials Processing Technology* 202(1-3): pp. 96-106, (2008).

[Reggiani et al.,2010] Reggiani, B., Donati, L., Zhou, J. and Tomesani, L. "The role of creep and fatigue in determining the high-temperature behaviour of AISI H11 tempered steel for aluminium extrusion dies." *Journal of Materials Processing Technology* 210(12): pp. 1613-1623, (2010).

[Saha,2000] Saha, P. "Aluminum Extrusion technology", ASM International, p. 259, (2000).

[Special Metals] Special Metals "Inconel Alloy 718" (consulted webpage in March 2011) http://www.specialmetals.com/documents/Inconel%20alloy%20718.pdf.

[Subodh,2004] Subodh, K. "*Technical Solutions for the Aluminum Extrusion Industry*". Eighth International Aluminum Extrusion technology (2004).

[Xianghong et al.,2006] Xianghong, W., Guoqun, Z., Yiguo, L. and Xinwu, M. "Numerical simulation and die structure optimization of an aluminum rectangular hollow pipe extrusion process." *Materials Science and Engineering: A* 435-436: pp. 266-274, (2006).

Chapter II

Microstructure and mechanical properties of Inconel 718 alloy

"La bibliographie se fait après et non avant d'aborder un sujet de recherche"

Jean Perrin

Chapter II: Microstructure and mechanical properties of Inconel 718

VI Introduction

Nickel-based superalloys have been developed during the last 50 years in order to satisfy the different service requirements concerning, above all, the aeronautical and energy applications.

The aim of this literature review is to give a synthetic view of the wide variety of researches that have been previously carried out, in order to understand the mechanical and microstructural properties of the alloy. This preliminary chapter is considered as a pertinent support for the interpretation of the experimental results that will be reported in the second part of the manuscript (Chapter IV and Chapter V).

In the *first part* of the chapter, attention is focused, prevalently, on the review of the main microstructure dependent effects relative to:

- the alloying elements;
- the secondary phases and their strengthening effects;
- the thermal treatment parameters.

The *second part* deals with the mechanical properties of the alloy, with a particular interest on the cyclic behaviour. An examination of the main microstructural degradations associated to cyclic loading will be discussed in details, pointing out their effects on the global fatigue performances.

In the description of the different topics, a particular attention will be given to the alternative solutions (alternative thermal treatments, composition changes, forming processes) that were proposed by previous works in order to extend the domain of application of Inconel 718.

VII The nickel based superalloys

The nickel base superalloys represent a class of material that were developed to fullfill a need for stronger and more corrosion resistant alloys for high temperature applications. These superalloys associate a good workability (castability, thermal treatment sensitivity, machining, coating…) to a high mechanical strength at elevated temperature, typically above 540°C, where the standard hot work materials (Steels, Titanium alloys, copper..) fail to operate **[Guedou,2009]**.

These outstanding properties are obtained by a structural hardening within a FCC solid-solution matrix mainly strengthened by the addition of Aluminium, Titanium, Tantalum combined with nickel forming intermetallic γ’ phases (LI_2). The nickel chromium matrix is

very beneficial as nickel, in contrast to iron and titanium matrices, does not show allotropic transformations that might destabilize the structure, especially at high temperatures. The trend to form adherent thermally growth oxide (TGO) guarantees a good resistance against environmental attack by harmful elements such as oxygen and sulfur.**[Decker,2006]**

The hardening γ' phase shows a rapid and homogeneous growth in the range of 12-300 nm: the slight lattice mismatching with the matrix increase the resistance to the dislocation movement, limiting the deformation process under high loads. In addition, the face-centred-cubic (fcc) crystal structure generates multiple slip systems assuring a good ductility and formability with minimum texturing. **[Decker,2006]**

Typical application of nickel base superalloys is the aerospace, industrial gas turbine and marine turbine industry, where the service temperature is closed to the melting point of the material. In addition, their high strength, coupled with a good corrosion resistance, allows their application in the biomedical field.

The future development of the nickel base superalloys will be focus on the optimisation of their general properties to fit a specific application or process **[Donachie,2002]**: this is the challenge that we are concerned with, for the present work, in order to optimise the material to the specific solicitations imposed by the extrusion process.

VIII Metallurgy and composition of Inconel 718

Inconel 718 is a nickel base superalloy initially introduced by Herbert Eiselstein in 1959. Concerning chemical composition, this material differs from the other Ni base alloys as it contains iron (18%), which influences the precipitation process and some Nb (5%), which contributes to the hardening mechanisms **[Alexandre,2004]**.

The alloy composition (Table II. 1) is based on a variety of alloying elements, each of them have a specific role to adjust material properties. Some elements, such as Nb, Al and Ti, take part in the formation of hardening phases. Others, like Cr, contribute to the oxidation resistance, whereas Mo enhances the mechanical resistance of the austenitic matrix at room temperature, but also at high temperature. **[Slama et al.,2000]**

Element [%]	**Ni**	**C**	**Cr**	**Fe**	**Nb**	**Mo**	**Ti**	**Al**
Min	Base	0.02	17.00	15.00	4.75	2.80	0.75	0.30
Max	Base	0.08	21.00	21.00	5.50	3.30	1.15	0.70

Table II. 1 : Chemical composition of Inconel 718 alloy (% weight).

The strengthening effects are ensured by the precipitation of the γ" phases, Ni_3Nb, with a body centred tetragonal ($D0_{22}$) crystal structure and an average size in the range 200-600 Å (Figure II. 1). The precipitates are coherent disk-shaped particles that form with an approximate thickness of 50-90 Å. In Inconel 718, the main contribution to hardening is

related to the coherency strains between γ" and the matrix. The crystal parameter misfit becomes more significant (~3%) along the tetragonal axis, as compared to the strain obtained on the plane of the disk (~1%). This element provides a higher strength than that associated to a traditional LI_2 precipitate such as γ'. The precipitates have the following orientation relationship with the matrix: $([1\bar{1}0]_\gamma$ // $[1\bar{1}0]_{\gamma"}$ and $(111)_\gamma$ // $(112)_{\gamma"}$ where the c axis of the tetragonal cell could be aligned along the three <001> directions of the matrix. In such a way, three variants of γ" can be detected in agreement with the following orientations: Variant 1: $[001]_{\gamma"}$ //$[001]_\gamma$; Variant 2: $[001]_{\gamma"}$ //$[010]_\gamma$; Variant 3: $[001]_{\gamma"}$ //$[100]_\gamma$ **[Strondl et al.,2008; Niang,2010]**. Figure II. 1 illustrates the morphology of the three variants of γ" phases Figure II. 1(b).

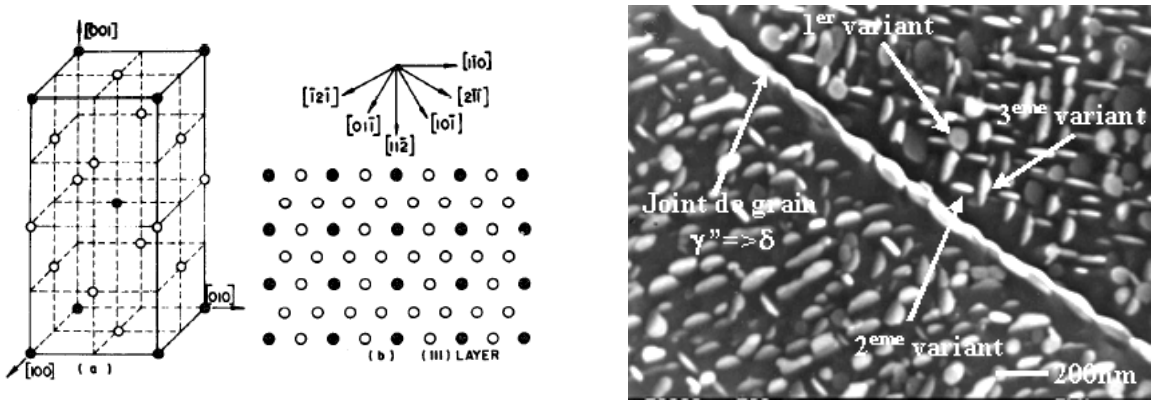

Figure II. 1 : Unit cell of DO_{22} structure (γ"-Ni_3Nb) structure and arrangement of atoms in the (111) plane (a) [Sundararaman et al.,1994], various variants of γ" phases detected in Inconel 718 microstructure (b) [Alexandre,2004].

The strengthening mechanism is completed by the presence of the γ' phase , which is common to all nickel based superalloys, displaying a primitive $L1_2$ structure (Figure II. 2) with Aluminium atoms at the cube corners and Nickel atoms at the centres of the faces.

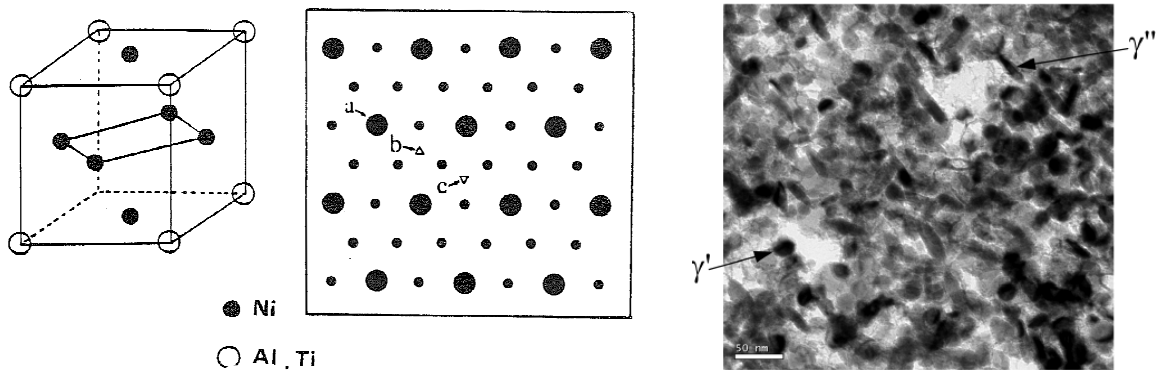

Figure II. 2 :Unit cell of LI_2 (γ') precipitates and distribution of atoms on the (111) close packed plane (a) [Andrieu,1987], TEM image in dark field conditions of γ' and γ" particles (b) [Bor et al.,2010].

In the austenitic superalloys, the γ' and γ" (A_3B) precipitates, due to a stacking sequences similar to that of the matrix, are the only phases prone to exhibit a homogeneous and coherent precipitation. The alloy contains about 15% of γ" and 4% of γ': the γ" precipitates ensures a high resistance to the shearing, providing higher coherency hardening, but they are less stable at high temperature where δ precipitates form, with same composition (Ni_3Nb). This phase is based on a orthorhombic structure (type $D0_a$) and precipitates for temperatures

ranging between 700°C and the solvus temperature (990°C) (Figure II. 3). Delta phase generally appears in the shape of plate, although the occurrence of a globular morphology was reported in previous works **[Ponnelle,2001]**. In general, δ phase shows an intergranular precipitation at grain or twin boundaries, which contributes to control the grain size. However, an intragranular precipitation may occur in association with the pre-existing γ" precipitates. **[Azadian,2004]**

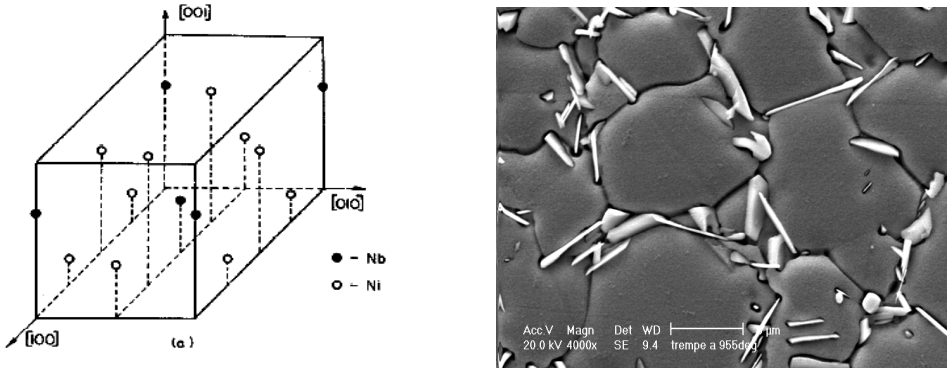

Figure II. 3 : Unit cell of DO_a (δ –Ni_3Nb) structure (a) [Sundararaman et al.,1994], needle-like morphology of delta precipitates at the grain boundaries (b).

The atomic cell associated to δ phase, where the (010) plane is the closed packed plane, shows a rectangular arrangement of niobium atoms identical to that obtained for the γ" structure. However, whereas the γ" precipitates displays a stacking sequence ABCABC, the δ phase structure shows a two layers stacking sequence ABABAB. Kirman **[Kirman et al.,1970]** reported that the nucleation of the intragranular δ platelets could be connected to the occurrence of stacking faults in the metastable γ" structure. These conditions can be associated to the shearing mechanism operated by the motion of dislocations on every alternate (111) plane, which results in the creation of ABABAB type layers, characteristic of the crystal structure of the δ phase. This mechanism enhances the nucleation and growth of δ through several γ" planes.

In addition to the hardening phases, the alloy is enriched with some carbides which precipitate during the heat treatments. The solubility of carbon in the austenite is limited by the high content of carbide forming elements (such as W, Ti, Mo and Nb). The high niobium content improves the formation of the Nb rich MC phases. Those carbides appear as globular and irregularly shaped particles (average size 1-5 µm), generally, at grain boundaries or along incoherent segments of twin boundaries. An over-aging treatment or an extended service exposure at high temperature induces their transformation into secondary carbides (such as M_6C or $M_{23}C_6$ where M is the metallic element), which continue to precipitate at the grain boundaries **[Ponnelle,2001]**.

Earlier investigations have demonstrated that carbides do not enhance the hardening mechanism. Nevertheless, there is some evidences that carbide precipitates strongly influence the fracture mode of the alloy, promoting an intergranular damage through micro-cracking at the interface between the carbide and the matrix.**[Sundararaman et al.,1997]**

To complete this description of the Inconel 718 metallurgy, it is worth to mention the possible presence of σ and µ phases, brittle intermetallic precipitates, with irregular globular

shapes, resulting in detrimental effects on the mechanical properties. The volume fraction of these phases has to be thoroughly controlled during the metallurgical processes: for aeronautical applications their precipitation is strategically avoided. **[Donachie,2002]**

IX Secondary phases and strengthening effects

The mechanical properties of Inconel 718 alloy are based on a precipitation strengthening mechanism which is controlled by the size, the morphology, the volume fraction and the distribution of the hardening phases (γ',γ"). These microstructural features could be optimized by an appropriate choice of thermal treatment parameters, having a strong impact on the mechanical properties.

The nickel based superalloys are particularly sensitive to the effect of the thermal treatment. A double steps process, including a solution annealing followed by a precipitation ageing process, is generally used for the optimisation of these materials.

The solution annealing consists in dissolution of the second phases in order to prepare the alloy to the subsequent ageing. The dissolution could be partial or total as a function of temperature and the holding time used for the treatment. In the case of Inconel 718, the main objective of this preliminary step is an optimization of the content of Ni_3Nb which may precipitates as γ" or δ phase. The annealing process is followed by a rapid quenching which contributes to retain, at room temperature, the supersaturated solid solution. Traditional cooling methods include oil and water quenching, as well as various forms of inert gas or air cooling. Inconel 718 is usually solution annealed near the delta solvus: as reported before, these precipitates are used to control the grain size in wrought alloys by a pinning mechanism of grain boundaries. For this reason the choice of the annealed conditions (temperature, time and cooling rate) is associated to the applications and to the required mechanical properties. In the aeronautical field, Inconel 718 is used for its high mechanical strength and fatigue resistance. For this scope, a solution treatment of 1 hour at 955°C, slightly below the delta solvus, ensures high mechanical properties by a specific control of the delta phase content and morphology.

After solution treatment, a two stages ageing is commonly applied. The ageing procedure contributes to the strengthening of the alloy by a precipitation of γ' and γ" phases from the supersatured matrix. The precipitation temperatures determine not only the type but also the size distribution of the precipitates. A double ageing treatment is usually applied to wrought superalloys in order to control the morphology of the strengthening phases and the carbides size.

In Inconel 718, the precipitation is based on a double ageing procedure with sequentially lowered temperatures. A preliminary step, at 720°C for 8 hours, induces a significant precipitation of the strengthening phases. The second ageing at 620°C for 8 hours, contributes to optimise the precipitates size. A cooling cycle at 50°C/h is employed between the two isothermal processes.

The procedure, schematically drawn in Figure II. 4, constitutes the standard cycle of

thermal treatment used for Inconel 718. In the industrial practice, the precipitation treatments are selected in order to find the better compromise between the microstructural adjustment and the industrial costs.

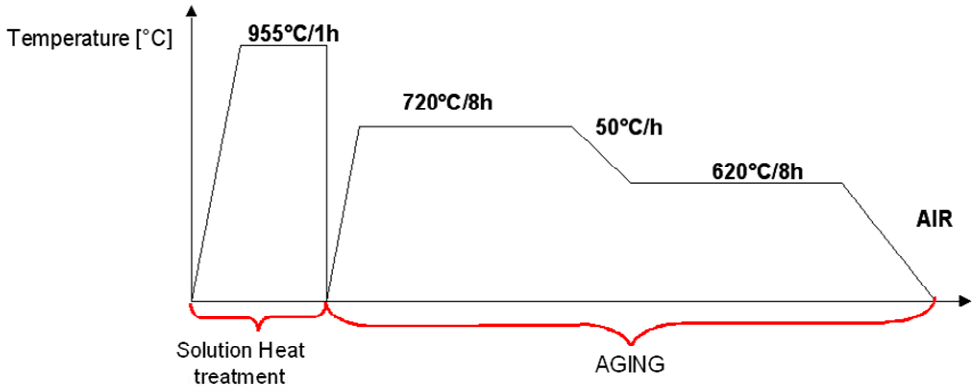

Figure II. 4 : Standard cycle of thermal treatment adopted for Inconel 718.

Figure II. 5(a) shows the microstructure obtained by the application of this treatment. The average grain size is in the range 10-12 µm. Needle-like δ phase precipitates decorate grain boundaries whereas primary carbides (NbC and TiC) are randomly distributed through the matrix (Figure II. 5(b)).

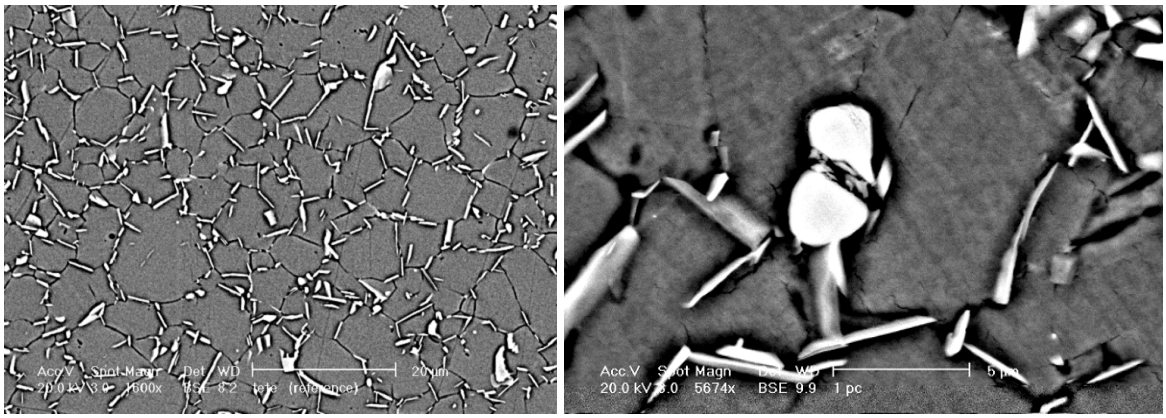

(a) **(b)**

Figure II. 5 : Microstructure of Inconel 718 obtained by a standard treatment (a), SEM micrograph of a Niobium carbide (b).

The double ageing treatment does not affect the grain size or the amount of δ phase, but strictly controls the distribution of γ' and γ". Previous works reported that the preliminary ageing step (at 720°C) induces a continuous growth of both γ' and γ" particles, whereas during the second ageing γ" stops growing, while γ' size continues to increase. Figure II. 6 reports the TTT diagram of the Inconel 718 alloy, pointing out the effects of the different parameters (time, temperature, cooling rate…) on the precipitation.

During the last 20 years, new modified heat treatments have been developed for Inconel 718. The main objective is to introduce a tailored microstructure in order to obtain a good compromise between grain size, grain boundary structure, specific mechanical performances and thermal stability.

Koul **[Koul et al.,1988]** has developed a damage tolerant microstructure able to reduce the

elevated temperature creep and fatigue crack growth rates. This heat treatment consists in a solution treatment at 1032°C followed by a holding time at 843°C for 4h in order to obtain a serrated grain boundary structure around acicular δ phase precipitates. The material is partially solution treated at 926°C for 1 hour to dissolve the intragranular γ" precipitates and is then subject to the conventional double ageing treatment. The resulting microstructure, showed in Figure II. 7(a), improves the resistance of the grain boundaries to the sliding mechanism induced by the high applied loads. As a consequence, the risks of intergranular damage, mainly due to the interaction between the mechanical solicitations and the environmental conditions (oxidation), is drastically reduced.

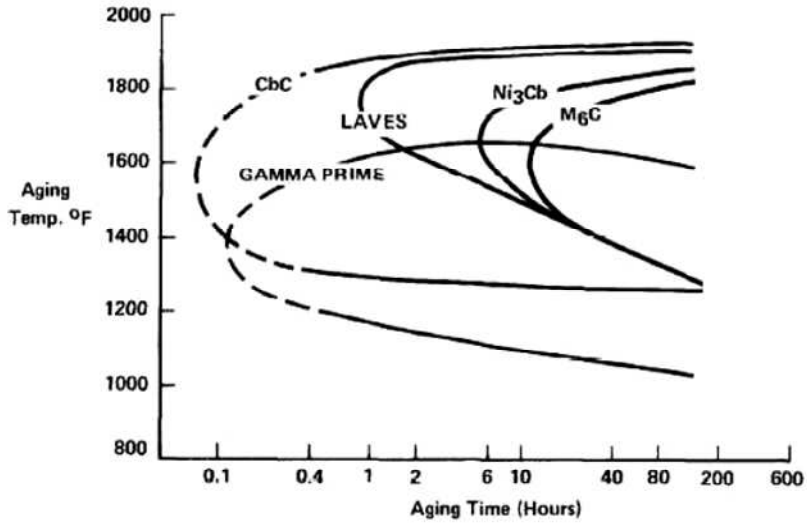

Figure II. 6 : Time-Temperature-Transformation (TTT) diagram of Inconel 718 [Lingenfelter,1989].

The development of alternative thermal treatments was carried out by Guedou **[Guedou et al.,1994]** who investigated the possibility to extend the Inconel 718 applications at temperatures above 650°C. The author proposed the application of an over-aging step at 750°C for 50 hours, as a modification of the standard treatment, in order to obtain an improvement of the crack propagation resistance above 650°C. This alternative procedure offers clear benefits in terms of damage tolerance through an increase of the precipitates size and a modification of the grain boundary morphology, tending to roughen as previously identified by Koul.**[Koul et al.,1988]**

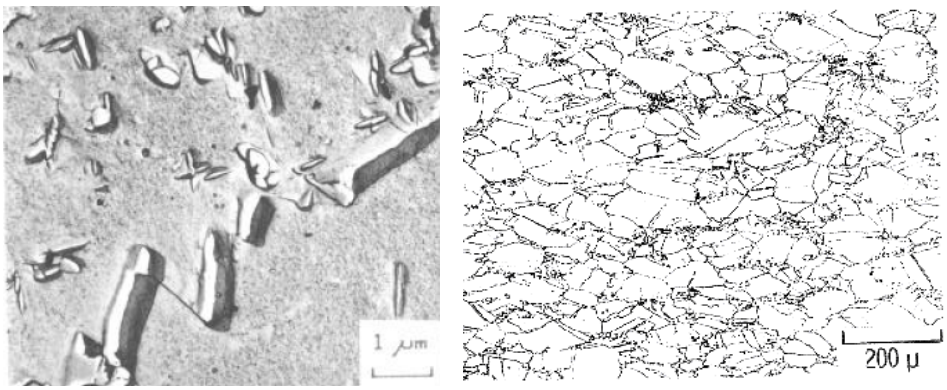

(a) **(b)**

Figure II. 7 : Serrated grain boundary morphology obtained by an alternative treatment [Koul et al.,1988] (a) , neck lace structure of a Direct Aged Inconel 718 alloy [James,1986] (b).

For highest strength levels, an alternative thermal treatment, called Direct Age (DA), was developed. Material is subject to larger forging reduction at low temperatures (980°C), is then water quenched and finally directly aged.

By performing forging reduction below the delta phase solvus, a small volume fraction of this phase is fractured and dispersed in the matrix during the deformation process thus providing resistance to grain boundary migration which allows controlling the final grain size. Omitting the conventional solution treatment step increases the hardening rate within grains, contributing to the improved strengthening of the alloy. The deformation substructure is then stabilized by traditional aging steps, ensuring a 10-20% increase of the tensile strength as compared to conventionally processed material.**[Warren et al.,2006]**

As previously defined, the Direct Age treatment consists in a thermo-mechanical process, based on a hot deformation of the material. Under these conditions, Inconel 718 develops a dynamic recrystallization during hot working. The evolution of the dynamic recrystallized microstructure (DRX), in polycrystals, starts with an initial nucleation at grain boundaries which extends into the non-recrystallyzed volume. The DRX proceeds via a regular nucleation at the interface between recrystallized and non-recrystallyzed grains. The process results in a non-uniform distribution of dislocations in the microstructure, where regions of high dislocation density coexist with almost dislocation free zones.**[Horvath et al.,2001]**

The final microstructure consists in a “necklace” structure (Figure II. 7(b)) with large warm-worked grains surrounded by very small grains.**[James,1986]**

IX.1 Effect of alloying elements on the precipitation behaviour.

Conventional Inconel 718 alloy is characterized by a large volume fraction of plate-like γ” precipitates and a supplementary precipitation of γ’ (Figure II. 8) which determines the high mechanical performances of the material. The fraction of these strengthening phases depends on the content of the main alloying elements, such as Al, Ti and Nb, which play an important role in the precipitation behaviour. **[Xie et al.,2010]**

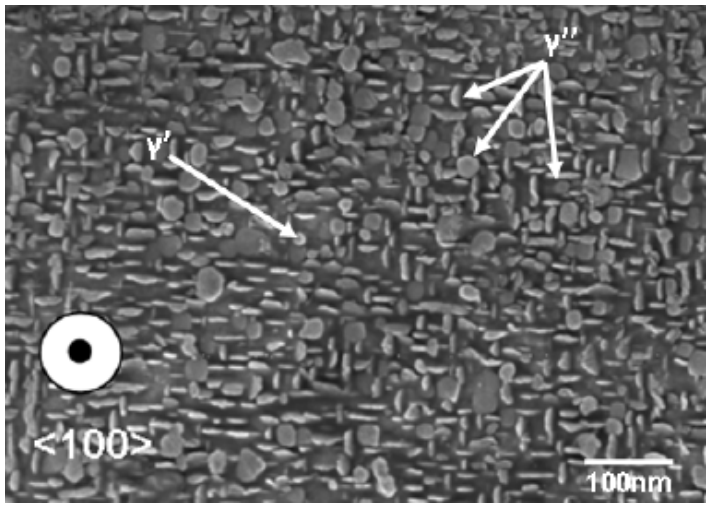

Figure II. 8 : Morphology and distribution of the intermetallic hardening phases γ’ and γ” [Ter-Ovanessian,2011].

Aluminium is the most important element in the formation of γ' phases. Thermodynamics calculations, reported by Fu **[Fu et al.,2009]**, showed that increasing Al content results in an increase of the γ' solvus temperature. However, an excessive amount of this element could favour the formation of the σ phases which degrades the alloy stability. For this reason, an optimum Al content is fixed in the range 0.5-1%.

Titanium plays also an important role in the definition of the γ' composition and morphology. This element promotes the transformation of the globular $Ni_3(Al,Ti)$ in long plate-like particles that form, in some cases, as Widmanstatten structure. An increase of the Ti content, as shown for Al **[Fu et al.,2009]**, induces a decrease of the volume fraction of delta phase with no clear modification of the solvus temperature.

As previously reported, Inconel 718 differs from the other Nickel-base superalloys as it contains Nb. This element, essential for strengthening, must be carefully controlled as, at high concentration, it enhances the formation of δ phase as the expense of γ". This microstructural fluctuation involves a loose of the mechanical properties (mainly tensile strength). From this point of view, the optimum content is limited at a maximum of 5.5%.

In addition to the precipitates hardening, the matrix can be strengthened by a solid solution through the addition of W and Co, which do not show a strong impact on the volume fraction of γ' or δ. According to the previous considerations, the sum of the main alloying elements (Al+Ti+Nb), for a traditional Inconel 718, is in the range 5.5-6 at% which corresponds to a ratio, (Al+Ti)/Nb, equal to 0.7. **[Xie et al.,2005]**

In 1973, Cozar and Pineau **[Cozar et al.,1973]** designed a modified Inconel 718 alloy where the ratio (Al+Ti)/Nb was fixed in the range between 0.9 and 1%. This alternative composition transforms the strengthening precipitates into a compact morphology which improves the thermal stability of the alloy. Cube shaped γ' particles are coated with a γ" thin shell on each of their six faces (Figure II. 9).

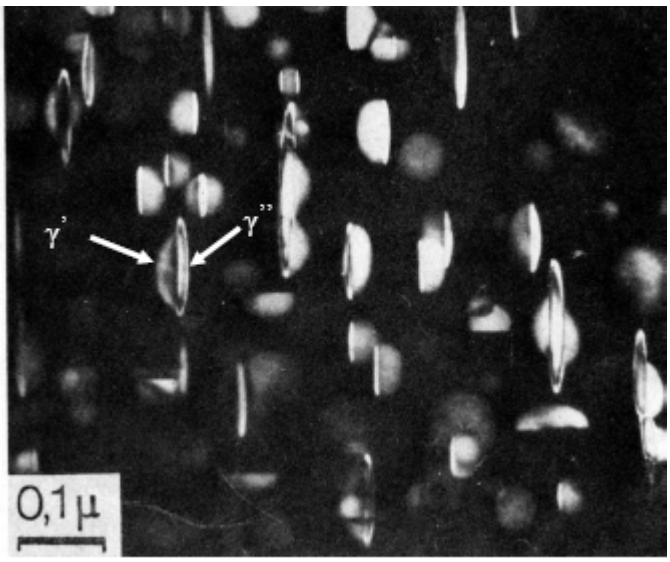

Figure II. 9 : γ'-γ'' compact morphology in a modified Inconel 781 alloy [Cozar et al.,1973].

Conversely to the traditional Inconel 718 behaviour, the compact morphology is prone to limit the continuous coarsening of the γ" particles during over-aging (Figure II. 10). The

growth of the γ" particles is mechanically blocked by the other two variants of precipitates. This specific morphology confers to the material a better stability at high temperature, widening the applications of the alloy.**[He et al.,1998]**

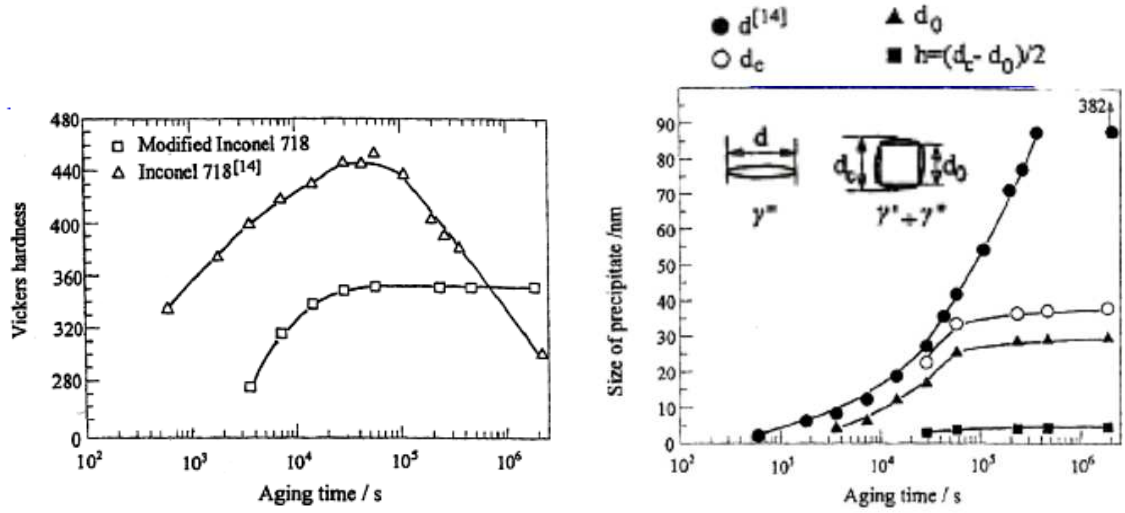

(a) **(b)**

Figure II. 10 : Effect of ageing time on hardness (a) and γ" morphology of standard and modified Inconel 718 (b) [He et al.,1998].

IX.2 The precipitation behaviour in Inconel 718

Inconel 718 derives its high mechanical properties from a fine dispersion of ordered precipitates within a face centred cubic matrix. The understanding of the precipitation behaviour is essential to a better optimisation and development of the material.

The microstructural evolution of the alloy is based on three parameters:

1. The γ' and γ" precipitates volume fraction and morphology;
2. The grain size;
3. The carbides distribution.

Considering that the strengthening phases form in specific temperature ranges, a careful choice of the heat treatment parameters ensures the control of the quantity and size of these precipitates. The nature of the precipitations strongly depends on the initial conditions of the material. The degree of residual stress, the amount of delta phase after the solution treatment and the segregation of Nb are the main variables to take into consideration. [He,1994]

The nose of the TTT curve (Figure II. 6) relative to delta phase shows that the precipitation occurs at 950°C for much less that 0.2 h. Kirman [Kirman et al.,1970] reported that the delta phase grows, as laths, along {111}γ: the small mismatch between the two close-packed planes, (010)δ and (111)γ is accommodated by an array of interfacial dislocations. The delta precipitates are initially plate-like particles which progressively increase their thickness as they consume Nb. Azadian [Azadian et al.,2004] showed that, for a given ageing time, the mean plate thickness increases with temperature, while it remains constant with time.

The presence of delta precipitates does not contribute to the hardening of the alloy, but it

leads to a depletion of γ". The TTT diagram shows that the γ" phase precipitates during isothermal ageing in the range 550-900°C. The incubation time for the onset of γ" precipitation is the shortest (7 minutes) for temperatures closed to 760°C [He,1994].

In a conventional Inconel 718, γ' and γ" are characterised by a random distribution. Different types of precipitates nucleate independently and the strengthening γ" phases are rarely in contact with γ'.

When a double step ageing is applied to the material, it is difficult to determine if γ" precipitates prior than γ'. The microstructural investigations, reported in Chapter V, in perfect agreement with other works, will point out a simultaneous precipitation of the two phases (γ" and γ') during the isothermal ageing.

The isothermal coarsening of γ", controlled by niobium volume diffusion in the matrix, is the most relevant limit for the application of the material at high temperature. At the beginning of the ageing process (600 s), the precipitates display a cubic shape which becomes elliptical with the increase of the ageing time[He,1994].

Sundaraman **[Sundararaman et al.,1994]** reported that the average half-length of these particles is linearly related to the cube root of the ageing time. These results are in agreement with the coarsening theory presented by Lifshitz, Slyozov and Wagner (LSW Theory), which is hypothetically based on a volume diffusion growth. Following these mechanisms, two different scenarii are defined: in the case of short ageing period, the density of γ" precipitates increases with the aging time, whereas in the case of long period, the density tends to decrease.

In the conditions of high precipitates density, coalescence occurs along the tetragonal axis of the particles belonging to the same variant. Han and He [Han et al.,1982; He,1994] observed that, during the growing mechanism, the γ" inter-particle distance is progressively reduced: The contact between the two boundaries induces the formation of a "neck" which causes the coalescence of the two particles and the formation of a new one. The coarsening behaviour, which induces a loss of coherency (Figure II. 11) between the precipitates and the matrix [Devaux et al.,2008], has a detrimental effect on the mechanical properties and it limits the application of the Inconel 718 alloy at a temperature above 650°C.

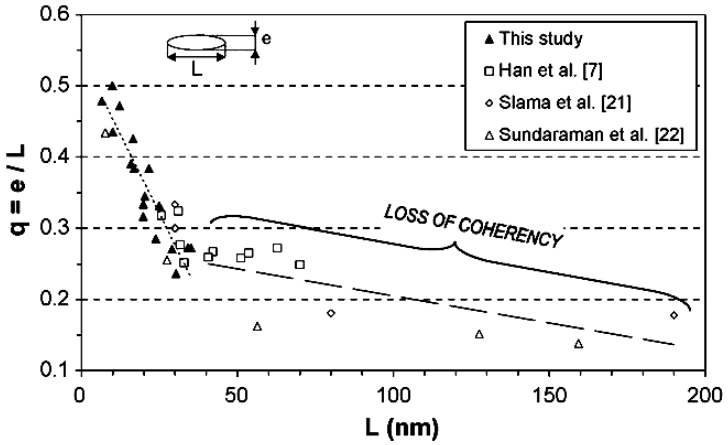

Figure II. 11 : Morphology evolution of γ'' precipitates [Devaux et al.,2008].

X Deformation mechanisms in Inconel 718

As discussed above, in Inconel 718, the γ' and γ" particles are dispersed in the alloy to create a strain field that produces some residual micro stresses acting as barriers to the dislocation motion, limiting the plastic deformation mechanisms. For γ' particles, the residual stresses derive from the differences in terms of elastic modulus between the precipitates and the matrix, whereas for γ" particles, as consequence of its tetragonal structure, a specific distortion of the atomic lattice inducing a significant strengthening of the alloy occurs.

After solution annealing, the material includes a fine a dispersion of solute atoms in the austenitic matrix. During subsequent ageing, activating the diffusion of the solute atoms, the formation of second phases occurs by nucleation and growth of precipitates. This process results in a continuous variation in the particles sizes and inter-particles distances which influences the deformation behaviour. A basic understanding of the mechanical performances of Inconel 718 is possible on the basis of the interactions of dislocations with the dispersed strengthening particles. For these reasons, the gliding dislocations must overcome a potential energy barrier mainly related to the distance between precipitates.

The dislocations movement can progress following different configurations: Figure II. 12 reports the evolution of the critical resolved stress as a function of the precipitates diameter, showing a shear mechanism below a critical diameter (d_C) and a by passing process, above the critical distance, due to the formation of the Orowan loops.

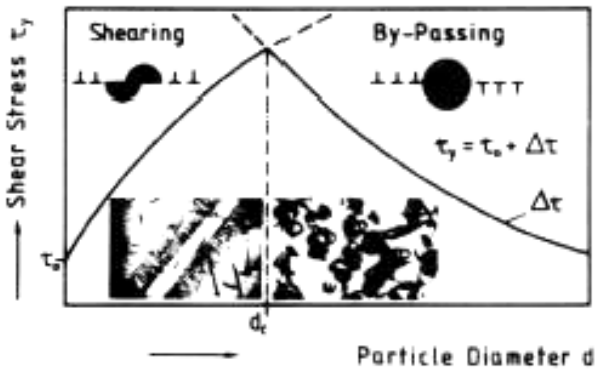

Figure II. 12 : Shear stress evolution as a function of hardening precipitates diameter [Hornbogen et al.,1981].

This latter condition can be achieved by an over ageing treatment. The dispersion size exceeds the critical distance and continues to increase with the evolution of the ageing time, causing a modification of the stress-strain behaviour.

Considering the limited size of the γ" precipitates, the shearing mechanism is considered as the main deformation process in Inconel 718. A specific flow stress, equal to the resolved shear stress, is required to initiate slip into the grains promoting the following mechanisms **[Mendoza et al.,1989]**:

- Creation of new dislocations sources and increase of the dislocations density;
- Activation of dislocations movement along specific slip systems;
- Unlocking of the pinned dislocations from obstacles (precipitates, grain

boundaries…)

These mechanical properties are directly connected to the material microstructure. During the solidification, all grains nucleate and grow in different directions causing an individual mismatching of each grain with respect to its neighbours. The slip mechanism starts in grains favourably oriented in terms of Schmid factor of dislocations slip systems. Slip is consequently spread over a series of adjacent grains when dislocations pileups form, predominantly at the boundaries, creating a stress concentration which allow the unlocking of the pinned dislocations. The dislocations continue moving through the microstructure of the material, expanding towards the boundary and moving out.

In FCC lattice, dislocations slip takes place in {111} planes and <110> directions: this mechanism evolves into concentrated slip bands, with a thickness of few thousands of atomic distances, that causes the reorganisation of the grain by grain sliding, rotation (twinning), fracture or compaction. When the yielding point is overcome, new dislocations sources are activated, increasing the dislocation density. The dislocation movement is impeded by the interaction with the new formed dislocations which cause a pinning at the interior points, inducing a work hardening process.

During the slip evolution, the dislocations are expected to interact with the strengthening phases (γ") in different ways:

1. *Shearing operated by perfect dislocations*: in this case only the γ" variant, whose c-axis is parallel to the [001] directions of the austenitic matrix, allows the passage of paired dislocations (a/2 [110]) which restore the order along the slip plane and limit the high energy anti-phase zones **[Xie et al.,2010]**. For the other variants **[Sundaraman et al.,1993]** deformation may occur by the passage of quadruplets of dislocations (of the type a/2 [110])) which shear the γ" particles restoring the order. This mechanism avoids the creation of stacking faults, but it is difficult to activate.

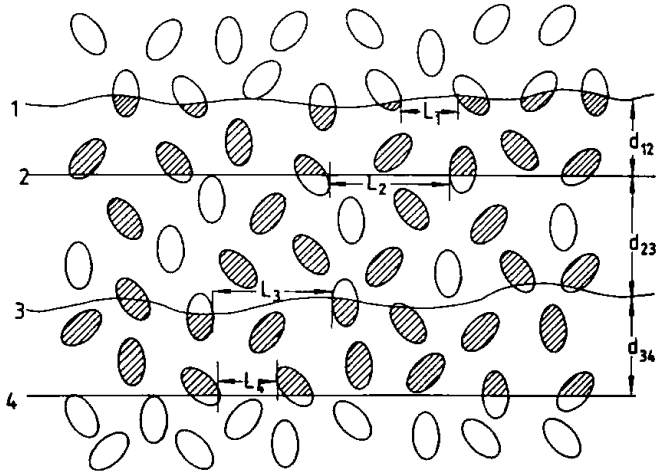

Figure II. 13 : Schematic representation of the shearing process of γ" precipitates operated by quadruplets of dislocations [Sundaraman et al.,1993].

2. *Shearing operated by partial dislocations*: this mechanism was initially highlighted by Kirman and Warrington **[Kirman et al.,1970]** who studied the dissociation of perfect dislocations into two partials separated by a region of stacking faults whose width is dictated by γ" staking faults energy. Considering a dissociation of the dislocation, at the γ" interface onto Shockley partials, following the mechanism a/2 [110] => a/6 [211] + a/6 [12$\bar{1}$], a geometric staking fault is generated on the (111) plane of a $[001]_{\gamma"}$ variant . In such a way, the B_1 layer of the DO_{22} stacking sequence $A_1B_1C_1$ $A_2B_2C_2$ $A_1B_1C_1$ $A_2B_2C_2$ is transformed into $A_1B_1C_1A_2B_2C_2$ $A_1C_2A_1$ $B_1C_1A_2B_2$. This mechanism induces the formation of four successive layers ($C_2A_1C_2A_1$) which corresponds to the A_3 stacking sequence of the delta phase, which nucleates by the growth of these faults into the matrix, replacing the pre-existing γ" particles **[Sundararaman et al.,1994]** (Figure II. 15 (a)).

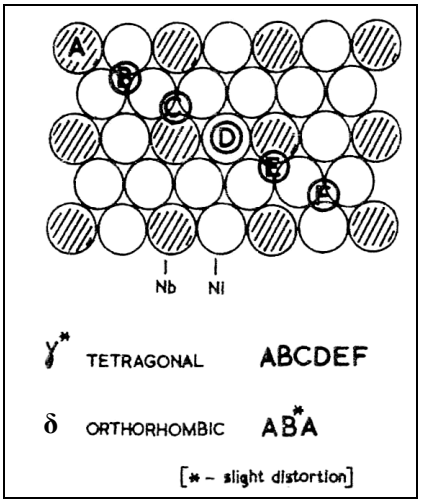

Figure II. 14 : γ" precipitates shearing operated by partial dislocation where the a/6 <112>- type shear of layer C transform the γ" stacking into δ stacking [Kirman et al.,1970].

3. *Deformation twinning:* a slip to twin transition occurs in the mode of precipitates shearing when the material contains coarse γ" phases (Figure II. 15(b)). This mechanism is another example of interaction between partial dislocations and precipitates: the passage of Shockley partials on every {111} plane would generate a twin orientation with respect to the original crystal lattice. The majority of twins is located within the precipitates without any propagation effects into the matrix. The value of the critical resolved shear stress (CRSS), required for a twinning to occur, is lower in the BCT structure (γ") than in the austenitic phase (γ) **[Fournier et al.,1977; Sundararaman et al.,1994]**.

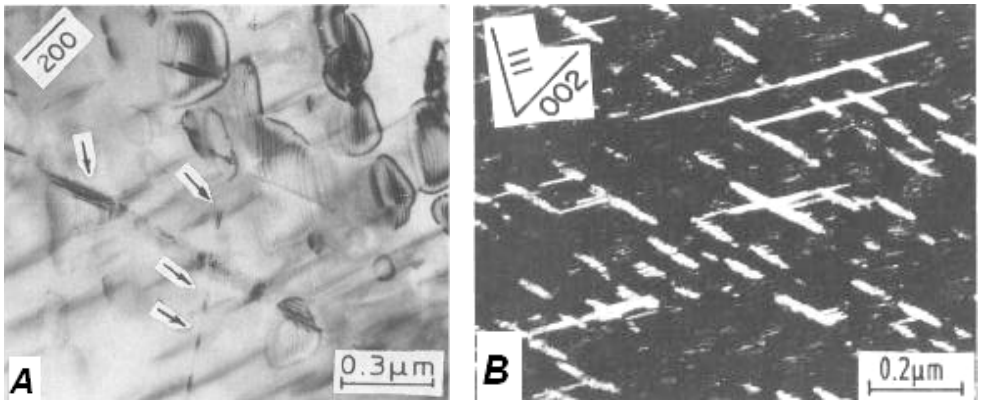

Figure II. 15 : Staking faults within γ" particles produced dislocations (a), dark field micrograph showing distribution of microtwins (b) [Sundararaman et al.,1994].

The deformation mode in Inconel 718 is strongly influenced by the size of the γ" precipitates. The CRSS displays a $R^{-1/2}$ dependence where the three deformation mechanisms depend on the precipitate radii (Figure II. 16). The diagram exhibits a critical size, about 10 nm, where a slip to twin transition could happen. It is important to point out that the CRSS, required for deformation twinning, is lower than the stress associated to the Orowan bypassing mechanisms. These considerations justify the profuse and rapid deformation twinning of γ", especially when long aging treatments, inducing particles size increase, are applied to the material.

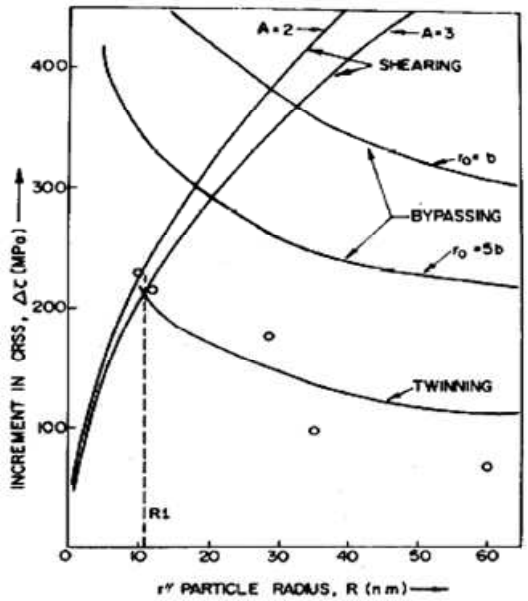

Figure II. 16 : Calculated values of shear stress as a function of γ" particle radius. [Sundararaman et al.,1994]

Depending on the applied loading, the material experiences a specific deformation behaviour which has a direct impact on the mechanical performances of the alloy. The following sections will focus on the effects of the deformation mechanisms on the tensile and fatigue behaviour of Inconel 718.

X.1 Tensile behaviour

The large variety of applications for Inconel 718 derives mainly from its outstanding mechanical performances at high temperature. The evolution of these properties is anyway influenced by the in-service temperature which can induce structural changes (**Figure II. 17**).

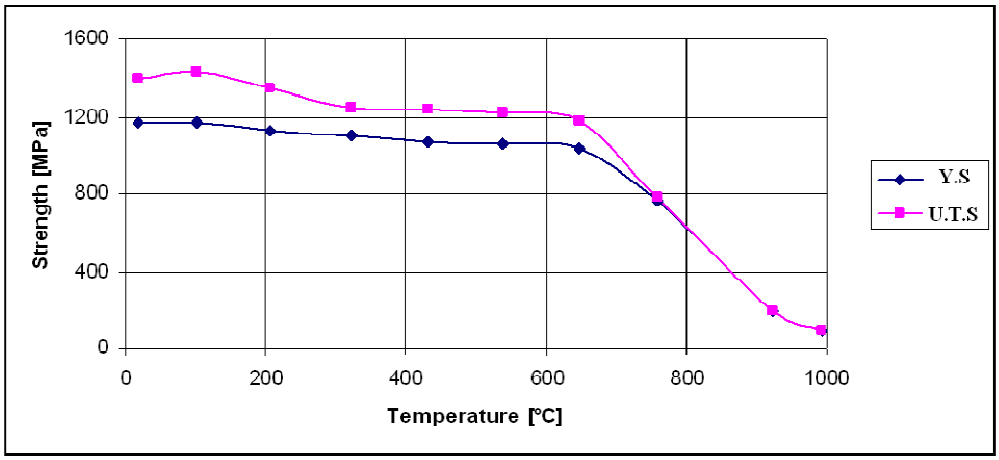

Figure II. 17 : Evolution of the mechanical properties of Inconel 718 as function of temperature [Zemzemi,2007].

On the other hand, the mechanical behaviour, for a specific time at a fixed temperature, can generate time dependent or time-independent mechanical properties due to the different interactions between dislocations and strengthening phases. The microstructural investigations reported by Clavel **[Clavel,1980]** on fractured specimen after tensile tests at room temperature, pointed out a deformation mechanism based on a planar slip where the slip lines are regularly distributed inside the grains.

The mechanical static properties are directly dependent on the thermal treatment which is initially applied to the material. The distance between precipitates must be optimized by an appropriate choice of parameters (solution temperature and ageing time) in order to increase the number of barriers acting as obstacle to dislocation motion.

Decreasing the solution treatment temperature, without changing the ageing time, decreases the amount of alloying elements available for the precipitation **[Mendoza et al.,1989]**. Slama **[Slama,1993]** investigated the effects of the ageing treatment on the tensile properties of Inconel 718 in the temperature range between 550-750°C and a holding time between 4 and 100h. The evolution of the yield strength (0.2% Y.S) is similar to the ultimate tensile strength (U.T.S). For a temperature below 680°C, the Y.S increases with an increase of the ageing time and temperature. Fixing an ageing time of 4 hours, the above mentioned mechanical properties (Yield strength and Ultimate tensile strength) clearly increase when the temperature is raised from 680°C to 750°C (Figure II. 18), enhancing the material toughness.

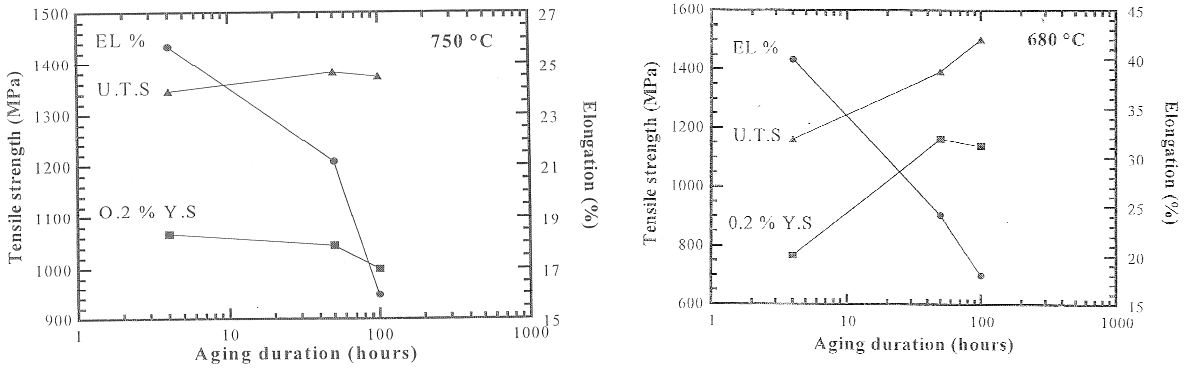

(a) **(b)**

Figure II. 18 : Room temperature tensile properties as function of the aging time at 750°C (a) and 680°C (b) [Slama et al.,2005].

In addition to the above considerations, the application of a thermo-mechanical treatment, like Direct Age, consisting of ageing right after forging and quenching, provides a significant improvement in strength (Figure II. 19) as compared both to the standard treatment (STD) and to a modified DA treatment (HS). Inconel 718, in direct age conditions, keeps higher mechanical properties over the full range of tensile tests temperatures. This is due, mainly, to its smaller grain size and to work hardening effects.

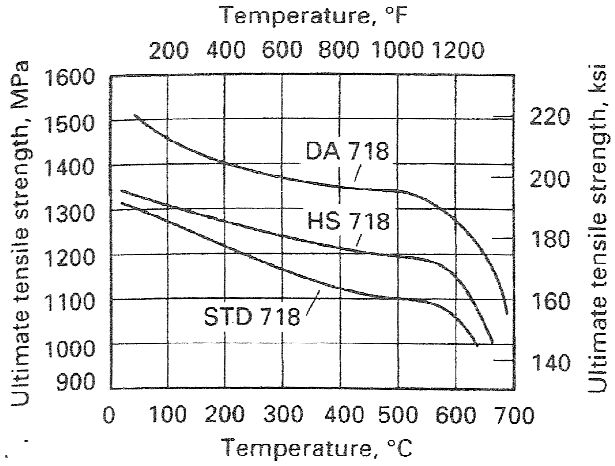

Figure II. 19 : Mechanical tensile properties of Inconel 718 at different processing conditions: DA, direct age; HS, high-strength processed; STD standard heat treatment [Krueger,1989].

X.2 Cyclic Deformation behaviour of Inconel 718

Fatigue is defined as the damage occurring in a material subject to conditions of cyclic stresses and strains possibly leading to complete fracture. Basic information on the cyclic stress-train behaviour are provided in the form of hysteresis loops, where the plastic strain range, $\Delta\varepsilon_p$, can be determined as the maximum loop width (Figure II. 20).

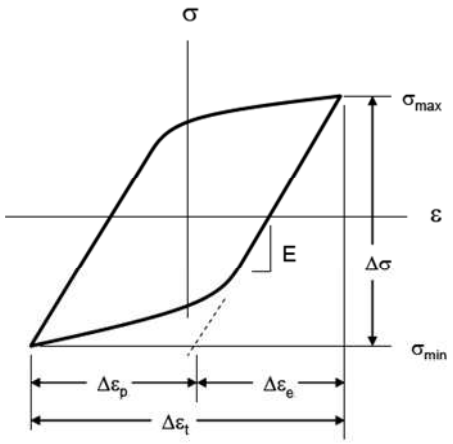

Figure II. 20 : Stable hysteresis loop associated to a cyclic loading [Velay,2003].

During fatigue loading, particular transient cyclic phenomena can occur: depending on the initial state, material shows either full stability, softening or hardening.

- *Strain hardening* is considered as an increase of stress amplitude, with time, during constant strain controlled tests. In case of stress controlled tests, this mechanism leads to a decrease of the plastic strain amplitude increasing the number of cycles.
- *Strain softening* consists of a stress reduction with time during constant strain controlled test. The magnitude of the maximum and minimum stress in the hysteresis loop is progressively reduced **[Clavel et al.,1982]**.

Under cyclic loading, the deformation microstructure consists in spaced arrays of planar deformation bands. Xiao **[Xiao et al.,2008]** reported the existence of two groups of bands that lie on $(1\bar{1}1)$ and $(11\bar{1})$ slip planes. This mechanism is enhanced by the low stacking fault energy (SFE) in the FCC structure which induce the formation of extended dislocations, reducing their tendency to operate cross-slip into other slip planes. In the case of Inconel 718, the activation of an array of planar bands is based on a simultaneous activation of multiple slip systems, which intersect each others, giving the typical saturated-diamond shaped deformation structure in the fatigued specimens (Figure II. 21).

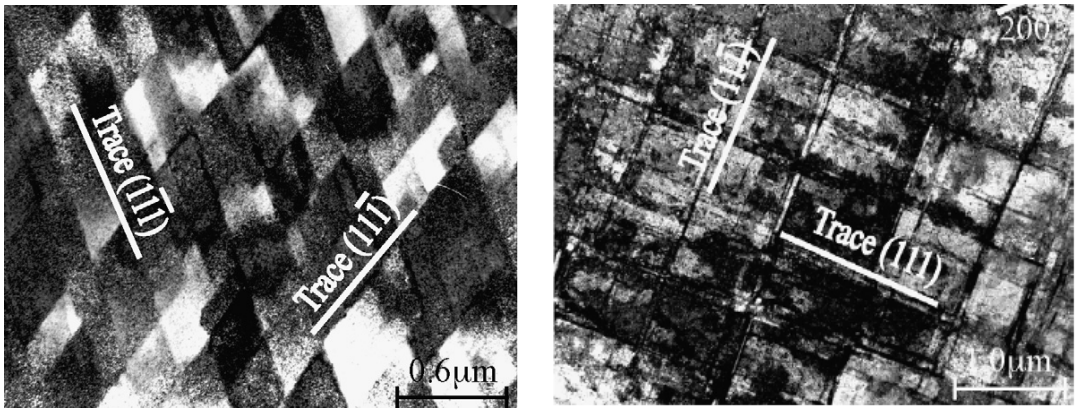

(a) **(b)**

Figure II. 21 : Group of planar slip bands exhibited in cross section areas of deformed Inconel 718 specimens respectively at room temperature (a) and 920 K (b) [Xiao et al.,2008].

The origins of this heterogeneous deformation process were studied by Worthem

[Worthem et al.,1990] who investigated about the development of new dislocation bands at a given strain or stress. These studies showed that the complexity of the dislocations arrangement, in contrast with the results obtained for copper, strongly depends on the applied strain and not on the number of cycles. The nucleation of a new dislocations bands occurs when a previous one is locked on obstacles. In terms of energy, it is easier for the system to activate a new band rather than progress the deformation along the pre-existing bands.

Although as the slip bands penetrate the entire grain area, a distribution of dislocations sources is detected along the boundaries. They include few compliant sources and a great number of stiff sources, able to operate at low and high stresses. After nucleation, dislocations are distributed along the bands. As the strain accumulation is progressively increased, the movement of dislocations becomes difficult, due to the interaction with the precipitates (*dislocations pile-up*). Furthermore, the interaction mechanisms between dislocations and dislocation debris enhance work hardening process based on the accumulation of forest dislocations. The hardening effects is explained as a competition effect between precipitate shearing, which induces a material softening, and the increase of slip bands density, that contributes to the work-hardening of the alloy.

The cyclic stress response curves, reported in Figure II. 22(a), display at room temperature a short period of cyclic hardening at the beginning of the test, especially at higher strain amplitudes ($\Delta\varepsilon_t \geq 0.8\%$). On the other hand, the comparison between the cyclic behaviour of specimens, tested at different temperature, is reported in Figure II. 22(b). The stress evolution is clearly different from the room temperature conditions, exhibiting a strong softening from the first cycle.

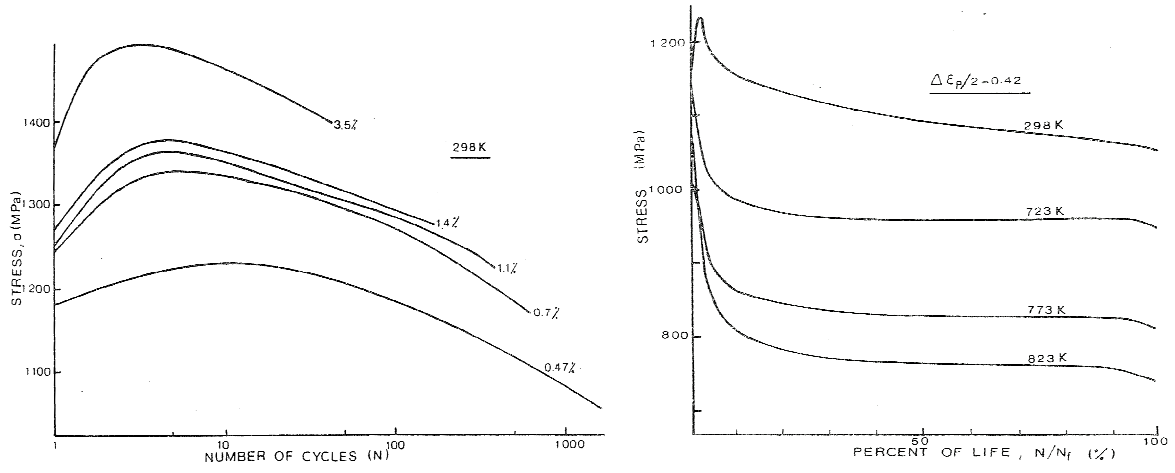

Figure II. 22 : Evolution of the cyclic tensile stress with the number of cycles at room temperature for different plastic strain (a) and high temperature for a plastic strain amplitude of 0.42% (b) [Fournier et al.,1977].

Under cyclic loading, the cyclic strain proceeds through the formation of intense slip bands which progressively shear the γ" precipitates at room temperature and also at elevated temperatures. This process of particles shearing is repeated several times. The size of γ" phases is continuously reduced, limiting their interaction with dislocations (Figure II. 23(a)). For this reason, the stress required to shear the smaller particles is reduced as the number of

cycles increases. The deformation bands are depleted with precipitates, establishing a preferential path for dislocations (Figure II. 23(b)) **[Xiao et al.,2005]**.

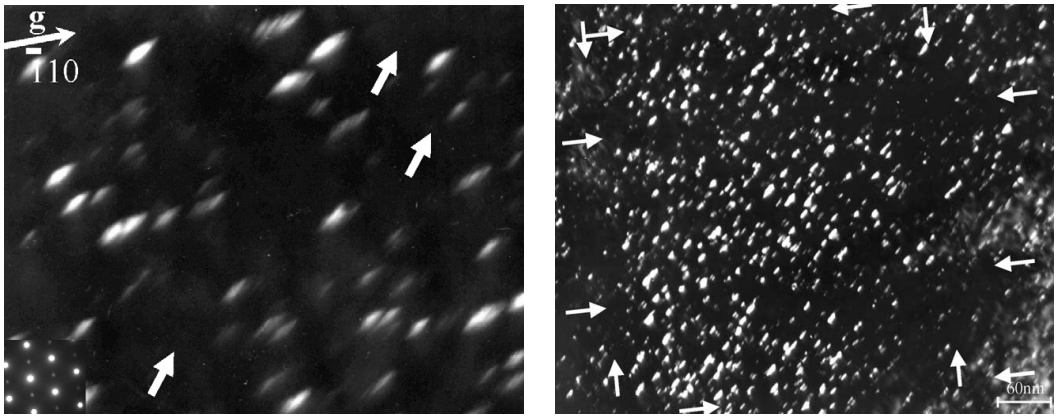

(a) **(b)**

Figure II. 23 : Dark field micrographs showing sheared precipitates (a) and precipitates-free bands (b) in a Inconel 718 specimen deformed at 650°C[Xiao et al.,2005].

The most common mode to analyse the LCF test results is to plot the plastic strain range at half life $\Delta\varepsilon_{pl}$ against the fatigue life (N). This type of relation is known as the Manson–Coffin relation written **[Coffin,1968]** :

$$\frac{\Delta\varepsilon_p}{2} = \varepsilon'_f (2N)^C \qquad \textbf{Eq.II. 1}$$

Where:

$\Delta\varepsilon_p$ /2 is the plastic strain amplitude;

- ε_f' is a constant known as the *fatigue ductility coefficient*
- N is the number of cycles to failure;
- c is an empirical constant known as the *fatigue ductility exponent*, commonly ranging from -0.5 to -0.7 for metals.

At high temperature, the fatigue life is extremely complex because of the occurrence of intergranular oxidation effects. Figure II. 24 compares the Manson-Coffin relation evaluated at different temperatures, showing a strong reduction of the fatigue performance in the range 500-650°C.

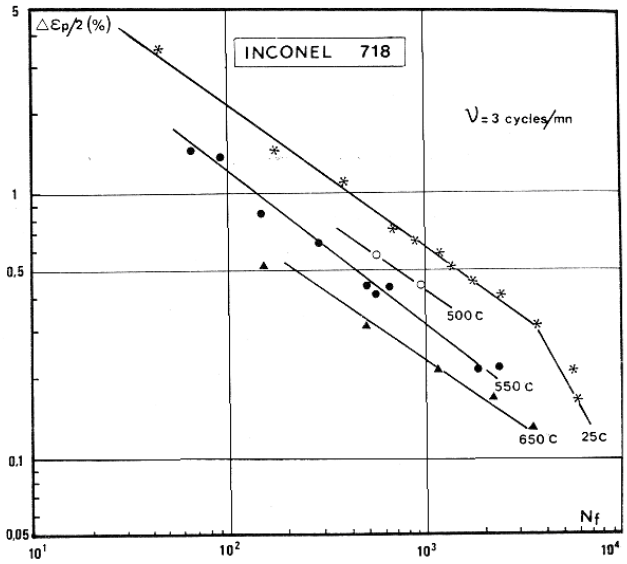

Figure II. 24 : Manson –Coffin relation for Inconel 718 at different temperatures. [Clavel,1980]

At room temperature, the heterogeneous deformation, just discussed above, is revealed by a bilinear Manson coffin relations **[Bhattacharyya et al.,1997]**; where the fatigue ductility exponent is higher for elevated strain than for low strain (Figure II. 25). These effects were noticed not only at room temperature but also in the range 125-425°C **[Sanders et al.,1981]**. This dual slope is an effect of strain localization. The amplitude of the plastic strain directly depends on the heterogeneity of the deformation. When very high strain amplitude is applied to the material, deformation homogeneously evolves through the microstructure, whereas it tends to be more localized for lower strain magnitudes **[Fournier et al.,1977]**. In the first regime (high strain amplitude) Inconel 718 exhibits evidence of twinning, which influences the hardening effects limited to the early cycles. However, at higher strain amplitude, twinning is replaced by the propagation of planar slip bands whose density increases with the applied plastic strain amplitude. The heterogeneous nature of the deformation, in contrast with the results reported for Waspalloy, is maintained up to 650°.**[Clavel,1980]**

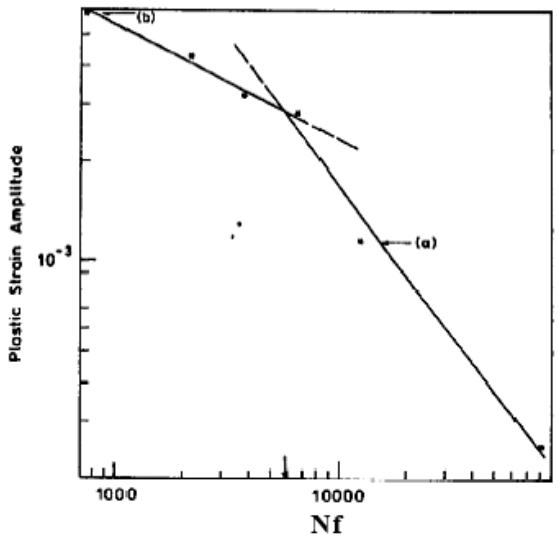

Figure II. 25 : Dual slope Manson-Coffin relationship for Inconel 718 at room temperature. [Bhattacharyya et al.,1997]

XI Fatigue damage

The fatigue damage is one of the primary degradation mechanism that limits the service life of Inconel 718 components. In general, the application of a cyclic loading generates the initiation of cracks resulting from the interaction between the material microstructure and the service conditions loading.

The fatigue process occurs over a period of time, but the consequent failure can be very sudden, even if the involved mechanism has been operating since the preliminary phases of the component service. This damaging process tends to be localised in specific zones rather than through the entire structure of the material. These areas exhibit higher stresses and strains concentrations due to external load transfer, changes in geometry, temperature gradients and material defects. The ultimate cause of fatigue failures is associated to the rapid crack propagation once, for the specific stress considered, the critical crack size is reached (that is the material toughness is reached.

Generally speaking, the fatigue resistance is affected by the progression of different stages of damage, which can be resumed in the following ones **[Ellyin,1997]**:

- Sub-structural and microstructural deformation mechanisms causing the nucleation of microscopic cracks (Crack ***Initiation***).
- Stable propagation of the dominant crack (***Crack Propagation***), generally modelled by the Paris law;
- Structural instability as critical crack size is reached and/or complete fracture.

It is important to point out that the fatigue life, under LCF conditions, is divided into two defined sequences: the crack initiation and the crack propagation. The material, as a function of its tailored microstructure obtained by a careful choice of the composition and thermal treatment, may favour a good crack *nucleation resistance* or a good microcrack /macrocrack *growth resistance*, but not necessarily both.

The characteristics of each stage of the fatigue process differently develops as a function of the applied load (tension-compression, holding time, strain rate) and the “service” conditions (temperature, environment…). The following sections will focus on the causes and mechanisms related to the activation and development of the fatigue damage of Inconel 718.

XI.1 Crack initiation

This specific stage of the fatigue process was defined by Jacquelin **[Jacquelin,1983]** as the number of cycles needed to propagate the prevalent crack up to a dimension similar to the grain size.

In the LCF range, it is well known that the crack initiation mechanisms are often associated with slip band emergence at the free surface of the component **[Villechaise et al.,2002]**. This process is based on an irreversible dislocations movement under cyclic loading. Dislocations agglomerate into bundles within the matrix, leading to a localised

deformation along persistent slip bands (PSB). The density of these bands increases with the cyclic loading and may fill the entire volume of the microstructure, generating a significant inelastic strain.

The space between the PSB and the matrix is characterized by a high strain gradient due to the difference of compliance of the two parts. This process results in high shear stresses related to the intrusion and the extrusion of the edges of these slip bands. In the case of polycrystals superalloys, cracks initiate at the stress concentration zones produced by the net extrusion effects, leading to a *transcrystaline* crack initiation.

This mechanism of crack initiation, as reported in Figure II. 26(a), is characterized by a crack initiation along the plane of maximum shear stress (Stage I): this growth is quite limited, usually on the order of some grains, then it becomes predominantly controlled by the maximum tensile stress range (Stage II). **[Stephens et al.,2001]**

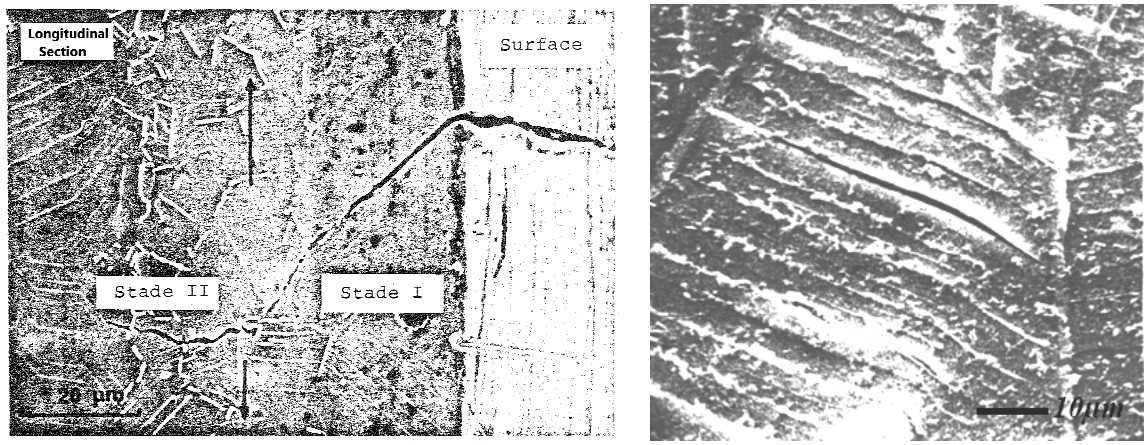

(a) **(b)**

Figure II. 26 : Stage I and Stage II of the crack propagation in Inconel 718 as a function of the tensile stress direction (black arrows) (a) [Jacquelin,1983], crack initiation along slip bands (b) [Fournier et al.,1977].

The number of cycles required to initiate a crack may be estimated by several methods: the equation derived by Tanaka and Mura **[Tanaka et al.,1981]**, particularly suitable for crack initiation in Stage I on grains, establishes the dependence between the microstructure of the material and the strain amplitude **[Alexandre,2004]**.

$$N_i = \frac{1}{d}\frac{A_{stadeI}}{(\Delta\varepsilon_p)^2} \qquad \textbf{Eq.II. 2}$$

Where A_{stadeI} is a constant, d is the grain size and $\Delta\varepsilon_p$ the amplitude of the plastic strain.

It is clear that the time scale of the Stage I is particularly affected by the grain size and the amplitude of the plastic strain.

In addition to these considerations, previous works discussed the role of carbides on the crack initiation. Spath **[Spath et al.,2001]** observed the presence of some failures originated from carbides near the surface or within the specimen. The effect is common when the carbides become as large as the grain size. In some cases a competition for crack initiation

processing can occur between carbides and grain boundaries. This phenomenon may be observed in the alloy treated by Direct Age, where the high resistance could favour a crack initiation on particles.

Other authors have studied the role of carbides in the determination of LCF life of notched Inconel 718 specimens. At lower temperature (20° C and 290° C) the initiation on carbides is relevant leading to multiple micro-cracks in the vicinity of the notch because of the brittleness of the particles **[Bhowal et al.,2005]**.

This mechanism of fatigue initiation, on second phase particles, is particularly significant at high temperature, because of the oxidation effects on NbC and TiC. During thermal exposure, the onset of NbC oxidation occurs at the outer surface and propagates within the carbides. In the case of TiC, oxidation rarely extends into the carbide. However, oxidation rate still increases with increasing oxidation time and temperature. Considering the Gibbs free energy associated to the oxidation reactions, NbC exhibits a lower value which explain its strong facility, compared to TiC, to transform into the oxide **[Hong et al.,2005]**. Pure NbC, in the range between 490°C and 600°C, is extremely prone to form Nb_2O_5, that is polymorphic and potentially observed in various crystalline (orthorhombic and monoclinic) and amorphous forms. These mechanisms are characterised by a volume expansion in the range 1.96-2.38 **[Connolley et al.,2000]**, appreciated by the Pilling Bedworth ratio. The mismatching stresses due to the volume change are sufficiently high to cause plastic deformation of the surrounding matrix, forming a plastic zone ranging from 1.6 to 3.4 times the particle radius. These mechanisms create local strains high enough to initiate cracks. In such a way, the crack surfaces provide a path to further diffuse O_2 towards sub-surface particles. These primary carbides evolve forming bulge-like defects on the material surface (Figure II. 27), limiting the fatigue performances of the alloy.

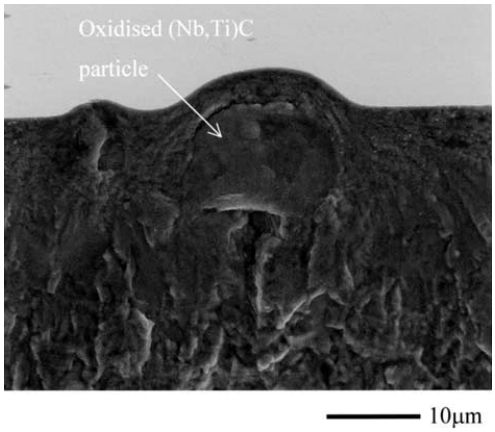

Figure II. 27 : Bulge-like defect causing crack initiation in alloy 718 [Connolley et al.,2003].

In other cases, when primary carbides intersect the surface, the volume expansion results in an eruption of the particles on the faces of the specimen (Figure II. 28(a)), as a result of a lamellar oxidation. The oxide/carbide interfaces, temporarily created, act as preferential oxygen diffusion paths, enhancing the oxide layers, hence initiating a fatigue crack. The eruption phenomena depend on the temperature and exposure time as reported in Figure II. 28(b).

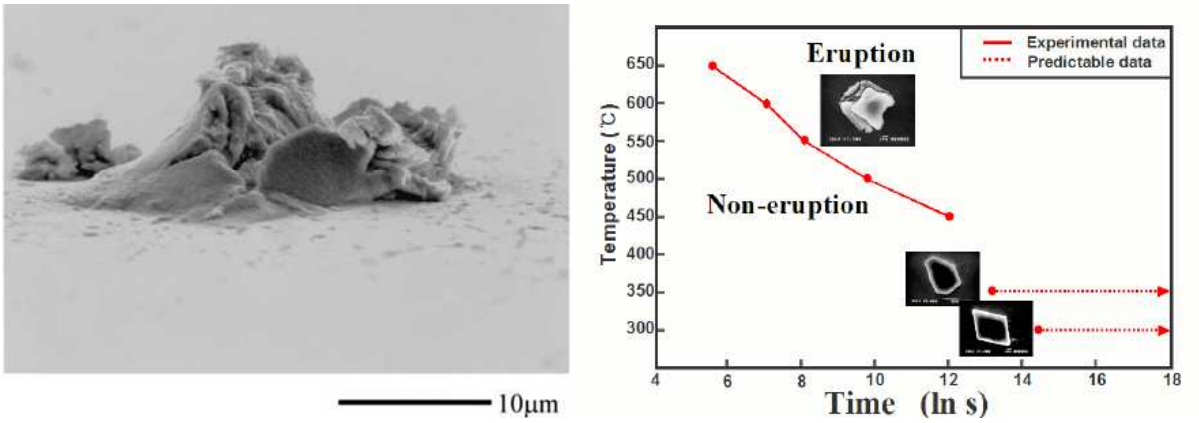

(a) (b)

Figure II. 28 Eruption of oxidised (Nb,Ti)C (a) [Connolley et al.,2003], dependence of thermal exposure and temperature on carbides eruption phenomena[Hong et al.,2005].

These results confirm the evidence that a volume expansion of oxidising primary carbides constitutes a mechanism of environmentally assisted crack initiation, that affects the fatigue life of Inconel 718.

XI.2 Crack propagation

Once a crack initiates, it may grow as a result of extended cyclic loading. As discussed early, the propagation path shows a transition from a growth mechanism along the active slip direction (Stage I) to a deviation on a non-crystallographic plane (Stage II) which occurs over few grains. The stage II is often considered as corresponding to a continuum mechanism which influences the fatigue performances of the alloy. The study and the understanding of the mechanisms of Fatigue Crack propagation (FCP) are critical steps in the optimisation of the material. A large number of research programs have been carried out over the last fifty years, in order to investigate the influence of various parameters on the crack growth.

The grain size plays an important role not only for crack initiation, but also for damage propagation: Pedron **[Pedron et al.,1982]** compared the FCG behaviour of three different microstructures, using a trapezoidal signal with a hold period of 300 seconds at 650°C (Figure II. 29). More precisely, the author compared a fine grained microstructure (ASTM 6-8) with a coarse grained microstructure (ASTM 3-4) and a necklace microstructure (ASTM 3-4 and 8-10). Results showed that the necklace structure gives the best properties while the worst situation is encountered with the fine grain structure. This last structure is considered as the most sensitive to the environmental effects: grain boundaries, as it will be discussed in the next section, are considered as oxidation paths prone to accelerate the intergranular rupture of the alloy. These considerations were confirmed by a series of tests performed under vacuum where all materials exhibited similar behaviour.

The observations on the necklace resistance to crack propagation are in perfect agreement with the studies reported by Lynch **[Lynch et al.,1994]**, who compared the behaviour of a direct age Inconel alloy to a standard treatment. Figure II. 30(a) shows that the direct age structure exhibits a higher resistance to the crack propagation, when tested under creep-fatigue conditions. The limited effects of frequency on this specific material derive from its

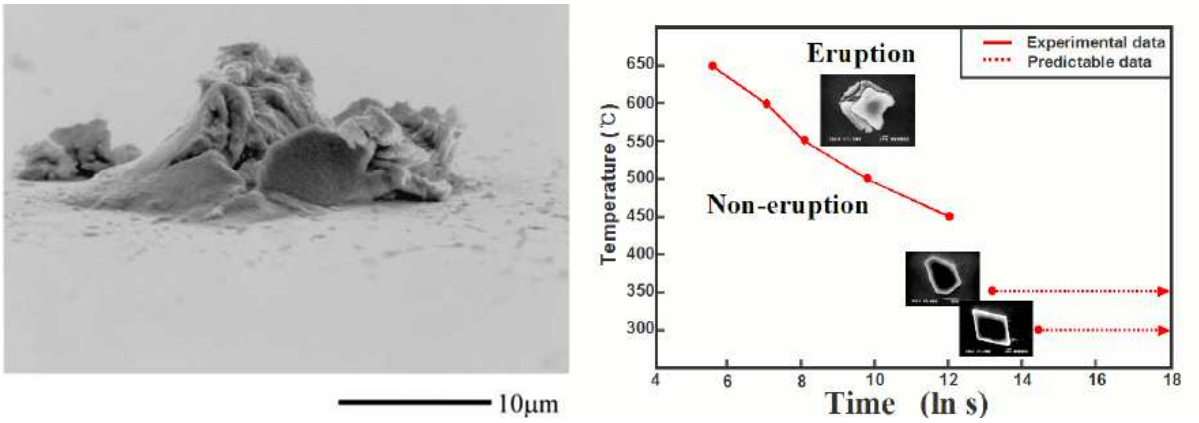

(a) (b)

Figure II. 28 Eruption of oxidised (Nb,Ti)C (a) [Connolley et al.,2003], dependence of thermal exposure and temperature on carbides eruption phenomena[Hong et al.,2005].

These results confirm the evidence that a volume expansion of oxidising primary carbides constitutes a mechanism of environmentally assisted crack initiation, that affects the fatigue life of Inconel 718.

XI.2 Crack propagation

Once a crack initiates, it may grow as a result of extended cyclic loading. As discussed early, the propagation path shows a transition from a growth mechanism along the active slip direction (Stage I) to a deviation on a non-crystallographic plane (Stage II) which occurs over few grains. The stage II is often considered as corresponding to a continuum mechanism which influences the fatigue performances of the alloy. The study and the understanding of the mechanisms of Fatigue Crack propagation (FCP) are critical steps in the optimisation of the material. A large number of research programs have been carried out over the last fifty years, in order to investigate the influence of various parameters on the crack growth.

The grain size plays an important role not only for crack initiation, but also for damage propagation: Pedron **[Pedron et al.,1982]** compared the FCG behaviour of three different microstructures, using a trapezoidal signal with a hold period of 300 seconds at 650°C (Figure II. 29). More precisely, the author compared a fine grained microstructure (ASTM 6-8) with a coarse grained microstructure (ASTM 3-4) and a necklace microstructure (ASTM 3-4 and 8-10). Results showed that the necklace structure gives the best properties while the worst situation is encountered with the fine grain structure. This last structure is considered as the most sensitive to the environmental effects: grain boundaries, as it will be discussed in the next section, are considered as oxidation paths prone to accelerate the intergranular rupture of the alloy. These considerations were confirmed by a series of tests performed under vacuum where all materials exhibited similar behaviour.

The observations on the necklace resistance to crack propagation are in perfect agreement with the studies reported by Lynch **[Lynch et al.,1994]**, who compared the behaviour of a direct age Inconel alloy to a standard treatment. Figure II. 30(a) shows that the direct age structure exhibits a higher resistance to the crack propagation, when tested under creep-fatigue conditions. The limited effects of frequency on this specific material derive from its

high resistance to the crack propagation under creep-fatigue conditions.

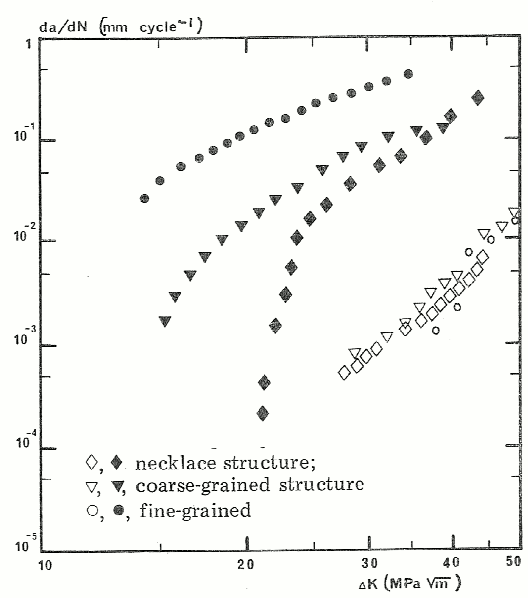

Figure II. 29 : Effect of microstructure and environment on the FCP at 650°C: open symbols vacuum, full symbols air [Pedron et al.,1982].

The negative effects of the microstructure on the propagation process, particularly noticed for the standard grade, could be limited by a careful control of the grain boundaries morphology. For this purpose, an innovative thermal treatment (DT 718) was developed by Guedou **[Guedou et al.,1994]** in order to improve the crack-propagation resistance at high temperature 700-750°C. This procedure, based on an over-aging treatment at 750°C for 50 hours, subsequent to a standard treatment, leads to a microstructural alteration. The grain morphology is more serrated as a result of the heterogeneous distribution of the delta phase at the grain boundaries. Figure II. 30(b) reports the result obtained by the application of a fatigue-creep loading with a dwell time of 90 seconds. It is clear that the benefit of using DT 718 increases with temperature. The superior crack propagation resistance of the modified heat treated materials is due to the presence of serrated grain boundaries which suppress grains sliding as confirmed in earlier studies **[Koul et al.,1988]**. In addition, a double precipitation/coarsening of γ' and γ" phases leads to a more homogeneous slip deformation which limits the oxygen penetration along the affected grains. Consequently, the oxidation effects at the crack tip, which contribute to high cracking rates, are prevented.

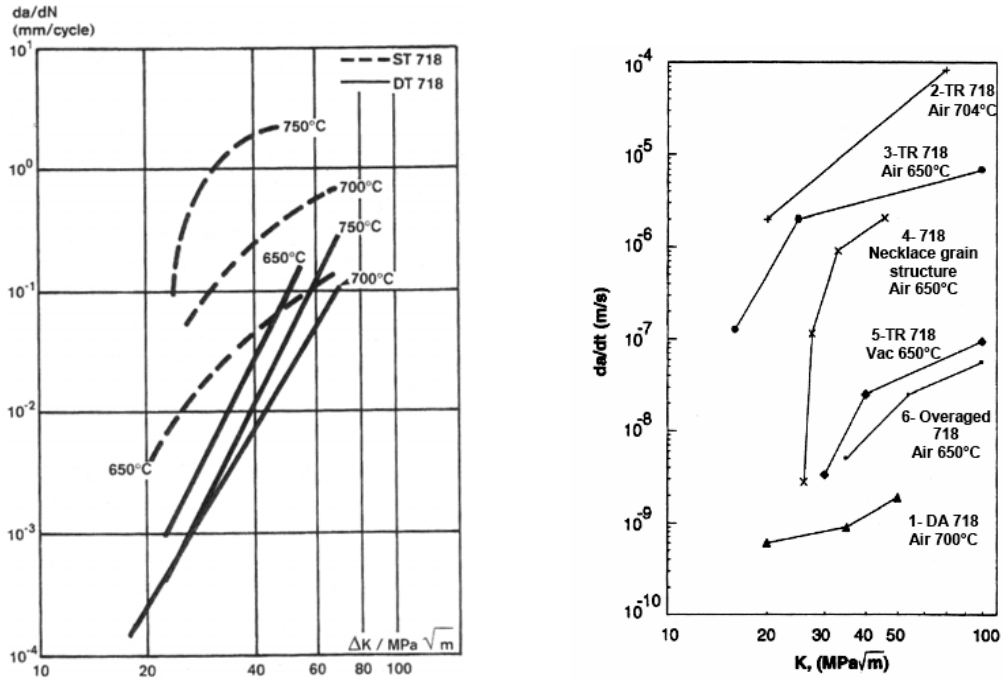

(a) **(b)**

Figure II. 30 Crack propagation rate evolution as function of different microstructures (a) [Lynch et al.,1994] and alternative thermal treatments (b) [Guedou et al.,1994].

The previous considerations have pointed out the role of the microstructure on the initiation and propagation of cracks. It is obvious that the microstructure has also an important impact on the fatigue performances of the alloy. Figure II. 31 illustrates the effects of the grain size at 350°C **[Spath et al.,2001]**.

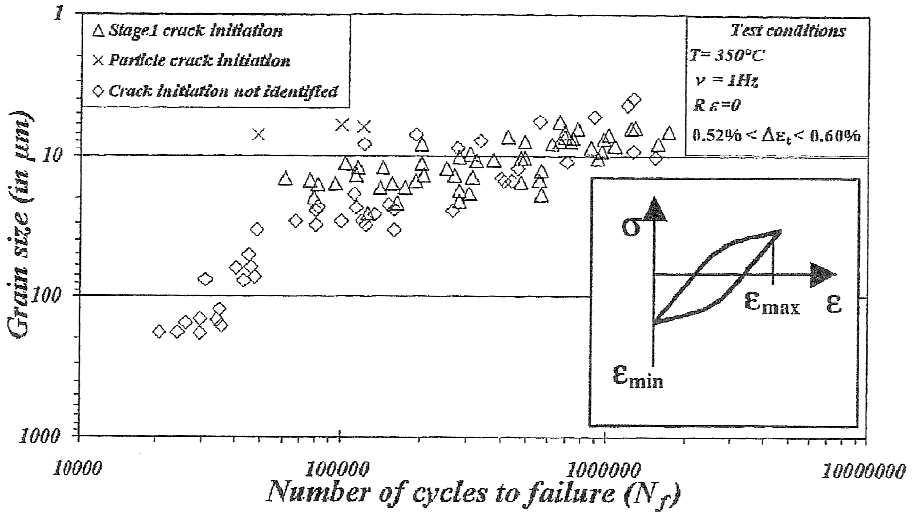

Figure II. 31 : Variation of the fatigue life with microstructure. LCF test realised at 350°C at low frequency (1 Hz) [Spath et al.,2001].

These results highlight that a fine grain structure, in the range ASTM 10-12, leads to a substantial fatigue life increase if compared to a coarse grain structure. When the initiation sites are localized on grains, the material exhibits a higher fatigue life, in contrast to a particle initiation which degrades the mechanical properties of Inconel 718. It can be concluded that if high fatigue resistance is required for a specific application, then fine grains must be

preferred.

XI.3 Environmental effects

The environmental effects on the fatigue behaviour of Inconel 718 occur in several ways, causing an embrittlement of the material. The previous results, reported for description of the crack growth behaviour, have shown a particular influence of the environment on the propagation rate. The detrimental effects of the air environment are largely documented in the literature. The observations of the fatigue surfaces of specimens, reported by Pedron **[Pedron et al.,1982]**, have shown that oxygen, at 650°C, is responsible for the occurrence of brittle intergranular fractures. Tests carried out under vacuum exhibit a fracture surface fully transgranular with the presence of local deformations at grain boundaries.

The intergranular nature of the crack path, associated to a high growth rate, depends on a oxidation mechanism which reduces the ductility of the grain boundaries. These effects are considered as a strong interaction between the mechanical behaviour and the environment, supported by the occurrence of an oxidation phenomenon. This is considered as a diffusional process, mainly influenced by time and temperature. The oxygen activity could be identified in terms of short or long range interaction **[Andrieu et al.,1992]**. The first mechanism is responsible for the growth of an oxide layer at the crack tip, whereas for the second mechanism, the oxygen penetrates along slip planes and grain boundaries. These processes lead to an inhibition of sliding and a migration of the grain boundaries reducing their ability to release the local stresses deriving from the deformation evolution. Molins **[Molins,1995]** showed that the oxidation process in Inconel 718 is based on two different stages. Oxidation tests, performed in-situ at 650°C, have shown that some preliminary homogeneously distributed nuclei of (Ni,Fe)O form, at the early stages of the process on the grain surfaces. On the inner subsurface, chromium oxide (*Chromia* Cr_2O_3) homogeneously forms. The coalescence of the oxide nuclei leads to the formation of a continuous layer with parabolic kinetics. The porous morphology of FeO and NiO oxides stands for a selective path for oxygen diffusion, promoting chromia formation.

Previous works **[Andrieu et al.,1992; Molins et al.,1997; Bache et al.,1999]** investigated the effect of the oxygen partial pressure PO_2^T on the preferential formation of oxides. A transition pressure, independent from the mechanical loading, was detected in Inconel 718 alloy as a function of the alloy chromium content. At the lowest pressures (lower than 10^{-2} Pa) chromia oxide initially forms, inhibiting the development of a continuous layer of nickel oxide on the outer surface. However, when the oxygen partial pressure is higher than 1 Pa, a nickel rich oxide forms. As discussed before, the oxidation process is influenced by time. At atmospheric pressure, the time (t_p) required to activate a passivation process (formation of a continuous layer of Cr_2O_3) is estimated to be in the range 5-8 min (Figure II. 32) **[Andrieu et al.,1992]**. When these conditions are satisfied, no further oxygen penetration can take place along the affected grain boundary paths. Figure II. 32 reports the suggested mechanisms for grain boundary oxidation as a function of time.

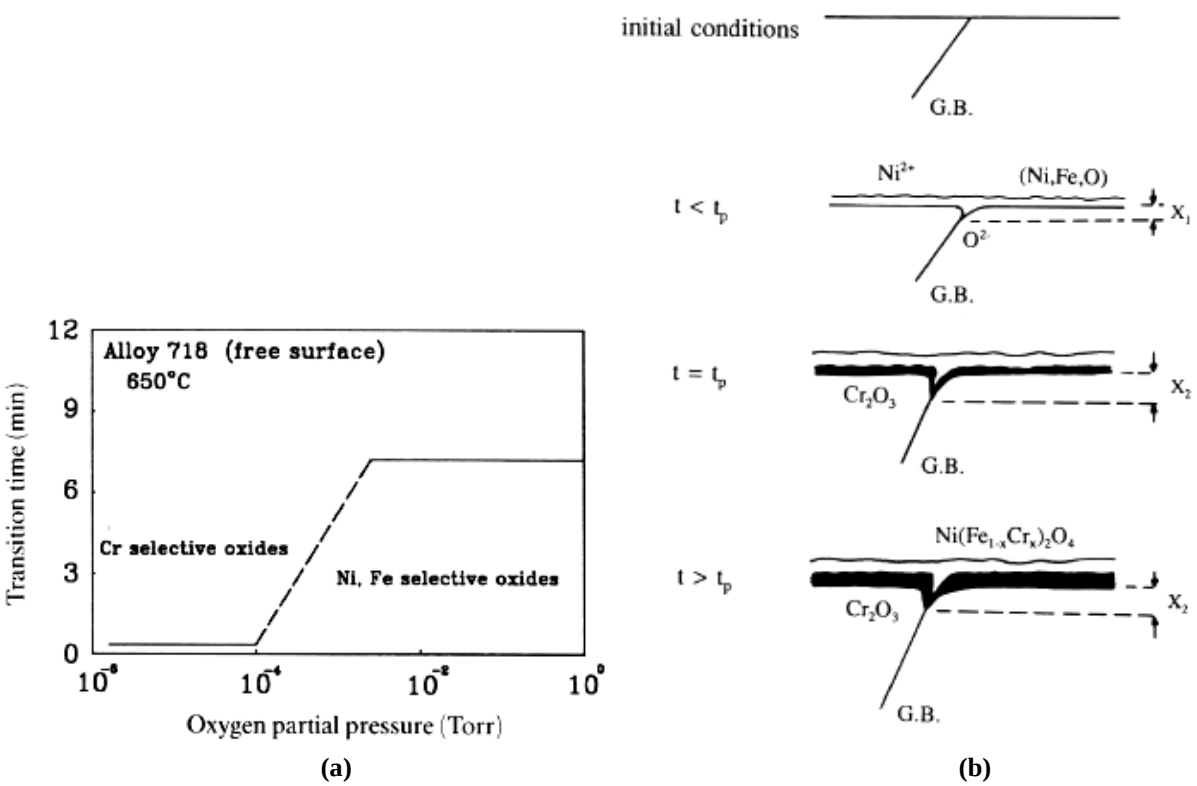

(a) **(b)**

Figure II. 32 : Types of oxides as function of partial pressure and time (a), oxidation mechanisms at grain boundaries (b) [Andrieu et al.,1992].

The transition found in the oxidation process affects the crack growth rate of the alloy. The formation of the "wedge-shaped" oxide layers along the crack front, followed by their subsequent rupture at the boundary intersections, can increase the crack growth rate. Figure II. 33 illustrates the impact of oxygen partial pressure on the FCP. At pressures lower than PO_2^T the crack growth rate is independent of the pressure, whereas, beyond this critical value, the crack propagation rate increases with the pressure. The material embrittlement could be explained considering the oxidation kinetics. When the cracks propagate faster than the time required to form chromia, NiO nuclei appear on the fresh crack surfaces. During the growth mechanism of the nickel oxide, the outer diffusion of Nickel cations Ni^{2+} is associated to a inner flux of vacancies which can not be annihilated at the oxide/metal interface, because of the coherency relationship between the oxide and the metal. The diffusion process promotes, then, the formation of vacancies at the crack tip. The embrittlement of the alloy results from the condensation of vacancies at the grain boundaries which reduces the crack propagation resistance. The stress relaxation at the crack tip is associated to a plastic strain. It can be noticed that the environmental effects are active until this deformation is positive, due to the interaction between dislocations and oxidation processes. **[Ponnelle,2001]**

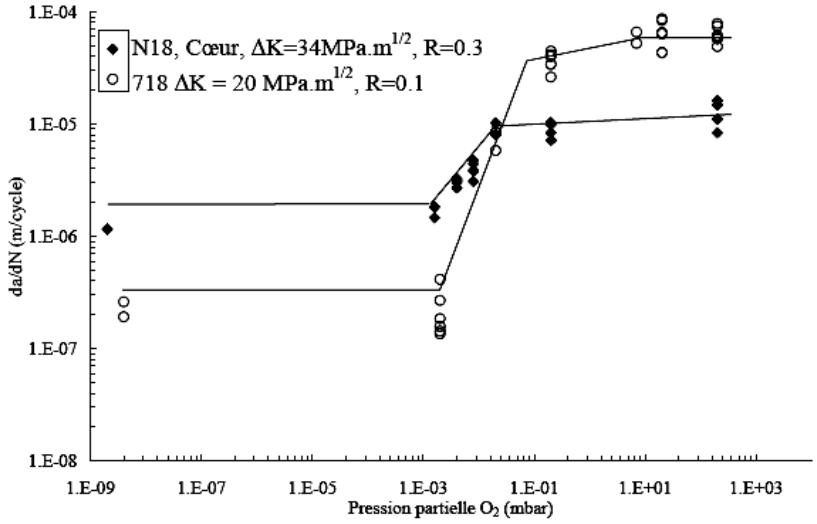

Figure II. 33 : Fatigue crack growth as a function of the oxygen partial pressure. [Molins et al.,1997]

It is clear that the material sensitivity to the environmental effects is strongly dependent on its utility to release the stress at the crack tip. For this reason the application of modified thermal treatments, is discussed in the section dedicated to the crack propagation, is considered as a promising solution. The aim is to modify the microstructure in order to optimise the creep properties of the alloy and ensure a fast relaxation of stresses. The application of an over-ageing is a good compromise to guarantee a high crack propagation strength without affecting the static and dynamic mechanical properties (yield strength and creep resistance).**[Molins,1995]**

XI.4 Effect of the loading cycle on the fatigue properties of Inconel 718

In industry, materials are usually loaded in complex fatigue conditions including variable holding time under stress/strain, cycle frequency, stress/strain ratio, resulting in a wide range of loading wave shapes. In many applications the mechanical components is subject to fluctuating and steady loadings, deriving from specific in-service conditions.

It is found that at high temperature, the material resistance degrades when a hold period is included in the load cycle. The amplitude of these effects depends on the duration of the steady state, the thermo-mechanical history (softening, hardening…) and the location of the holding period within the cycle (Tension and/or compression period).

The loading waveform has an important effect on the fatigue crack propagation. When a holding time is applied, especially at maximal load, a time dependent behaviour may be introduced. The material tends to be damaged trough O_2 diffusion which decreases its resistance to cracking. The variations in the time spent at peak stress affect the fracture profiles and the crack growth rates. Ponnelle **[Ponnelle,2001]** showed that the application of steady period of 300 seconds at maximal loading increases the crack growth rate by a factor 7.5 at 550°C, 50 at 600°C and 100 between 650°C and 675°C (Figure II. 34).

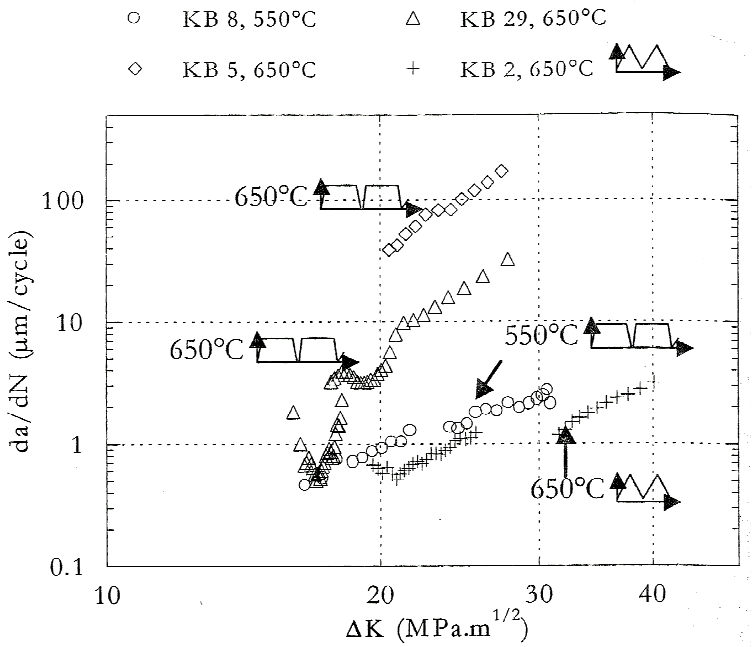

Figure II. 34 : Effect of the application of a holding time of 300 s on the crack propagation rate of Inconel 718 at high temperature. [Ponnelle,2001]

During the holding time an interaction between fatigue and creep effects can be assumed. The introduction of holding period in strain controlled fatigue tests generates a conversion of the elastic strain to plastic strain, due to the stress relaxation effects (Figure II. 35) . The level of the relaxed stress is proportional to the length of the holding period. The inelastic strain range associated to each fatigue cycle is based on two components:

$$\varepsilon_{in} = \varepsilon_p + \varepsilon_{cp} \qquad \textbf{Eq.II. 3}$$

Where:

- $\Delta\varepsilon_p$ is determined by the hysteresis loop without the hold time
- $\Delta\varepsilon_{cp}$ is related to the stress relaxation during holding time by the following equation:

$$\varepsilon_{cp} = \Delta\sigma_r / E \qquad \textbf{Eq.II. 4}$$

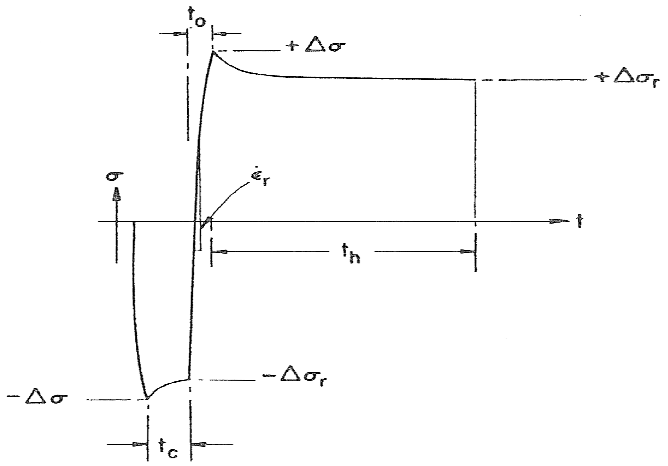

Figure II. 35: Stress relaxation during the application of a holding time. [Min et al.,1978]

The effects of the holding time on the fatigue performances depends on the test conditions. At temperatures below that defining the creep regime of the material, the holding time application has no effects on specimen life. Figure II. 36 illustrates the effect of different dwell times at 649°C under a continuous fatigue behaviour. **[Korth,1991]**

Since the amplitude of the hysteresis loop is proportional to the plastic strain range, the relaxation rate is influenced by the conversion of elastic strain to plastic. Considering the importance and the impact of the crack closure process, it is clear that a compressive holding period is less damaging than a tensile one. The crack closure effect decreases with the increase of the inelastic strain, where the crack growth, during tensile relaxation, becomes significant. **[Coffin,1968]**

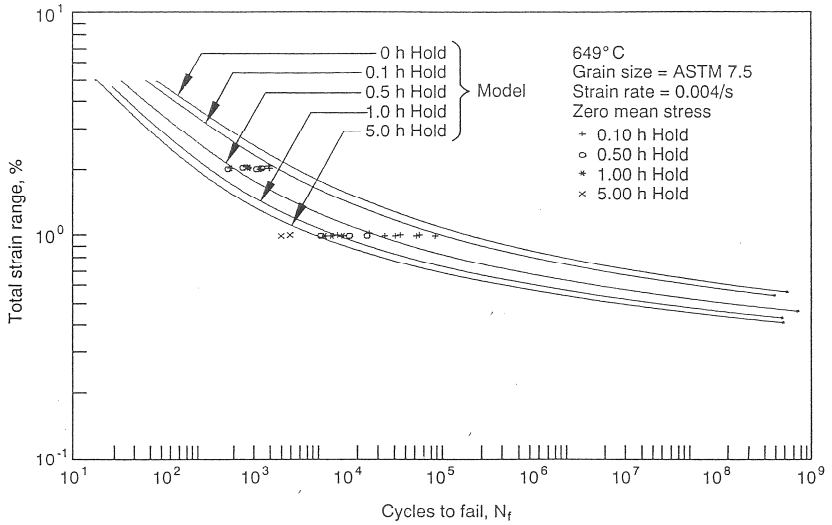

Figure II. 36 : Effect of different holding times on the fatigue behaviour of Inconel 718 at 649°C [Korth,1991].

Frequency is also observed to impact cycle life mainly in the low-cycle regime. The results reported by Clavel and Pineau **[Clavel et al.,1978]** showed that, at 550°C, the fatigue growth rate is almost independent of frequency in the range 0.5 Hz to 20Hz. However, when frequency is decreased below 0.5 Hz, the crack propagation rate is strongly increased as compared to the case of higher frequencies.

Focusing on the deformation structure, the authors pointed out a strong inhomogeneity in the plastic deformation, shown, at low frequency, by the occurrence of twinning. Conversely, at room temperature, the material exhibits a homogeneous plastic zone where the deformation occurs through planar slip even at high crack propagation rates (da/dN > 0.01 μm/cycle). It is clear that temperature plays an important role in the deformation mechanism enhancing the impact of frequency on the mechanical properties.

Figure II. 37 reports the evolution of the stress amplitude versus fatigue for tests performed at 3 cycles/minute and 0.3 cycles/minute. A lower frequency corresponds to a fast softening which leads to a decrease in the fatigue life.

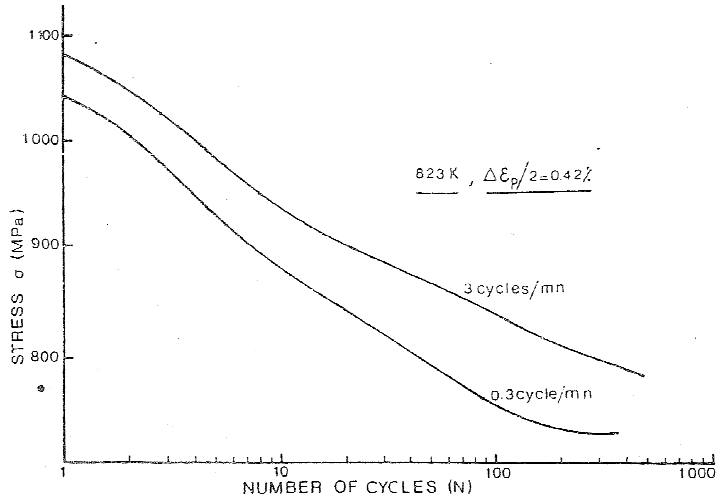

Figure II. 37 : Evolution of the stress amplitude of a LCF test with strain rate at 550°C.[Fournier et al.,1977]

Pedron **[Pedron et al.,1982]** studied the effects of frequency on the fracture profile. The graph, reported in Figure II. 38, shows the existence of two regimes: a first regime ***"cycle dependent"***, at high frequency, where the fracture is fully transgranular and independent of the test frequency, and a second one , so called ***"time dependent"***, at low frequency, where the propagation becomes intergranular and increases with decreasing frequency. These effects are further emphasized by an increase in test temperature.

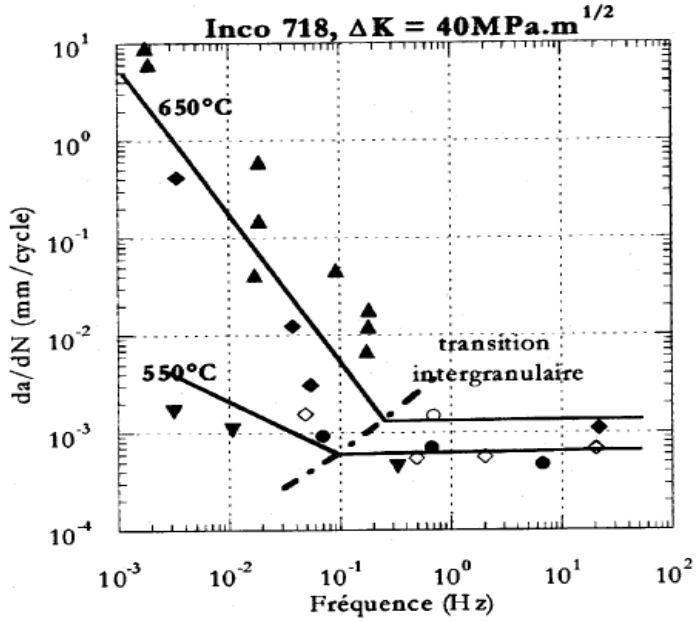

Figure II. 38 : Variation in the Fatigue Crack growth with the test frequency and temperature for Inconel 718. [Pedron et al.,1982]

The influence of the frequency on the fatigue life of Inconel 718 was explained by Andrieu **[Andrieu,1987]** as resulting from a direct interaction between damaging mechanisms and environmental effects . The oxides formation, at high temperature, is strongly influenced by the localisation of the plastic strain. When material is *homogenously* deformed, the presence of multiple slip bands at the crack surfaces enhances the diffusion of Cr, facilitating the instantaneous formation of a chromia layer. In such a way, the mechanical properties of the

grain boundaries are not affected by the oxidation process, reducing the crack propagation rate.**[Molins,1995]**

However, when the deformation mechanism becomes *heterogeneous*, especially at low frequencies, a transient embrittlement occurs through the activation of an intergranular oxidation process (NiO) which accelerates the crack propagation and delays the passivation process **[Molins et al.,1997]**.

All the assumptions have pointed out the dependence of the material behaviour on its specific microstructure. Advanced applications at high temperature are often limited by the tensile, creep, and fatigue mechanical properties of the alloy. These mechanical properties vary with the size, shape and quantity of the strengthening precipitates. It is therefore important to quantify these precipitate parameters and relate them to mechanical properties. For these reasons, a detailed description of the individual effects of the precipitates on the mechanical behaviour of the alloy is reported in the next section.

XII Influence of the intergranular precipitates and solute atoms on the mechanical behaviour

XII.1 Delta phase impact on the mechanical behaviour

Delta phase has an important effect on the microstructure and the mechanical resistance of Inconel 718. In general, precipitates are discontinuously distributed at grain boundary under normal heat treatment conditions. In some cases, Delta phase was observed within grains showing a cluster appearance with several orientation relationships.

As reported in section X, Inconel 718 is subject to a deformation process based on the dislocations movement along primary slip bands (PSB). Previous works have shown that Delta phase usually precipitates along $\{111\}_\gamma$ planes which correspond to the main slip systems. In these circumstances, the heterogeneous bands, whose width is about 0.4-0.6 μm, are extended into needle-like δ particles at grain boundaries, which delays their translation. These mechanisms are not associated to the occurrence of voids or cracks at the intersecting points of δ phases and slip lines **[Yuan et al.,2005]**.

Desvallées **[Desvallées et al.,1994]** investigated the effect of delta phase on the tensile properties of Inconel 718: the author compared a "standard thermal treatment alloy", where δ particles are only present at grain boundaries, to an alternative material with a microstructure characterised by a high amount (10% volume fraction) of intergranular/transgranular δ phase. The results showed a detrimental effect of the presence of delta phase on the yield strength of the alloy, reduced by 10%.

A specific control of the microstructure, of the distribution and morphology of the delta phase is essential to improve the cracking resistance of the alloy. As described before (Paragraph XI.2), the coupled effects of mechanical loading and environmental attack lead to an intergranular crack propagation. In this case delta phase plays a role as obstacle able to block the grain boundary propagation. Guided by these particles, crack follows a zig-zag path (Figure II. 39 (a)). These considerations were improved by the studies reported by Li **[Li et al.,1994]** who analysed several microstructures obtained by a direct ageing treatment. All the tests were carried out at a 650°C under creep-fatigue conditions. Results confirmed that a high amount of delta phase decreases the crack propagation rate of the alloy (Figure II. 39 (b)).

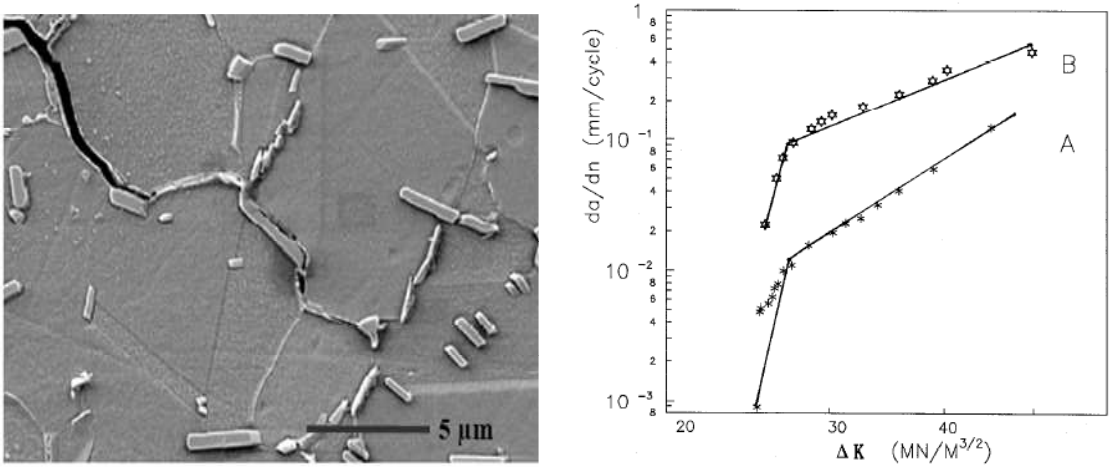

(a) **(b)**

Figure II. 39 : Role of delta precipitates on the crack propagation mechanisms (a) [Ponnelle,2001], crack propagation rates at 650°C as a function of the amount of delta precipitates (Treatment A contains more delta phase than treatment B) (b) [Li et al.,1994].

The improvement of the fatigue resistance, especially at high temperature, is associated to the interaction between the precipitation of these intergranular particles with the other strengthening phases. Delta phase formation is a Nb diffusion control process. Often δ phase is surrounded by a zone depleted in Nb, free of γ" precipitates and particularly ductile. These areas, as illustrated in Figure II. 40, still contain γ' particles, especially when ageing is carried out at temperature below the γ' solvus **[Sundararaman et al.,1994]**. The ductile regions can rapidly release the stress concentration at grain boundaries, delaying crack propagation and limiting the environmental effects.

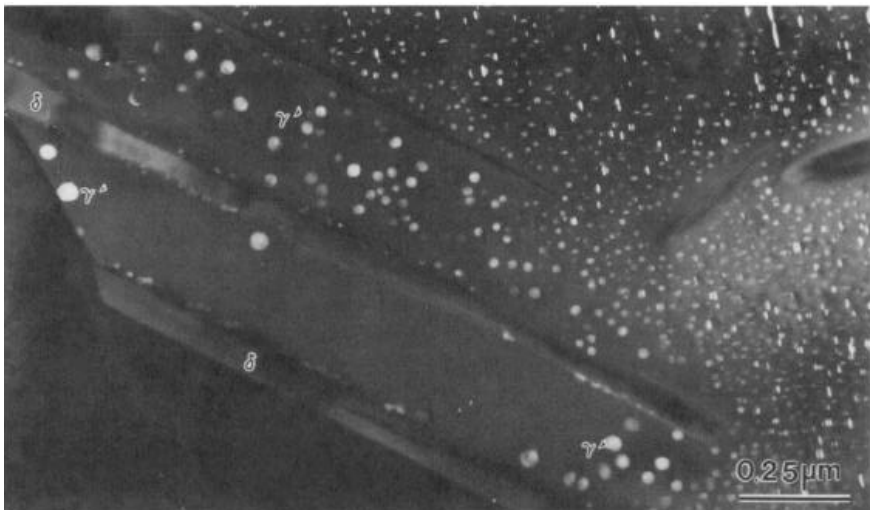

Figure II. 40 : TEM micrograph of the precipitates-free zone around δ precipitates [Burke et al.,2000].

During forging, the material is subjected to several thermo-mechanical operations leading to a microstructural orientation of the delta phase and carbide particles. Ponnelle **[Ponnelle et al.,2001]** analysed the role of these Forming Induced Arrangement (FIA) on the propagation resistance of Inconel 718. The various crack front shapes and propagation rates were explained as a function of the interaction between the crack tips and the delta phases. An increase in the growth rate is associated to crack propagation between the δ phase

alignments. It is important to point out that these alignments act as preferential path for the oxygen diffusion, increasing the embrittling effects of the environment. However, when crack front is normal to the delta arrangements, a *delamination* mechanism is activated. This process decreases the stress triaxiality leading to a reduction of the crack propagation rate.

The delta phase has also an important effect in the definition of the microstructural features, acting as an effective barrier to static recrystallization. The particles tend to precipitate heavily in strained grains at 990°C or below and resist to grain boundary migration even if such particles are a spheroidal. When the temperature is well above 990°C, i.e., 1010 to 1025'C, delta particles dissolution and rapid grain growth occur **[Radavich et al.,1989]**.

When the material is processed by a Direct Age treatment, multiple hot deformation process act on the microstructure of the alloy in order to ensure a dynamic recrystallization (DRX). The plate-like delta phases, whose orientation is not perpendicular to the compression direction, are submitted to a continuous deformation breakage which leads to a *spheroidization* **[Zhang et al.]** of the particles (Figure II. 41). In such a way, dislocations are accumulated around δ phases as strain increases. This mechanism increases the rate of dislocation nucleation, promoting Dynamic Recrystallization. The thermo-mechanical process leads to an ultra fine structure providing high mechanical properties **[Wang et al.,2009]**.

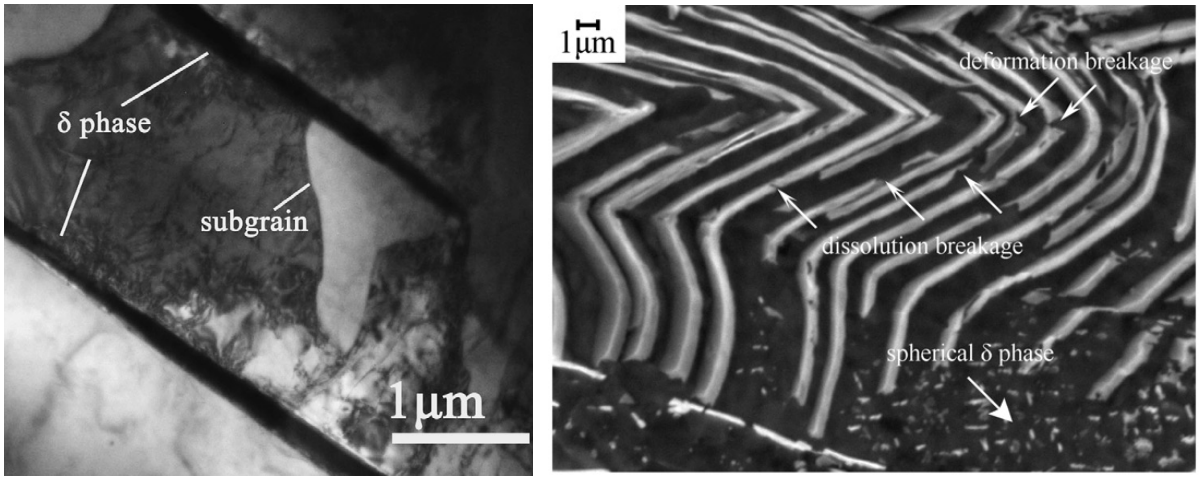

(a) **(b)**

Figure II. 41 : Role of the delta phase in the dynamic recrystallization (a) [Wang et al.,2009], dissolution breakage and creation of globular delta particles (b) [Zhang et al.].

XII.2 The Dynamic Strain Aging (DSA)

Previous sections have shown that the LCF behaviour is often influenced by various test parameters like frequency (strain rate), wave form and holding time under stress.

In addition to the time dependent mechanisms, the Dynamic strain aging is considered as a process, typical of many superalloys, prone to influence the cyclic behaviour of Inconel 718. DSA is a time dependent process based on an interaction between solute atoms and mobile dislocations during plastic deformation. In terms of deformation behaviour, this particular

mechanism is associated to a progressive decrease of the strain rate sensitivity parameter (SRS) which becomes negative in a limited range of temperature and strain rate:

$$SRS = \left(\frac{\delta\sigma}{\delta \log \dot{\varepsilon}_p} \right) T, \varepsilon_p \qquad \textbf{Eq.II. 5}$$

Where σ is the flow stress, T the temperature, ε_p the plastic strain and $\dot{\varepsilon}_p$ the applied strain rate.

Different manifestation of the DSA mechanism can be noticed, such as yield stress plateau, reduced tensile elongation, sharp upper yield points and serrated stress-strain curves generally associated to Portevin-Le Chatelier (PLC) effects.

This phenomenon, generally considered as a plastic instability, is based on an intensive interaction between diffusive processes of solute atoms and mobile dislocations. Three types of plastic heterogeneities are identified (Figure II. 42): continuously propagating Type A, intermittently propagating Type B and random nucleating and propagating Type C. Previous works showed the activation of type C serration, for Inconel 718, in the temperature range 798-923 K. It's interesting to point out that each load drop, in monotonic tensile stress, can be accompanied by acoustically identified emissions during testing **[Hale et al.,2001]**.

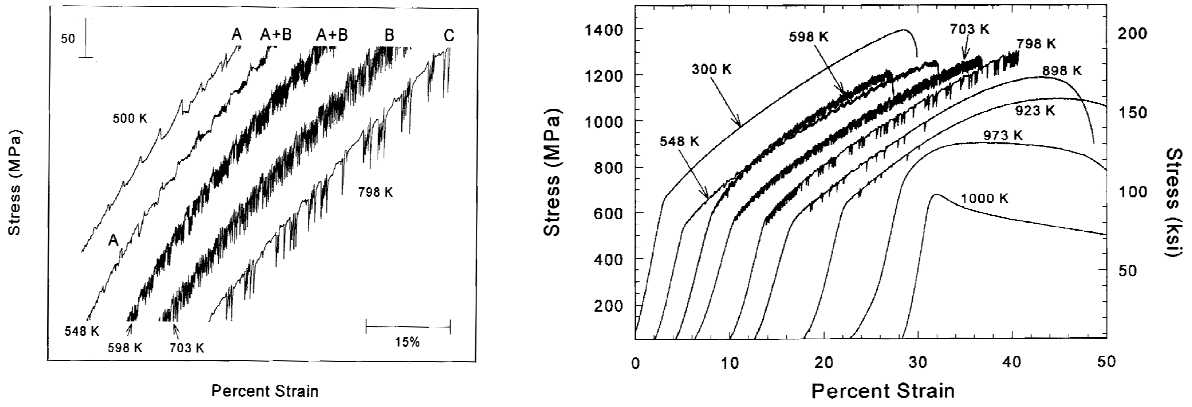

Figure II. 42 : Various types of serrated flow observed in stress-strain curves of Inconel 718 (a), typical tensile tests of Inconel 718 at various temperatures showing plastic instabilities. [Hale et al.,2001]

The aspect of the PLC bands is influenced by the dislocations dynamics and work hardening, and is further complexified by the presence of different diffusion mechanisms **[Klose et al.,2003]**. According to Cottrell theory**[Cottrell,1949]**, strain-aging results from an interaction between moving dislocations and foreign atoms diffusing with a velocity of the same order of magnitude. This classical approach is based on a *long range diffusion* of solute atoms towards dislocations, forming the "Cottrell atmosphere" around each dislocation edge. The interstitial atoms, having a size lower than that of the matrix atoms, can diffuse towards the compressive part of the stress field of dislocations, while the substitutional atoms, with diameter greater than that of the matrix atoms, can diffuse towards the tensile zone of the stress field of dislocations.

The kinetic aspects of the serrated flow can be expressed according to an Arrhenius

relationship. Activation energy calculations, evaluated for Inconel 718 Type C serrations, suggest that plastic instabilities result from lattice diffusion of substitutional solutes, likely Cr, at high temperatures. These fast diffusing atoms block the mobile dislocations until the stress is high enough to release its pinning points between mobile and forest dislocations. With an increase in stress, the forest dislocation density increases. The larger amount of diffusion paths improve the efficiency of DSA resulting in stronger pinning and increased jumps. A critical value of inelastic strain is required to activate the PLC mechanisms. This is a necessary condition to increase the vacancies concentrations, produced by the dislocations glide, enhancing diffusion **[Mulford et al.,1979]**. Jiang **[Jiang et al.,2007]** reported that solute concentration decreases with increasing strain rate. Solute is usually localised around dislocations, but its presence tends to be more diluted when elevated strain rates are considered. However, at lower strain rates the solute concentration reaches its saturated value and dislocations are pinned and immobilized.

The influence of the DSA on the mechanical properties of Inconel 718 is schematically represented in Figure II. 43. In general, the effects can be synthesised in a decrease of the yield stress, an increase in the yielding rate (the parameter n of the Hollomon law $\sigma = \varepsilon^n$) and a decrease of ductility. DSA occurs also in the cyclic deformation in the form of serrations in stress-strain hysteresis loops over a wider range of temperature than in monotonic deformation. The degree of inhomogeneity of strain during cyclic loading is enhanced and strain is localised in regions characterised by alternative high and low amplitudes of dislocation movements. The DSA process inhibits slip motion and limits the plasticity associated to the fatigue loading. The result is a decreased crack propagation rate and an improvement in the fatigue resistance by dynamic hardening. **[Lee et al.,1995]**. LCF tests carried out at 723 and 823 K, for PE-16 superalloys, showed an increase in fatigue life with an increase of the strain rate from $3x10^{-5}$ to $3x10^{-3}$ s^{-1} **[Valsan et al.,1994]**.

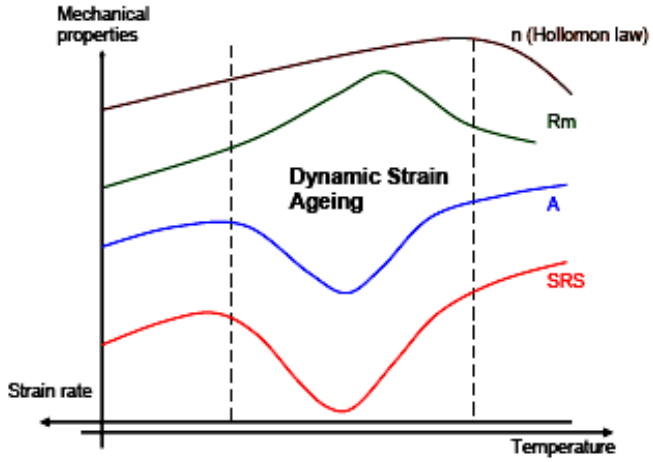

Figure II. 43 : Evolution of the mechanical properties as function of the dynamic strain aging (DSA) [Graff,2006]

An interesting discussion about the interaction between PLC serrations and the fatigue rupture mode was reported by Garat **[Garat et al.,2008]**. In particular, the author showed how the Portevin-Le Chatelier (PLC) effects play an important role in the inhibition of the

intergranular crack propagation. As a matter of fact, the crack initiation sites and the nucleation zones of strain serrations are located in the same regions of the polycrystal. Strain rate becomes a discriminating factor for the activation of the PLC mechanism. As reported in Figure II. 44, at 550°C, two regimes are proposed by the authors. At very low strain rate (lower than $3x10^{-4}$ s^{-1}) the PLC effects are not activated and the fatigue failure is intergranular, while at high strain rate (higher than $3x10^{-4}$ s^{-1}), strain jumps occur and the failure mode is fully transgranular.

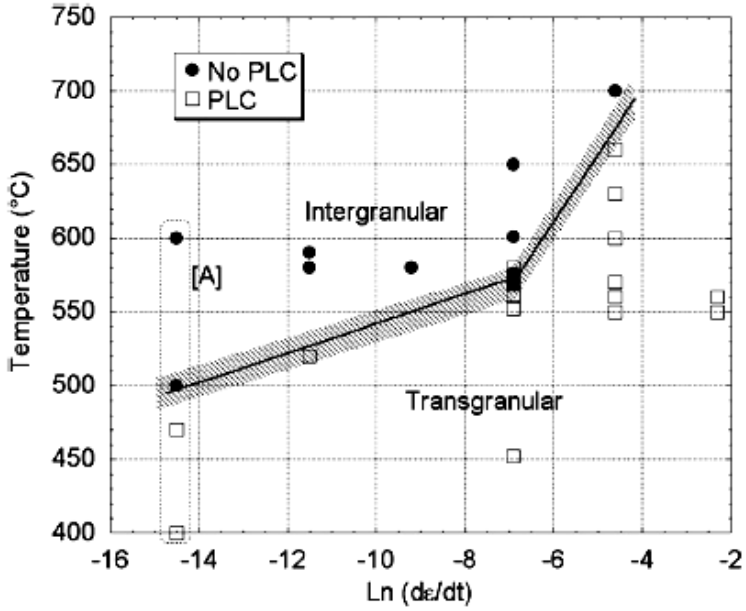

Figure II. 44 : Influence of the PLC effects on the rupture mode of Inconel 718 [Garat et al.,2008].

Probably, the PLC bands participate to a redistribution of the local stresses and they simultaneously reduce the flux of embrittling species. Ter-Ovanessian **[Ter-Ovanessian et al.,2008]** showed that PLC serration tend to trap interstitial solute atoms in the zones where the dislocations are pinned. In such a way, the interaction between oxygen and interstitial atoms is avoided at grain boundaries and intergranular failure is inhibited. This assumption permits to conclude that the DSA have a strong effect on the fatigue behaviour of Inconel 718 especially at high temperature.

XIII Conclusions

The nickel base superalloys are a class of materials developed to fulfil a need for stronger and more corrosion resistant alloys for high temperature applications.

Inconel 718 belongs to this class of high performing materials, ensuring high mechanical properties at temperatures up to 650°C. These properties are based on a precipitation strengthening mechanism which is controlled by the size, the morphology, the content and the distribution of the hardening phases (γ'and γ"). The microstructure is completed by the presence of the δ phase, which limits the grain expansion without taking part in the strengthening mechanisms and other primary carbides such as NbC and TiC.

The nickel based superalloys are particularly sensitive to the effect of the thermal treatment. A double steps process, including a solution annealing followed by a precipitation ageing, is generally used to optimise the material. The volume fraction of the strengthening phases depends on the content of the major alloying elements, such as Al, Ti and Nb, which play an important role in the precipitation behaviour.

The mechanical behaviour is strongly dependent on the in-service temperature which can induce structural changes.

Under cyclic loading (fatigue regime), particular transient cyclic phenomena can occur. Depending on the initial state, material can show either full stability, softening or hardening.

At elevated temperature, Inconel 718 exhibits strong softening from the first cycle: the cyclic deformation proceeds by the formation of intense slip bands which progressively shear the γ" precipitates, establishing a preferential path for dislocations.

The wave form, associated to the loading signal, could influence the fatigue performances of the material, especially when the frequency is decreased or a holding time is included in the cycle activating time-dependent mechanisms.

Under these conditions, the material tends to be damaged by the simultaneous interaction of the deformation mechanisms and the environmental degradation. The diffusion of oxygen at grain boundaries decreases the mechanical resistance affecting the fracture profiles and the crack growth rates. Crack propagation could be divided into two regimes: a first regime **"*cycle dependent*"**, at high frequencies, where the fracture is completely transgranular and independent on the test frequency, and a second one, defined as **"*time dependent*"**, at low frequency, where the propagation becomes intergranular and increases with decreasing frequency. These effects are further emphasized by the increase of the test temperature.

XIV References

[Alexandre,2004] Alexandre, F. "*Aspects Probabilistes et microstructuraux de l'amorçage des fissures de fatigue dans l'alliage Inco 718*". PhD Thesis, Ecole des Mines de Paris (2004).

[Andrieu,1987] Andrieu, E. "*Influence de l'environnement sur la propagation des fissures dans un superalliage base nickel: l'Inconel 718*". PhD Thesis, Ecole Nationale Superieure des Mines de Paris (1987).

[Andrieu et al.,1992] Andrieu, E., Molins, R., Ghonem, H. and Pineau, A. "Intergranular crack tip oxidation mechanism in a nickel-based superalloy." *Materials Science and Engineering: A* 154(1): pp. 21-28, (1992).

[Azadian et al.,2004] Azadian, S., Wei, L.-Y. and Warren, R. "Delta phase precipitation in Inconel 718." *Materials Characterization* 53(1): pp. 7-16, (2004).

[Bache et al.,1999] Bache, M. R., Evans, W. J. and Hardy, M. C. "The effects of environment and loading waveform on fatigue crack growth in Inconel 718." *International Journal of Fatigue* 21(1): pp. 69-77, (1999).

[Bhattacharyya et al.,1997] Bhattacharyya, A., Sastry, G. V. S. and Kutumbarao, V. V. "On the dual slope Coffin-Manson relationship during low cycle fatigue of Ni-base alloy in 718." *Scripta Materialia* 36(4): pp. 411-415, (1997).

[Bhowal et al.,2005] Bhowal, P. R. and Wusatowska-Sarnek, A. M. "Carbides and their influence on notched low cycle fatigue behavior of fine-grained IN718 gas turbine disk material." *Superalloys 718, 625, 706 and Derivatives, Proceedings*: pp. 341-349, (2005).

[Bor et al.,2010] Bor, H., Chao-Nan Wei, Huu Tri Nguyen, An-Chou Yeh and Kuo, C.-M. "*Aging effects on γ'and γ" precipitates of Inconel 718 Superalloy*". 7th International Symposium on Superalloy 718 and Derivatives (2010).

[Burke et al.,2000] Burke, M. G. and Miller, M. K. "The application of AEM and APFIM to the analysis of precipitation behaviour in Alloy 718." *Microbeam Analysis 2000, Proceedings*(165): pp. 161-162, (2000).

[Clavel,1980] Clavel, M. "*Fatigue plastique et fissuration de deux alliages durcis par des précipités cohérents. Etude comparative des mécanismes*". PhD Thesis, Université de Poitiers (1980).

[Clavel et al.,1978] Clavel, M. and Pineau, A. "Frequency and wave-form effects on the fatigue crack growth behaviour of alloy 718 at 298 K and 823 K." *Metallurgical and Materials Transactions A* 9(4): pp. 471-480, (1978).

[Clavel et al.,1982] Clavel, M. and Pineau, A. "Fatigue behaviour of two Nickel base alloys I: Experimental results on Low-Cycle fatigue crack propagation and substructures." *Materials Science and Engineering* 55(2): pp. 157-171, (1982).

[Coffin,1968] Coffin, L. "Introduction to high-temperature low-cycle fatigue." *Experimental Mechanics* 8(5): pp. 218-224, (1968).

[Connolley et al.,2003] Connolley, T., Reed, P. A. S. and Starink, M. J. "Short crack initiation and growth at 600 °C in notched specimens of Inconel718." *Materials Science and Engineering A* 340(1-2): pp. 139-154, (2003).

[Connolley et al.,2000] Connolley, T., Starink, M. J. and Reed, P. A. S. "Effect of oxidation on high temperature fatigue crack initiation and short crack growth in Inconel 718." *Superalloys 2000*: pp. 435-444, (2000).

[Cottrell,1949] Cottrell, A. H. "Theory of dislocations." *Progress in Metal Physics* 1: pp. 77-96, IN1-IN2, 97-126, (1949).

[Cozar et al.,1973] Cozar, R. and Pineau, A. "Morphology of γ' and γ" precipitates and thermal stability of inconel 718 type alloys." *Metallurgical and Materials Transactions B* 4(1): pp. 47-59, (1973).

[Decker,2006] Decker, R. F. "The evolution of wrought age-hardenable superalloys." *Jom* 58(9): pp. 32-36, (2006).

[Desvallées et al.,1994] Desvallées, Y., Bouzidi, M., Bois, F. and Beaude, N. "*Delta phase in Inconel 718: mechanical properties and forging process requirements*". Superalloys 718, 625, 706 and Various Derivatives (1994).

[Devaux et al.,2008] Devaux, A., Nazé, L., Molins, R., Pineau, A., Organista, A., Guédou, J. Y., Uginet, J. F. and Héritier, P. "Gamma double prime precipitation kinetic in Alloy 718." *Materials Science and Engineering: A* 486(1-2): pp. 117-122, (2008).

[Donachie,2002] Donachie, M. J. "Superalloys: a technical guide", ASM International, p., (2002).

[Ellyin,1997] Ellyin, F. "Fatigue damage, crack growth, and life prediction", p., (1997).

[Fournier et al.,1977] Fournier, D. and Pineau, A. "Low fatigue cycle behaviour of Inconel 718 at 293 K and 823 K." *Metallurgical Transactions a-Physical Metallurgy and Materials Science* 8(7): pp. 1095-1105, (1977).

[Fu et al.,2009] Fu, S. H., Dong, J. X., Zhang, M. C. and Xie, X. S. "Alloy design and development of INCONEL718 type alloy." *Materials Science and Engineering a-Structural Materials Properties Microstructure and Processing* 499(1-2): pp. 215-220, (2009).

[Garat et al.,2008] Garat, V., Cloue, J. M., Poquillon, D. and Andrieu, E. "Influence of Portevin-Le Chatelier effect on rupture mode of alloy 718 specimens." *Journal of Nuclear Materials* 375(1): pp. 95-101, (2008).

[Graff,2006] Graff, S. "*Viscoplastic behaviour of zirconium alloys in the temperatures range 20°C–400°C: characterization and modelling of strain ageing phenomena*". Paris, Ecole Nationale Supérieure des Mines de Paris**:** 319 (2006).

[Guedou,2009] Guedou, J. Y. "Optimisation des traitements thermiques dans les alliages de titane et de nickel pour pièces structurales de turboréacteurs aéronautiques." *Matériaux et Techniques* 97: pp. 99-108, (2009).

[Guedou et al.,1994] Guedou, J. Y., Simon, G. and Rongvaux, J. M. "Development of damage tolerant INCO 718." *Superalloys 718, 625, 706 1994*: pp., (1994).

[Hale et al.,2001] Hale, C. L., Rollings, W. S. and Weaver, M. L. "Activation energy calculations for discontinuous yielding in Inconel 718SPF." *Materials Science and Engineering A* 300(1-2): pp. 153-164, (2001).

[Han et al.,1982] Han, Y. F., Deb, P. and Chaturvedi, M. C. "Coarsening behaviour of γ" particles and γ' particles in Inconel Alloy 718." *Metal Science* 16(12): pp. 555-561, (1982).

[He,1994] He, J. "γ" Precipitate in Inconel 718." *J.Mater.Sci.Technol.* 10: pp. 293-303, (1994).

[He et al.,1998] He, J., Han, G., Fukuyama, S. and Yokogawa, K. "Interfaces in a modified Inconel 718 with compact precipitates." *Acta Materialia* 46(1): pp. 215-223, (1998).

[Hong et al.,2005] Hong, J. K., Park, N. K., Kim, S. J. and Kang, C. Y. "Microstructures of oxidized primary carbides on superalloy Inconel 718." *New Frontiers of Processing and Engineering in Advanced Materials* 502: pp. 249-253, (2005).

[Hornbogen et al.,1981] Hornbogen, E., Thumann, M. and Verpoort, C. "Fatigue crack inititation at slip steps." *Journal of Metals* 33(9): pp. A63-A63, (1981).

[Horvath et al.,2001] Horvath, W., Zechner, W., Tockner, J., Berchthaler, M., Weber, G. and Werner, E. A. "*The effectiveness of direct aging on Inconel 718 forgings produced at high strain rates as obtained on a screw press*". Superalloys 718, 625, 706 and Various Derivatives**:** 223-228 (2001).

[Jacquelin,1983] Jacquelin, B. "*Amorçage des fissures en fatigue oligocyclique sous chargement multiaxial*". PhD Thesis, Ecoles des Mines de Paris (1983).

[James,1986] James, L. A. "The effect of grain size upon the fatigue-crack propagation behaviour of alloy 718 under hold-time cycling at elevated temperature." *Engineering Fracture Mechanics* 25(3): pp. 305-314, (1986).

[Jiang et al.,2007] Jiang, H., Zhang, Q., Chen, X., Chen, Z., Jiang, Z., Wu, X. and Fan, J. "Three types of Portevin-Le Chatelier effects: Experiment and modelling." *Acta Materialia* 55(7): pp. 2219-2228, (2007).

[Kirman et al.,1970] Kirman, I. and Warrington, D. "The precipitation of Ni3Nb phases in a Ni−Fe−Cr−Nb alloy." *Metallurgical and Materials Transactions B* 1(10): pp. 2667-2675, (1970).

[Klose et al.,2003] Klose, F. B., Ziegenbein, A., Weidenmüller, J., Neuhäuser, H. and Hähner, P. "Portevin-LeChatelier effect in strain and stress controlled tensile tests." *Computational Materials Science* 26: pp. 80-86, (2003).

[Korth,1991] Korth, G. E. "*Effects of various parameters on the Fatigue life of alloy 718*". Superalloys 718, 625, 706 and Derivatives, Proceedings (1991).

[Koul et al.,1988] Koul, A. K., Au P., Bellinger N. and R., T. "Development of a damage tolerant microstructure for Inconel 718 turbine disc material." *Superalloys 1988*: pp. 3-12, (1988).

[Krueger,1989] Krueger "The development of direct age 718 for Gas Turbine Engine disks applications". Superalloy 718-Metallurgy and Applications. M. M. S. The Minerals (1989).

[Lee et al.,1995] Lee, B. H. and Kim, I. S. "Dynamic Strain Aging in the high temperature Low-Cycle Fatigue of SA508 Cl. 3 forging steel." *Journal of Nuclear Materials* 226(1-2): pp. 216-225, (1995).

[Li et al.,1994] Li, S., Jingyum, Z., Qun, D. and Jinhui, D. "*The effect of delta phase on crack propagation under creep and fatigue conditions in alloy 718*". Superalloys 718, 625, 706 and Various Derivatives (1994).

[Lingenfelter,1989] Lingenfelter, A. "*Welding of Inconel Alloy 718: A Historical Overview*". Superalloy 718, Metallurgy & Applications**:** 673 (1989).

[Lynch et al.,1994] Lynch, S. P., Radtke, T. C., Wicks, B. J. and Byrnes, R. T. "Fatigue crack growth in nickel based superalloys at 500-700°C. Direct Aged alloy 718." *Fatigue & Fracture of Engineering Materials & Structures* 17(3): pp. 313-325, (1994).

[Mendoza et al.,1989] Mendoza, O. and Feldstein, H. "*Analysis and Elimination of high temperature notch induced microcrack initiation in Inconel 718 Nickel-based alloy*". Report. San Antonio, DTIC Electe (1989).

[Min et al.,1978] Min, B. K. and Raj, R. "Hold Time Effects in High-Temperature Fatigue." *Acta Metallurgica* 26(6): pp. 1007-1022, (1978).

[Molins,1995] Molins, R. "*Oxydation des superalliages à base de Nickel : identification des mécanismes et conséquences sur le mode de propagation des fissures en fatigue à haute température*". PhD Thesis, Ecole Nationale Superieure des Mines de Paris (1995).

[Molins et al.,1997] Molins, R., Hochstetter, G., Chassaigne, J. C. and Andrieu, E. "Oxidation effects on the fatigue crack growth behaviour of alloy 718 at high temperature." *Acta Materialia* 45(2): pp. 663-674, (1997).

[Mulford et al.,1979] Mulford, R. A. and Kocks, U. F. "New observations on the mechanisms of dynamic strain aging of jerky flow." *Acta Metallurgica* 27(7): pp. 1125-1134, (1979).

[Niang,2010] Niang, A. "*Contribution à l'étude de la précipitation des phases intermétalliques dans l'alliage 718*". PhD Thesis, INP Toulouse (2010).

[Pedron et al.,1982] Pedron, J. P. and Pineau, A. "The effect of microstructure and environment on the crack-growth behaviour of Inconel 718 alloy at 650 °C under fatigue, creep and combined loading." *Materials Science and Engineering* 56(2): pp. 143-156, (1982).

[Ponnelle,2001] Ponnelle, S. "*Propagation des fissures par fatigue à haute température dans l'Inconel 718: effets de microstructure et de chargements complexes*". PhD Thesis, Ecole des Mines de Paris (2001).

[Ponnelle et al.,2001] Ponnelle, S., Brethes, B. and Pineau, A. "Orientational effects and influence of delta phase on fatigue crack growth rates in a forged disc of INCO718 superalloy." *Superalloys 718, 625, 706 and Various Derivatives*: pp. 501-510, (2001).

[Radavich et al.,1989] Radavich, J. F. and Couts, W. H. "*Factors affecting delta phase precipitation and growth at hot work temperatures*". Superalloys 718, 625, 706 and Derivatives, Proceedings (1989).

[Sanders et al.,1981] Sanders, T., Frishmuth, R. and Embley, G. "Temperature Dependent Deformation Mechanisms of Alloy 718 in Low Cycle Fatigue." *METALLURGICAL AND MATERIALS TRANSACTIONS A* 12(6): pp. 1003-1010, (1981).

[Slama et al.,2005] Slama, C, Abdellaoui and M "Mechanical properties of the inconel 718 aged at 680 and 750 °C." *Physical and Chemical News*(22): pp. 8, (2005).

[Slama,1993] Slama, C. "*Analyse des évolutions structurales et des processus de précipitation intervenant dans l'alliage à base de nickel INCONEL 718 (NC 19Fe Nb). Incidence de la microstructure sur les propriétés mécaniques.*". PhD Thesis, Université de Paris Sud- Centre d'Orsay (1993).

[Slama et al.,2000] Slama, C. and Abdellaoui, M. "Structural characterization of the aged Inconel 718." *Journal of Alloys and Compounds* 306(1-2): pp. 277-284, (2000).

[Spath et al.,2001] Spath, N., Zerrouki, V., Poubanne, P. and Guedou, J. Y. "718 superalloy forging simulation : A way to improve process and material potentialities." *Superalloys 718, 625, 706 and Various Derivatives*: pp. 173-183, (2001).

[Stephens et al.,2001] Stephens, R. I. and Fuchs, H. O. "Metal Fatigue in Engineering (Second Edition)", John Wiley & Sons, p., (2001).

[Strondl et al.,2008] Strondl, A., Fischer, R., Frommeyer, G. and Schneider, A. "Investigations of MX and γ'/γ" precipitates in the nickel-based superalloy 718 produced by electron beam melting." *Materials Science and Engineering: A* 480(1-2): pp. 138-147, (2008).

[Sundaraman et al.,1993] Sundaraman, M., Singh, J. B. and Mukhopadhyay, P. "Estimation of order strengthening in Inconel 718 type alloys containing all γ" precipitate variants." *Scripta Metallurgica Et Materialia* 29: pp. 557-562, (1993).

[Sundararaman et al.,1994] Sundararaman, M., Mukhopadhyay, P. and Banerjee, S. "*Precipitation and room temperature deformation behaviour of Inconel 718*". Superalloys 718, 625, 706 &nd Various Derivatives (1994).

[Sundararaman et al.,1997] Sundararaman, M., Mukhopadhyay, P. and Banerjee, S. "*Carbide precipitation in nickel base superalloys 718 and 625 and their effect on mechanical properties*". Superalloys 718, 625, 706 and Various Derivatives (1997).

[Tanaka et al.,1981] Tanaka, K. and Mura, T. "A dislocation model for fatigue crack initiation." *Journal of Applied Mechanics* 48: pp. 97-103, (1981).

[Ter-Ovanessian,2011] Ter-Ovanessian, B. "*Etude comparative de différents superalliages base Ni pour ressorts de systèmes de maintien*". PhD Thesis, INP Toulouse (2011).

[Ter-Ovanessian et al.,2008] Ter-Ovanessian, B., Deleume, J., Cloue, J. M. and Andrieu, E. "Influence of interstitials content on the sensitivity of alloy 718 to oxidation assisted intergranular fracture." *High Temperature Corrosion and Protection of Materials 7, Pts 1 and 2* 595-598: pp. 951-958, (2008).

[Valsan et al.,1994] Valsan, M., Sastry, D. H., Rao, K. B. S. and Mannan, S. L. "Effect of strain rate on the High-Temperature Low-Cycle Fatigue properties of a Nimonic PE-16 Superalloy." *Metallurgical and Materials Transactions a-Physical Metallurgy and Materials Science* 25(1): pp. 159-171, (1994).

[Velay,2003] Velay, V. "*Modélisation du comportement cyclique et de la durée de vie d'aciers à outils martensitiques*". PhD Thesis, Ecole des Mines de Paris (2003).

[Villechaise et al.,2002] Villechaise, P., Sabatier, L. and Girard, J. C. "On slip band features and crack initiation in fatigued 316L austenitic stainless steel: Part 1: Analysis by electron back-scattered diffraction and atomic force microscopy." *Materials Science and Engineering A* 323(1-2): pp. 377-385, (2002).

[Wang et al.,2009] Wang, Y., Zhen, L., Shao, W. Z., Yang, L. and Zhang, X. M. "Hot working characteristics and dynamic recrystallization of delta-processed superalloy 718." *Journal of Alloys and Compounds* 474(1-2): pp. 341-346, (2009).

[Warren et al.,2006] Warren, J. and Wei, D. Y. "The cyclic fatigue behaviour of direct age 718 at 149, 315, 454 and 538 °C." *Materials Science and Engineering: A* 428(1-2): pp. 106-115, (2006).

[Worthem et al.,1990] Worthem, D., Robertson, I., Leckie, F., Socie, D. and Altstetter, C. "Inhomogeneous deformation in INCONEL 718 during monotonic and cyclic loadings." *Metallurgical and Materials Transactions A* 21(12): pp. 3215-3220, (1990).

[Xiao et al.,2005] Xiao, L., Chen, D. L. and Chaturvedi, M. C. "Shearing of γ" precipitates and formation of planar slip bands in Inconel 718 during cyclic deformation." *Scripta Materialia* 52(7): pp. 603-607, (2005).

[Xiao et al.,2008] Xiao, L., Chen, D. L. and Chaturvedi, M. C. "Cyclic deformation mechanisms of precipitation-hardened Inconel 718 superalloy." *Materials Science and Engineering: A* 483-484: pp. 369-372, (2008).

[Xie et al.,2005] Xie, X. S., Dong, J. X., Wang, G. L. and You, W. "The effect of Nb, Ti, Al on precipitation and strengthening behavior of 718 type superalloys." *Superalloys 718, 625, 706 and Derivatives, Proceedings*: pp. 287-298, (2005).

[Xie et al.,2010] Xie, X. S., Fu, S. H., Zhao, S. Q. and Dong, J. X. "The Precipitation Strengthening Effect of Nb, Ti and Al in Cast/Wrought Ni-Base Superalloys." *Thermec 2009, Pts 1-4* 638-642: pp. 2363-2368, (2010).

[Yuan et al.,2005] Yuan, H. and Liu, W. C. "Effect of the [delta] phase on the hot deformation behavior of Inconel 718." *Materials Science and Engineering: A* 408(1-2): pp. 281-289, (2005).

[Zemzemi,2007] Zemzemi, F. "*Caracterisation de modeles de frottement aux interfaces piece-outil-copeau en usinage: application au cas de l'usinage des aciers et de l'Inconel 718*". PhD Thesis, Ecole centrale de Lyon (2007).

[Zhang et al.] Zhang, H. Y., Zhang, S. H., Cheng, M. and Li, Z. X. "Deformation characteristics of [delta] phase in the delta-processed Inconel 718 alloy." *Materials Characterization* 61(1): pp. 49-53,

Chapter III

Strategy for Inconel 718 microstructure design and experimental methodology

"Que la stratégie soit belle est un fait, mais n'oubliez pas de regarder le résultat"

Winston Churchill

Chapter III: Strategy for Inconel 718 microstructure design and experimental methodology

I Introduction

The study of the LCF behaviour and the optimisation of the microstructural features needs the application of a large variety of experimental methods appropriate to the range of magnification needed for the understanding of different phenomena.

The material optimization, focused on the improvement of the extrusion die properties, could be achieved through the integration of different research and testing methodologies.

In this way, a series of order of magnitudes are needed to move from the macroscopic structure (Extrusion Die) to the atomic arrangement (Inter-metallic phases size and morphology).

The understanding of the mechanical behaviour and the damage mechanisms are based on the relationships between different analysis methodologies. The results combination permits a multi-disciplinary approach based on mechanical tests and simulations, metallurgy and solid-state physics investigations (Figure III. 1).

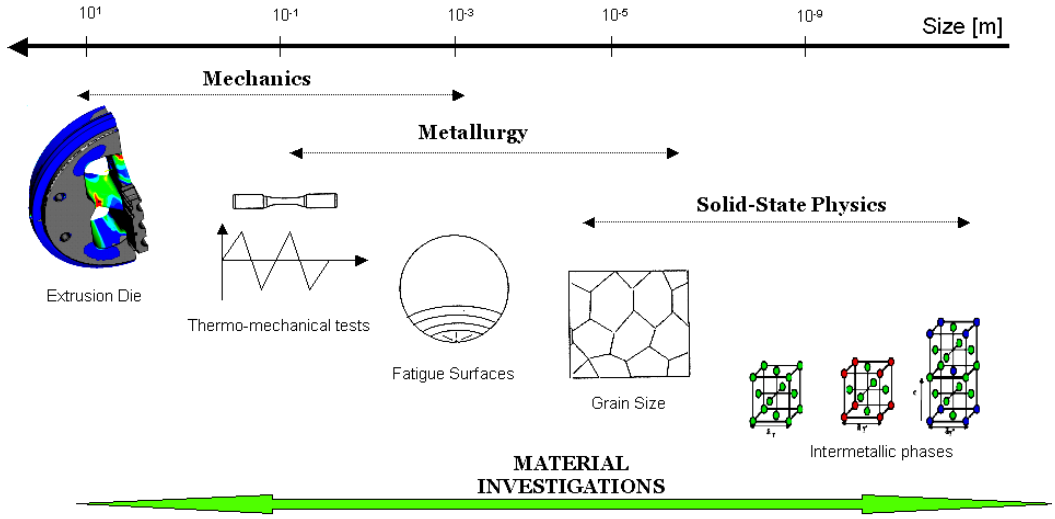

Figure III. 1 : Multi-disciplinary approach for material investigations.

This chapter is divided into two parts. The first part is focused on the presentation of the microstructural features associated to the standard grade of Inconel 718, adopted for the preliminary LCF tests. This sequence includes a detailed description of the research strategies adopted for the metallurgical optimization of the alloy, introducing some alternative thermal treatments that will be considered for the mechanical tests reported in chapter V. The last part is dedicated to the presentation of the different experimental methods used for the metallurgical and mechanical characterisation of the alloy.

II Microstructure of standard Inconel 718

II.1 Composition

The material investigated for all analyses is an Inconel 718 alloy. The elaboration was based on a double melting process (VIM-Vacuum induction melting and VAR Vacuum Arc Remelting) ensuring a high metallurgical quality.

The material is received in the form of 20 mm diameter forged bars from which all samples are extracted, for fatigue tests and metallurgical investigations are extracted.

The alloy composition is reported in Table III. 1:

Element	Ni	C	Cr	Fe	Nb	Ta	Mo	Ti	Al
[% weight]	53.5	0.024	17.8	18.8	5.28	0.01	2.98	0.89	0.50

Table III. 1 : Weight percent analysis of the standard grade of Inconel 718.

The alloy is characterized by a high amount of niobium and a limited content in aluminium, to promote the precipitation of γ' and γ" phases. As described in the literature, the variation in Al content can change the precipitation behaviour: the thermodynamic calculations reported by Fu **[Fu et al.,2009]** showed that Al addition (>2 wt.%) leads to a strong increase in γ' volume fraction, but promotes the formation of σ and Laves phases that degrade the alloy microstructure. For this reason, the alloying elements are carefully balanced in order to limit the embrittlement and enhance the material stability. A reduced carbon amount (0.04 wt.%) is also an important requirement to limit the carbides precipitation.

II.2 Thermal treatment

Samples from the as received Inconel 718 are exposed to a conventional heat treatment (Figure III. 2) following the ASTM B637 specification:

- *Solution thermal treatment*: at 954°C for 1 hour and air-cooling to room temperature.
- *Ageing treatment*: at 718°C for 8 hours, furnace cooled to 621°C and held at 621°C for a total ageing-time of 18 hours followed by air-cooling to room temperature.

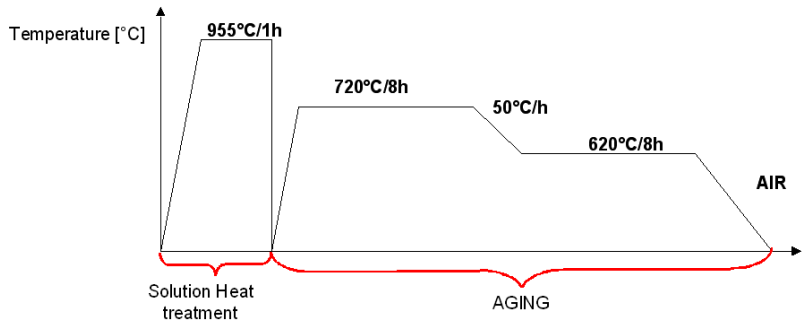

Figure III. 2 : Standard thermal treatment for Inconel 718 following ASTM B637 specification.

It is important to point out that the solutionizing temperature, expressly chosen below the delta solvus, inhibits a fast grain growth and allows a controlled precipitation of the intermetallic phases, in order to attain the required properties.

II.3 Microstructure

The microstructure of the material, resulting from the conventional thermal treatment, consists of fine equiaxe grain (ASTM 12). Grains are decorated with a clear presence of delta phase, in the shape of thin platelets, preferentially formed at grain boundaries with an average length of 1.5 μm (Figure III. 3).

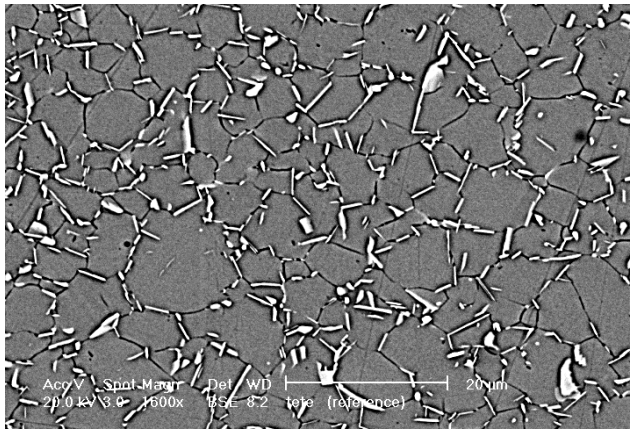

Figure III. 3 : Microstructure of Inconel 718 after conventional heat treatment [Taina et al.,2010].

A number of MC type primary carbides (Figure III. 4), inhomogeneously distributed throughout the structure, is observed. They consist of typical NbC or TiC carbides that exhibit irregular or quadrangular shapes showing various contrasts, on etched cross-sections, depending on their composition (orange for TiC and grey for NbC).

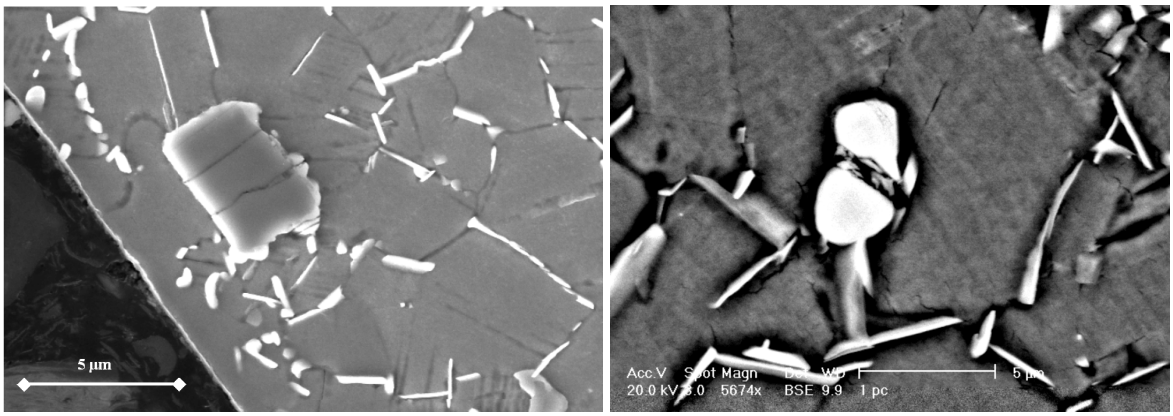

(a) **(b)**

Figure III. 4 : Typical examples of TiC (a) and NbC (b) particles detected by SEM investigation in IN718.

Figure III. 5 reports the EDS spot analyses obtained respectively for delta (δ) phase and MC particles. These phases exhibit a primary peak associated to Nb, while Ti and C show lower contents.

The Delta phase pattern, on the contrary, reveals peaks relative to Nb and Ni, but it shows also the presence of the main matrix alloying elements such as Cr, Fe, Ti and C.

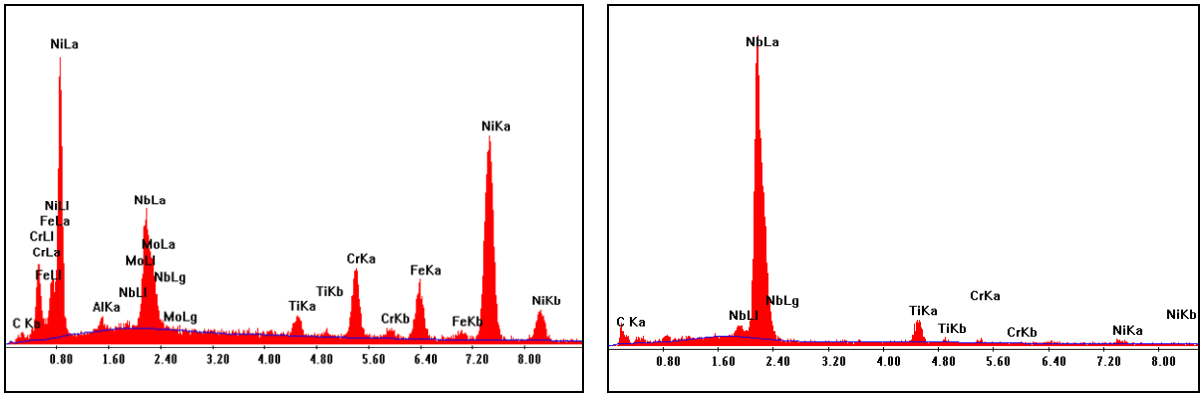

(a) **(b)**

Figure III. 5 : EDAX spot patterns evaluated for Delta phase (a) and MC carbides (b) particles.

High resolution diffraction experiments, carried out by Synchrotron XRD, give more information on the hardening phases. The high intensity associated to the synchrotron leads to the detection of γ' and γ".

In general, the precipitates size is too small to be detected by conventional X ray diffraction experiments. Synchrotron XRD ensures a better resolution for identifying these nanometric particles, improving the microstructural investigation.

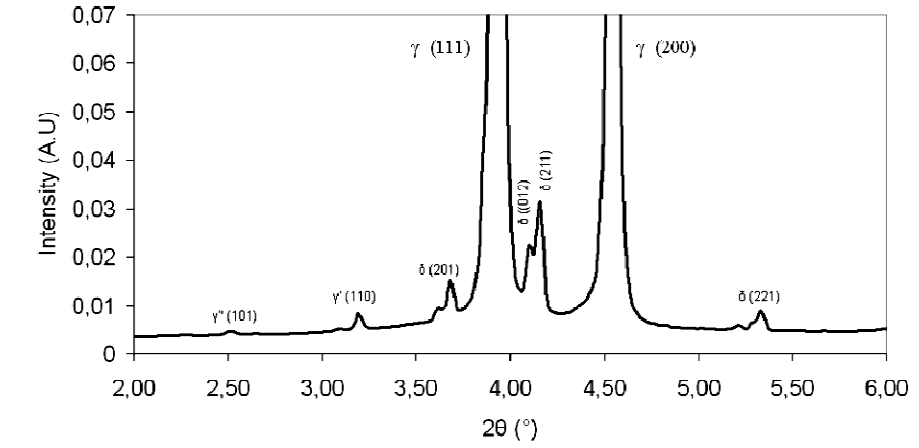

(a)

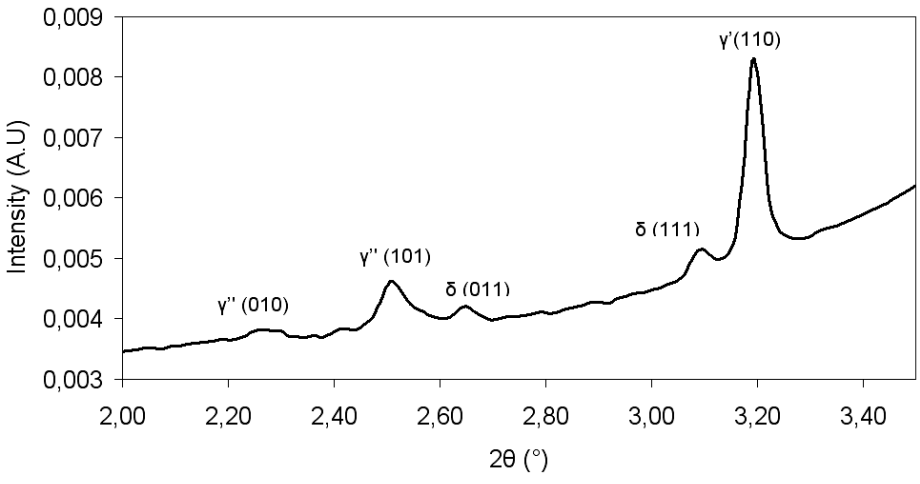

(b)

Figure III. 6 : DRX-Synchrotron patterns evaluated on Standard Inconel 718.

Diffractograms in Figure III. 6, evaluated in the range 2θ=2-6°, exhibit high intensity peaks associated to the matrix (γ) (Figure III. 6(a)), and low intensity peaks associated to the intermetallic phases (δ, γ' and γ") (Figure III. 6(b)).

The X-ray Synchrotron diffraction experiments, added to the SEM investigations, constitute a valid support to analyse the microstructural evolution upon thermal treatment.

II.4 Tensile strength

The static mechanical properties are measured by tensile tests carried out at 550°C with a strain rate of 10^{-3} s^{-1}. The tensile curve, reported in Figure III. 7, exhibits a Portevin-Le Chatelier effect as indicated by stress serrations with amplitudes ranging between 100 and 200 MPa.

As confirmed by previous studies, the stress drops are due to the localisation of strain in the form of deformation bands, as a consequence of an heterogeneous plastic flow **[Rodriguez et al.,1995]**. The mechanism originates from fast diffusing solute atoms that block the mobile dislocations until the stress is high enough to overcome the obstacle. According to Garat and Rodriguez **[Rodriguez et al.,1995; Garat et al.,2008]**, these serrations can be defined as type C Portevin-Le Chatelier because they appear as load drops below the general level of the stress-strain curve.

At the test temperature, the solutes diffusivity is high enough to recapture the mobile dislocations during the motion, initiating stress instabilities. Each load drop is associated to an acoustic emission during the test. With an increase in stress, dislocations density increases resulting in some work hardening **[Klose et al.,2003]**.

The tensile curve shows that stress serrations are activated by a critical plastic strain, 0.25 %, where the stress/strain concentrations enhance the appearance of the jerky flow.

The alloy is characterised by a high Yield Strength (998 MPa) which delays the plastic flow ensuring high performances at high temperature (Table III. 2).

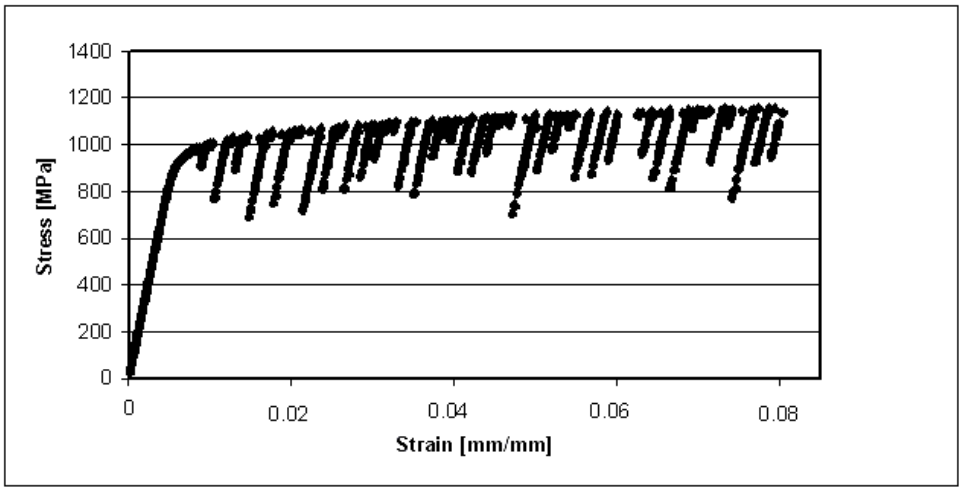

Figure III. 7 : Typical stress-strain relation for a uni-axial tensile test at 550°C.

	HEAT TREATMENTS PARAMATERS					TENSILE TESTS DATA			
Heat Treatment	T_a (°C)	T_{R1} (°C)	t_{R1} (h)	T_{R2} (°C)	t_{R2} (h)	YS [MPa]	E [MPa]	UTS [MPa]	A [%]
STANDARD	955	720	8	620	8	**998**	**163216**	**1228**	**35.3**

Table III. 2 : Experimental parameters and mechanical properties of standard Inconel 718 grade.

III Alternative Inconel 718 grades

As described in Chapter I, one of the main objectives of this work consists in the optimisation of the material properties to improve its strength under extrusion loading. Generally speaking, materials are characterised by several parameters, intimately related to their microstructures, which are difficult to modify. These are the intrinsic properties depending on the atomic bonds and arrangements. On the contrary, other properties could be considerably optimised by a change in composition or the application of appropriate thermal or thermo-mechanical treatments. By a proper control of processing parameters, specific microstructures can be achieved in order to enhance tensile and fatigue properties.

The starting point of our optimisation consist in a standard grade of Inconel 718, heat treated following the conventional process described above. The general approach, employed for the achievement of tailored microstructural properties is schematically reported in Figure III. 8 .

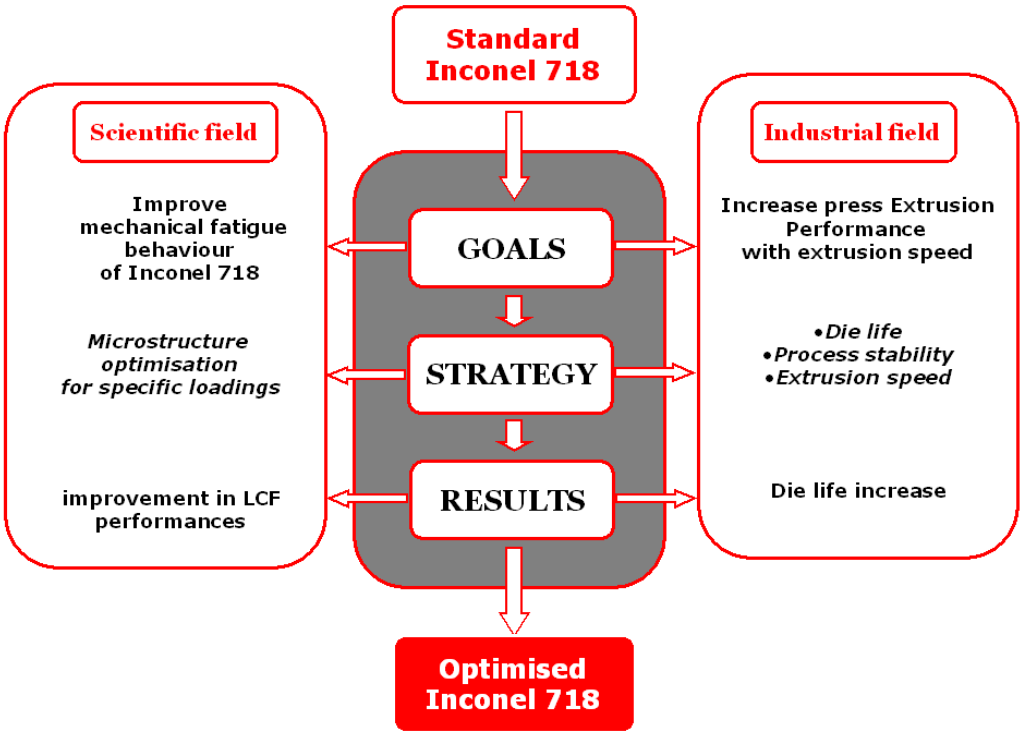

Figure III. 8 : General approach adopted for the optimisation of Inconel 718.

The material development is organized considering both industrial and scientific requirements. The main *goals* of this approach consist in the improvement of the fatigue life of Inconel 718 that directly impact on the durability of the extrusion dies. As a result, the applied *strategy* is based on the microstructural optimisation of the alloy in order to reduce

the risks of failure under extrusion conditions and ensure the process stability. The design of alternative thermal treatments, prone to improve the LCF resistance of Inconel 718 constitutes the main *result* of this PhD work.

Donachie **[Donachie,2002]** described the thermal treatment as "*the logical consequence of the processing requirements as well as the logical precursors for the generation of optimal properties*". Following this definition the thermal treatment can be defined as a valid way to transform the standard Inconel 718 alloy into a material specifically adapted to the extrusion conditions.

Figure III. 9 illustrates the experimental approach adopted for the optimization of the material heat treatment. Two investigation directions can be considered: the first consists in the optimization of the heat treatment parameters as a function of the required mechanical properties, while the second is base on the adoption of thermo-mechanical processes where not only the heat treatment, but also the forging procedure is refined.

Considering the heat treatment optimization, the procedure used for standard Inconel 718 follows a series of requirements contained in the ASTM B637 specification **[ASTMB637]**. This document, designed for precipitation hardening nickel alloys, recommends specific range of temperature and time for each stage of the heat treatment, prone to ensure high mechanical properties.

The reported recommendations are the following:

Solution treatment

- Solution temperature: 924°C < T < 1010°C.
- Solution Time: 0.5 h minimum, cool at rate equivalent to air cool or faster.

Ageing Treatment

- First ageing: T = 718 ± 14 °C, holding at temperature for 8 hours, furnace cooling to 621 ± 14 °C.
- Second ageing T = 621 ± 14 °C holding until total precipitation heat treatment time has reached 18h and then air cooling.

Following the constraints applied by the specification, we opt for a heat treatment optimization where the specific parameters are chosen following two strategies:

1. Intra-specification design: the solution treatment temperature are selected in the range reported by ASTM B 637 (924°C < T < 1010°C).
2. Extra-specification design: high solution treatment temperatures, above the specification range (T> 1010°C).

This approach allows the consideration of a large variety of process parameters that can be adopted separately or combined, in order to improve the material efficiency. Two alternative Inconel 718 grades (Tr. 990 and Tr.1000) are defined following an intra-specification design, whereas a further heat treatment procedure (API 6A) is optimized by an extra-specification

approach. Finally, the thermo-mechanical approach is based on the application of a direct ageing (DA) procedure which has been presented in the literature review (Chapter II).

These alternative strategies will be described in detail in the following sections.

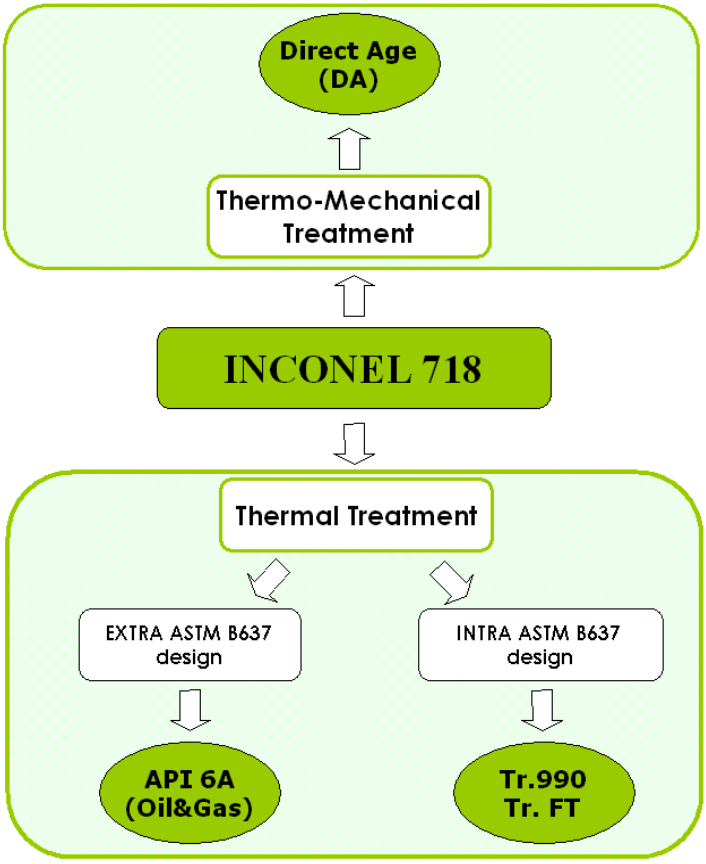

Figure III. 9 : Adopted strategies for Inconel 718 thermal treatment optimization.

III.1 Intra-specification heat treatment design

The optimization of the heat treatment parameters is ensured by the application of the Taguchi method. This approach is an efficient tool for the design of experiments (DOE) based on orthogonal array experiments that provide a reduction of the number of activities with an optimum control of the individual parameter contributions. During the extrusion cycle, the mechanisms of cyclic plasticity is concentrated in specific zones of the tool (hot spots), where the fatigue damage occurs, limiting the die life.

For this reason, the current study considers Yield Strength and Ultimate Tensile Strength as the optimization criteria. The purpose is to maximize Y.S in order to reduce plasticity and improve the fatigue behavior of the alloy. The aim of this work is not only to point out the contributions of individual parameters, but also to understand the relationships existing between them.

Eight process parameters are selected for designing and carrying out an experimental plan. The employed method is a stable Taguchi L8 matrix which consists of five columns of process parameters and eight lines representing different process conditions (Table III. 3).

The design parameters of this study are:

1. *The solution treatment temperature (T_a)*: four levels of solutioning temperature are considered (955, 980, 990 and 1000°C) in the range recommended by the ASTM specification. Specimens are hold at temperature for 1 h and air cooled to room temperature.
2. *The first ageing temperature (T_{R1}):* two levels of temperature are considered (720 and 750 °C).
3. *The first ageing time (t_{R1}):* two levels of time are chosen (4 and 8 h). The furnace cooling rate between the first and the second ageing is fixed at 55°C/h.
4. *The second ageing temperature (T_{R2}):* it is fixed at 620°C.
5. *The second ageing time (t_{R2}):* two times are chosen (4 and 8 h).

N° EXPERIMENT	HEAT TREATMENT PARAMATERS					TENSILE TESTS DATA			
	T_a (°C)	T_{R1} (°C)	t_{R1} (h)	T_{R2} (°C)	t_{R2} (h)	YS [MPa]	E [MPa]	UTS [MPa]	A [%]
1	955	720	4	620	8	**980**	**165200**	**1214**	**33,8**
2	980	750	8	620	8	**1097**	**165500**	**1297**	**38**
3	990	720	8	620	8	**1078**	**164500**	**1271**	**36**
4	1000	750	4	620	8	**1116**	**165600**	**1297**	**34,6**
5	955	750	8	620	8	**1010**	**163200**	**1264**	**33**
6	980	720	4	620	8	**995**	**167700**	**1224**	**33**
7	990	750	4	620	8	**1060**	**165800**	**1283**	**38**
8	1000	720	8	620	8	**1085**	**163100**	**1297**	**40**

Table III. 3 : Experimental design using a Taguchi L8 orthogonal array and outline results.

Each line corresponds to a specific thermal treatment investigated by a conventional tensile test carried out at 550°C. U.T.S and Y.S along with E and A% are the output values of the tests.

Figure III. 10 shows the average effect of each parameter on yield strength. The analysis, limited to the main parameters (T_a, T_{R1} *and* t_{R1}), gives the optimal conditions that are: solution treatment at 1000°C and first ageing at 750° for 8h.

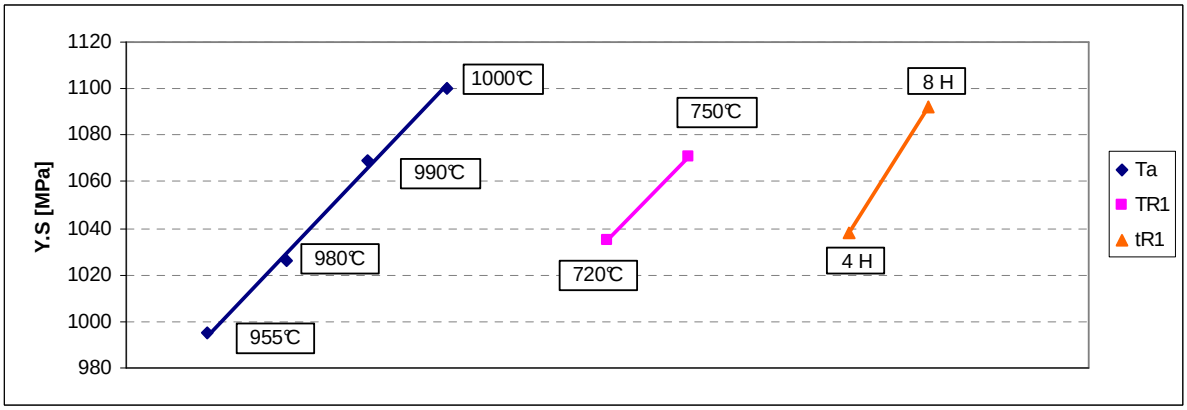

Figure III. 10 : Individual effects of heat treatment parameters on Yield Strength.

The diagram points out the effect of the annealing temperature which has the maximum contributions on the mechanical properties of the alloy.

Another important aspect to explore is the impact of the two-fold interactions on the

response (Y.S). These analyses are represented in form of linear graphs where the average output values are reported (Figure III. 11). The non-parallelism of the plots indicate that an interaction exists between the two factors. From Figure III. 11(b) it can be seen that a quite strong interaction exists between the first ageing temperature and the holding time. An ageing process carried out at 750°C for 4h is the best solution to optimize the Y.S value.

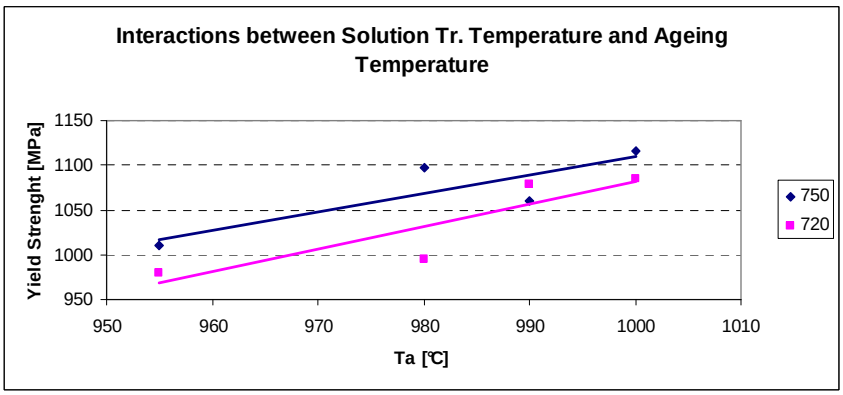

(a)

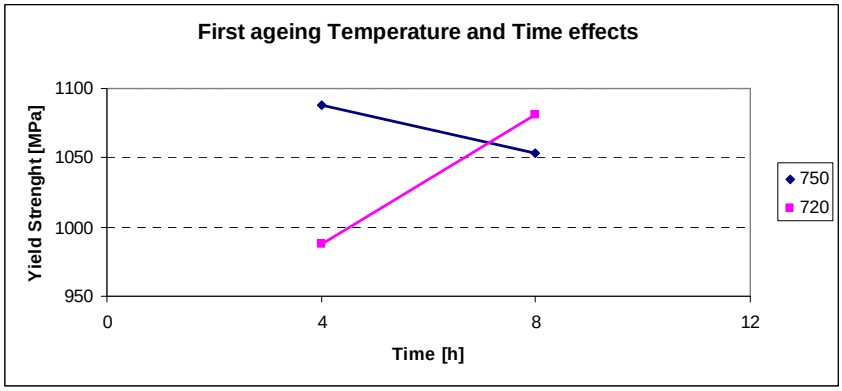

(b)

Figure III. 11 : Two-ways interactions between solution and ageing process parameters.

As described above, current study considers Yield Strength ad the discriminating parameter for choosing alternative thermal treatments.

Following these considerations, two heat treatments, the number 3 and 4, are selected as alternative solutions to be tested under LCF conditions. The experiment N°4, renamed “Tr. 1000” (Table III. 4), is a particular optimization of the standard process where all the parameters, except those relative to the second ageing, have been refined. This treatment has ensured the maximum Y.S value and their parameters are in perfect agreement with the interactions analysis reported above.

Experiment N° 3, defined as “Tr.990“(Table III. 4), is another powerful process which is based on a single variation of the standard cycle. The increase in solution temperature ensures a significant improvement of the mechanical properties and justify its choice for the fatigue investigations.

	HEAT TREATMENT PARAMATERS					TENSILE TESTS DATA			
Heat Treatment	T_a (°C)	T_{R1} (°C)	t_{R1} (h)	T_{R2} (°C)	t_{R2} (h)	YS [MPa]	E [MPa]	UTS [MPa]	A [%]
Tr.990	990 [1h]	720	8	620	8	**1078**	**164500**	**1271**	**36**
Tr.1000	1000 [1h]	750	4	620	8	**1116**	**165600**	**1297**	**34.6**

Table III. 4 : Summary of the selected thermal treatments associated to the intra-specification design.

III.2 Extra-specification heat treatment design

In this case the selection of an alternative thermal treatment is based on the adoption of a process largely employed in the Oil & Gas industry.

Inconel 718 possesses the attributes of aqueous and high temperature corrosion resistance, added to weldability and formability that are needed for this application. The actual tendency of the Oil and Gas application is to operate with higher pressures and higher temperature corrosive fluids that increase the risks of hydrogen embrittlement and stress corrosion cracking **[Barbadillo de et al.,2010]**.

For these severe service conditions, the high-strength condition, ensured by the conventional heat treatment, are not desirable for maximum yield strength material, but a specific thermal treatment is required to optimize microstructure for toughness and corrosion resistance.

The Oil and gas industry is governed by NACE standard MR-0175/API 6A **[NACE/MR0175]** for sour service applications, where the heat treatment is performed in agreement with the following procedure:

- Solution treatment at a temperature from 1021°C to 1052°C during 1 to 2.5 hours.
- Cooling in air, water, polymer or oil to ambient temperature.
- Age hardening at a temperature of 774°C-802°C for six to eight hours, followed by an air cool or faster to ambient temperature.

In this frame and for our applications, the heat treatment procedure and the relative mechanical properties are reported in Table III. 5:

	HEAT TREATMENT PARAMATERS					TENSILE TESTS DATA			
Heat Treatment	T_a (°C)	T_{R1} (°C)	t_{R1} (h)	T_{R2} (°C)	t_{R2} (h)	YS [MPa]	E [MPa]	UTS [MPa]	A [%]
API 6A	1030 [1.5h]	785	6	/	/	**755**	**162700**	**996**	**46**
STANDARD	955 [1h]	720	8	620	8	**998**	**163200**	**1228**	**35.3**

Table III. 5 : Experimental parameters and mechanical properties of API 6A treatment.

The alloy is characterized by a 37 HRC hardness and exhibits a very low delta phase content, due to the high solution temperature, giving an important grain growth (ASTM 5-7). All microstructural investigations will be reported in Chapter V.

Beyond the relative microstructural evolutions, the choice of this alternative thermal treatment is justified, from an industrial point of view, by technico-economic reasons. This alternative use of Inconel 718 is facilitated by a large availability of stocks opportunely treated in accordance with the API 6A specification. In such a way, the material could be found in large quantity and purchased with an average 30% cost reduction.

III.3 Thermo-mechanical treatment

The literature review, reported in Chapter II, showed that mechanical properties of Inconel 718 are closely related to the microstructure which is controlled by processing and heat treatment.

In general, Thermo-mechanical processing is the practice of exploiting temperature and strain interactions to enhance specific mechanical properties such as:

- Tensile strength and ductility;
- Fatigue/strength, life;
- Crack growth rate;
- Fracture Toughness
- Creep stress rupture

The final optimization of the alloy is usually a compromise between some of the above listed properties, through a good control of the interactions between chemical composition, solidification and hot working.

The strategy adopted for the thermo-mechanical treatment consists in the maximization of the cyclic capability and tensile properties through the application of a direct ageing (DA) procedure.

The material elaboration is carried out in collaboration with Aubert & Duval (Les Ancizes) by a specific control of the forging procedures (temperature, deformation, strain rate) and the quality of the in-put material (composition and grain size).

Material, in the form of double melted ingot (VIM-VAR), is thermo-mechanically processed by open die forging to a final pancake of 300 mm diameter and 80 mm height. The process involves a multiple step forging process of the work-piece, in a range of temperature between 985-1040 °C, to achieve the final diameter and a sufficiently fine grain size. Forging temperature is usually selected to limit the delta phase dissolution in order to ensure a minimal quantity of these phases prone to pin the boundaries of the new dynamic recrystallized grains, limiting grain growth.

The general procedure consists in rotating the work-piece (through 45° to 90°C, for instance) at the end of each pass in order to obtain a homogeneous cross section. Pancake is then water quenched after hot working, preserving the partially recrystallized structure and avoiding a re-arrangement of dislocations in low energy configurations.

The product exhibits a resulting grain size of ASTM 5-6 at the surface and ASTM 12-13 at the center where material is partially recrystallized. Pancake is finally treated in Direct Age conditions with the omission of the solution treatment and the application of the traditional double step ageing (720°C/8h and 620°C/8h).

Two tensile specimens are extracted from the homogeneous zones of the pancake and tests performed at 550°C. Table III. 6 reports a comparison between the Direct age material and the standard material.

Heat Treatment	HEAT TREATMENT PARAMATERS					TENSILE TESTS DATA			
	T_a (°C)	T_{R1} (°C)	t_{R1} (h)	T_{R2} (°C)	t_{R2} (h)	YS [MPa]	E [MPa]	UTS [MPa]	A [%]
DIRECT AGE (DA)	/	720	8	620	8	**1133**	**165500**	**1280**	**33**
STANDARD	955 [1h]	720	8	620	8	**998**	**163200**	**1228**	**35.3**

Table III. 6 : Experimental parameters and mechanical properties of Direct Age Inconel 718.

Results show a yield and tensile strength improvement of respectively 15% and 6% over the conventional grade. In particular the close values of Y.S and U.T.S, due to the work-hardening effects of the thermo-mechanical process, limit plastic strain mechanisms.

Horvath **[Horvath et al.,2001]** showed that dynamic recrystallization leads to a non uniform distribution of dislocations where regions of high dislocations density coexist with dislocation free areas.

The high value of the yield strength, associated to Direct Age treatment, is an indication of the inhomogeneous arrangement of dislocations due to a fast cooling after hot forging. The onset of plastic deformation is based on the motion of these pinned dislocations that require the application of increased stress levels.

These high mechanical responses associated to the Direct Age process, justify the use of this alternative treatment for extrusion die bulk material, assuming that its high mechanical properties could ensure, under cyclic loadings, a delay in crack initiation and propagation.

The investigation of the as-forged microstructures as well as a detailed understanding of its cyclic behavior will be reported in chapter V.

IV Thermo-mechanical investigation

One of the major goal of this work consists in a thermo-mechanical characterisation of Inconel 718 alloy. For this reason, a large amount uni-axial low cycle fatigue tests is carried out at 550°C, using different loading wave-forms. A detailed description of the tests method will be reported in the following paragraphs, focusing on the test equipments and procedures.

IV.1 Low cycle fatigue test method

All LCF tests are conducted using a uni-axial 250 kN Schenck fatigue machine coupled with an induction heating device. Figure III. 12 illustrates a LCF specimen placed in the fatigue machine and surrounded by the induction coil. The specimen tying consists in water cooled screwed grips. An alignment system placed between the force detector and the upper grip ensure the alignment of the sample.

A digital controller allows the connection between the personal computer and the machine. Three input signals could be collected: strain, force and piston displacement. The evolution of a LCF cycle is monitored and progressively measured via the Testar2® software developed by MTS, whereas the temperature regulation is ensured by an Eurotherm 900HP® controller.

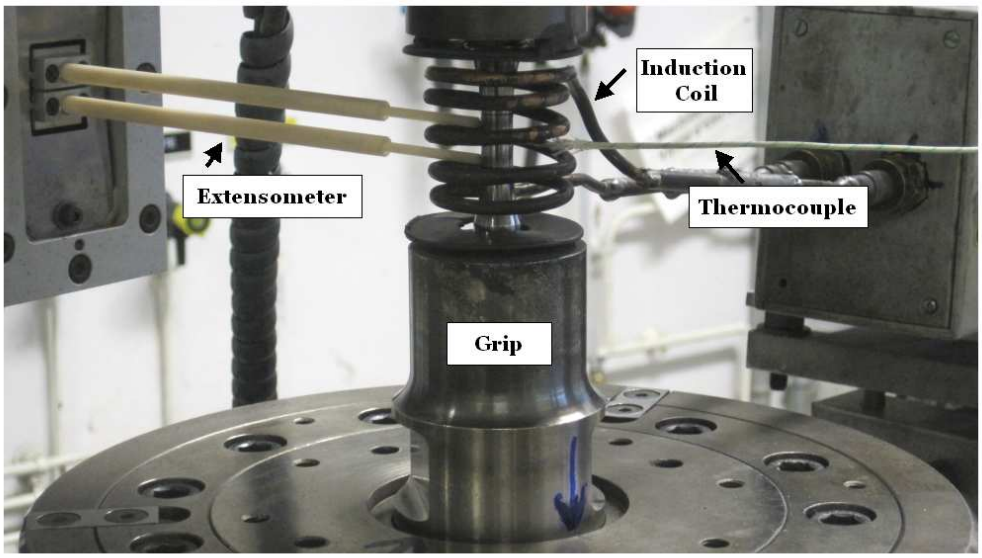

Figure III. 12 : Low cycle fatigue test meyhod

IV.1.A Induction heating

Specimens are induction heated with a Celes high frequency power supply. A specific water cooled induction coil is designed and manufactured to ensure uniform temperature along the isothermal gauge of the specimen. The induction coil is calibrated by a specific sample equipped by 9 thermocouples spot welded on its surface. Longitudinal and circumferential thermal gradients, along the gauge length, are respectively within 15°C and 5°C ensuring the isothermal conditions over the test.

During the cyclic loading application, thermocouples are not spot welded on the specimen, to avoid early crack initiation closed to the welding locations. A flatted 0.2 mm diameter K-type thermocouples is half wounded around the specimen in centreline. This thermocouple monitors the thermal cycles via the Eurotherm temperature controller (Eurotherm). To avoid any accidents, a security temperature controller is also installed in order to cut off all signals to the inductor generator in case of over-shoot or thermocouple failure.

IV.1.B Strain measurements

The strain measurement is achieved by a longitudinal extensometer properly adapted to high temperature tests. This extensometer, provided with a gauge length of 10 mm, is provided with a cooling fan that ensures that the body temperature stays below 150°C. The system is equipped of two high purity alumina rods, whose extremities are in contact with the sample and allow the transmission of the strain to the sensor. The system is accurately calibrated before every test campaign using a specific calibrator.

IV.1.C Specimens

Solid smooth cylindrical specimens with $\Phi=9\ mm$ diameter and 15 mm cylindrical calibrated gauge length are used to perform tests (Figure III. 13). All the specimens are manufactured from forged cylindrical bars ($\Phi=20mm$) and polished to achieve an inner and

outer surface roughness of R_a= 0.015 µm. Polishing procedure includes the use of emery SiC papers (80 to 1200 grade) and a finishing operation obtained using 6, 3 and 1 µm diamond suspensions.

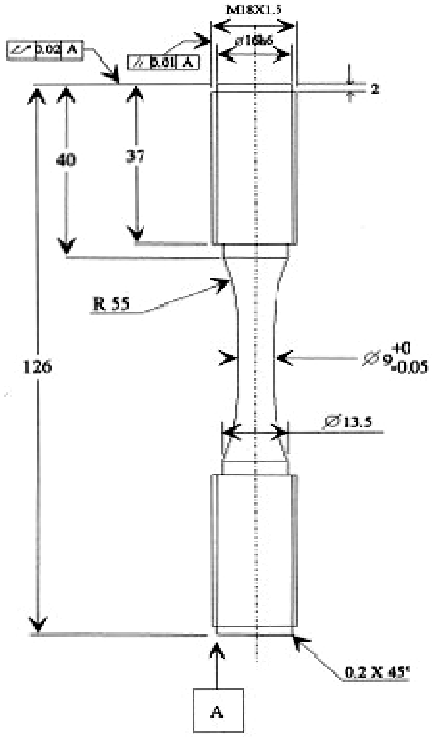

Figure III. 13 : LCF test sample [Delagnes,1998].

IV.1.D LCF test procedure

All the tests are carried out in air atmosphere, employing the following launching procedure:

1. Thermal stabilization of the system (specimen, extensometer, grips) at 550°C.
2. Determination of the thermal expansion coefficient.
3. Evaluation of the elasticity modulus to check if the system and the sample are operating as expected.
4. LCF test starting.

Fatigue life is commonly defined as the number of cycles at which the maximal stress or stress range drops sharply with a percentage of the pseudo stabilised stress.

As it will be reported in Chapter IV, Inconel 718 shows, at 550°C, a decrease of the cyclic stress with the number of cycles. However, the material exhibits a pseudo-stabilised stage where stress amplitudes are approximately constant. For this reason, tests were stopped at a stress drop of 10% of the stabilized stress range, which is normally achieved between 11 and 25 cycles. The test interruption, before final rupture, avoids additional oxidation effects and preserve the morphological features of the fracture surfaces.

IV.2 Low cycle fatigue test conditions

As mentioned in the preliminary chapter, the cyclic loading experienced by an extrusion die could be different as function of the profile geometry, the extruded alloy and/or the extrusion speed. For this reason, various LCF test conditions are examined in order to experimentally reproduce the loading of a large variety of extrusion dies.

Two types of isothermal (550°C) fatigue tests are performed, respectively in reversed total strain:

Simple cyclic tests

Simple cyclic tests are conducted employing a triangular symmetrical waveform (R= -1). The total strain amplitude is varied in the range from ±0.6 to ±1.65%, whereas frequency is held constant at 1 Hz. The aim of this preliminary campaign is to investigate the cyclic behaviour of Inconel 718, focusing on the damage mechanisms and on the softening behaviour of the alloy.

Dwell cyclic test

The response of the material under extrusion loading conditions is investigated by the application of trapezoidal wave-forms with total strain amplitude ranging from ±0.8 % to ±1.50%. The reference loading signal is illustrated in Chapter I. Tests are initially run with a strain rate of $5 \cdot 10^{-3} s^{-1}$ which reproduce the usual extrusion rate.

The employed loading waveforms are defined by the loading times, in seconds, at maximal and minimal strain. The standard cycle, for example, characterised by a dwell time of 150 s at maximal strain and 20 s at minimal strain, could be defined as 150-20. In a second time, two extra durations for the tensile dwell period are considered: 45 and 300 seconds. The time spent at minimal compression strain is hold at 20 sec in order to isolate the influence of the holding time in tensile conditions.

The impact of the extrusion extrinsic parameters on the Inconel 718 fatigue behaviour is completed by the studyof two alternative strain rates, respectively equal to $5 \cdot 10^{-3} s^{-1}$ and $5 \cdot 10^{-4} s^{-1.}$

IV.3 Tensile test conditions

Isothermal tensile tests are performed using the same induction heating device and push-pull fatigue machine employed for LCF tests. Identical smooth cylindrical specimens are adopted. A K-type thermocouple is spot welded at the base of the sample to ensure a better control of the thermal gradient. All tests are carried out in total strain control, with a strain rate equal to $10^{-3} s^{-1}$.

V Microstructural investigation

An important component of the materials characterization involves the knowledge of the structure of materials which has an important effect on its mechanical behaviour.

Several characterization techniques allow the understanding of the relationships between

material structure and mechanical behaviour. Each methodology is used for a specific application, as a function of the resolution and metallurgical interests.

Figure III. 14 illustrates the different analyse methods with their respective applications and magnification ranges. It is important to point out that all the methodologies could be applied both for the microstructure optimisation and fatigue fracture investigations.

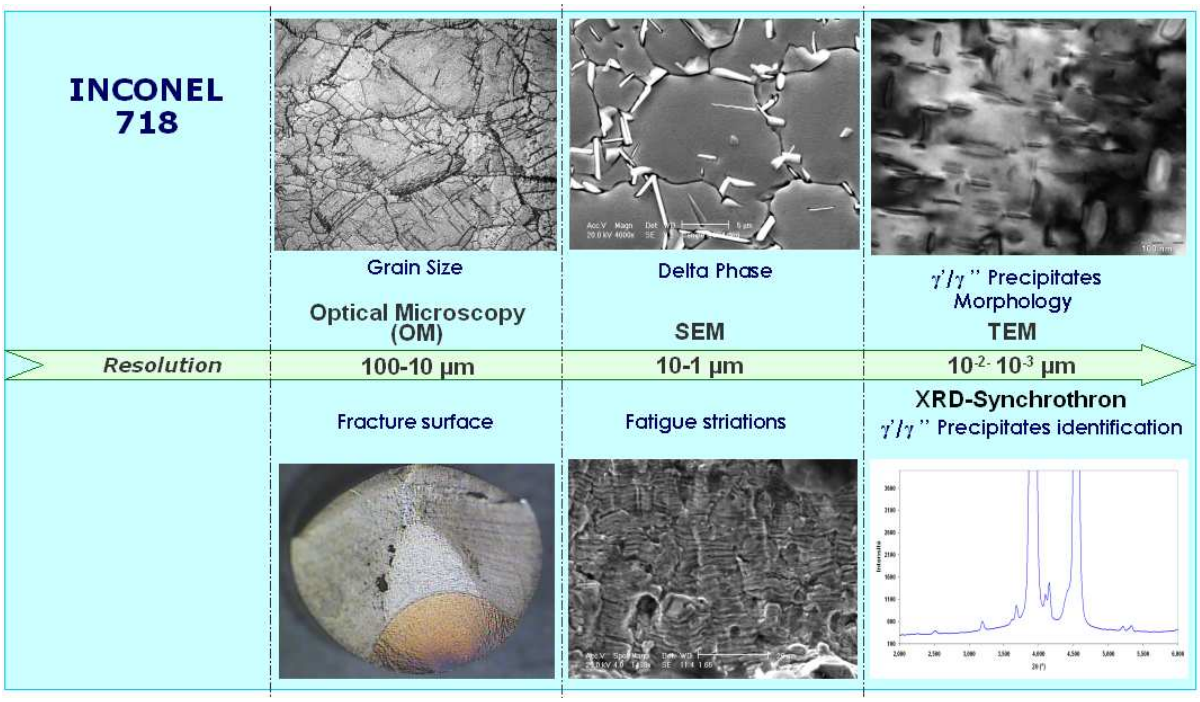

Figure III. 14 : Representation of the microstructural investigation methods used for Inconel 718.

In the following paragraphs, the different characterisation techniques will be presented with a particular attention to their technical instrumentations and applications.

V.1 Hardness measurements

Hardness measurements are carried out on an Instron® tester. The Vickers hardness is measured on polished samples, using 30 kg load. At least three measurements are evaluated across a surface.

V.2 Optical Microscopy

The study of the macrostructural appearance of the forged material is carried out by a Leica LEITZ DMRX instrument. Samples are prepared by a chemical etching in a bath containing hydrochloric acid (15 cc), Glycerol (10 cc) and nitric acid (5 cc).

V.3 Scanning Electrons Microscopy (SEM)

Microstructural investigations are performed by a Scanning Electron Microscopy (SEM-FEG XL 30) provided with secondary and back scattering electrons detectors. The system is also equipped with an energy dispersion spectrometer (EDAX DX4) that defines the X-ray emission pattern of the investigated zone.

Analyses are carried out following two main directions:

Post mortem specimen investigations: A detailed examination of the fracture surfaces of the fatigued samples are conducted in order to investigate the different damage stages, that are crack initiation, crack propagation and final catastrophic fracture. Considering crack initiation, post-mortem samples are investigated through an accurate observation of the longitudinal cross-sections. Generally, at the end of the LCF test the specimen is fractured, by a tensile loading, in two parts. One of them is conserved for further analyses, while the other part is cut along the sample axis and prepared for failure analysis. SEM investigations are then conducted on these longitudinal sections in order to point out the effect of the microstructure on the crack initiation. Fracture surfaces are finally analysed to investigate the crack propagation path as well as the crack propagation mode (transgranular or intergranular).

Microstructural evolution investigations: the optimisation of the thermal treatment parameters is strongly examined by a main investigation of their single effects on the microstructural properties. Results are reported in chapter V where particular attention is given to the impact of solutionizing temperature on the content of the delta phase and on the evolution of the grain size.

V.3.A Metallographic samples preparation

Samples for SEM investigations are mounted in conducting thermosetting resins and ground down under running water using a series of silicon carbides papers finishing on 1200 grit. Polishing is carried out using 6, 3 and 1μm diamond pastes.

An electrolytic etching at 2.5 V potential in a bath containing 10 ml H_2SO_4 in 100 ml of water is used to reveal microstructural details.

V.4 Transmission Electron Microscopy (TEM)

The transmission electron microscopy (TEM) is a microscopy technique whereby a beam of electrons is transmitted through an ultra thin specimen, interacting with it and revealing the finest details of the material structure. Because the wavelength of electrons is much smaller than that of photons (where wave-length corresponds to the visible region of the spectrum), the optimal resolution attainable for TEM images is many orders of magnitude better than that from a light microscope

Sample preparation is a necessary prerequisite: a specific thickness is required to allow the electrons transmission through the sample.

The first step consists in sectioning the material into thin wafers, approximately 0.1 μm in thickness. This operation determines the orientation of the sample in the microscope, especially when the crystallographic orientation is investigated.

The sample is then submitted to a mechanical polishing employing SiC disks driven by motors of adjustable speed. Polishing begins with a coarse abrasive and carries on

progressively with finer abrasive grains. This produces a surface of decreasing roughness and homogeneously eroded.

The specimen, consisting in thin plate of 30 µm thickness, is then subjected to an electrolytic thinning with a STRUERS Tenupol-5® equipment. The electrolytic bath consists of a solution of 900 ml of methanol, 100 ml of perchloric acid and 200 ml of Butyl Cellosolve. The procedure is carried out at –15°C applying a current ranging between 500 and 600 mA. Dissolution takes place on both faces until the specimen is perforated. The voltage is turned off to avoid further dissolution of the hole thin edges. The specimen, placed on a support microscope grid, is ready to be observed.

Investigation are performed at CEMES-CNRS laboratory in Toulouse using a JEOL-JEM 2010 microscope equipped with a single crystal LaB6 filament and an accelerating voltage equal to 200kV. This system ensures a better brightness than a common Tungsten filament and a high resolution imaging with 0.23 nm point resolution.

V.5 Image Analysis

The image analysis is an analytical technique prone to exploit the information contained in pictures. The main objective associated to this methodology consists in a specific modification of the picture to quantify the relevant information.

For our researches, the technique is used for a stereological analysis of the delta (δ) phase in order to quantify the surface fraction and the morphology of the precipitates. The employed methodology is based on a series of operations based on mathematical concepts. Analyses are performed using Aphelion® software: every stage of the study is considered into a specific algorithm composed of four main operations. The preliminary stage is based on a pre-treatment/ filtering operation prone to increase the image quality through a contour smoothing and contrast enhancement. The image treatment is followed by a contrast inversion and binarization (Figure III. 15). Delta precipitates are then isolated from the background (matrix) and the procedure is concluded by a morphological characterisation prone to describe their sizes and shapes through quantitative parameters. The algorithm contains also a specific function which allows the erosion of all particles having connections with the image edges.

Two parameters are associated to the circularity and elongation of each precipitate: the relative values range between 0 and 1.

Circularity (called C(x)) is defined as the ratio between the equivalent area circle perimeter divided by the actual particle perimeter. When C(x) =1, the particle is perfectly circular. Conversely, when the circularity value is closed to zero, the precipitate exhibits irregular edges.

Elongation (called R(x)) is calculated from one minus the ratio between the ellipse axes (major axis L and minor axis l). Considering a perfect circular particle (L=l), elongation is equal to zero.

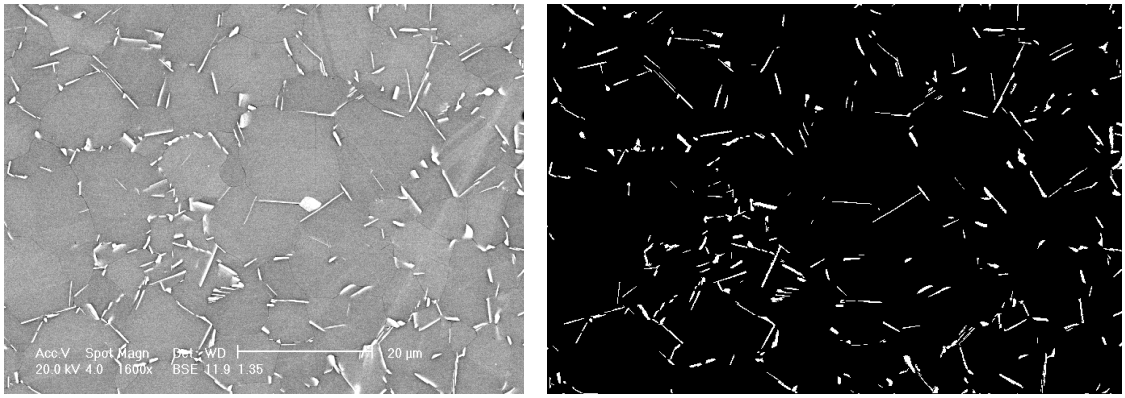

(a) **(b)**

Figure III. 15 : Image analysis - original picture (a) and relative binarization (b).

V.6 Synchrotron X-ray diffraction

Synchrothon XRD represents an advanced method for the determination of macromolecular structures that are unsuitable to detect using conventional XRD sources.

In this study, measurements are made at the European Synchrotron Radiation technique (ESRF, Grenoble, France) where the radiation could be accessed at 30 beam-lines. All tests have been carried out using the ID15 line which is dedicated to the high energy diffraction.

The interest of these studies is the exploitation of the high intensity and penetration depth of the synchrotron radiation for the intermetallic phases detection in Inconel 718. The photon energy used is equal to 87 keV, corresponding to the wavelength of 0.1414 Å.

The technique involves a direct collection of diffracted patterns in digital form, using a high resolution CCD camera. All the diffraction data are collected in one measurement: the ring-like pattern, produced on a plane normal to the incident beam, is then acquired using an X-ray image intensifier. The number of complete diffraction rings is optimised by choosing the appropriate distance between the sample and the CCD camera.

The radial integration of the ring intensity, around the entire radius, gives a conventional one-dimensional pattern which can be exploited by the same method used for XRD.

V.7 Thermo-analytical techniques

Thermal analysis stands for a group of techniques in which the properties of the alloy are monitored as function of time and temperature. Basically, methods of thermal analysis allow the study of chemical/metallurgical processes that are associated to heating or cooling.

The aim of this work is to characterize the microstructural evolutions of Inconel during the thermal treatment. For this purpose, as indicated in Figure III. 16, the thermo-analytical methods improve the knowledge provided by the image techniques (SEM, Image analysis and TEM) monitoring the phases transformations mechanisms and their kinetics.

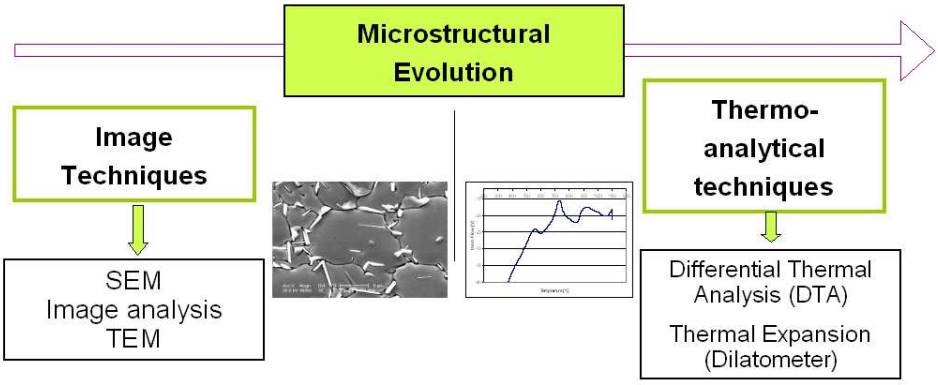

Figure III. 16 : Analytical techniques for the study of structural evolutions.

V.7.A Differential Thermal Analysis (DTA)

Differential thermal analysis (DTA) measurements are conducted with a Setaram SETSYS 16/18 system. The test specimen, whose weight is equal to 0.1 g, is situated in high purity recrystallized alumina crucible that is suspended from the top of the vacuum resistance-heated furnace. The heating ramp is fixed at 10°C/min in order to provide a good resolution in the peaks observation. All tests are carried out under helium atmosphere to reduce the oxidation risks. Prior to the first run, the DTA cells were completely purged with the inert gas. this methodology is applied to the study of Inconel 718 by the aim to define the solvus temperaturew of the various intermetallic phases (δ, γ' and γ"),

V.7.B Thermal Expansion measurements

Comparative measurements to DTA are carried out with an horizontal push-rod dilatometer (Netsch DIL 402 C) with a resolution up to 8 nm/digit.

The dilatometer consists of a double wall alumina tube, an alumina push rod and a movable furnace (Figure III. 17). The inner alumina tube contains the sample support, the thermocouple and guides the push-rod, while the outer tube acts as vacuum chamber. The alumina push-rod is balanced by a counter weight to avoid pressure on the sample, while the change in length are inductively measured by a LVDT system **[Hermann et al.,2003]**.

Cylindrical samples, with a diameter of 8 mm and a length of 8 mm, are used. Measurements are performed with heating and cooling rates equal to 10°C/min, under helium atmosphere.

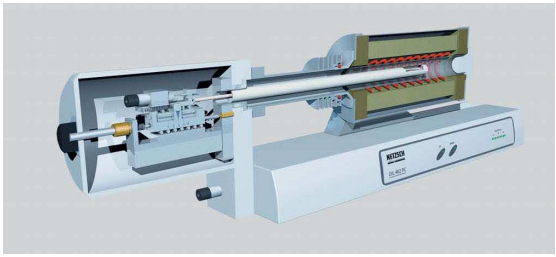

Figure III. 17 : Schematic representation of the dilatometer.

Thermal expansion measurements provide provide information to the DTA data, investigating, in detail, the microstructural evolution of the alloy under the effect of the

thermal treatment.

V.8 Thermal treatments method

In order to characterize the microstructural evolutions of Inconel 718 and the effect of microstructure on the fatigue behaviour, different thermal treatments are conducted, as it will be reported at the end of the chapter.

Two modalities of tests are considered as function of the specific objective:

Microstructural characterisation: all heat treatments are performed in a laboratory vertical furnace under an argon atmosphere. Small cylindrical samples (Φ= 18 mm and l= 25 mm), extracted from the LCF specimen heads are considered for these treatments. Assumption is made that no changes occurs in this parts of specimen during the thermo-mechanical tests thanks to the water cooled fixtures that enable the over-heating of the material. All samples are cooled in air at the end of thermal treatment.

Material optimisation for fatigue tests: in this case all treatments are carried out in an industrial furnace in collaboration with Thermi-Garonne in Toulouse. The solutionizing treatments are carried out under vacuum at different temperatures using an irradiation heating system and employing oil or air quench, depending from the treatment specification . Ageing treatments have been conducted under convective heating which allows a better control of temperature especially at low temperature (below 850°C). Temperatures are strictly controlled by the use of a thermocouple placed at the heart of a reference sample of Inconel 718.

V.9 Isolation and determination of the lattice misfit of intermetallic phases

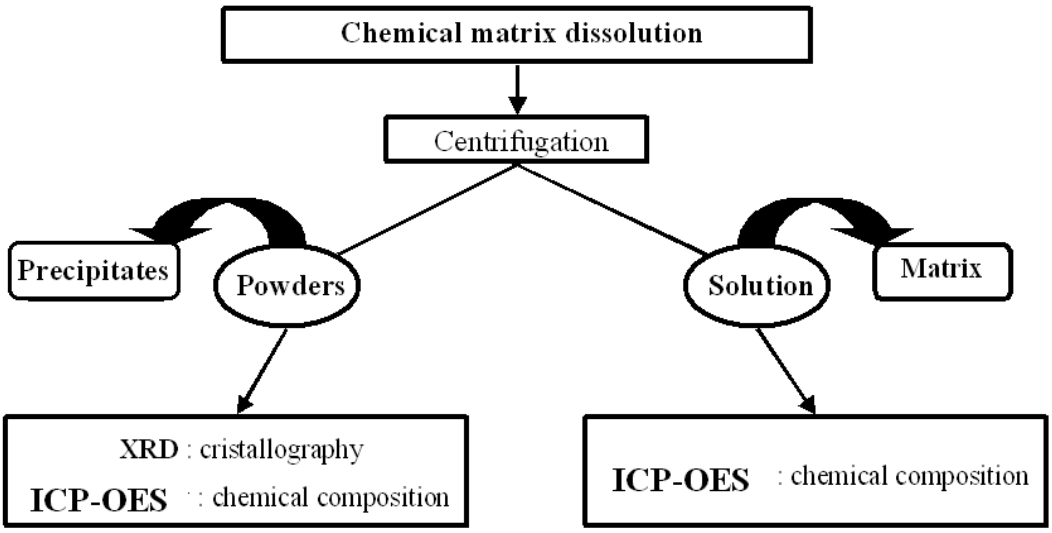

Figure III. 18 : Experimental method adopted for intermetallic phases extraction and determination.

V.9.A Precipitates extraction

Intermetallic precipitates (δ, γ' and γ") are extracted using anode selective electrolysis. To determine the conditions under which the processes of electrolytic extraction should be conducted, the anodic polarisation curves have been evaluated. Adequately prepared heat treated samples are immersed, at a temperature of 25 °C, in an electrolyte solution whose composition is confidential. A three electrodes electrochemical cell using Inconel 718 sample as the working electrode, while a platinum auxiliary electrode and a Calomel reference electrode. Typically, one hour of electrolytic dissolution leads to a precipitates extraction of 6 g/l. The solution is then centrifuged during 40 minutes with a Beckman Coulter Avanti J-30I centrifugal machine equipped with a JA-30.50Ti rotor. The adopted radial acceleration is approximately 110 000G. After centrifugation, the powder is ultrasonically cleaned and then placed in a vortex mixer. Afterwards, a second centrifugation under the same experimental conditions is performed. After three cycles, the powder is dried at 65°C for 12 hours.

V.9.B X-ray diffraction

In our specific studies, XRD is employed for the identification of the extracted intermetallic phases (δ, γ' and γ") and for the study of the relative experimental lattice parameters.

The XRD analyses are carried out by a Philips X-PERT diffractometer equipped of a Cu anticathode (λ_{Cu}=0.154 nm) whereas the exploitation of the diffraction patterns is realised by X'PERT High Score® software developed by PANalytical®.

The experimental configuration, used for all tests, is reported in Figure III. 19.

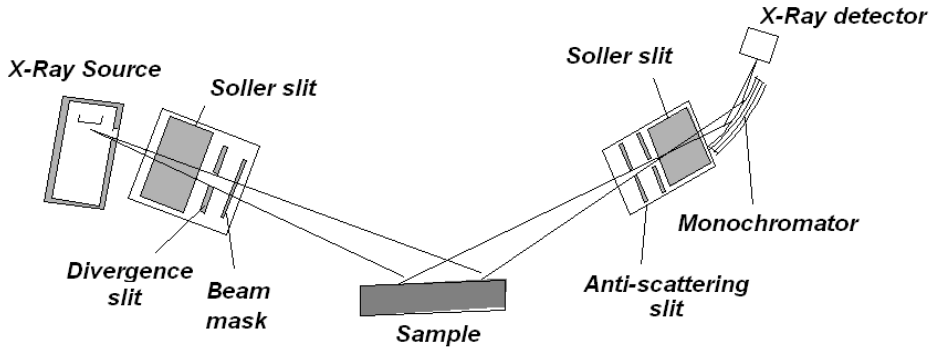

Figure III. 19 : Experimental configuration for XRD analyses.

In our specific studies, XRD is employed for the identification of the extracted intermetallic phases (δ, γ' and γ") and for the study of the relative experimental lattice parameters.

V.9.C Crystallographic lattice parameters evaluation

The XRD patterns obtained from individual precipitates extraction give important information about the size and the shape of the unit cells, which determine the relative position of the diffraction peaks.

According to Bragg law, $\lambda = 2d\sin\theta$, it can be written:

$$\frac{1}{d_{hkl}^{\ 2}} = \frac{4\sin^2\vartheta}{\lambda^2} \qquad \textbf{Eq. III. 1}$$

In such a way, through the study of the properly indexed XRD patterns, the lattice parameters can be evaluated combining the Bragg law with the plane spacing equation.

VI Conclusions

The chapter has been dedicated to the description of the experimental methods used for the research studies. Three types of investigation techniques are considered: thermo-mechanical, microstructural and thermo-analytical methods.

A detailed description of the standard grade of Inconel 718 has been reported in the second part of the chapter. A particular attention has been given to the microstructure features and to the standard heat treatment process. Finally, a specific experimental approach for the microstructural optimization is presented. Alternative thermal treatments have been designed in order to maximize the mechanical properties of the alloy.

Table III. 7 reports the alternative grades of Inconel 718 that will be considered for the microstructural and thermo-mechanical characterizations, carried out in Chapter IV (standard grade in various LCF test conditions) and in Chapter V (alternative grades under LCF typical of extrusion conditions).

	HEAT TREATMENT PARAMATERS					TENSILE TESTS DATA			
Heat Treatment	T_a (°C)	T_{R1} (°C)	t_{R1} (h)	T_{R2} (°C)	t_{R2} (h)	YS [MPa]	E [MPa]	UTS [MPa]	A [%]
STANDARD	955 [1h]	720	8	620	8	**998**	**163216**	**1228**	**35.3**
Tr.990	990 [1h]	720	8	620	8	**1078**	**164495**	**1271**	**36**
Tr.1000	1000 [1h]	750	4	620	8	**1116**	**165596**	**1297**	**34.6**
API 6A	1032 [1.5h]	785	6	/	/	**755**	**162691**	**996**	**46**
DIRECT AGE (DA)	/	720	8	620	8	**1133**	**165500**	**1280**	**33**

Table III. 7 : Summary of Inconel 718 thermal treatments

VII References

[ASTMB637] ASTMB637 "*Standard Specification for precipitation-hardening Nickel alloys, bars forgings and forging stock for high temperature Service*"

[Barbadillo de et al.,2010] Barbadillo de, J. J. and Mannan, S. K. "*Alloy 718 for Oilfiel Applications*". 7th International Symposium on Superalloy 718 and Derivatives (2010).

[Delagnes,1998] Delagnes, D. "*Comportement et tenue en fatigue isotherme d'aciers à outils Z 38 CDV5 autour de la transition fatigue oligocyclique endurance*". PhD Thesis, Ecole des Mines de Paris (1998).

[Donachie,2002] Donachie, M. J. "Superalloys: a technical guide", ASM International, p., (2002).

[Fu et al.,2009] Fu, S. H., Dong, J. X., Zhang, M. C. and Xie, X. S. "Alloy design and development of INCONEL718 type alloy." *Materials Science and Engineering a-Structural Materials Properties Microstructure and Processing* 499(1-2): pp. 215-220, (2009).

[Garat et al.,2008] Garat, V., Cloue, J. M., Poquillon, D. and Andrieu, E. "Influence of Portevin-Le Chatelier effect on rupture mode of alloy 718 specimens." *Journal of Nuclear Materials* 375(1): pp. 95-101, (2008).

[Hermann et al.,2003] Hermann, W., Neuer, G., Leitner, G., Poeßnecker, W., Quested, P., Richter, F. and Sockel, H. G. "Thermophysical Properties Benchmark Tests on a Monocrystalline Ni-base Alloy." *Advanced Engineering Materials* 5(1-2): pp. 46-51, (2003).

[Horvath et al.,2001] Horvath, W., Zechner, W., Tockner, J., Berchthaler, M., Weber, G. and Werner, E. A. "*The effectiveness of direct aging on Inconel 718 forgings produced at high strain rates as obtained on a screw press*". Superalloys 718, 625, 706 and Various Derivatives**:** 223-228 (2001).

[Klose et al.,2003] Klose, F. B., Ziegenbein, A., Weidenmüller, J., Neuhäuser, H. and Hähner, P. "Portevin-LeChatelier effect in strain and stress controlled tensile tests." *Computational Materials Science* 26: pp. 80-86, (2003).

[NACE/MR0175] NACE/MR0175 "*NACE MR0175-2003 Impact on API 6A Equipment and Customers*"

[Rodriguez et al.,1995] Rodriguez, P. and Venkadesan, S. "Serrated Plastic Flow Revisited." *Solid State Phenomena* 42-43: pp. 257-266, (1995).

[Taina et al.,2010] Taina, F., Pasqualon, M., Delagnes, D., Velay, V. and Lours, P. "*Effect of the LCF loading cycle characteristics on the fatigue life of Inconel 718 at high temperature*". 7th International Symposium on Superalloy 718 and Derivatives (2010).

Chapter IV

Fatigue performances of standard Inconel 718: the influence of material-extrinsic parameters

"Seule la paresse fatigue le cerveau".

Louis Pauwels

Chapter IV - Fatigue performances of standard Inconel 718: the influence of material-extrinsic parameters

I Introduction

The aim of this chapter is to assess the fatigue behaviour of Inconel 718, at 550°C, under various LCF conditions. The first part deals with the cyclic behaviour of the alloy. Different examples of tests are carried out in order to define a cyclic model prone to evaluate the stress-strain state in an extrusion die. Some parameters are used to describe and characterize the cyclic behaviour of Inconel 718. Secondary, a series of strain-controlled low cycle fatigue tests is conducted to investigate the impact of various parameters on the behaviour of the material. Namely, focus is placed on the influence of the *extrinsic parameters* such as the cycle frequency, the strain rate, the holding time under load and the stress relaxation. A detailed characterisation of the fatigue-induced rupture surfaces is performed to analyse the role of the alloy microstructure on the mode of crack propagation. In order to account for the time dependent effect of the mechanical response of the alloy, the Portevin-Le Châtelier effect and the oxidation behaviour of the material are discussed. Results are analysed in terms of Manson-Coffin plots to discriminate the relative impact of the various tested parameters on the stress/strain response and the fatigue life of the material.

Finally, a fractographic method, based on microscopical investigations, is proposed in order to predict the crack growth rate of prevalent cracks under LCF conditions.

II Cyclic behaviour of Inconel 718

During hot extrusion, dies experience thermo-mechanical loading, whose magnitude depends on the working conditions (extrusion speed, ratio,) and the billet material. The critical regions of the tools are generally edges, section changes and areas under high stress triaxialities and large accumulated inelastic strains. The failure usually originates from a combination of different factors, like an arising local overload, material defects, wear at the contact surface tool-billet, as well as creep-fatigue damage.

The extrusion industry tries to accelerate the manufacturing process by increasing the billet temperature and by accelerating the press speed. These parameters contribute to modify the loading conditions which have a negative impact on the service life of the tools. As a consequence, each component of the extrusion tool (die, backer, container and dummy block) must be carefully designed in order to find optimum process conditions and reduce the risks of failure. Numerical simulation seems to be adequate to provide the strain-stress response induced at different locations of the tool and to compare different operating conditions (extrusion speed, die design, billet materials)**[Krumphals et al.,2010]**.

Most of today's Hydro Aluminium extrusion die developments are based on numerical simulations performed using static material model (isotropic hardening model based on 550°C tensile test results) to provide the strain-stress response at different locations of the tool. The progressing use of Inconel 718 to manufacture extrusion dies has provided significant increase performance and profitability in association with high die cost. It is of interest, in some clear cases, to have the possibility to simulate the actual behaviour of the die material towards Creep-Low Cycle fatigue. The die experiences this type of loading through extrusion cycles and a progressive, non-linear plastic deformation leads to the loss of extruded profile tolerances. For these reasons, it could be critical to assess the "lifetime potential" of a given die design by Finite Elements (FE) analysis using a ***"dynamic material model"***. The output may simplify the decision to manufacture the die using such design.

Some prerequisites are, however, mandatory to achieve these results. First, a cyclic elasto plastic behaviour model has to be identified from one dimensional fatigue tests. The complexity of its formulation depends on the considered thermo-mechanical loading conditions. Finally, the model will be integrated into a FE code in order to perform dynamic calculations at the scale of the extrusion dies. Results provided by these analyses can be compared to the stress-strain level and die deflection cyclically measured on the extrusion dies and calculated by the traditional FE simulation. These topics will be described in the next sections, with a particular attention to the adopted experimental procedure.

II.1 Experimental procedure for behaviour model identification

An optimized test procedure has been developed within the ICA laboratory in order to reduce the number of test specimens and to decrease manpower and time required for model parameter identification.

Strain controlled fatigue tests including different strain rates, tensile and compressive dwell times will be performed. These tests play an important role in the assessment of the Baushinger effects, cyclic softening, strain rate sensitivity and stress relaxation during holding time. All tests have been performed using LCF specimens treated with the Tr.990 procedure.

All parameters of these tests have been carefully selected in order to represent the typical loads expected in dies giving a general validity of the model whatever the extrusion process. Figure IV. 1 illustrates the experimental procedure and the related identification methodology considered in this study.

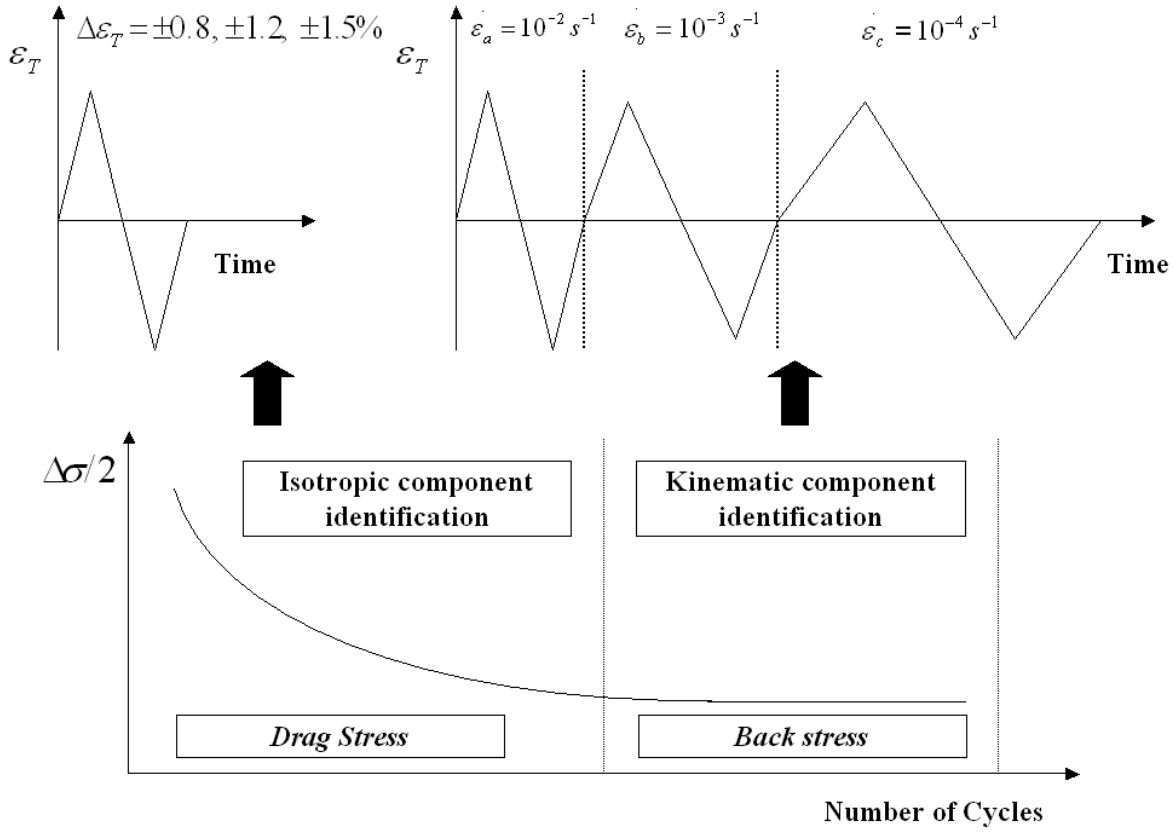

Figure IV. 1 : Experimental tests and related identification methodology [Velay,2003].

The fatigue test procedure is defined by a symmetrical total strain push-pull test with a fixed strain range $\Delta\varepsilon_T$ and a constant strain rate $\dot{\varepsilon}$. The adopted total strain range is varied from ±0.8% to ±1.5%. The number of cycles is selected to reach a cumulative plastic strain close to 3 for each applied strain range. Then, when the pseudo-stabilised cycle (linear softening) is reached, cyclic tests are performed with a variation of strain rate. Three levels of strain rate are considered: $\dot{\varepsilon}_a = 10^{-2}\,s^{-1}$, $\dot{\varepsilon}_b = 10^{-3}\,s^{-1}$ and $\dot{\varepsilon}_a = 10^{-4}\,s^{-1}$. For all the tests, only one level of temperature T=550°C is investigated. Table IV. 1 illustrates the different fatigue

test conditions.

	Strain range $\Delta\varepsilon_T$ **[%]**	**Strain rate** $\dot{\varepsilon}$ **[s^{-1}]**	**Stabilised cycle**
Test 1	±0.8	10^{-2}	350
Test 2	±0.8	10^{-3}	300
Test 3	±1.2	10^{-2}	150
Test 4	±1.2	10^{-3}	150
Test 5	±1.5	10^{-3}	80

Table IV. 1 : Experimental LCF test conditions.

Figure IV. 2- Figure IV. 5 present some experimental results. Figure IV. 2 and Figure IV. 3 show that no significant effect of the strain rate is observed, cyclic plasticity induced in both tests is very close. The viscous effect can be assumed negligible. Moreover, an increase of the strain amplitude applied leads to a more important cyclic plasticity and higher stress levels (Figure IV. 4). This phenomenon can also be observed on the stabilised cycle (Figure IV. 5).

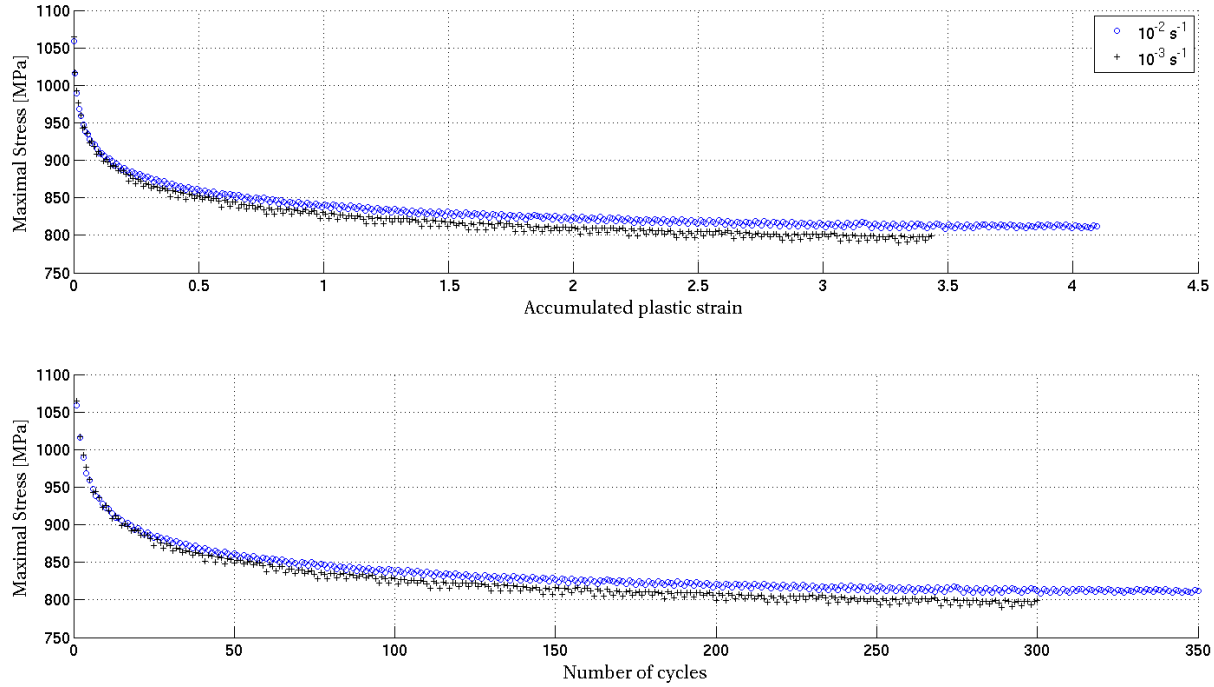

Figure IV. 2 : Strain controlled fatigue tests with a total strain amplitude of ±0.8% (T=550°C).

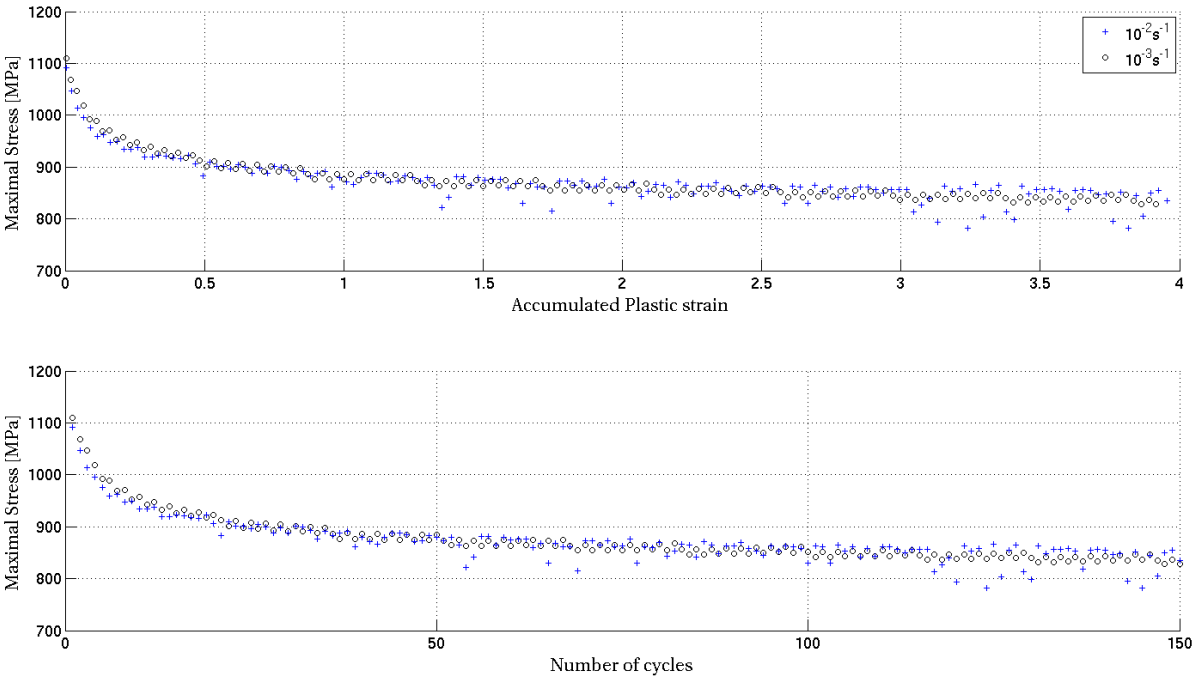

Figure IV. 3 : Strain controlled fatigue tests with a total strain amplitude of ±1.2% (T=550°C).

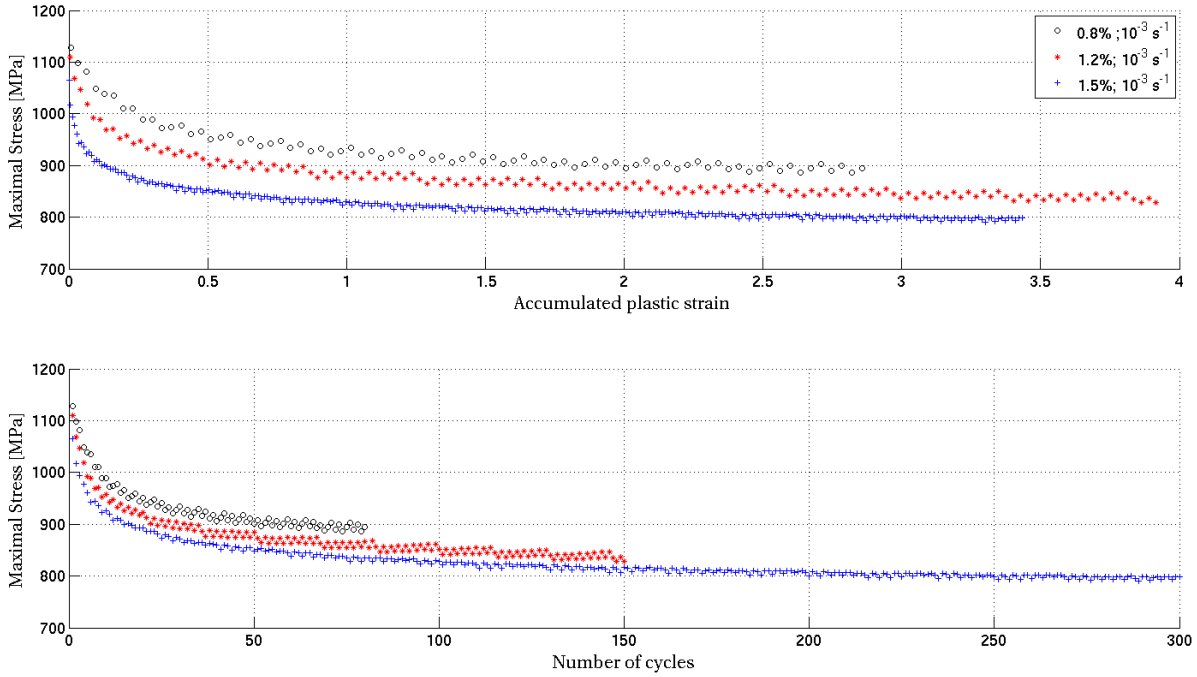

Figure IV. 4 : Comparison of strain controlled fatigue tests at different strain amplitudes: ±0.8, ±1.2%. and ±1.5.% (T=550°C).

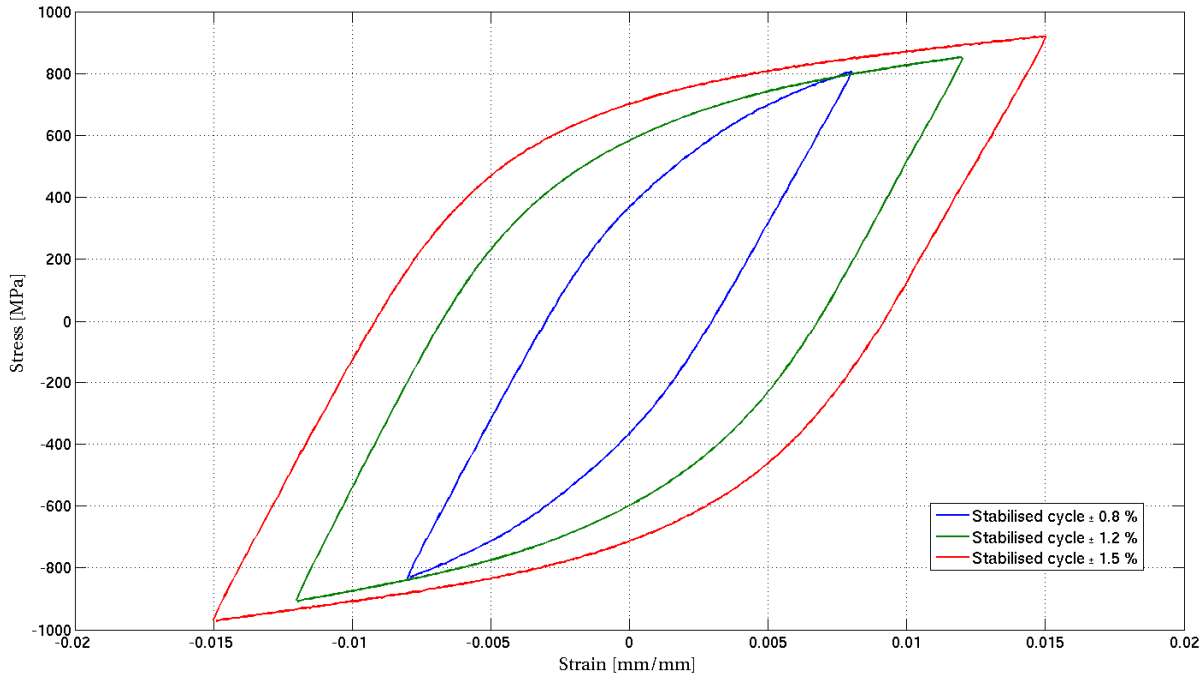

Figure IV. 5 : Stabilised stress-strain responses for different strain ranges (T=550°C).

II.2 Identification and validation of a cyclic elasto-plastic model

The considered material model is a rate-independent version of the nonlinear kinematic hardening model proposed by Chaboche **[Lemaitre et al.,1987; Chaboche et al.,1994; Ponnelle,2001; Velay,2003]**, whose formulation, according to the von Mises criterion, is expressed as:

$$F = \left(\frac{3}{2} (\{s\} - \{\alpha\}) : (\{s\} - \{\alpha\}) \right)^{\frac{1}{2}} - R = \sigma_{eq} - R \qquad \textbf{Eq. IV. 1}$$

Where R is the isotropic hardening and $\{\alpha\}$ the kinematic hardening.

According to the normality rule, the associated flow rule becomes:

$$\left\{ \dot{\varepsilon}_{pl} \right\} = \dot{\lambda} \frac{\partial F}{\partial \{\sigma\}} = \frac{3}{2} \dot{\lambda} \frac{(\{s\} - \{\alpha\})}{\sigma_{eq}} \qquad \textbf{Eq. IV. 2}$$

Where $\dot{\lambda}$ is the plastic multiplier.

The development of the internal back-stress tensor $\{\alpha\}$ represents a strain-induced anisotropy. The evolution of $\{\alpha\}$ is related to the Bauschinger effect via the displacement of the midpoint of the elastic range, the so called kinematic hardening.

As a consequence, the back stress is defined as a superposition of two kinematic hardening models:

$$\{\alpha_1\} = \{\alpha_1\} + \{\alpha_2\} \qquad \textbf{Eq. IV. 3}$$

Where $\{\alpha_1\}$ represents the fast nonlinear kinematic hardening at low inelastic strain and $\{\alpha_2\}$describes the slower hardening with inelastic strain at larger deformation ($\Delta\varepsilon_p$>1%).

The kinematic hardening evolution is defined as:

$$\left\{ \dot{\alpha}_i \right\} = \frac{2}{3} C_i \left\{ \dot{\varepsilon}_{pl} \right\} - \gamma_i \{\alpha_i\} \dot{\lambda} \qquad \textbf{Eq. IV. 4}$$

Where C_i and $\gamma_i \cdot (i = 1,2)$ are temperature and material dependent parameters.

Moreover, the plastic multiplier can also be noted as:

$$\dot{\lambda} = \sqrt{\frac{2}{3} \left\{ \dot{\varepsilon}_{pl} \right\} : \left\{ \dot{\varepsilon}_{pl} \right\}} = \dot{\hat{\varepsilon}}_{pl} \qquad \textbf{Eq. IV. 5}$$

The increase (R) of the initial elastic limit (k) describes the expansion of the elastic range, the so called isotropic hardening

In such a way, the isotropic hardening variable (*drag stress*) takes the following form:

$$R = k + R_0 \hat{\varepsilon}_{pl} + R_\infty \left(1 - e^{-b \hat{\varepsilon}_{pl}} \right) \quad \textbf{Eq. IV. 6}$$

Where k is the elastic limit, R_0, R_∞ and b are temperature and material dependent parameters.

To be more precise, R_0 reflects the linear softening of the material, b characterizes the rate of isotropic hardening with the cumulated inelastic strain $\hat{\varepsilon}_{pl}$ and R_∞ the asymptotic value assumed by R where $\hat{\varepsilon}_{pl} \to \infty$ (Cyclic softening).

The whole model includes 9 parameters to be determined, 4 parameters to define the isotropic component (k, R_0, R_∞ and b) and 4 parameters to define the kinematic component C_i and $\gamma_i (i = 1,2)$. The Young modulus (E) is also required.

The identification process requires a calibration of the coefficients based on the raw data of the isothermal LCF tests. Solutions are obtained using optimization algorithms (such as Levenberg-Marquardt algorithm in Z-set software) and adopting a step by step procedure. In this way, the coefficients associated to the kinematic law are identified analyzing the pseudo-stabilized cycles obtained from the LCF tests performed at different strain rates.

Then, the previously calibrated parameters represent a good base for the next steps, allowing good quality solutions for the isotropic coefficients. The method consists in a minimization of the error function which represents the difference between the experimental and the simulated data. The calibrated values are presented in Table IV. 2.

E [MPa]	***k*** [MPa]	C_1 [MPa]	γ_1	C_2 [MPa]	γ_2	R_0 [MPa]	R_∞ [MPa]	***b***
160200	670	223140	1000	38510	145	-13.25	-190	+3.41

Table IV. 2 : Identified model behaviour parameters for Inconel 718 at 550°C.

Figure IV. 6 presents the comparison between experimental and calculated strain-stress responses for the stabilised cycle, selected at half life, for three different strain ranges (±0.8%, ±1.2% and ±1.5%). Figure IV. 7 shows the evolution of the maximal stress at each cycle versus the cumulated plastic strain. The behaviour model is able to take into account the cyclic softening of the material.

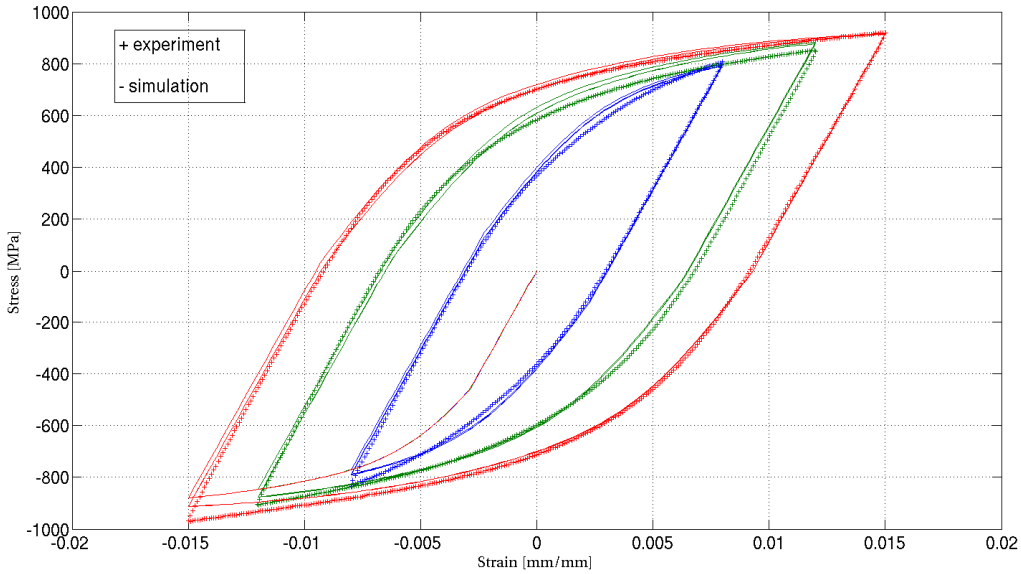

Figure IV. 6 : Comparison of the strain-stress loops for different strain ranges at a strain rate of 10^{-3} s^{-1} (Stabilised cycle)

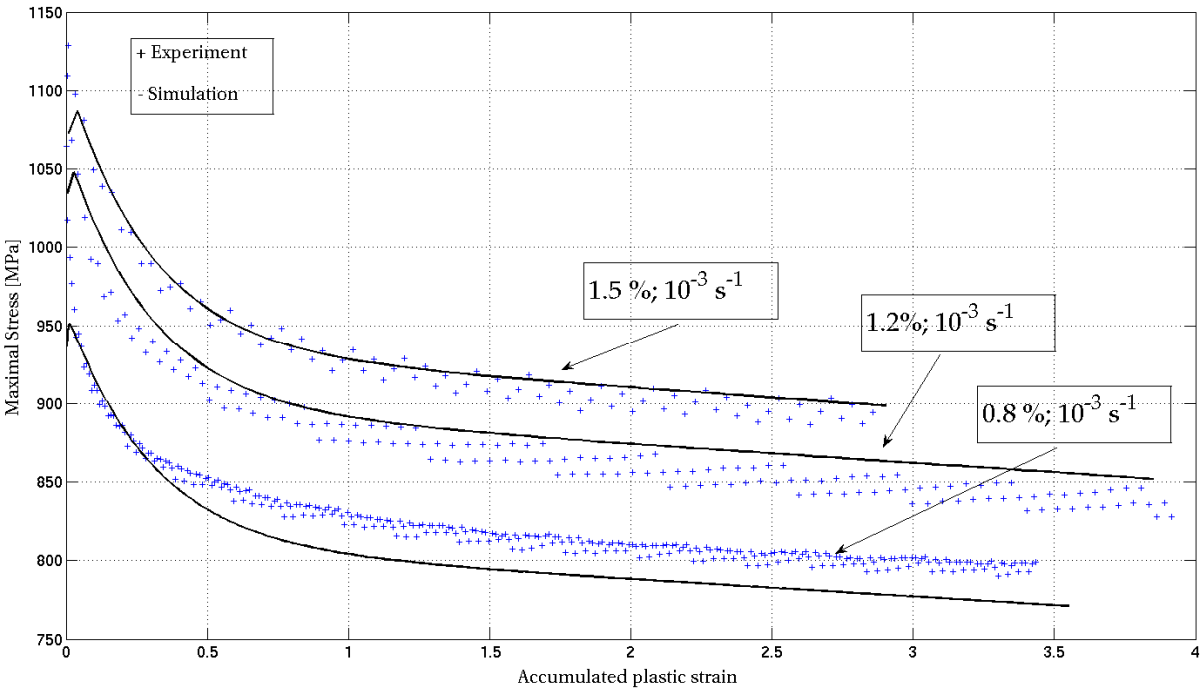

Figure IV. 7 : Cyclic softening for various strain ranges; comparison of simulation and experiment.

Finally, once the constitutive parameters have been identified, the model needs to be validated for various mechanical conditions. Experimental fatigue tests carried out at 550°C by the application of a trapezoidal signal in total strain control (extrusion conditions simulation (see chapter I)), are considered and the stress-strain responses are compared with those assessed by the elasto-plastic model. The selected lifetime tests include total strain amplitudes ranging between 1.0 and 1.5 % at a strain rate of $5x10^{-3}$ s^{-1}. Figure IV. 8 reports a comparison of the simulated and experimental stress-strain responses respectively evaluated at the first cycle (a), during preliminary softening stage (10^{th} cycle) (b), and at the half-life (stabilised stage) (c).

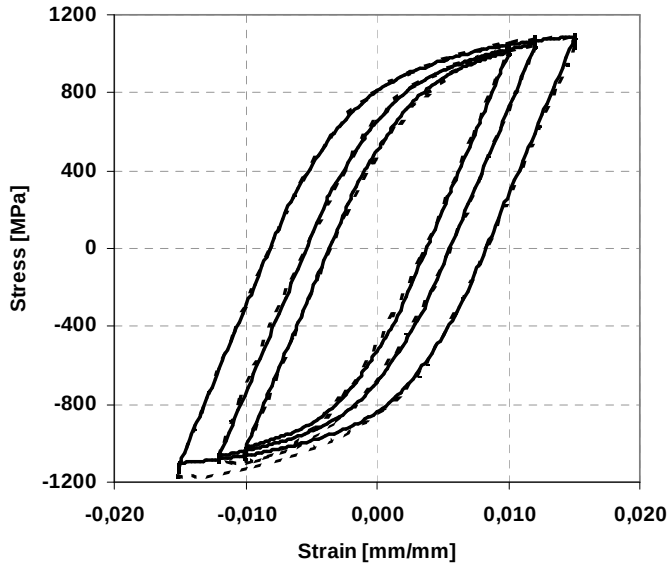

(a)

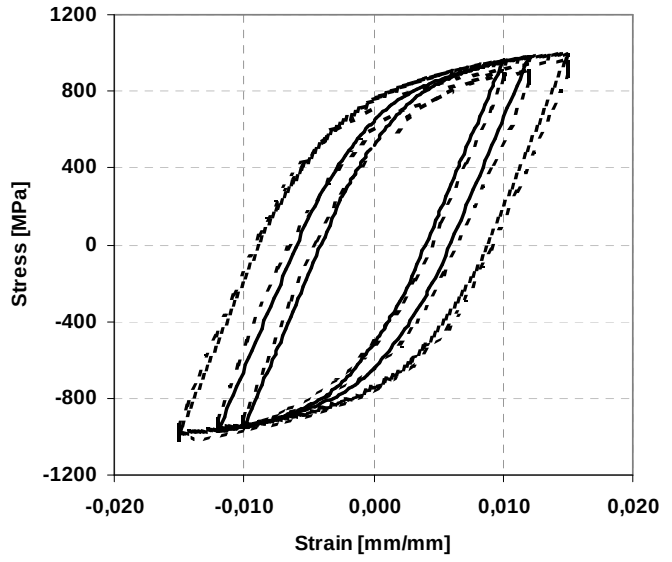

(b)

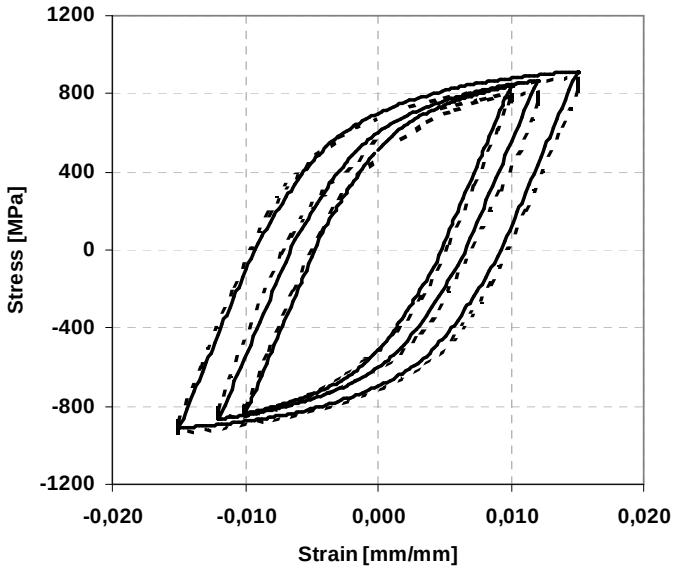

(c)

Figure IV. 8 : Stabilised stress-strain responses for various total strain (±1%,±1.2% and ±1.5%) at different stages of the LCF test. Dotted lines: experimental; Continuous line: simulation.

(a) first cycle; (b) preliminary softening (10th cycle); (c) stabilized cycle (half-life)

It is evident that the model is able to provide good agreement with all experimental evidences. The use of a cyclic behaviour model has been identified as a valid alternative to describe mechanical loadings close to those induced in the extrusion dies. It allows describing the Baushinger effect through a kinematic component and the cyclic softening of the material through a linear-non linear isotropic component. However, viscous effects, like strain rate effects or stress relaxation during holding time at maximum strain, are not considered in the model formulation. Moreover, the present model can be integrated in a Finite Elements code, prone to predict the stress-strain distribution at different locations of an extrusion die.

II.3 The application of the Dynamic Modelling to an industrial case: the Inconel 718 base tube extrusion die.

II.3.A Case description and model integration

The base tube die is a modular extrusion tool used to produce large volume of high strength Aluminium alloy D x t = 25 x 2 mm extruded tube. Figure IV. 9 shows the details of the die and its relative assembling configuration in the extrusion press (Longitudinal section view). A die plate insert bearing ring made of a heat resistant material (C) and a plate holder (D) is fitted into the die holder (A). A mandrel ring (B) is tightly adjusted on pole (E) on the holder **[Pasqualon,2010]**.

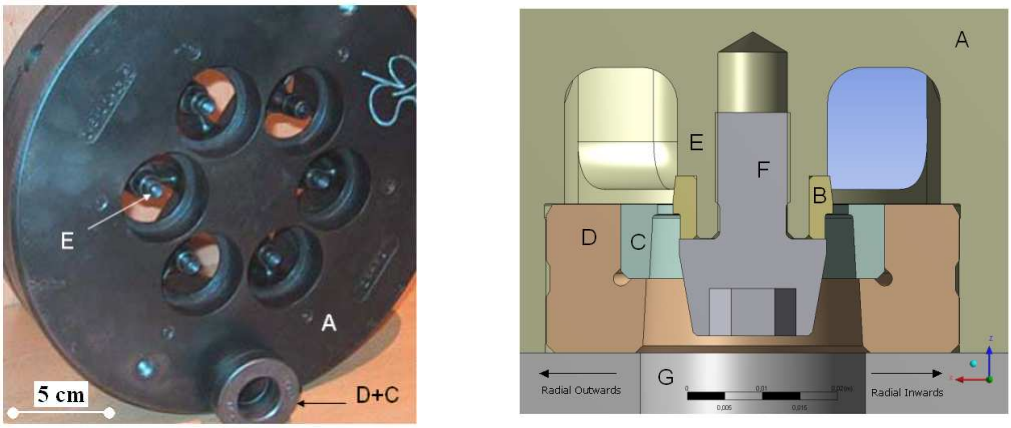

(a) **(b)**

Figure IV. 9 : Details (a) and assembling (b) of a base tube die for base tube extrusion.

Usually, the die holder (A) is made of H13 hot-work tool steel as well as the plate holder (D). Most of manufacturing tolerances of the die insert diameters are $\leq$ 0,01mm.

In extruding high strength alloy, a large press force is needed and repeated dies deflection lead to permanent centrifuge displacement of the mandrel pole (E) leading to Al-tube eccentricity defect. Out of tolerance tubes for eccentricity cannot be allowed in subsequent drawing process steps, low life die holders are then scrapped at significant cost.

Figure IV. 10 shows a x50 magnified displacement of die holder cross-section (upper part) showing the radial outward displacement of the pole E and attached ring B.

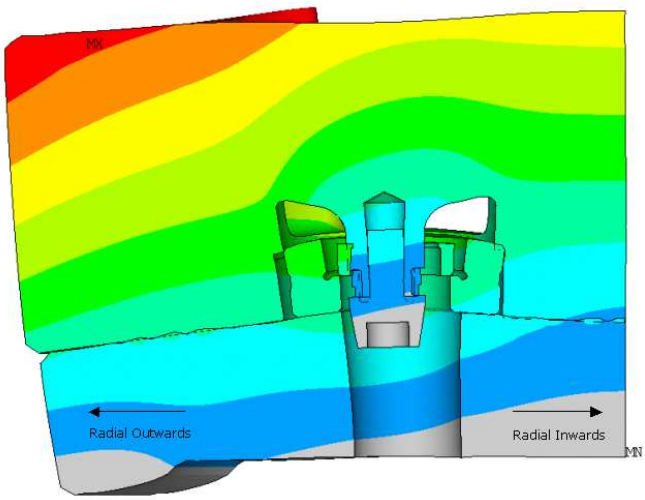

Figure IV. 10 : Magnified displacement (50x) of base tube die during early stage of press cycle showing outwards movement of the mandrel pole and ring.

A Ni-superalloy Modular Extrusion Die (Hydro Aluminium patent pending) including a holder (A) made of Inconel 718 was designed in order to improve life by controlling above rapid growing permanent displacement observed in H13 tool. The die assembling is completed by a simple bolt locking the mandrel insert and a backer die made in H13 steel (G).

To compensate the deflection of the poles, a mandrel to plate shift of 0.05 mm was introduced on the Inconel 718 holder.

Eccentricity assessment is performed on Al-tubes at end of each production run, following the practice illustrated in Figure IV. 11. Maximum eccentricity defined as the tube thickness difference in 6 and 12 o'clock positions is picked for each of the 6 cavities and plotted. Maximum permitted eccentricity being 0.2 mm.

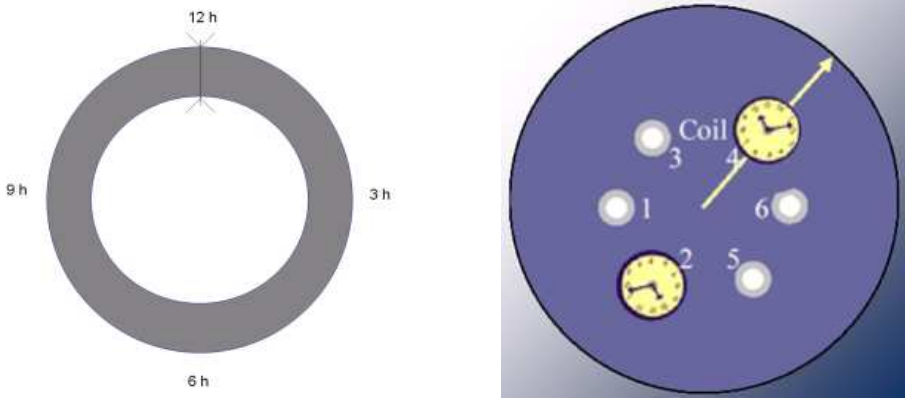

Figure IV. 11 : Tube eccentricity assessed by measurement of tube thickness at end of each production run. Measurements are performed at 6 and 12 o'clock positions along die radial axis.

The eccentricity evolution is the direct consequence of continuous deformation acting on specific zones of the die. For this reason, a specific knowledge of the stress/strain distribution through the tool during the extrusion process could be a valid support for an optimisation of the tool design and the enhancement of the product quality. In such a way, the elato-plastic model presented in the previous section could be integrated into a Finite Elements (FE) code in order to perform dynamic calculation at the scale of the base tube extrusion die for the first 25 cycles. All calculations were performed by a Hydro Aluminium external partner using

Ansys Software, taking into account the hydrostatic pressure die distribution, friction loading at the contact surfaces between die and alloy, force applied directly on the die by container during press cycle. Appropriate overall model symmetry are considered to optimize calculation time and simulation applies on a 1/12 "pie" shape section of the tool stack.

Figure IV. 12 shows output of the FE Analysis as the plastic strain distribution on a single cavity of the base tube holder respectively for the first and twenty-fifth cycle.

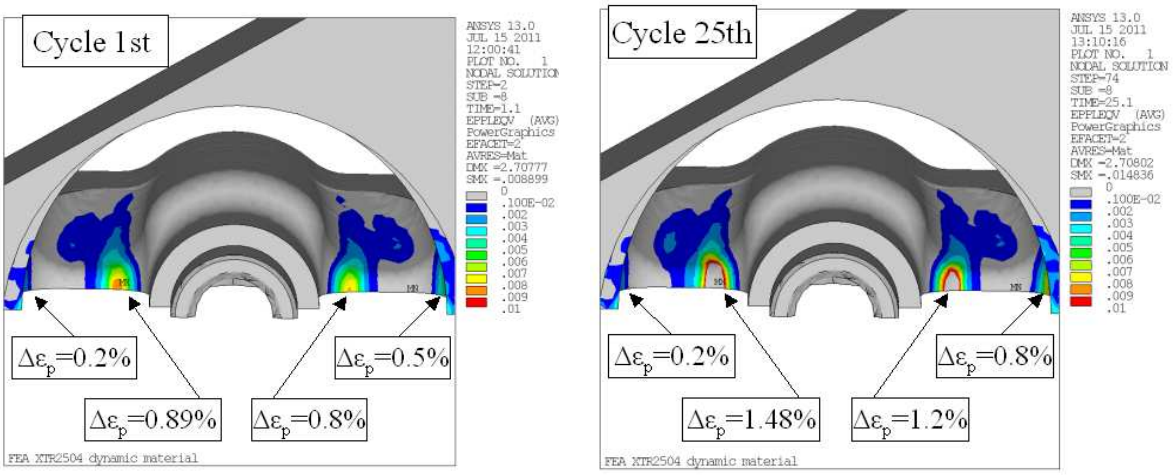

Figure IV. 12 : FE simulation obtained by the application of the Dynamic Modelling: Inelastic strain representations through the extrusion die for the 1st and the 25th cycle.

Pictures demonstrate that zones of transition between the bridge web and the mandrel pole exhibits highest stress concentration, called "Hot Spots" (see chapter I), well above the yield strength of the material generating a plastic deformation. Additional results of the FE simulations are reported in Appendix A.

These analyses corresponds to a specific instant of the extrusions cycle, called 'End of the press cycle", which corresponds to the extrusion of the final part of billet. This moment in the cycle corresponds to maximum deformation induced by combined loading effects on the holder.

Figure IV. 13 displays the evolution of the total, plastic and elastic strain acting in the most critical hot spot as a function of the number of simulated extrusion cycles. A significant enhancement of the plastic and total deformation is exhibited during the very first cycles, followed by a pseudo-stabilized stage where the inelastic strain increases much more slowly. As a result, the elastic strain, which is defined as the difference between the total and the plastic deformation, progressively decreases from the first cycle till assuming an asymptotic value.

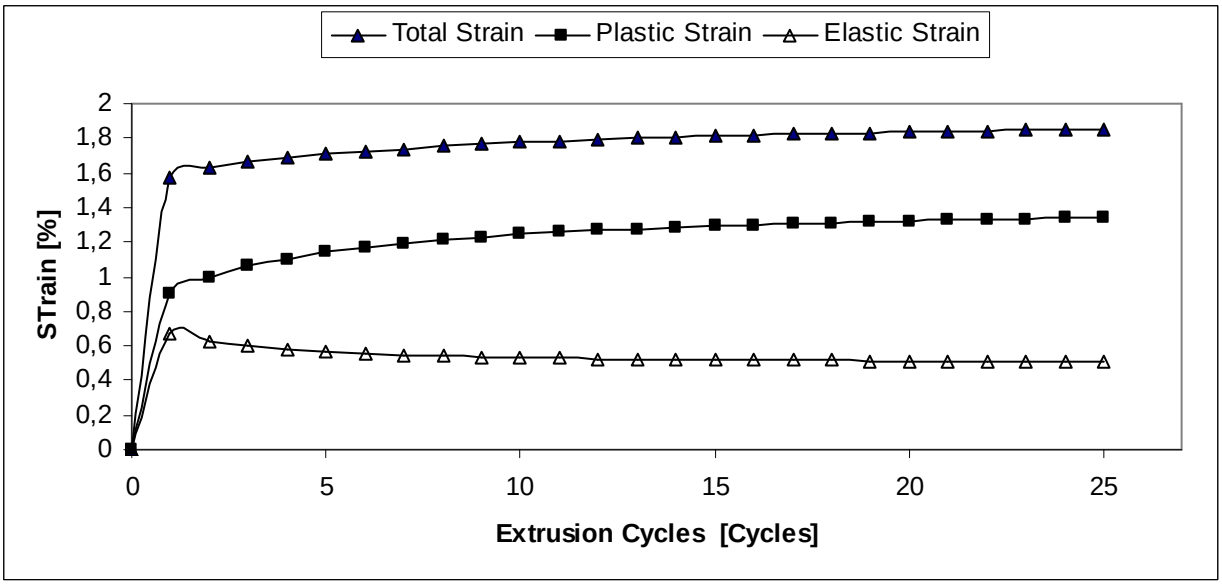

Figure IV. 13 : Evolution of the total, plastic and inelastic strains, predicted by FE in the most critical hot spot, as a function of the extrusion cycles

This specific strain evolution can be explained by a detailed investigation of stress distribution in the die. In addition to the simulations reported in Appendix A, that show the "σ_1" (S1) stress assessment for all extrusion cycles (1-25), Figure IV. 14 displays the evolution of the equivalent stress (Von Mises) in the most critical hot spot.

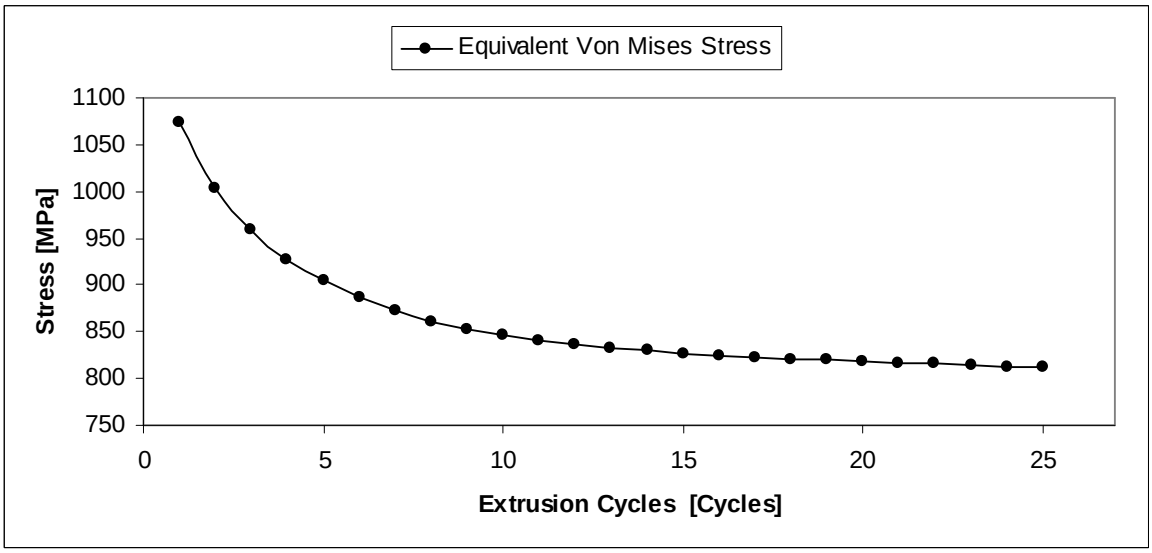

Figure IV. 14 : Evolution of the equivalent Von Mises stress, predicted by FE in the most critical hot spot, as a function of the extrusion cycles.

As expected, these regions exhibit a preliminary softening stage, where a severe decreases of the stress and an increase of the plastic strain occur, followed by a "pseudo stabilized-stage" where strain and stress amplitudes are approximately constant.

As reported in Chapter II, the cyclic response of the material is related to microstructural

evolutions. The shearing of γ" particles, operated by partial dislocations, is closely related to the preliminary fatigue stage. The precipitates cutting decreases the apparent mean area intercepted by dislocations along their slip planes, giving rise to a strong decrease of the applied stress. When the accumulated plastic strain increases, the deformation structure becomes more and more heterogeneous. Plasticity is associated to the deformation of intense deformation bands, identified by Fournier **[Fournier et al.,1977]** as twins, which control the pseudo-stabilized stage. The mechanical shearing of the precipitates, associated to a reduction of their size, is the main explanation for cyclic softening **[Kalluri et al.,2004]**.

II.3.B Dynamic model validation

The results obtained by the integration of the dynamic modeling into a FEA code needs to be confirmed experimentally. Also it is interesting to compare this material model with a simpler kinematic hardening model. For this purpose, two approaches could be followed:

- **FE benchmark with static model**: the results provided by the dynamic modelling are compared to those obtained by the traditional FE analyses performed on the same die design using a isotropic hardening material model (tensile test data).
- **Industrial benchmark**: the most limiting aspect associated to the base tube die consists in the centrifuge displacement of the mandrel pole leading to Al-tube eccentricity defects. In such a way, the FE results are an important support to predict the mandrel deformation, cycle by cycle, and the consequent eccentricity produced on the extruded profile. As consequence, a direct benchmarking between the predicted values of eccentricity by the dynamic modelling during first few cycles and the reference data measured on tubes, for a brand new die holder, shall increase confidence in the correctness of the material model formulation to simulate the behaviour of dies. This verification is on-going work at Hydro Aluminium. Preliminary observations show a good correlation between macroscopic deformation (eccentricity) provided at 25 cycles and the first industrial production base on assessements at a larger number of cycles. Eccentricity measurements at each of the first 25 cycles on a new die is planned.

In the following section, the FE benchmark with static model is described in detail.

II.3.B.1 Experimental approach – FE benchmark with static model

The first task to check the output of the Dynamic Modelling consists in a direct benchmark of the results obtained by this new method with those provided by the traditional approach. This latter is based on the integration of an isotropic hardening model, calibrated on Inconel 718 tensile test data evaluated at 550°C, in a FE code.

Figure IV. 15 compares the two approaches applied to the case of the base tube extrusion die. The predicted inelastic strains in the hot spot area are in good agreement.

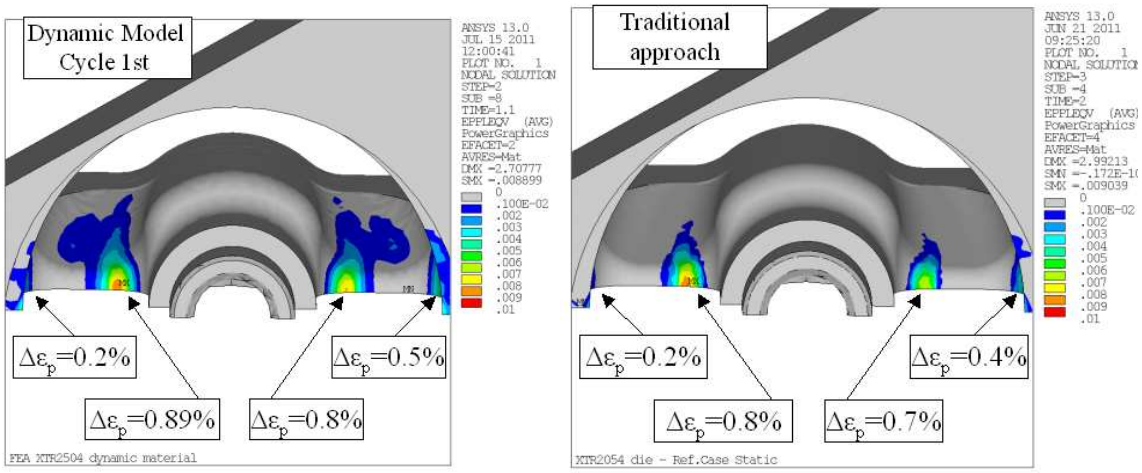

Figure IV. 15 : Comparison of the FE results obtained by the traditional experimental approach (isotropic hardening law) and the Dynamic Model (elasto-plastic model).

Table reports the values of the predicted values of tube thicknesses and the relative eccentricity calculated for both methods.

Experimental approach	***T_{IN} [mm]***	***T_{OUT} [mm]***	***Eccentricity [mm]***
Dynamic Modelling (1st cycle)	2.156	1.994	-0.161
Traditional Approach	2.153	1.997	-0.157

Table IV. 3 : Comparison of the predicted tube eccentricity obtained by the two experimental methods.

The calculations carried out by both methods are similar. However, the traditional approach does not take into consideration the evolution of the loading state that takes place, through the die, cycle by cycle. In such a way, the results provided by the FE analyses are in agreement with the Dynamic Modelling only for the first cycle but they do not implement the transient mechanisms (such as the Inconel 718 softening) occurring during the following cycles.

II.4 Partial Conclusions

The first part of this chapter has been dedicated to the study of the cyclic behaviour of Inconel 718. A cyclic behaviour model has been calibrated and validated by numerous comparisons with data obtained from LCF tests. The considered model is a strain rate independent version of the non-linear kinematic hardening model proposed by Chaboche **[Chaboche et al.,1994]**. The constitutive equations have been integrated in a FE code to predict the evolution of the stress-strain state in an extrusion die. Good control of the cyclic behaviour and deformation mechanisms through the die is of primary importance for extrusion product quality. The application of the so called "Dynamic Material Modelling" constitutes an important alternatives to the costly and time-consuming trials and errors in die design based on the know-how acquired through the current practice **[Fiétier et al.,2009]**.

The model has been applied to the industrial case in order to simulate the loading state of the "Base tube extrusion die" used by Hydro Aluminium to produce large volume of Aluminium high strength alloy extruded tube. A large press force needed to produce the extruded profile induces a permanent centrifuge displacement of the mandrel pole leading to

Al-tube eccentricity defect.

A first benchmark with reference practice was made to compare the simulated results obtained by the “dynamic model” with those reproduced by the traditional isotropic hardening model based on tensile test data at 550C.First cycle benchmark delivers similar results for both dynamic and kinematic hardening model showing that integration of the dynamic material model in ANSYS provide comparable output with current simpler modelling approach.

Verification of the delivered macroscopic displacement by the dynamic modelling is on-going at Hydro Aluminium. The model seems to be able to predict eccentricity measured on production parts at a larger amount of cycles, however, some practical geometrical consideration of the Model itself need to be discussed further prior to definitive conclusion.

Practical measurements of the tube eccentricity over the first 25 cycles will be practiced in a soon future at Hydro Aluminium.

III Fatigue life of Inconel 718 under isothermal LCF conditions

III.1 Introduction

The isothermal LCF properties of Inconel 718 are assessed by strain-controlled tests at 550°C carried out on samples treated according to the standard heat procedure. Results are presented in the form of Manson Coffin and Basquin relationships.

III.2 Fatigue life assessment

Low cycle fatigue is defined as the damage occurring after a limited number of cycles, typically lower than 10,000, as a consequence of high stresses resulting in significant plastic strain at each cycle. This type of fatigue must be considered when designing many industrial components, especially when, because of geometrical singularities for instance, high stress can concentrate in specific locations. Generally speaking, the LCF results are assessed by the following two power laws:

1. **Manson-Coffin law**:

$$\frac{\Delta\varepsilon_p}{2} = \varepsilon_f \cdot (2N_R)^c \qquad \textbf{Eq. IV. 7}$$

Where:

- $\Delta\varepsilon_p$ is the plastic strain amplitude at half life;
- ε_f' is an empirical constant known as the *fatigue ductility coefficient*;
- N_R is the number of cycles to failure;
- c is an empirical constant known as the *fatigue ductility exponent*, commonly ranging from -0.5 to -0.7 for metals.

2. **Basquin Law**:

$$\frac{\Delta\sigma}{2} = C_e \cdot (N_R)^p \qquad \textbf{Eq. IV. 8}$$

Where:

- $\Delta\sigma$ is the stress amplitude at half life;
- N_R is the number of cycles to failure
- C_e and p are empirical constants depending on material and test conditions.

A first approach to the fatigue life of Inconel 718 is based on a first series of tests carried out, in total strain control at 550°C, considering a triangular loading (R=-1) and a frequency of 1 Hz.

Figure IV. 16 shows the Manson Coffin relation relative to these type of tests compared to

a series of tool steels with various hardness. The slope of the straight line for Inconel 718, in a bi-logarithmic plot, is equal to –0.58, in good agreement with the previous description.

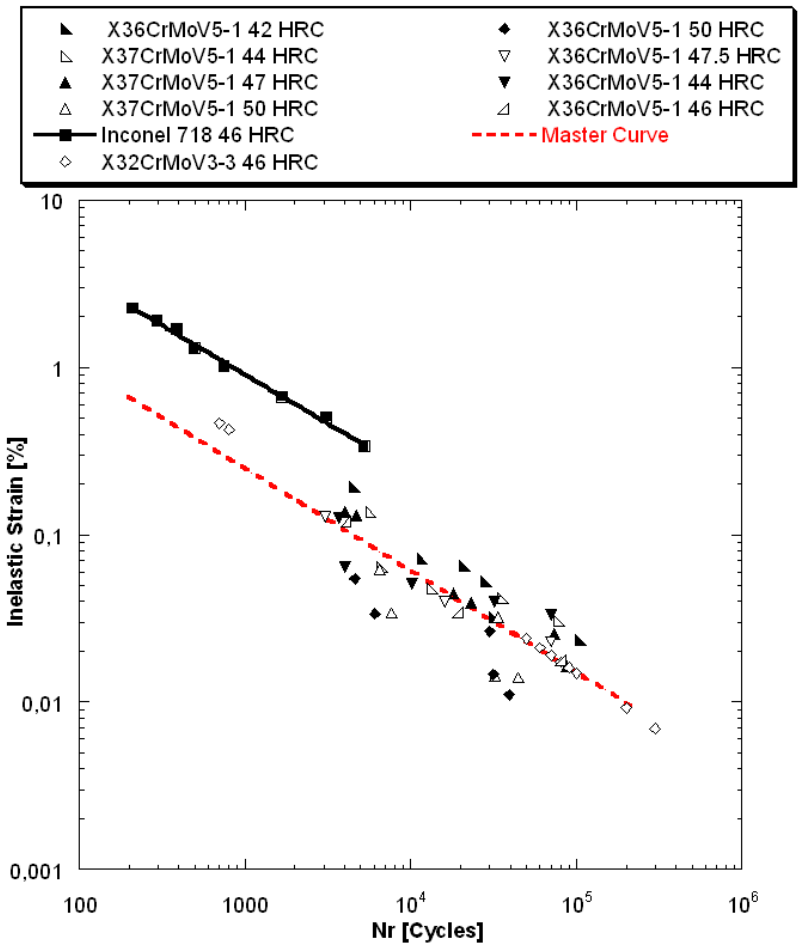

Figure IV. 16 : Manson coffin diagram for LCF tests at 550°C/1Hz : comparison of Hot Work steels [Delagnes,1998; Velay,2003; Bergstrom et al.,2006] and Inconel 718 results.

The diagram reports a direct benchmark of the fatigue properties of the main hot work steels reported in literature. All data are derived from LCF tests carried out at 550°C at a frequency of 1 Hz **[Delagnes,1998; Velay,2003; Bergstrom et al.,2006]**.

In agreement with Bergstrom, a unique "Master fatigue life curve" can be drawn in the Manson-Coffin diagram with the aim to predict, with reasonable accuracy, the average fatigue life for different grades of steels. In such a way, Inconel 718 shows better properties that the traditional hot-work steels. For a similar applied inelastic strain ($\Delta\varepsilon_p$) the superalloy exhibits a longer fatigue life than steels. The "Master curve" is evaluated by a linear regression method that considers all the experimental results referring to steels: the slope of the Manson-Coffin law, in the bi-logarithmic diagram, is equal to –0.61 and it is closed to the fatigue ductility exponent (-0.58) characteristic of Inconel 718. The plots may be considered as parallel, assuming an average exponent (c) equal to –0.60. In such a way it is possible to define a factor $F_{\Delta\varepsilon p}$ that corresponds to the ratio between the two fatigue lives as function of a similar plastic strain amplitude:

$$F_{\Delta\varepsilon_p} = \frac{N_{R(INCONEL\,718)}}{N_{R(Steels)}} = \frac{\left(\frac{\Delta\varepsilon_p}{2\cdot\varepsilon_{f(INCONEL)}}\right)^{\frac{1}{c}}}{\left(\frac{\Delta\varepsilon_p}{2\cdot\varepsilon_{f(Steel)}}\right)^{\frac{1}{c}}} = \left(\frac{\varepsilon_{f(Steel)}}{\varepsilon_{f(INCONEL)}}\right)^{\frac{1}{c}} \qquad \textbf{Eq. III.2}$$

the numerical application gives:

$$F_{\Delta\varepsilon_p} = 6.65$$

It is important to point out that the $F_{\Delta\varepsilon p}$ factor is independent of the fatigue life.

We can conclude that the use of Inconel 718 under LCF conditions improves fatigue life by a factor of 6.65 as compared to traditional hot-work tool steels.

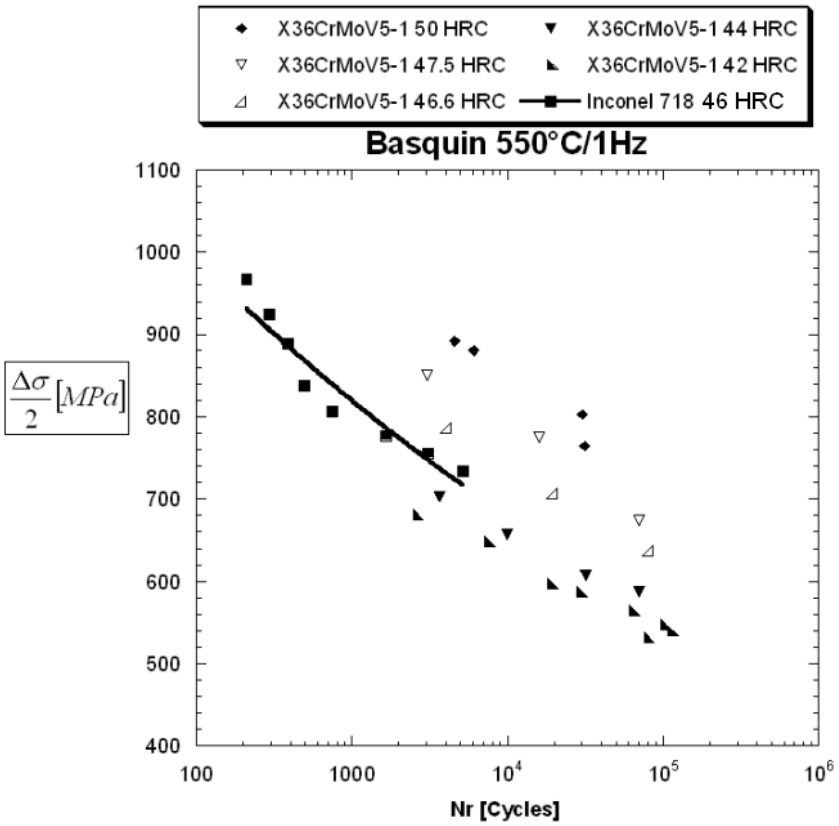

Figure IV. 17 : Basquin diagram for LCF tests at 550°C/1 Hz: comparison between Hot Work steels and Inconel 718 results.

Figure IV. 17 reports the Basquin laws relative to Inconel 718 and steels, where the half stress amplitude (Δσ/2) is plotted as a function of the number of cycles to failure. This representation reflects the material behavior in high-cycle fatigue (HCF) situations, where the deformation is primarily elastic and more than 10^4 cycles are required to failure. In these conditions (T=550°C), when the applied stress amplitudes are lower than the yield strength, the material does not ensure similar performances under fatigue loading as compared to the hot work steels. Recall that LCF is typically defined by stress amplitudes between yield and ultimate strength, and cyclic lives between 10^2 to 10^4 cycles. As a consequence, the Manson-Coffin diagram (Figure IV. 16) has pointed out the high fatigue strength of Inconel 718 when

large inelastic strain amplitudes are applied. These results point out that at 550°C, Inconel 718 exhibits a strong fatigue efficiency at high plasticity (LCF conditions), whereas it becomes less performing when deformation is primarily elastic (HCF conditions).

To better understand the different inelastic behavior of the alloys, Figure IV. 18 exhibits the same results reported in Figure IV. 17, where the stress amplitude ($\Delta\sigma/2$) is normalized as function of the Yield Strength at room temperature ($R_{P0.2}$). In this case, for a similar applied ratio, Inconel 718 exhibits a better fatigue life.

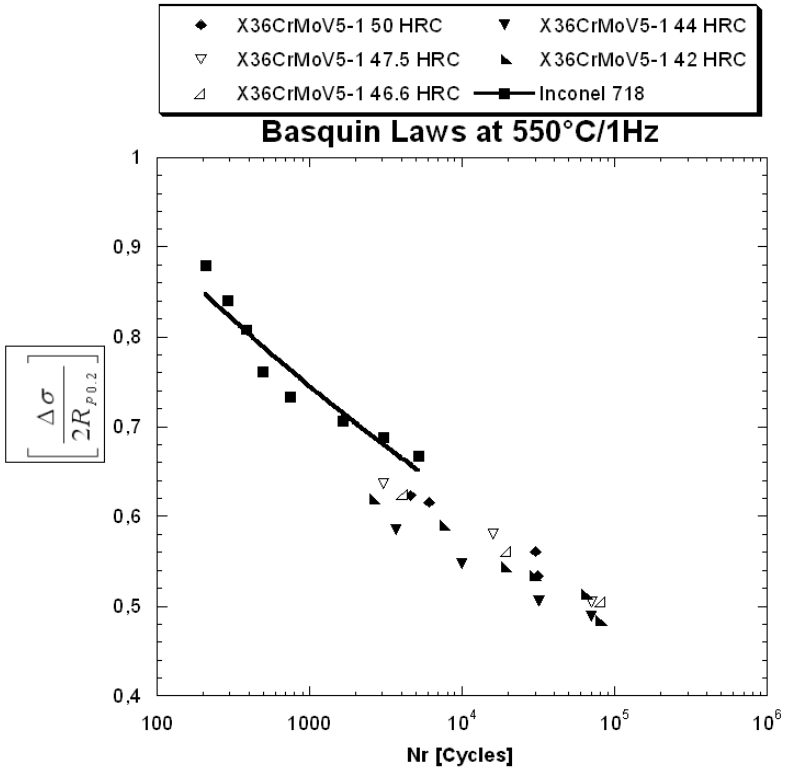

Figure IV. 18 : Basquin diagram for LCF tests at 550°C/1Hz: stress amplitude is normalized as function of the Yield Strength at room temperature.

A detailed examination of the fracture surfaces of the fatigued samples is conducted with a particular attention to the different damage stages, that are crack initiation, crack propagation and final catastrophic fracture. Clavel and Pineau **[Clavel et al.,1982]** showed that the mechanism of crack initiation is closely related to the development of intense deformation bands formed by twinning which look like the so-called slip-band extrusion. In our case, the crack initiation is investigated through a detailed observation of the longitudinal cross-sections of each sample. Figure IV. 19 shows the case of a sample loaded with a strain amplitude of 1.5%. This is a common Stage I initiation site: The crack propagates until it is decelerated by a microstructural barrier such as a grain boundary, inclusions, plate-like delta phase, which cannot accommodate the initial crack growth direction. The number of initiation sites is function of the amplitude of the plastic strain.

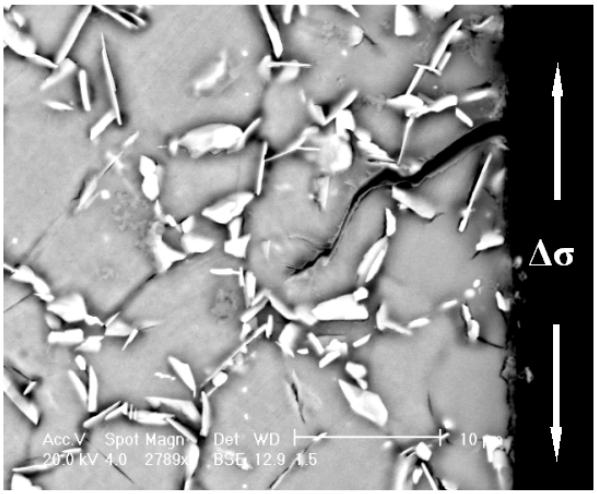

Figure IV. 19 : SEM investigation of a typical crack initiation of a secondary crack under LCF test at 550°C

The crack propagation is shown in Figure IV. 20, where fatigue striations are clearly revealed on the fracture surface.

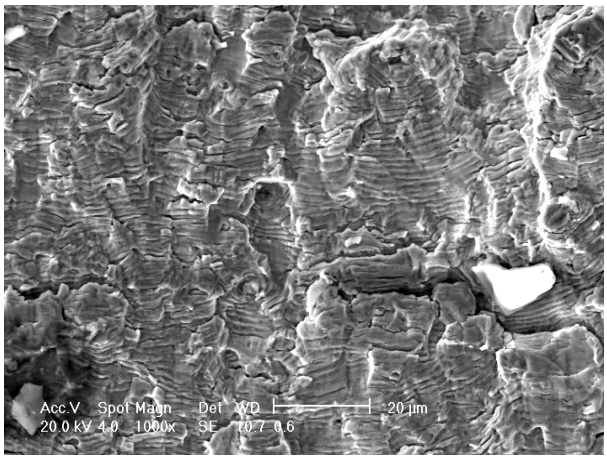

Figure IV. 20 : Scanning electron micrographs of fracture surfaces after LCF tests at 550°C using a triangular signal at 1Hz.

III.3 Cyclic stress-strain response

During fatigue loading, particular transient cyclic phenomenon can occur. Depending on the initial state, material can show full stability, softening or hardening. Following the considerations reported by Delagnes **[Delagnes,1998]**, different behaviors may be identified in Figure IV. 21 where the half stress amplitude, showing different variations, is plotted versus the number of cycles.

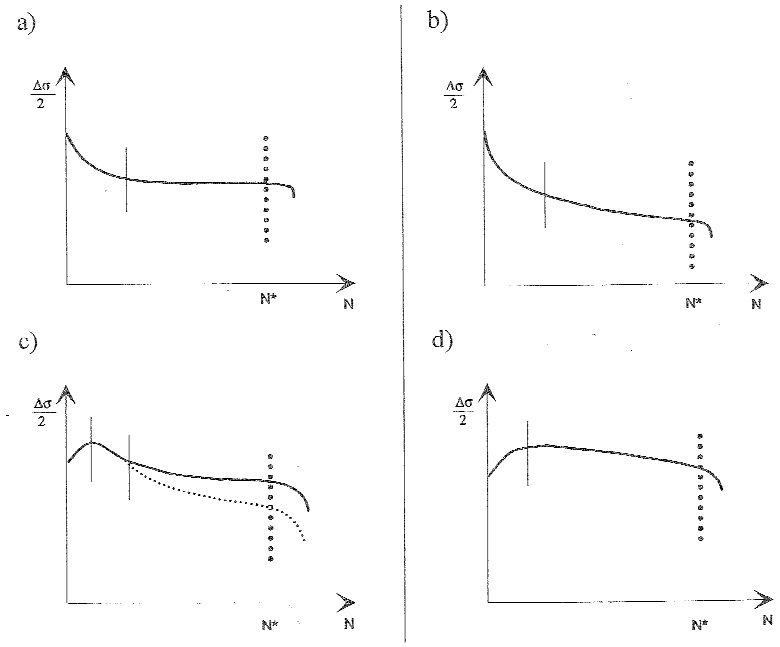

a) Preliminary softening + Stabilization;

b) Preliminary softening + Continuous softening;

c) Preliminary hardening + Softening + Stabilization or continuous softening;

d) Preliminary Hardening + Continuous softening

Figure IV. 21 : General cyclic stress responses [Delagnes,1998].

In general, a further distinction can be reported. In some cases, a pseudo stabilized stage is shown after a preliminary softening (Figure IV. 21(a)), whereas, in other cases, materials exhibit a secondary softening, less significant than the preliminary one, that progressively develops until the propagation of a macroscopic crack occurs.

The cyclic stress curves, established for the cyclic test results at 550°C/1Hz are reported in Figure IV. 22. Materials show, whatever the applied total strain is, a sharp softening from the very first cycles, inducing a strong decrease of the cyclic tensile stress with the number of cycles. This preliminary softening is followed by a stabilized stage where the stress amplitude remains constant.

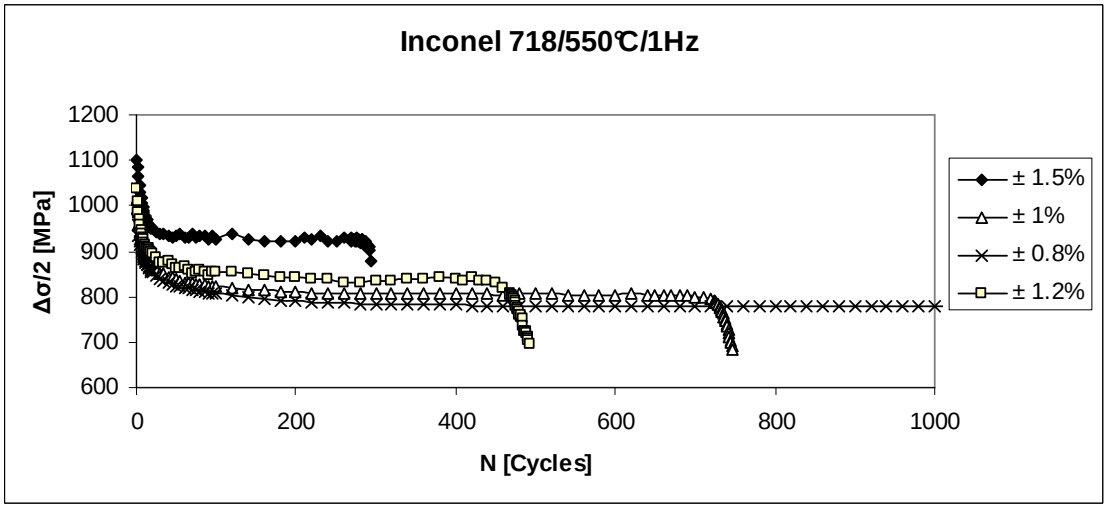

Figure IV. 22 : Evolution of the stress amplitude with the number of cycles at 550°C for different total strain amplitudes.

Based on the cyclic stress curves, three stages can be defined for Inconel 718:

- ***Preliminary softening stage***: a severe decrease of the stress occurs during the very first cycles, associated to a significant enhancement of the plastic strain.
- ***Pseudo stabilized stage***: the plastic strain and stress amplitudes are approximately constant while the material is continuously deformed along the hysteresis loop. This region of cyclic saturation extends over the major part of the fatigue life.
- ***Macro-cracking stage***: the drop in tensile stress is directly related to the rapid propagation of macro-cracks within the monitored gauge length.

Figure IV. 23 shows the evolution of the related plastic strain during a LCF test carried out at 550°C.

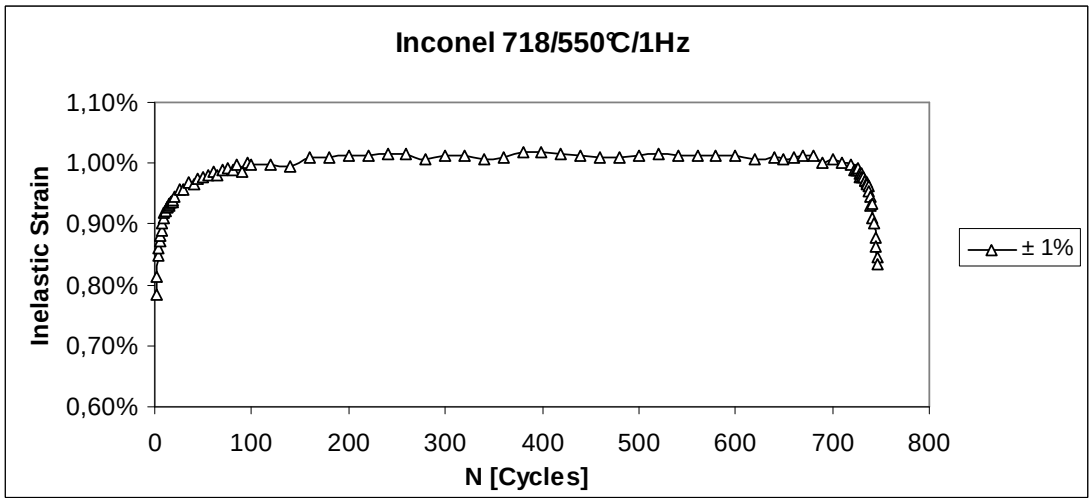

Figure IV. 23 : Evolution of the inelastic strain during a LCF test at 1 Hz ($\Delta\varepsilon_t$=±1%).

Results dealing with the softening behavior may be plotted using the ratio $\frac{\Delta\sigma_i}{\Delta\sigma_1}$, where Δσi

corresponds to the instantaneous stress amplitude and Δσ1 to the stress amplitude at the first cycle, according to the number of cycles. (Figure IV. 24). Accordingly, it can be pointed out that for all strain amplitudes, the preliminary softening stage shows a similar softening rate independently of the applied strain, giving rise to a stress reduction of almost 15% in relation to the first cycle.

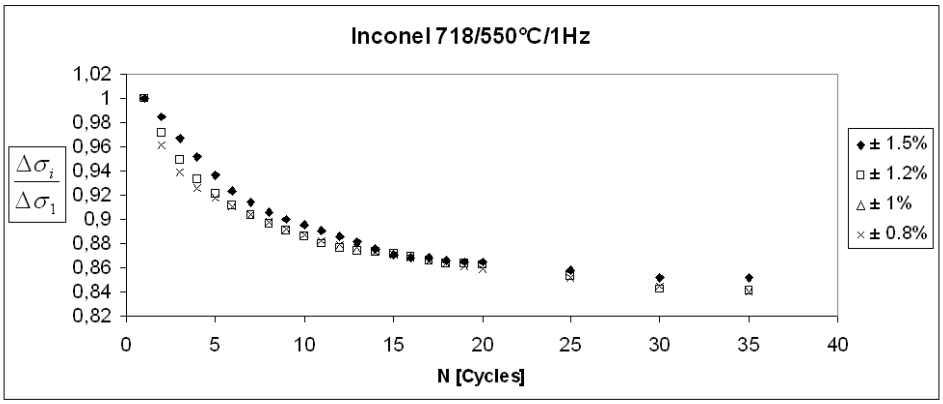

Figure IV. 24 : Normalized stress responses during the preliminary softening stage for different apllied total strains at 550°C.

Figure IV. 25 reports a modeling approach by a power law, showing good results. In such a way, a unique master curve may be plotted for the different applied total strain amplitude, leading to an qualitative prediction of the preliminary softening of Inconel 718 at 550°C.

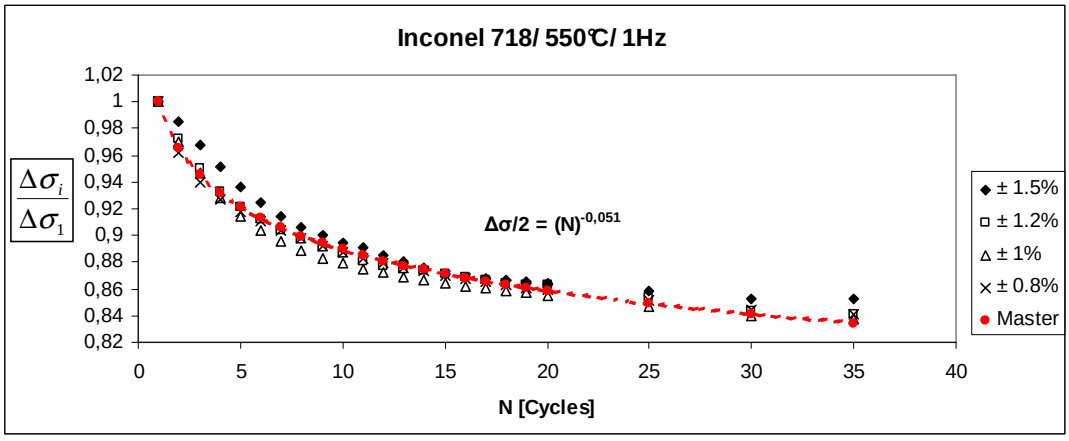

Figure IV. 25 : Modeling of the preliminary softening stage for different applied total strains.

As described in the first part of the Chapter, the cyclic softening of Inconel 718 is mainly associated to the mechanical shearing of the γ" precipitates limiting their interaction with dislocations.

In addition to the benchmarking analyses, reported for fatigue life in Figure IV. 16, between hot-work tool steels and Inconel 718, Figure IV. 26 exhibits a similar comparison in terms of cyclic stress response based on literature results **[Mebarki,2003]**.

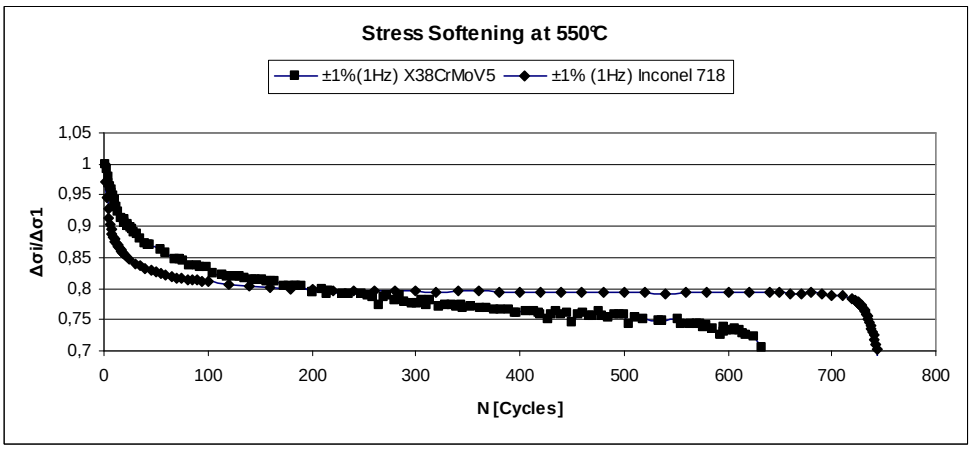

Figure IV. 26 : Comparison between X38CrMoV5 (42 HRC) and Inconel 718 stress responses during a test at 550°C/1Hz using a total strain amplitude of ±1%.

In this case it is still possible to describe a different behavior between the materials: X38CrMoV5 steels show a different softening mechanism where a preliminary strong accommodation is followed by a continuous linear softening that extends until the macro-cracking stage. This mechanism is due to a continuous arrangement of the dislocations entanglement, formed as a consequence of the quenching treatment. The dislocations annihilation, due to cross slip at high temperature, contributes to lower the dislocations density **[Delagnes,1998]**.

In addition, the increase of the precipitates size, at high temperature, enhances the cyclic softening. As a result, the coalescence of carbides, reduces the strengthening mechanisms obtained by a fine precipitation during the ageing treatment, improving the mobility of the dislocations. At equal total applied strain, steels consequently exhibit faster softening than Inconel 718.

III.4 Representation of extrusion loading by LCF tests

One of the aim of this PhD work is the simulation of the extrusion die loading by LCF tests. As anticipated in chapter I, the loading state can be approached by a trapezoidal waveform provided by a holding period of 150 s at maximal strain and 20 s at minimal strain. Tests are carried out at 550°C, in total strain control, with a strain rate of $5x10^{-3}$ s^{-1}. This latter value is chosen in order to be representative of the real loading ramp considered for the extrusion operations.

The results are reported in a Manson Coffin diagram and compared to the data associated to triangular waveform at 1 Hz with no holding time (Figure IV. 27). It is clear that the application of a trapezoidal signal induces a reduction of the fatigue life of Inconel 718.

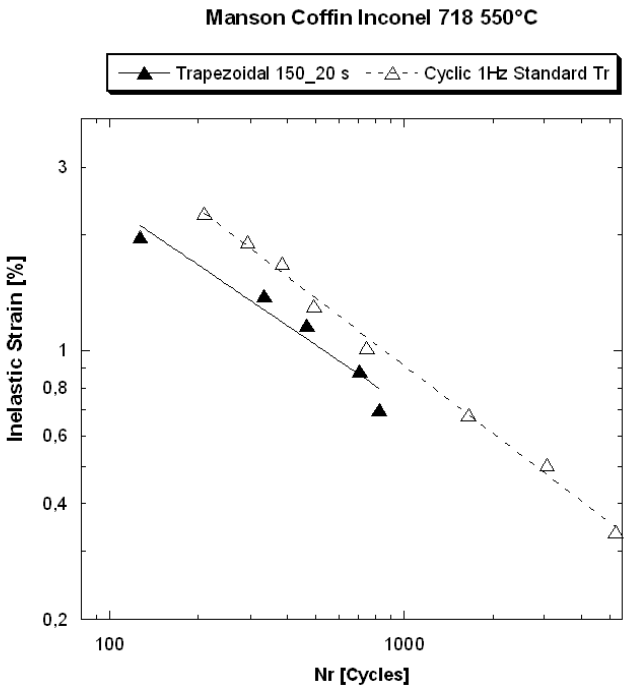

Figure IV. 27 : Effect of the trapezoidal signal on the fatigue performance of Inconel 718 at 550°C.

According to the expression reported in the previous section, the fatigue life ratio between the application of a cyclic triangular signal and to a trapezoidal signal (150_20 s) can be evaluated considering the two relationships as parallel straight lines:

$$F_{\Delta\varepsilon_p} = \frac{N_{R(Cyclic\cdot 1Hz)}}{N_{R(Trapezoidal\cdot 150\_20s)}} = \frac{\left(\frac{\Delta\varepsilon_p}{2\cdot\varepsilon_{f(Cyclic\cdot 1Hz)}}\right)^{\frac{1}{c}}}{\left(\frac{\Delta\varepsilon_p}{2\cdot\varepsilon_{f(Trapezoidal\cdot 150\_20s)}}\right)^{\frac{1}{c}}} = \left(\frac{\varepsilon_{f(Trapezoidal\cdot 150\_20s)}}{\varepsilon_{f(Cyclic\cdot 1Hz)}}\right)^{\frac{1}{c}} \qquad \textbf{Eq. IV. 9}$$

In such a way, following an average slope as c=-0.552, we obtain:

$$F_{\Delta\varepsilon_p} = 3.39$$

Figure IV. 28 shows the cyclic response of the material during a test carried out at a total strain amplitude of 2%: the extrusion cycle tends to enhance the cyclic softening, especially during the pseudo-stabilized stage. Furthermore, a preliminary crack initiation associated to the severity of the extrusion cycle, could be considered as a possible explanation of the rapid softening.

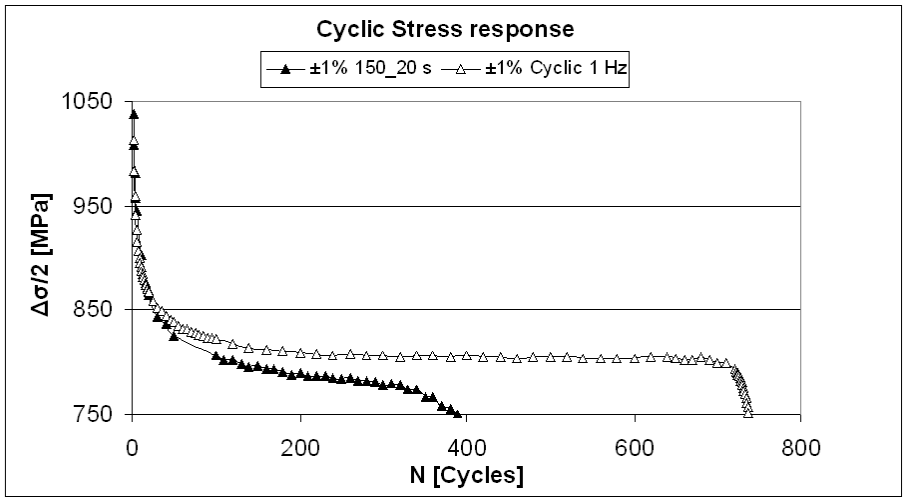

Figure IV. 28 : Evolution of the cyclic stress amplitude with the number of cycles at 550°C for a cyclic (1 Hz) and a trapezoidal (150_20 s) signal ($\Delta\varepsilon_t$=±1%).

Figure IV. 29 shows the evolution of the plastic strain amplitude at half life as a function of the total strain. The trapezoidal waveform increases the plastic strain amplitude due to the visco-plastic effects at 550°C. A possible explanation can be proposed considering the holding time effects as a time dependent problem. The stress relaxation, occurring at cycle *N*, while holding at constant strain, results in a decrease of the material yield strength leading to an increase of the plastic strain at cycle *N+1*. This instantaneous process, operating at each cycle, is characterized by a stress drop between 50 and 80 MPa in the hysteresis loops, and produced a global effect that can be noticed by an increase of the plastic strain at half life.

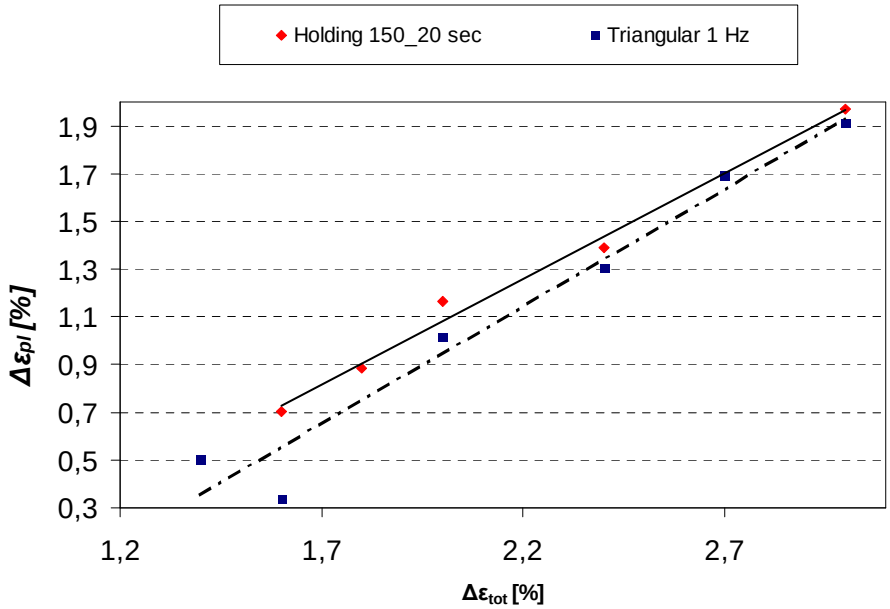

Figure IV. 29 : Relationship between the total strain and the plastic strain for LCF tests at 550°C under triangular signals at 1 Hz and trapezoidal waveforms (150 s holding time).

The effect of the stress relaxation on the inelastic strain is showed in Figure IV. 30, where a triangular cycle is compared to a trapezoidal cycle in terms of stress-strain response. Both

tests are carried out with total strain amplitude equal to 2%.

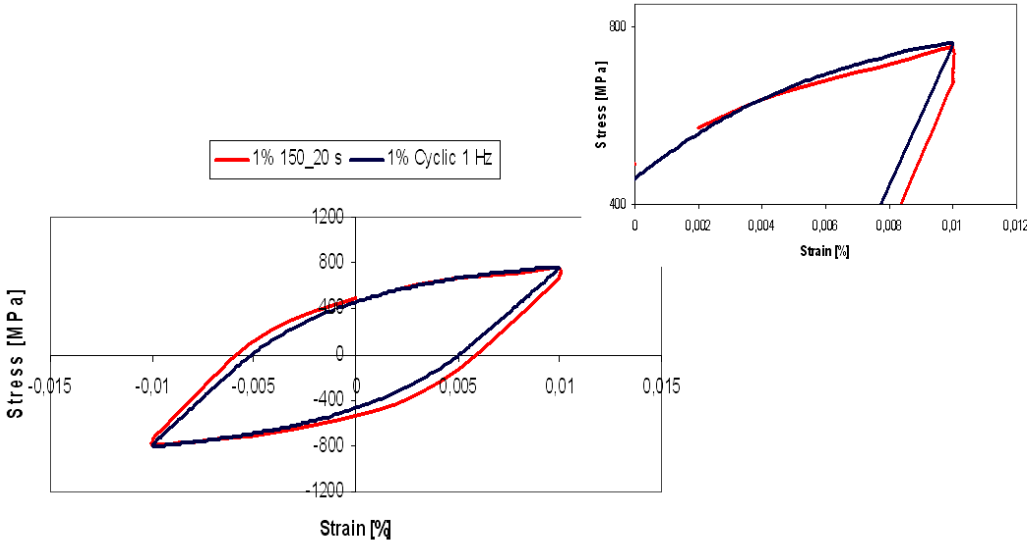

Figure IV. 30 : Stress-Strain curves exhibiting the stress relaxation effects induced by a holding time at tensile stress ($\Delta\varepsilon_t$=±1%).

The post mortem observation of the longitudinal section of a typical specimen (Figure IV. 31 (a)) shows a transgranular crack propagation of secondary cracks extending over a distance of one or two grains. Considering crack propagation, the fracture surfaces (Figure IV. 31 (b)) exhibits predominant transgranular propagation.

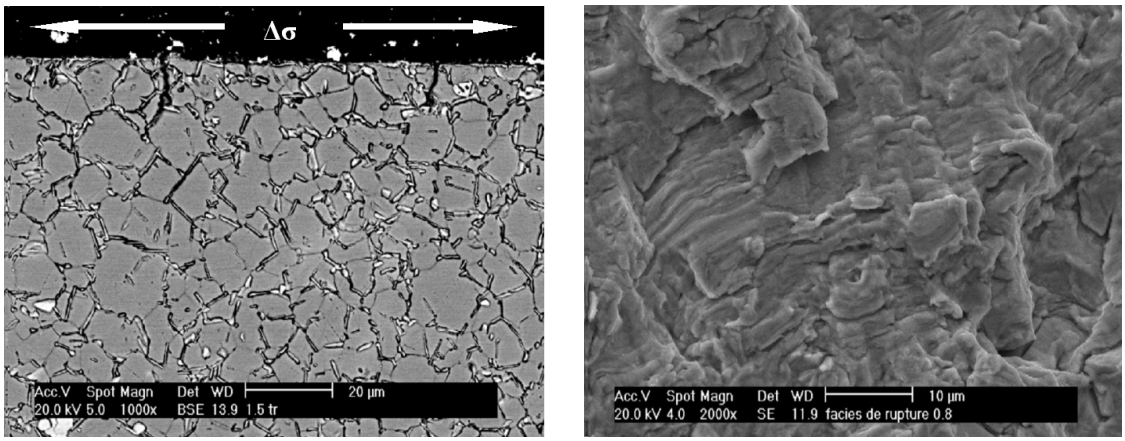

(a) **(b)**

Figure IV. 31 : SEM investigation of the longitudinal section (a) and fracture surfaces (b) of a post mortem specimen submitted to a trapezoidal (150_20 s) fatigue signal at 550°C.

It is obvious that the application of a trapezoidal fatigue cycle has a detrimental effect on the fatigue life. However, the application of holding times is not the only parameter that plays a significant role. The chosen strain rate ($5x10^{-3}$ s^{-1}) is lower than the value considered for the triangular cycle: the decrease in the fatigue properties could be attributed to the simultaneous impact of the strain rate and holding times on plastic deformation. The individual influence of these parameters is analyzed in the next sections.

III.4.A Effects of holding time on the fatigue behaviour

Although the effect of the holding time is well understood for fatigue crack propagation, further work is required to identify the mechanisms by which the application of the holding time influences the fatigue life performances. The introduction of holding periods to a low cycle fatigue test at high temperature can be considered as a frequency-related problem, which requires investigating the interaction between fatigue and creep, using trapezoidal cycles. They are defined by the loading times, in seconds, at maximal and minimal strain. For example, 150-20 indicates a wave-form with a holding time of150 s at maximal strain and 20 s at minimal strain. All tests are carried out in total strain controlled mode with an R ratio equal to –1 and a strain rate of $5 \cdot 10^{-3}$ s^{-1}. The investigation of the effect of holding time has a strong interest for understanding the extrusion process: the selection of different holding times allows the simulation of different billet lengths to be extruded. For this reason, only the holding time at maximal load, which represents the extrusion time, is varied in the range between 45 and 300 seconds, whereas the time held at minimal loading is kept constant (20 s). Results are presented in Figure IV. 32: it is important to point out that extending the holding time, from 45 to 300 seconds, does not further decrease the number of cycles to failure. All data satisfactorily fit a “Trapezoidal Master curve”, evaluated for the results obtained for trapezoidal cycles, and located below the straight line of 1 Hz tests, performed with the triangular cycles.

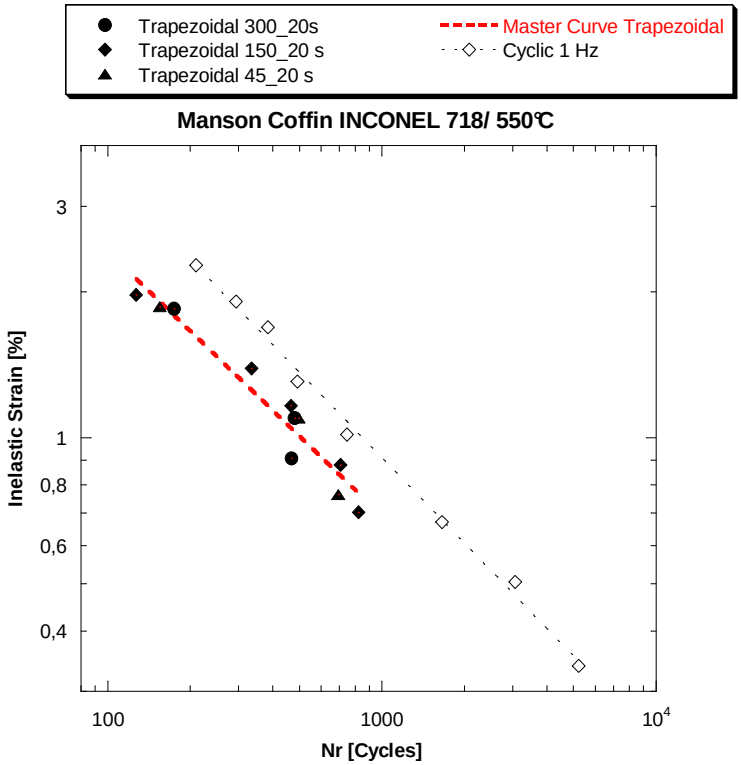

Figure IV. 32 : Effect of holding time on fatigue life of Inconel 718 at 550°C.

Figure IV. 33 focuses on the stress response. It shows that a variation of the holding time does not induce significant differences in softening: the three curves exhibit a similar behaviour leading to approximately same fatigue lives.

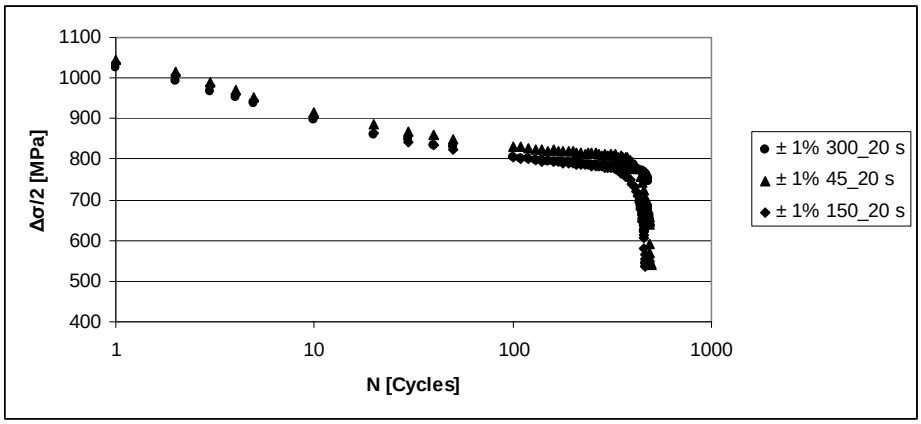

Figure IV. 33 : Cyclic stress response curves at 550°C for various holding times ($\Delta\varepsilon_t$=±1%)..

The similar behaviour for the different fatigue signals may be explained analysing the stress drop associated to the holding time. Figure IV. 34 shows the relaxation behaviour during a holding time at maximal load, occurring at half life. Relaxation can be divided into two different stages. A sharp stress decrease occurs within the first 25 seconds while a second linear softening prevails from 40 s till the end of the steady stage.

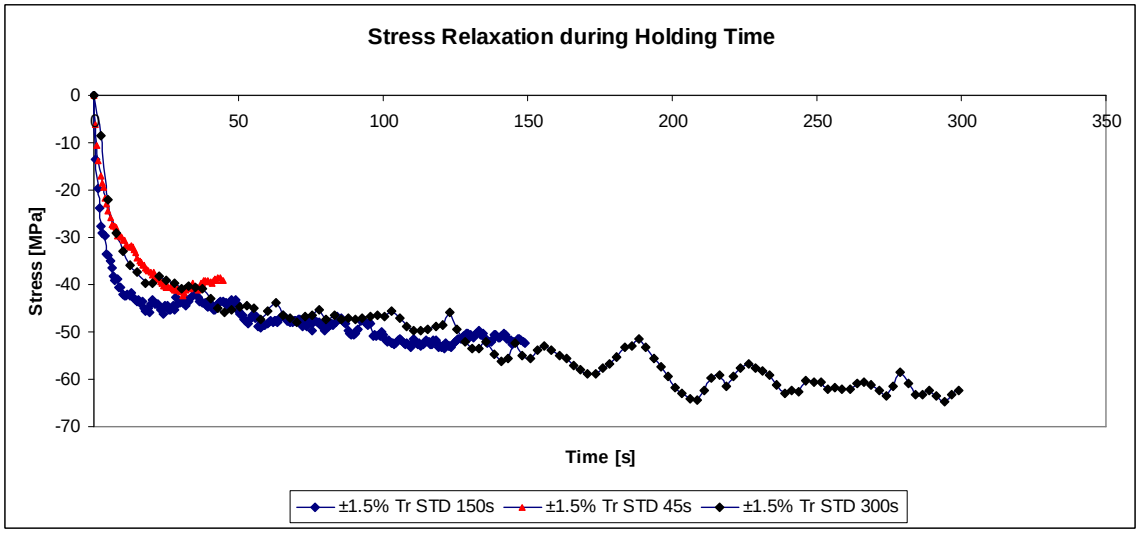

Figure IV. 34 : Evolution of the stress relaxation during holding time at maximal stress ($\Delta\varepsilon_t$=±1.5%).

Considering that stress relaxation is fully completed within 40 seconds, almost no further effect is expected while holding specimen for longer time under maximal strain. This explains the similar behaviour under LCF conditions between the three different loading cycles (holding time of 45, 150 and 300 seconds).

III.4.B Strain rate effects on fatigue behaviour

The fatigue life of Nickel based superalloys at elevated temperature is directly affected by strain rate. As reported by previous studies **[Mannan,1993; Valsan et al.,1994; Fournier et al.,2001; Hong et al.,2005]**, this parameter plays an important role in the deformation process leading to a series of changes in damage mechanisms such as slip modes, oxidation and dynamic strain aging (DSA). Generally speaking, the time related factors, such as hold time, strain rate and wave shape, may influence fatigue life either synergistically or independently

[Valsan et al.,1994]. The application of a trapezoidal cycle, to simulate the extrusion cycle, results in more extended damages than for triangular cycles at 1 Hz, associated to the simultaneous application of a reduced strain rate and a tensile/compression holding time.

The preliminary approach to study the strain rate effects is based on the analysis of a triangular signal, in total strain control, using a strain rate equal to the extrusion loading rate, $5x10^{-3}$ s^{-1}. Figure IV. 35 shows the results relative to these preliminary tests. The influence of the strain rate, between $5x10^{-3}$ s^{-1} and 1 Hz, where strain rate ranges between $6,6x10^{-2}$ s^{-1} (respectively for $\Delta\varepsilon_{tot}=\pm1.65\%$) and $2,4x10^{-2}$ s^{-1} (respectively for $\Delta\varepsilon_{tot}=\pm0.6\%$), results in a decrease in fatigue life as confirmed in previous studies **[Clavel et al.,1982]**.

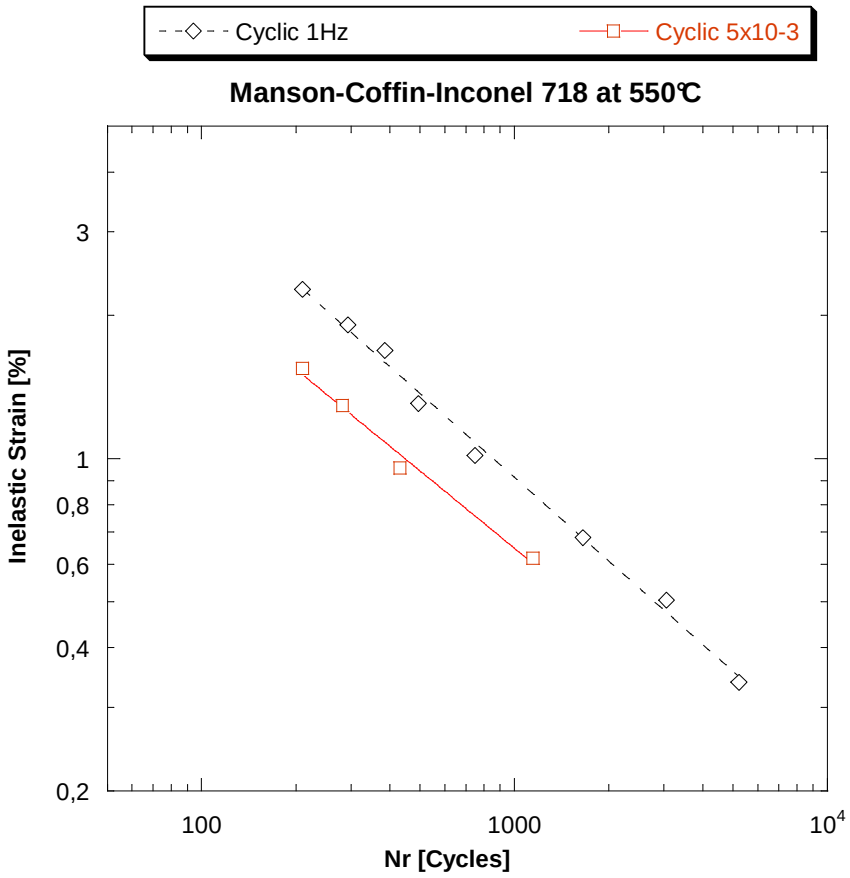

Figure IV. 35 : Influence of strain rate on the cycles to failure for Inconel 718 (Manson-Coffin curve obtained at 550°C for a fully reversed cyclic signal).

The fatigue life ratio for a similar inelastic strain may be expressed by:

$$F_{\Delta\varepsilon_p}=\frac{N_{R(Cyclic\cdot1Hz)}}{N_{R(Cyclic\cdot5\times10^{-3}s^{1})}}=\frac{\left(\frac{\Delta\varepsilon_p}{2\cdot\varepsilon_{f(Cyclic\cdot1Hz)}}\right)^{\frac{1}{c}}}{\left(\frac{\Delta\varepsilon_p}{2\cdot\varepsilon_{f(Cyclic\cdot5\times10^{-3}s^{1})}}\right)^{\frac{1}{c}}}=\left(\frac{\varepsilon_{f(Cyclic\cdot5\times10^{-3}s^{1})}}{\varepsilon_{f(Cyclic\cdot1Hz)}}\right)^{\frac{1}{c}} \qquad \textbf{Eq. IV. 10}$$

Assuming same slopes for both plots, *c= -0.562*, the fatigue ratio is:

$$F_{\Delta\varepsilon_p}=3.28$$

The cyclic stress responses are reported in Figure IV. 36 for a cyclic test conducted with a total strain amplitude of ±1%. The softening is more important at low frequencies, as noticed for the tests performed for the dynamic modeling; especially in the pseudo-stabilized stage where the curves tend to slightly separate.

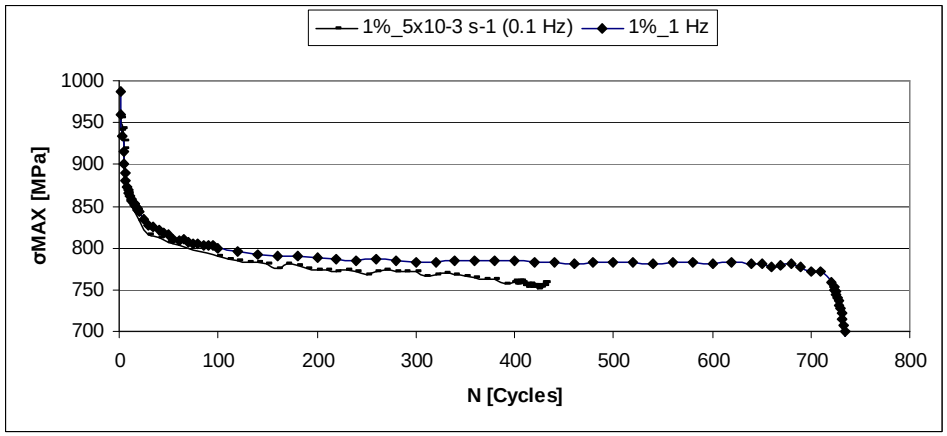

Figure IV. 36 : Cyclic stress response at 550C for different strain rates ($\Delta\varepsilon_t$=±1%).

The investigation on the strain rates effects is completed by a second series of test carried out with the trapezoidal (extrusion) cycle.

Two alternative strain rates, equal to $5x10^{-2}$ s^{-1} and $5x10^{-4}$ s^{-1}, are considered in addition to the standard one ($5x10^{-3}$ s^{-1}). Results are reported in Figure IV. 37

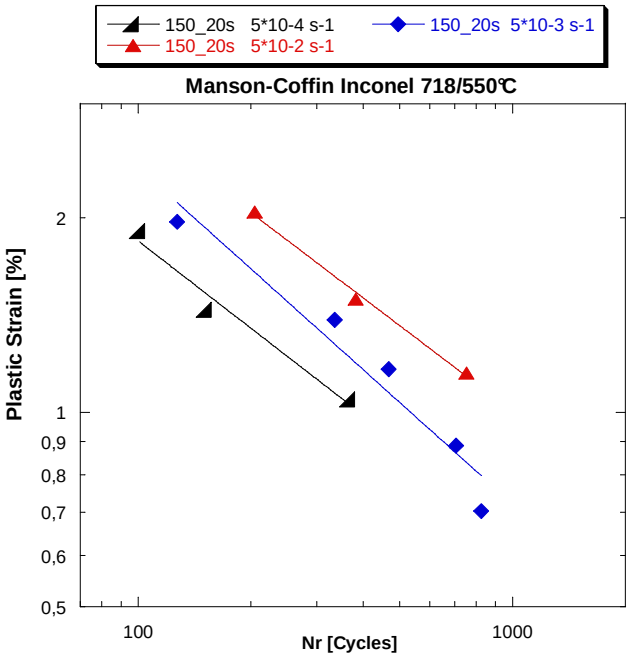

Figure IV. 37 : Fatigue life variation with strain rate, at 550°C, for a trapezoidal signal.

The Manson-Coffin diagram, associated to the trapezoidal wave-form, shows that a higher strain rate corresponds to a longer fatigue life.

Figure IV. 38 compares the half life hysteresis loops associated to different strain rates for a fatigue test carried out at strain amplitude of ±1.5%.

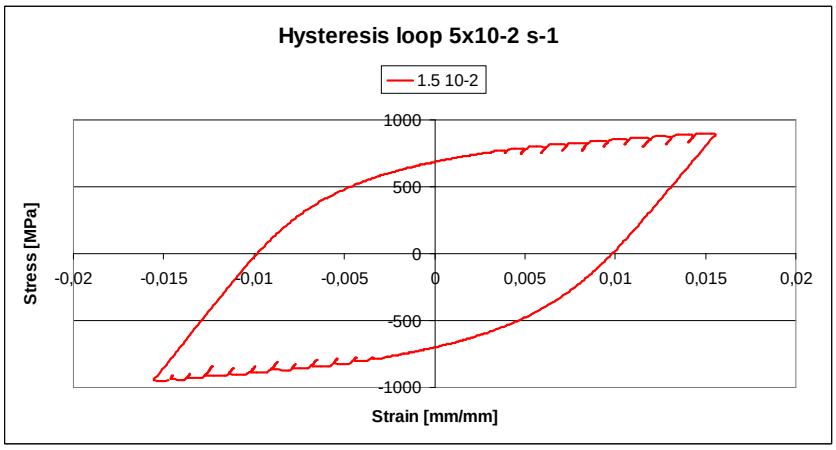

(a)

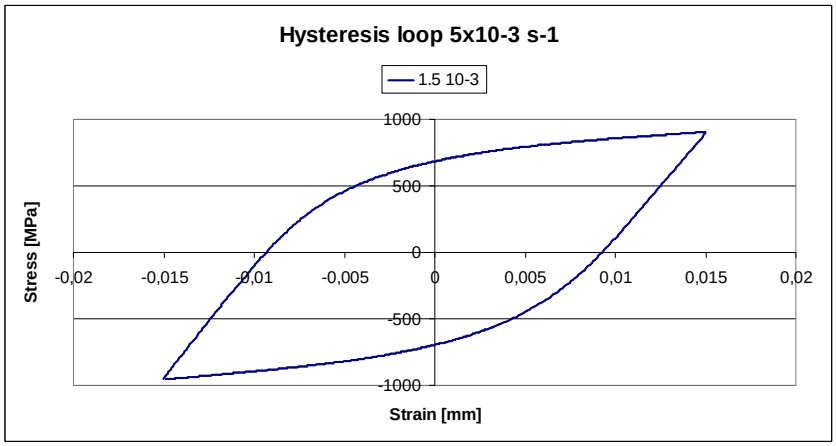

(b)

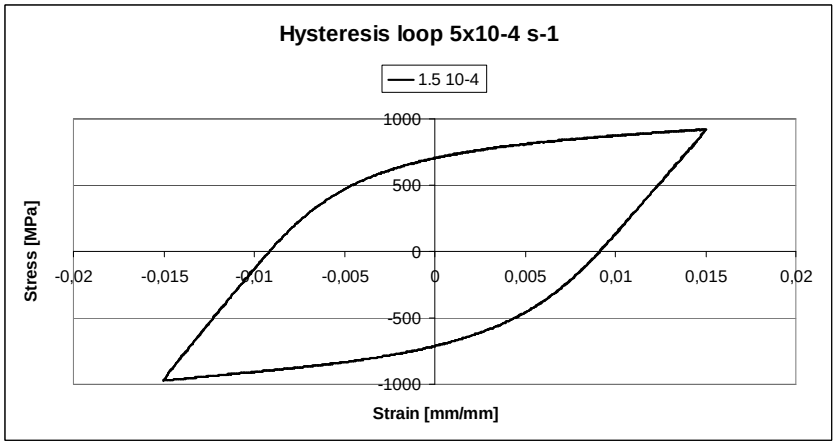

(c)

Figure IV. 38 : Cyclic stress-strain response at half life for different strain rates: (a) $5x10^{-2}$ s^{-1}, (b) $5x10^{-3}$ s^{-1}, (c) $5x10^{-4}$ s^{-1} ($\Delta\varepsilon_t$=±1.5%).

Clear unstable stress serrations can be noted in the plastic domain of the stress-strain curve associated to the highest strain rate ($5x10^{-2}$ s^{-1}). As reported in literature **[Mannan,1993; Valsan et al.,1994; Chihab,2004]**, these plastic instabilities play an important role in the damaging mechanisms associated to fatigue loading. Unsurprisingly, this macroscopic mechanical effect has been associated to a microstructure evolution. Kirman and Warrington **[Kirman et al.,1970]** have reported that the mechanisms of deformation in Inconel 718

induce the formation of stacking faults within the strengthening precipitates (γ"). Those faults locally reproduce the crystallographic sequence of the δ phase.

Clavel and Pineau **[Clavel et al.,1975]** have proposed a post deformation heat treatment, including a 80 hours holding at 770°C, prone to enhance the size of the δ phase nuclei. These precipitates, localised along the slip lines, allow a better observation of the plastic strains lower than about 1%. In Figure IV. 39 the effects of the post deformation treatment can be appreciated. The γ" => δ transformation is used to compare the different effects of strain rate.

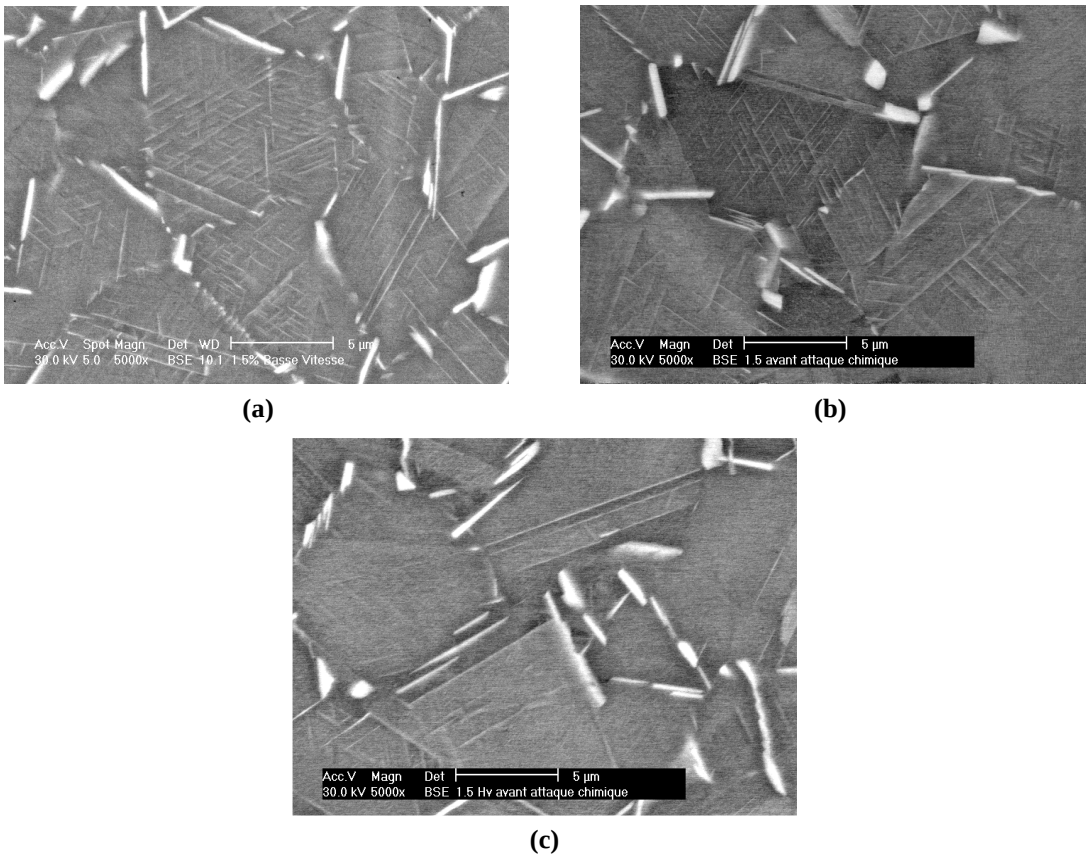

(a) **(b)**

(c)

Figure IV. 39 : Comparison of the deformation mechanisms observed under 150s/20s (1.5% Total applied strain) trapezoidal load at different strain rates: $5x10^{-4}$ s^{-1} (a), $5x10^{-3}$ s^{-1} (b) and $5x10^{-2}$ s^{-1} (c).

For low strain rates (Figure IV. 39 (a), (b)) grains contain multiple deformation bands that are delineated by a pronounced presence of δ phase (white contrast) indicating the occurrence of two activated slip planes. These slip lines, developing gradually during the softening of the alloy, are similar to the thin and long twins detected by Fournier in previous investigations **[Fournier et al.,1977]**.

Figure IV. 39 (c) details the deformed microstructure observed for a high strain rate. In this case, the density of slip lines drastically decreases as a consequence of a softening process and a further increase of inhomogeneity of fatigue deformation. Figure IV. 38 has showed that for high strain rate, Inconel 718 exhibits Portevin Le Chatelier (PLC) effects occurring through plastic serrations in stress-strain loops. As reported in Chapter II, this phenomenon results from the locking of mobile dislocations by substitutional solute atoms. As reported by Mannan **[Mannan,1993]**, the regions between the slip bands contain uniform distribution of dislocations: the dislocation velocities within the bands are too high to allow the solute-

dislocation interactions. In such a way, the PLC effects, exhibited at high strain rate, derive from the solute locking of the dislocation that move more slowly between slip bands. The enhancement of strain inhomogeneity, associated to high strain rates, derives from the differential movement of dislocations within and between the slip bands.

The variation of fatigue life as a function of strain rate could be explained by a detailed investigation of the interaction between deformation mechanisms and the fracture modes.

This particular point could be studied by observing the fracture surface with a particular attention to the two involved stages of the fatigue fracture, which are crack initiation and propagation.

III.4.B.1 Initiation of fatigue cracks

For the different applied strain rates, micro-cracks initiate along the slip bands connected to the specimen surface. This hypothesis is based on the general assumption that fatigue crack initiation is related to the formation of intense extrusion-intrusion bands associated to intense shear stresses. Fournier **[Fournier et al.,1977]** showed that this crack initiation mechanism takes place whatever the loading frequency is.

However, the increased density of slip bands, associated to low strain rates, results in the multiplication of crack initiation sites, localized at the intersection between slip bands and surface. Consequently, the crack initiation life is reduced.

III.4.B.2 Propagation of fatigue cracks

Figure IV. 40 reports the aspects of fractures surfaces for two different strain rates.

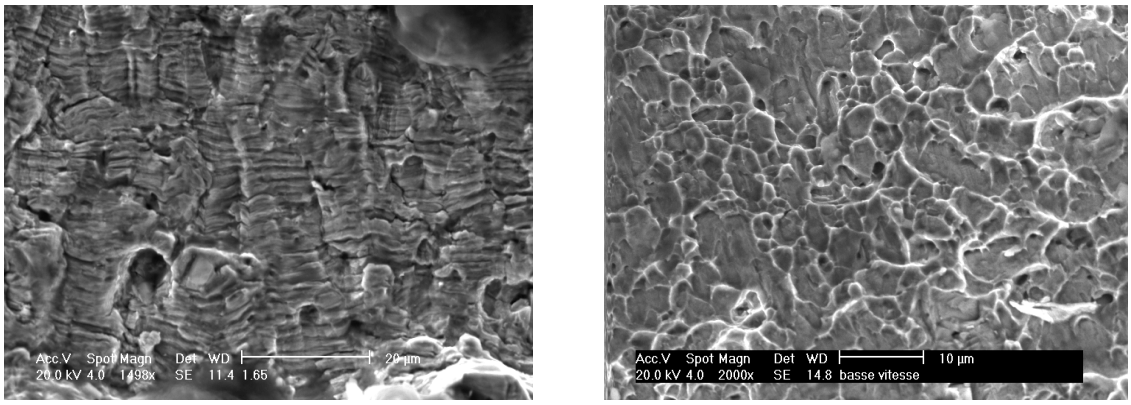

(a) **(b)**

Figure IV. 40 : Scanning electron micrographs of fracture surfaces after LCF tests at 550°C: high strain rate ($5x10^{-2}$ s^{-1}) (a) and low strain rate ($5x10^{-4}$ s^{-1}) (b).

At low strain rate ($5x10^{-4}$ s^{-1}), a simultaneous appearance of transgranular and intergranular cracking is observed along the crack propagation direction, especially at the edge of the crack propagation zone, where the strain rate is the lowest.

Conversely, at high strain rate ($5x10^{-2}$ s^{-1}), transgranular propagation is found on the fracture surfaces. This result is in perfect agreement with the studies of Fournier **[Fournier et al.,2001]** who clearly showed that the occurrence of PLC instabilities in alloy 718 avoids the intergranular crack propagation. The Portevin-Le Chatelier effects lead to specimen

unloadings that modify the interactions between dislocations and interstitial-solute atoms. Garat **[Garat et al.,2008]** proposed that the nucleation sites of strain jumps and the intergranular crack initiations are located in the same areas of the material microstructure.

These assumptions could be integrated considering that the evidence of the intergranular propagation features are the result of the environment, and more specifically oxygen.

Oxidation occurs preferentially along the intense deformation bands causing the embrittlement of these zones by oxygen diffusion and oxidation. It has been demonstrated that for dynamic (at the crack tip) and static embrittlement (stress free) the direct intergranular diffusion of oxygen is the dominant process **[Woodford,2006]**. The most common reactions include gas bubble (CO-CO_2) formation, as a result of oxidation of carbon or carbides, and the oxidation of oxide forming impurities or minor alloying elements. These mechanisms induce the formation of localised cavitation that leads to an intergranular propagation, reducing the ability to accommodate stress concentrations at sliding grain boundaries.

Following these considerations, Ter-Ovanessien **[Ter-Ovanessian et al.,2008]** have investigated the effect of the interstitial species concentrations on the rupture mode. These studies demonstrated that the flow instabilities are controlled by the interstitial content of alloying elements such as carbon, nitrogen and oxygen. The planar slip mechanism is responsible for the intergranular oxidation in Inconel 718: oxygen may react with interstitial carbons brought by dislocation at grain boundaries, forming gas bubbles. On the other hand, the occurrence of the PLC effects is based on strong interactions between dislocations and interstitial carbons: the atoms are localized on the sites where they pin dislocations and the intergranular oxidation is avoided. In such a way, independently of the deformation amplitude, the stress serrations (PLC) lead, systematically, to a transgranular ductile propagation.

These considerations point out the main roles played by the strain rate on the fatigue behaviour. Results have clearly shown the effects associated to the PLC mechanisms which act, mainly, on the stress-strain response, on the inhomogeneity of deformation mechanisms and on the resistance to intergranular cracking assisted by oxidation.

IV Quantitative analysis of fatigue crack growth by fractographic investigations

IV.1 Introduction

The microscopical investigations performed on fracture surfaces have shown that fatigue striations can spread, in transgranular fractures, over the major part of the flaw surface. The most interesting quantitative information associated to a fatigue fracture surface is related to striations. The description of fatigue cracks by a quantitative micro-fractography approach offers a potential basis for the reconstitution of the crack growth kinetics. According to previous studies, it is assumed that one striation corresponds to one cycle in ductile materials:

unloadings that modify the interactions between dislocations and interstitial-solute atoms. Garat **[Garat et al.,2008]** proposed that the nucleation sites of strain jumps and the intergranular crack initiations are located in the same areas of the material microstructure.

These assumptions could be integrated considering that the evidence of the intergranular propagation features are the result of the environment, and more specifically oxygen.

Oxidation occurs preferentially along the intense deformation bands causing the embrittlement of these zones by oxygen diffusion and oxidation. It has been demonstrated that for dynamic (at the crack tip) and static embrittlement (stress free) the direct intergranular diffusion of oxygen is the dominant process **[Woodford,2006]**. The most common reactions include gas bubble (CO-CO_2) formation, as a result of oxidation of carbon or carbides, and the oxidation of oxide forming impurities or minor alloying elements. These mechanisms induce the formation of localised cavitation that leads to an intergranular propagation, reducing the ability to accommodate stress concentrations at sliding grain boundaries.

Following these considerations, Ter-Ovanessien **[Ter-Ovanessian et al.,2008]** have investigated the effect of the interstitial species concentrations on the rupture mode. These studies demonstrated that the flow instabilities are controlled by the interstitial content of alloying elements such as carbon, nitrogen and oxygen. The planar slip mechanism is responsible for the intergranular oxidation in Inconel 718: oxygen may react with interstitial carbons brought by dislocation at grain boundaries, forming gas bubbles. On the other hand, the occurrence of the PLC effects is based on strong interactions between dislocations and interstitial carbons: the atoms are localized on the sites where they pin dislocations and the intergranular oxidation is avoided. In such a way, independently of the deformation amplitude, the stress serrations (PLC) lead, systematically, to a transgranular ductile propagation.

These considerations point out the main roles played by the strain rate on the fatigue behaviour. Results have clearly shown the effects associated to the PLC mechanisms which act, mainly, on the stress-strain response, on the inhomogeneity of deformation mechanisms and on the resistance to intergranular cracking assisted by oxidation.

IV Quantitative analysis of fatigue crack growth by fractographic investigations

IV.1 Introduction

The microscopical investigations performed on fracture surfaces have shown that fatigue striations can spread, in transgranular fractures, over the major part of the flaw surface. The most interesting quantitative information associated to a fatigue fracture surface is related to striations. The description of fatigue cracks by a quantitative micro-fractography approach offers a potential basis for the reconstitution of the crack growth kinetics. According to previous studies, it is assumed that one striation corresponds to one cycle in ductile materials:

the distance between two striations (*i*) is related to the instantaneous crack propagation rate da/dN at a given crack length (*a*). Fracture surfaces, characteristic of post mortem LCF specimens, are investigated using SEM measurements of fatigue striation spacing along the crack propagation direction. Different mechanical approaches and fractographic techniques are implemented for the analysis of the experimental data: the results of the fractographic reconstitutions are presented and directly compared to the crack growth rate published in the literature. The aim of this section is to investigate the crack propagation process. First, a brief review of the process of fatigue striation formation is presented, then, the experimental approaches used for the fractographic reconstitution and their relative results are discussed in detail.

IV.2 Fatigue striations formation

The crack propagation process has been widely studied in the past fifty years with a particular attention to its microstructural aspects. Before focusing on the investigation of the fracture surfaces, it is important to remind the common features of a typical fatigue failure. As shown in Figure IV. 41, the fracture surface exhibits two distinct regions. The cross section area corresponds to the fatigue crack region, whereas the coarse zone at the top of the final catastrophic failure is the remaining cross section that survived to the fatigue damage.

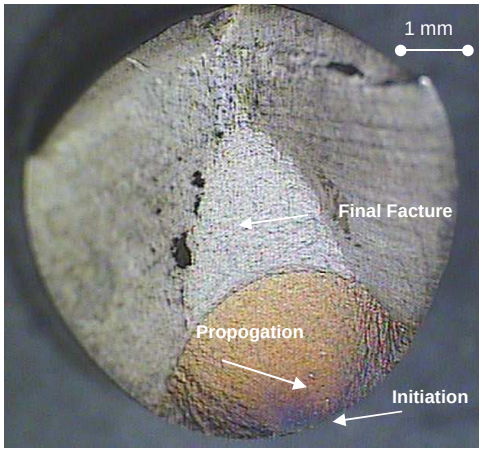

Figure IV. 41 : Typical appearance of a LCF fracture surface of IN718 at 550°C.

Initial cracks are observed close to the outer perimeter of the fatigue specimen: cracks develop with an angle of about 45° over a few microns before propagating perpendicular to the axial longitudinal loading. Higher magnification observations, performed along the crack propagation direction, show the presence of wavy darker and lighter bands that are commonly called “beach marks”. These marks contain thousands of “striations” assumed to be individual steps of crack propagation, with inter-distance that depends on the stress/strain range. Specific researches on the mechanism of fatigue striations were carried out by Laird and Smith and later by Neumann and Pelloux **[Pelloux,1970; Neumann,1974]**. The authors showed that in a high-strain loading cycle, crack extension is associated to a sliding off mechanism with blunting of the crack tip during loading and consequent re-sharpening upon unloading.

This mechanism, called “plastic blunting”, plays an important role in the damage process relative to the Stage II of the crack propagation. Figure IV. 42 reports a schematic attempt for

representing the different phases of the phenomenon. Under the application of the tensile load, metal plastifies plastically due to the high stress concentration. Plasticity is located along the slip planes of maximum shear stress (b) and crack tip blunts occur under further increase of the tensile load. This mechanisms leads to the displacement of the crack tip (c). Finally, when loading is reversed, the crack tip returns to a sharp configuration through the opening of newly created surfaces. This results in the formation of striation (d and e). Making the assumption that the compression loading is not sufficient to fully annihilate the crack tip blunting, a net crack growth occurs during the subsequent tensile load.

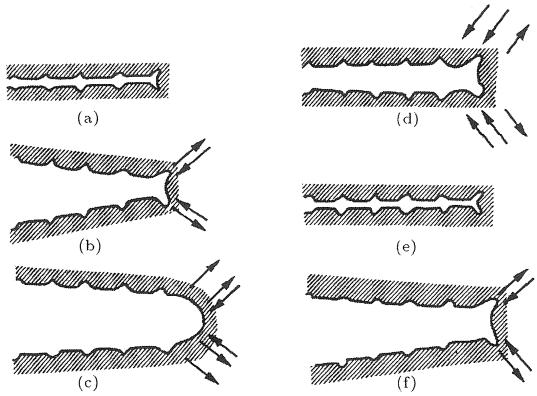

Figure IV. 42 : Plastic blunting process due to fatigue crack propagation in the Stage II mode, considering a vertical stress axis. [McEvily et al.,2010]

This process of fatigue crack growth, via striations formation, leads to the propagation of a fatigue crack on a cycle-by-cycle basis. As reported by Cai **[Cai et al.,2001]**, the crack extension occurs upon each single load cycle as a consequence of cyclic slip occurring at crack tip.

These assumptions are considered in detail for the fractographic investigations of the fatigue surfaces as reported in the next sections.

IV.3 Fatigue striations spacing (FSS) assessment

The relationships between microstructure and engineering properties represent one of the primary goals of this research work. Focusing on fatigue mechanisms, the understanding of the quantitative effects of various microstructural features on crack inititation and propagation is limited by the localized nature of the damage mechanisms. In the previous section, the presence of fatigue striation has been related to transgranular crack propagation, able to inhibit the development of time-dependent mechanisms (generally associated to intergranular propagation).

In addition to these features, a fractographic study of the fatigue surfaces is prone to allow the identification of the failure process history, in particular the description of fatigue crack growth as a function of time and space (distance from the initiation site) **[Levaillant et al.,1982]**.

The first step to the quantitative analysis of fracture profiles is based on the measurement of the fatigue striation spacing. The method, used here, consists in measuring the number (N) of striations intercepting a reference straight line (with length L_T) lying along the direction

normal to striations.

In such a way, the average center to center spacing i_m, between two adjacent striations, is expressed by the following ratio:

$$i_m = L_T/N \qquad \textbf{Eq. IV. 11}$$

Specimens are placed in the SEM with the plane of fracture accurately perpendicular to the electron beam axis. This configuration is an essential requirement because angular mis-orientations can be a source of significant error **[Connors,1994]**.

The measurements are carried out in a direction normal to the striations orientation, that is essentially grain-dependent (Figure IV. 43(a)). The obtained values must be recalculated by projecting them on the crack propagation direction (CPD) (Figure IV. 43(b)). The random distribution of the parallel striations requires the introduction of a correction factor. Underwood and Starke **[Underwood,1979]** studied the specific geometrical relations concerning the striation spacing. They observed that when striations are randomly oriented with respect to the direction of propagation, a correction factor (evaluated following the geometrical relationship between the CPD and the fatigue striations orientation) of $2/\pi$ is required. In this case, the striation spacing is expressed by:

$$i = 2/\pi * i_m \qquad \textbf{Eq. IV. 12}$$

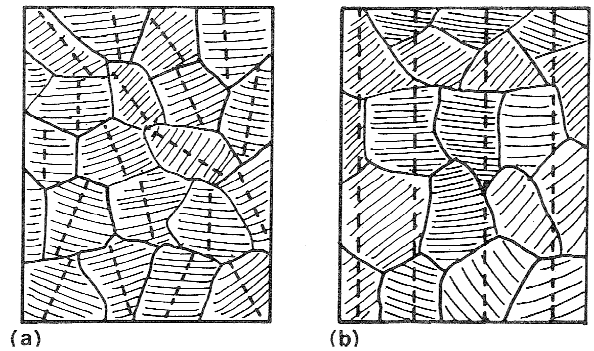

Figure IV. 43 : Methods of measurement of fatigue striation spacing on fatigue surfaces: (a) measurement normal to striations, (b) measurement normal to macroscopic direction of propagation [Chermant et al.,1979].

IV.4 Fractographic reconstitution methodology

The fractographic methodology, described above, is applied for the reconstitution of fatigue cracks of failed LCF specimens. In general, one or several cracks grow simultaneously in a direction perpendicular to the loading axis until the complete rupture of the sample occurs. The fracture surface is then assessed by SEM observations.

Measurements are carried out on three specimens, subject to LCF tests under cyclic loading (1 Hz) at different total strain amplitudes (±1%, ±1.2%, and ±0.6%). As illustrated in previous sections, the applications of this type of loading leads to a transgranular fracture characterized by significant striation.

The fracture surface in the region of the predominant crack is characterized by three different zones (Figure IV. 41):

- *Stage I: crack initiation and preliminary propagation zone (free of striations);*
- *Stage II: ductile propagation zone (with striations);*
- *Stage III: final propagation zone.*

The first zone corresponds to the Stage I: fatigue striations are not observed in this zone at least along distance lower than 25-50 µm from the outer surface of the sample (crack initiation site).

These observations are in agreement with the results reported by Jacquelin, for Inconel 718, **[Jacquelin,1983]** who defined the crack initiation onset as the number of cycles required to obtain a crack length close to the grain size. The standard microstructure, examined for these analyses, shows a small grain size, close to 20 µm, that is in agreement with the extent of crack initiation stage.

The largest part of the fatigue fracture surface corresponds to Stage II of crack propagation, where ductile striations are detected perpendicular to the direction of the loading axis. The striation spacing increases with the advance of the crack length (a). Figure IV. 44 reports a *qualitative* comparison of the striation spacing for different crack depths, for a sample loaded with a total strain amplitude of 1.0%.

Finally, stage III is related to unstable crack growth that is controlled by static modes of failure and is very sensitive to the microstructure, load ratio, and stress state (plane stress or plane strain loading).

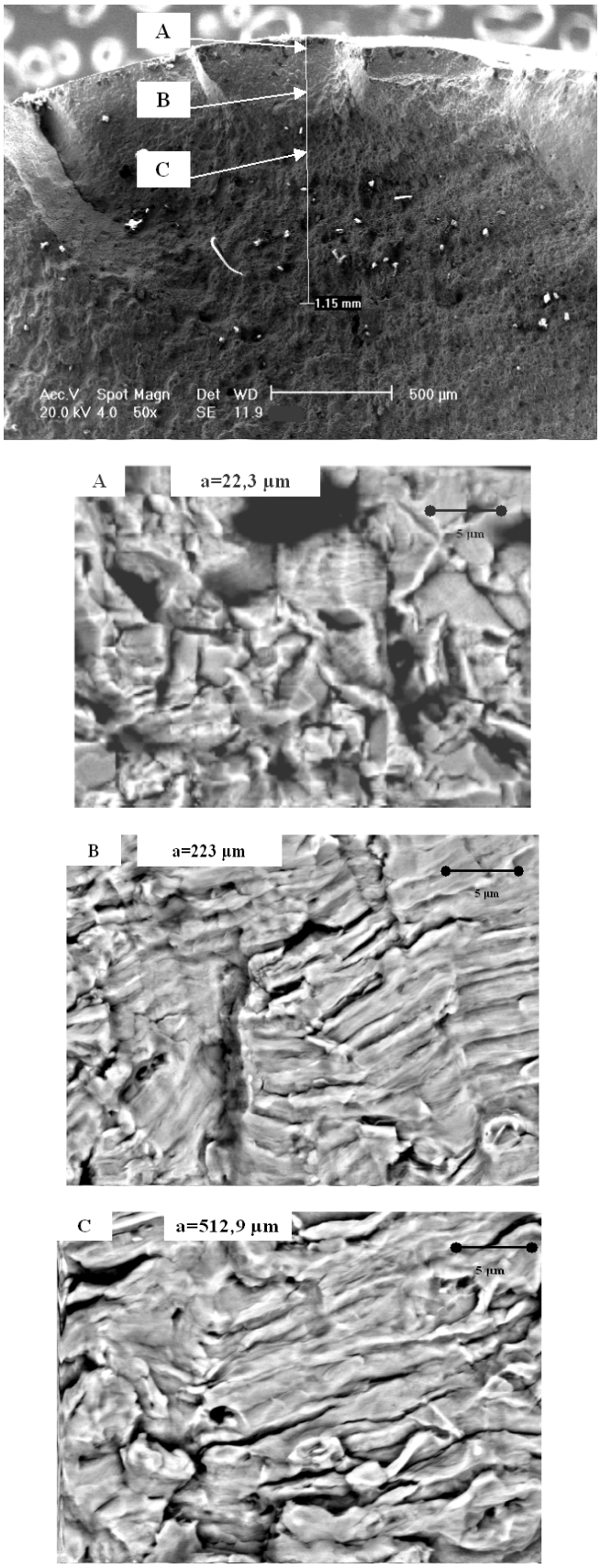

Figure IV. 44 : SEM investigation of fracture surfaces at different crack length: a=22,3 µm (A), a=223 µm (B) and a=512,9 µm (C)

Quantitatively, the results of these preliminary analyses are summed up in Figure IV. 45 where (i) is plotted against (a).

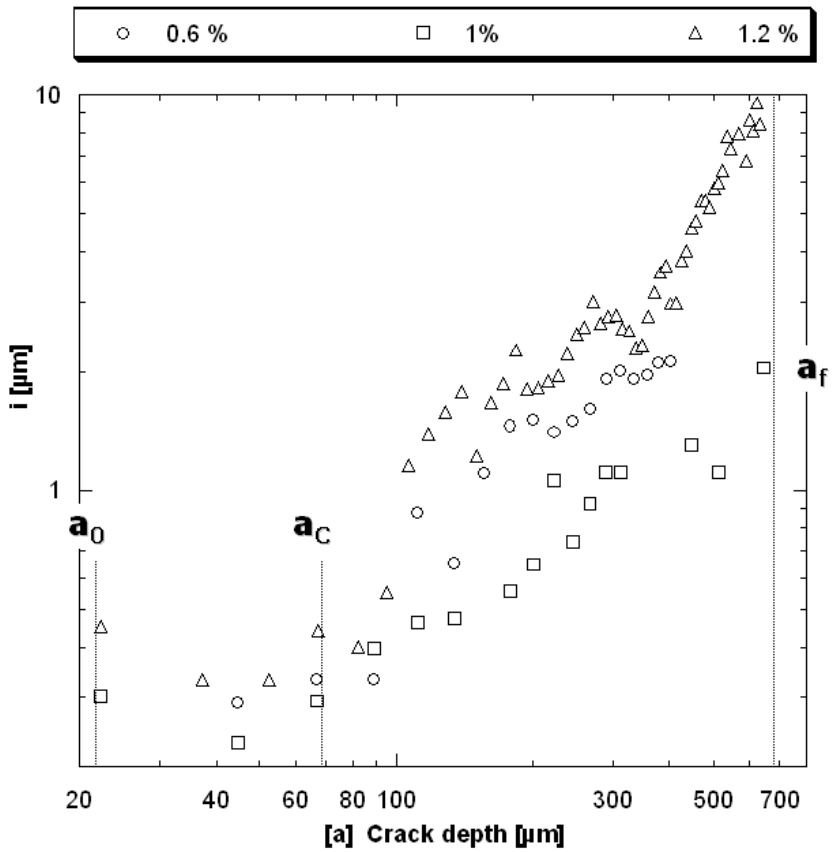

Figure IV. 45 : Typical examples of striation spacing as function of the crack length under various LCF conditions (a_0=22,3 µm, a_c=69 µm and a_f=680 µm) .

All specimens show a similar behaviour based on three different regimes associated to specific crack length ranges, that can be described as:

1. *Stage I* where $0 < a < a_0$: Once initiated, a fatigue microcrack ($a_0 \approx 20$ µm) propagates at the surface of the specimens along high shear stress planes. This zone is very limited as compared to the final crack depth. However the crack initiation, followed by a short crack growth stage, (free of fatigue striations) is a very long process which leads to a propagation rate of few Angstroms per cycle **[Bathias,1979]**.
2. *Stage II where* $a_0 < a < a_f$ *:* this stage is mainly characterized by the formation of fatigue striations on the fracture surface. Two different zones can be pointed out by a detailed study of the striation spacing:
   a) *The preliminary fatigue striations where* $a_0 < a < a_c$: the crack growth follows a nearly constant rate. The presence of this "steady state" may be explained considering two hypothesis:

- Fatigue striations are extremely fine and SEM measurement is not accurate enough to detect such slight variation in striation spacing.
- In the early stages of the crack propagation, the extent of plastic deformation at

the crack tip is generally small and the associated stress intensity factors do not induce rapid crack propagation.

b) *The continuous crack propagation where* $a_c < a < a_f$: the crack propagation continuously increases with the crack length up to the complete fracture of the specimen.

Following these assumptions and as generally admitted we can express the fatigue life as the sum of the initiation fatigue life Ni and the propagation fatigue life NP:

$$N_f = N_i + N_P \qquad \textbf{Eq. III.3}$$

Following the results reported by Oudin **[Oudin,2001]**, the propagation mechanism can be described in two steps:

1. N_{p1}: the number of cycles required to propagate the crack from a_0 *to* a_c under the effect of a nearly constant crack growth rate (ν).
2. N_{p2}: the number of cycles required to propagate the crack from a_c *to* a_f with increasing rate following a specific law.

$$N_p = N_{p1} + N_{p2} \qquad \textbf{Eq. III.4}$$

The number of cycles corresponding to the regime where crack propagation remains constant is:

$$N_{p1} = \frac{(a_c - a_0)}{\nu} \qquad \textbf{Eq. III.5}$$

On the other hand, propagation fatigue life can be evaluated considering the striation spacing as an input for the relation proposed by Nedbal **[Nedbal et al.,2008]**:

$$N_{p2} = \int_{a_c}^{a_f} \frac{da}{D(i) \cdot i(a)} \qquad \textbf{Eq. III.6}$$

Where a_f corresponds to the final crack length, a_c represents the crack length from which striation spacing starts progressively to increase and D(i) is the ratio between striation spacing (*i(a)*) and macroscopic crack growth rate ($\nu = da/dN$) [$D = \nu/i$]

The latter factor reflects the local microscopic processes that take place at the crack tip during the growth of the macroscopic fatigue crack. These phenomena are influenced by the heterogeneous microstructural features and by a continuous redistribution of the externally induced stress and strain fields.

In order to simplify the estimations and referring to results reported by de Matos **[de Matos et al.,2005]**, all integrations are carried out using D=1. In such a way we conclude that the distance between two striations (*i*) is specifically related to the instantaneous crack growth rate at a given crack depth (*a*).

Following these assumptions, the numerical integration of the experimental striations spacing curves is based on these assumptions:

- *The knowledge of one pair of data (N_i, a_i);*
- *D= v/i =1*

For each case, the couple of data is derived from the total number of cycles spent under LCF conditions (N_f) and the final crack length a_f that is assessed on fracture surfaces by SEM investigations.

Calculations provide the number of cycles necessary for crack propagation (N_p). As a consequence of these results, fatigue initiation life can be evaluated as the complementary fraction of the fatigue life:

$$N_i = N_f - N_P \qquad \textbf{Eq. IV. 13}$$

Results are showed in Figure IV. 46 where N_i is related to the number of cycles to failure N_f evaluated by the experimental LCF tests.

The diagram illustrates, for high strain amplitudes, a crack initiation process that represents the major part of the fatigue life, ranging between 75% and 90%. Results are closed to that reported by Jacquelin **[Jacquelin,1983]** for Inconel 718 LCF tests performed at 20°C.

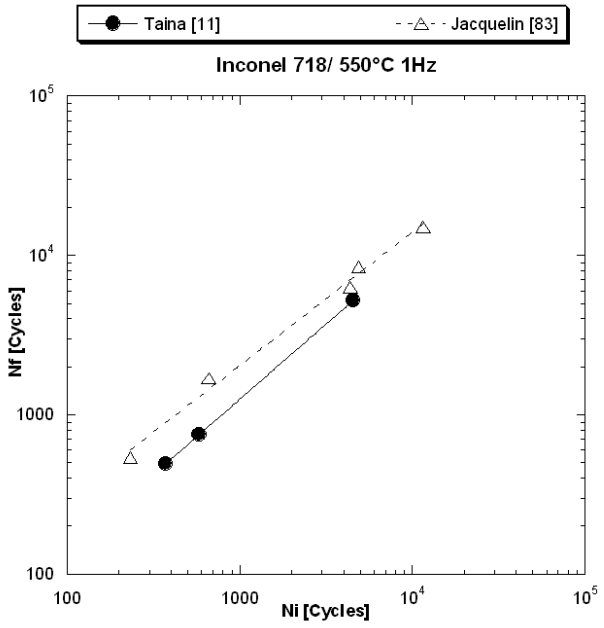

Figure IV. 46 : Correlation between crack initiation life (N_i) and total fatigue life (N_f)

In agreement with Oudin **[Oudin,2001]**, N_i and N_p could be represented as a function of the applied mechanical strain range as reported in Figure IV. 47. For both cases, data follow a power law type that is similar to the Manson-Coffin relationship commonly used to represent LCF data (N_f).

In such a way we can conclude that the initiation fatigue life is slightly improved when the applied strain is lowered, as a consequence of the minimized stress/strain concentrations acting to promote crack initiation.

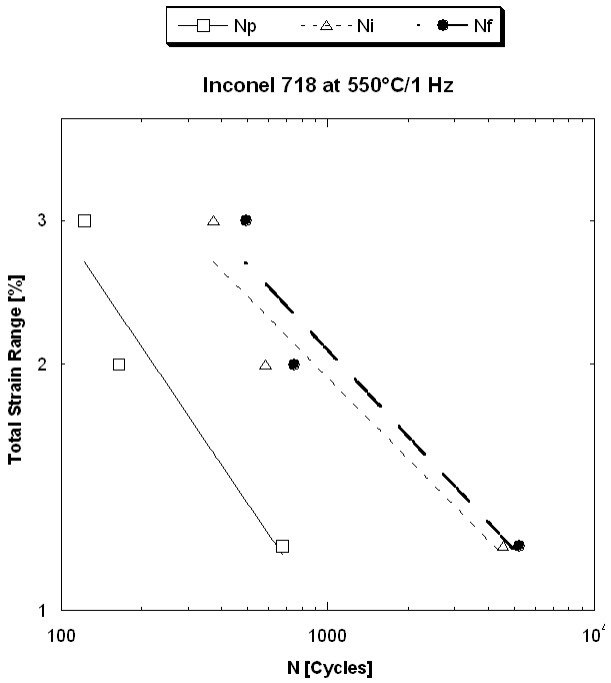

Figure IV. 47 : Mechanical strain range as function of N_P, N_i fraction lives and N_f fatigue life.

IV.5 Crack growth rate assessment

Low cycles fatigue is impacted by a large variety of mechanical and microstructural parameters. As described in the previous section, the fatigue behaviour is based on an extended fatigue crack initiation followed by a rapid propagation mechanism which determines the final fracture. The crack propagation mode determines the crack propagation rates: intergranular propagation (respectively transgranular) is associated to high growth rates (respectively low growth rates).

The propagation behaviour, under cyclic loading, is related to the crack size and to the mechanical behaviour of the damaged material. LCF specimens exhibit one or more prevalent small cracks that are significantly larger than the size of the local zone of plasticity. In this case, the Linear Elastic Fracture Mechanics (LEFM), which characterizes the growth of a linear elastic crack, can not be used, and an elasto-plastic approach is required because plasticity is not restricted in a delimited zone.

The aim of this section is to propose a method for predicting crack growth rate under LCF conditions. This study is based on the partition of the problem into three distinct tasks that can be solved independently:

1. **Microstructural analysis of the main crack**: the first problem consists in developing a fractographic study of the fatigue surfaces allowing the identification of the failure process history.
2. **Calculation of key fracture parameters**: once the explicit fractographic analysis is assessed, a failure criterion to evaluate the local crack-tip properties (stress, plasticity,

displacement) is required.

3. **Crack propagation rate prediction**: once the fracture parameters are available, the final step consists in establishing the relationships between the microstructural investigations and the engineering properties previously evaluated. In such a way, a prediction of the crack propagation rate under various loading conditions (different total strain amplitudes) can be assessed.

Previous sections focused on a detailed analysis of the fracture surfaces based on fatigue striations spacing measurement. The calculation of the key fracture parameters is discussed in the next sections. Finally, a direct comparison of the predicted crack propagation rates with the experimental results published in the literature is presented.

IV.5.A Relationship between Low Cycle Fatigue properties and crack growth rates

The Linear Elastic Fracture Mechanics is generally used to predict fatigue life of laboratory fatigue specimens crack propagation tests. The elastic stress intensity factor (ΔK) is considered as the key fracture parameters in fatigue crack growth under elastic conditions and when the plastic zone around the crack tip is small compared to the crack length. ΔK reflects the stress field near the crack tip, but also the plasticity occurring in this region.

If the above requirements are not met, the cyclic J-integral, in the frame the Elastic plastic Fracture mechanics (EPFM) may be employed. This approach was introduced in order to evaluate crack growth rate where deep cracks and large plasticity are achieved. This method accounts for the stress intensity field at the crack tip by evaluating the energy dissipated during fracture per unit of newly created fracture surface (strain energy release rate). This is a basic concept of fracture mechanics: the energy required by a crack tip to grow must be equal to the amount of energy dissipated for the creation of new surfaces and for inelastic mechanisms to operate. The J-integral approach provides a better understanding of the physical parameters of fracture for a dynamic crack tip in the case of extended plastic deformation.

From a theoretical point of view, the J-integral, as defined by Rice **[Rice,1968]**, is acceptable only for monotonic loadings. This method does not take into account the effects of the residual plasticity in the case of a cyclic loading applied to an elastic-plastic material. For this reason, Dowling and Begley **[Dowling et al.,1976]** proposed a correction to the standard approach in order to transform J in ΔJ.

This approximated solution assumes that fatigue crack propagation consists in a crack growth within a plastic zone and that the fatigue fracture behaviour of this specific area is similar to that of an LCF sample.

The ΔJ expression may be deduced from its original definition, corresponding to a monotonic loading, introducing the total applied strain and stress ranges ($\Delta\varepsilon$ and $\Delta\sigma$). Following these assumptions, the ΔJ_{Cycl} integral can be expressed as the sum of an elastic (ΔJ_{el}) and a plastic (ΔJ_{pl}) components related to the LCF data:

$$\Delta J_{Cycl} = \Delta J_{el} + \Delta J_{pl} \qquad \textbf{Eq. IV. 14}$$

Both terms of the relationship are subsequently examined paying attention to their scientific meaning and physical expression.

Focusing on the linear elastic component (ΔJ_{el}), the J integral corresponds to the strain energy rate. When the plane strain conditions and the isothermal test conditions are fullfilled, the J-integral may be expressed as following:

$$\Delta J_{el} = \frac{\Delta K^2}{E} \qquad \textbf{Eq. IV. 15}$$

(The modulus of elasticity (E) being deduced from the tensile test carried out at 550° C).

The previous equation can be transformed into:

$$\Delta J_{el} = \frac{1}{E} \cdot Y^2 \pi \cdot a \cdot \Delta\sigma^2 \qquad \textbf{Eq. IV. 16}$$

Where $\Delta\sigma$ is the applied stress range and Y is a geometrical correction factor, calculated by the approach described above.

The evaluation of this parameter for cylindrical component, such as fatigue specimens, is a complex problem that requires a three-dimensional approach.

According to Yang results **[Yang et al.,2006]**, the evolution of the crack shape may be approximated by an elliptical curve, as reported in Figure IV. 48, where 2b is the major axis and 2a the minor axis of the ellipse. As observed by other authors **[Branco et al.,2008]**, the early propagation is sensitive to the initial crack configuration. For the semi-circular (a/b=1) and elliptical tip (a/b<1) the crack advances more rapidly towards the centre of the specimen than along the free surface. This is due to the maximum stress intensity factor attained at the deepest point of the crack. As a consequence, the crack front tends to become curved and the aspect ratio a/b increases.

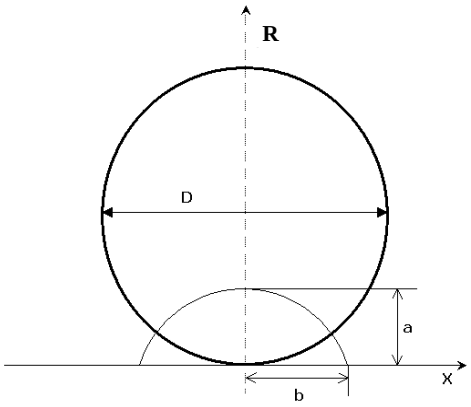

Figure IV. 48 : Geometrical configuration of a semi-elliptical crack in a round bar [Yang et al.,2006].

A mathematical correction approach, based on specific finite element analyses, was defined by Yang as a function of the relative crack length, respectively estimated at different locations

on the crack tip:

$$Y = 0.906 - 1.23 \cdot \left(\frac{a}{D}\right) + 0.599 \cdot \left(\frac{a}{D}\right)^2 + 12.0 \cdot \left(\frac{a}{D}\right)^3 - 11.2 \cdot \left(\frac{a}{D}\right)^4 \quad \textbf{Eq. IV. 17}$$

Where D is the specimen diameter.

In such a way, ΔJ_{el} can be calculated for every point along the crack tip, from the deepest point of the crack and assuming a semi-elliptical geometry.

Similarly to ΔJ_{el}, the plastic component ΔJ_{pl} can be calculated using a reference stress approach that follows the general relationship proposed by Liu **[Liu et al.]**:

$$\Delta J_{pl} = 2\pi Y^2 a \left(\int_0^{\Delta\varepsilon_p} \sigma d\varepsilon_P \right) \quad \textbf{Eq. IV. 18}$$

The integration factor corresponds to a cyclic stress/strain relationship that respects a power hardening law:

$$\sigma = C_0 \varepsilon_p^{\ n^*} \quad \textbf{Eq. IV. 19}$$

Where C_0 and n* are material dependent constants that can be evaluated from the tensile loading portion of the cyclic hysteresis loop corresponding to each LCF cycle.

Substituting the latter equation in the ΔJ_{pl} relationship, we obtain:

$$\Delta J_{pl} = 2\pi Y^2 a \left(\int_0^{\Delta\varepsilon_p} C_0 \varepsilon_p^{\ n^*} d\varepsilon_P \right) \quad \textbf{Eq. IV. 20}$$

$$\Delta J_{pl} = 2\pi Y^2 a \cdot \left(\frac{(C_0)(\Delta\varepsilon_p)^{1+n^*}}{(1+n^*)} \right) \quad \textbf{Eq. IV. 21}$$

A second form of the relationship can be expressed assuming the hardening equation of the cyclic stress/strain curve as:

$$\Delta\sigma/2 = k'\left(\Delta\varepsilon_p/2\right)^{n'} \quad \textbf{Eq. IV. 22}$$

where k' and n are material constants that can be related to C_0 and n* following Mowbray suggestions **[Mowbray et al.,1976]**. The authors considered the loading portion of the hysteresis loop equal to the cyclic stress/strain curve when the latter is expanded by a scale factor of 2. In such a way material constants are respectively:

$$n^* = n \quad \text{and} \quad C_0 = (2)^{1-n'} \cdot k' \quad \textbf{Eq. IV. 23}$$

Based on these considerations, the cyclic J integral is estimated by the following relationship:

$$\Delta J_{Cyclic} = 2\pi Y^2 a \cdot \left[(\Delta\sigma^2/2E) + (2^{1-n'} k' (\Delta\varepsilon_p)^{n'+1}/(n'+1) \right] \quad \textbf{Eq. IV. 24}$$

where *K', n', $\Delta\varepsilon_p$* and *$\Delta\sigma_p$* are related to LCF experiments.

For this reason, a different interpretation of the fractographic results may be considered, in

the form of a crack propagation curve that relates the crack length to the number of cycles (Figure IV. 49). The crack depth is measured by SEM investigation as the distance between the crack initiation site and the edge of the fatigue striations zone.

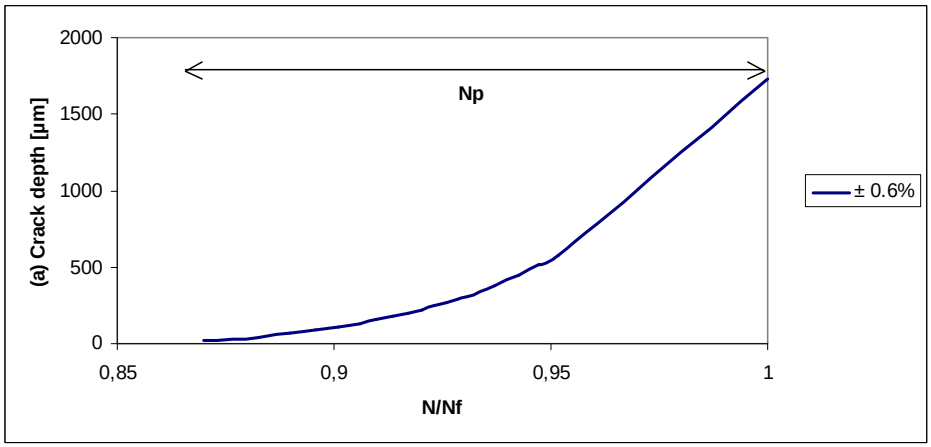

Figure IV. 49 : Fatigue crack history reconstitution for a fatigue test carried out with a total strain amplitude of ±0.6 %.

Following the fractographic reconstitution of crack growth with time, a=a(N), and analysing the stress-strain response under LCF conditions associated to each cycle, it is possible to evaluate all the parameters included in the J-integral relationship. In such a way, ΔJ_{Cycl} is estimated at the crack tip as a function of the increasing crack length (*a*).

Finally, the J-integral is used to predict the theoretical crack growth rate following the relationship proposed by Sadananda **[Sadananda,1984]**:

$$\frac{da}{dN} = A\left(\sqrt{\Delta J_{Cycl} E}\right)^m \qquad \textbf{Eq. IV. 25}$$

Where *A* and *m* are two constants relative to the material and *E* is the Young modulus.

Consequently, the crack growth rate curves may be assessed by using the $\sqrt{\Delta J_{Cycl} E}$ parameter as a Fatigue Crack Growth Rate (FCGR) criterion.

The general algorithm, considered for the fractographic reconstitution by the J-integral method, is reported in Figure IV. 50.

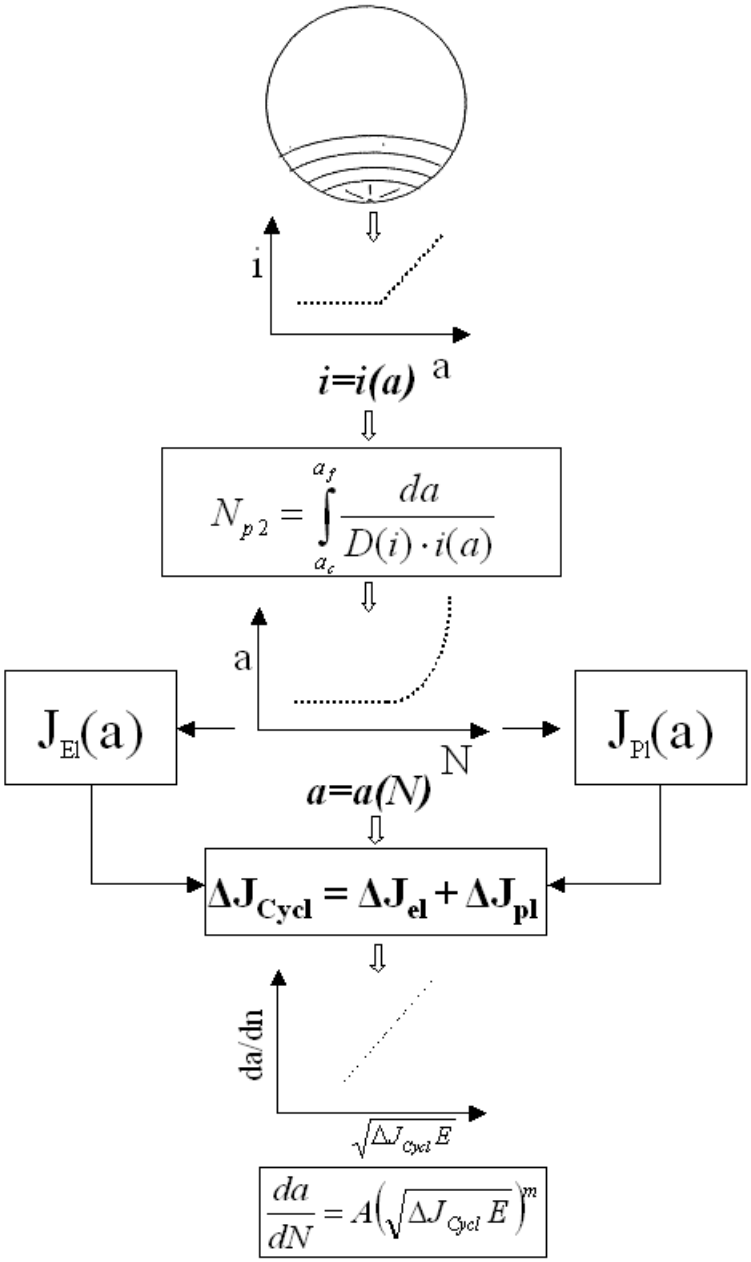

Figure IV. 50 : Algorithm for fractographic reconstitution by the J-integral approach.

The fractographic results, associated to the $\sqrt{\Delta J_{Cycl} E}$ parameter are reported in Figure IV. 51.

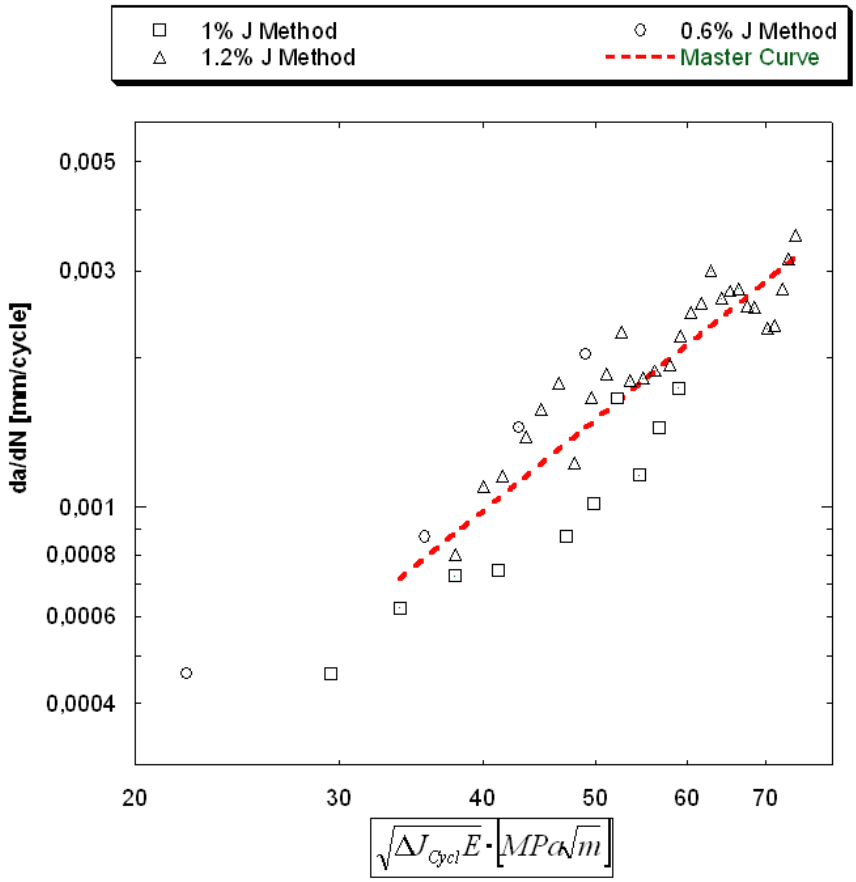

Figure IV. 51 : Crack growth rate reconstitution by striations spacing using the J-integral approach.

The crack growth parameters obtained for the three LCF tests used in this investigation are presented in Table IV. 4. A general Master curve is plotted by the aim to predict the average crack propagation rate for increasing $\sqrt{\Delta J_{Cycl} E}$ parameters.

$\Delta\varepsilon_{tot}$	A	m
± 0.6%	2.36 x 10^{-8}	2.27
± 1.0%	1.10 x 10^{-6}	1.77
± 1.2%	2.56 x 10^{-6}	1.65
Master Curve	8.69 x 10^{-7}	1.91

Table IV. 4 : Summary of the crack rate parameters obtained for different applied total strains under LCF conditions.

IV.5.B Comparison with experimental results

The final step of our investigation consists in a direct benchmarking with the experimental crack growth results, published in the literature **[James,1986; Ghonem et al.,1993; Xie et al.,1997]** and evaluated on Compact Test (CT) specimens. These reference data are plotted as a function of the stress intensity factor, ΔK evaluated by the Linear Elastic Fracture Mechanics (LEFM). In such a way test performed with a load control at temperatures closed or equal to 550°C have been selected even if the test parameters (such as frequency (f) and stress ratio (R)) differ from our standard LCF tests. Figure IV. 52 compares the literature data with the crack growth rates predicted by a J-integral approach.

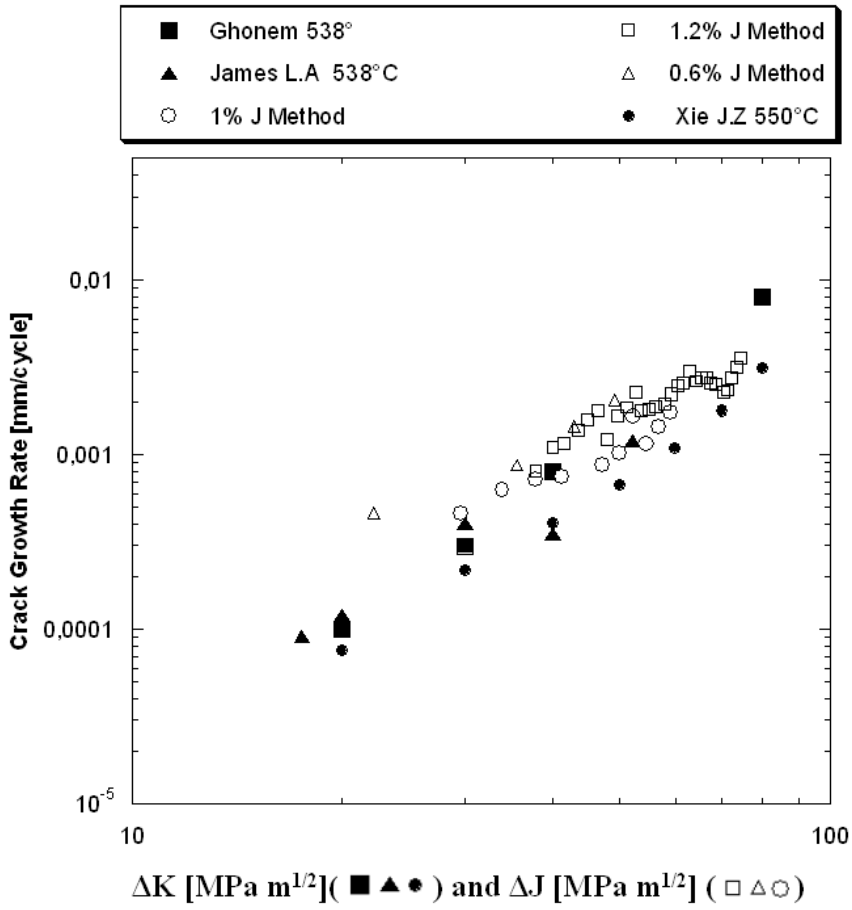

Figure IV. 52 : Comparison between the experimental crack growth rates, evaluated by a fractographic reconstitution of LCF tests, and the literature data obtained on C.T specimens.

Compared with elastic-plastic crack growth experimental data, this alternative approach shows good correspondence: the scatter is limited and the results are satisfactorily similar. The crack growth constants associated to the experimental results reported in literature, are listed in Table IV. 5.

Source	*T [°C]*	*A*	*m*	$\frac{\left(da/dN\right)}{\left(da/dN\right)_{J-Method}}$ *for* $\frac{\Delta K = 50MPa\sqrt{m}}{\sqrt{\Delta J_{Cycl} E} = 50MPa\sqrt{m}}$
[James,1986]	538	1.82×10^{-7}	2.17	0.6
[Ghonem et al.,1993]	538	6.42×10^{-9}	3,19	1.1
[Xie et al.,1997]	550	3.2×10^{-8}	2.58	0.5
J Method-Master Curve	550	8.69×10^{-7}	1.91	1.0

Table IV. 5 : Summary of the crack rate parameters associated to the experimental FCGR tests reported in literature.

Furthermore, the Table reports a ratio between the predicted crack propagation rate obtained through standard CT specimens, available in literature, and our crack growth rate obtained by fractographic analysis of LCF specimens for a value of $\Delta K \approx \sqrt{\Delta J_{Cycl} E}$ equal to $50\,MPa\sqrt{m}$.

The values assumed by this ratio, ranging between 0.5 and 1.1, justifies the validity of the theoretical model and points out a close link between the LCF properties and the FCG behaviour. The J-integral approach provides a good correlation between crack growth and crack length, in the case of extended plastic deformation.

However, the robustness of the method has to be assessed on other test data obtained under various loading histories (as well as frequency, strain, stress and temperature) in order to precisely determine where it can be generalized.

As described above, fatigue crack growth produces, on fracture surfaces, some striations that can help in understanding the location of the crack origin and the directionality of propagation. The practical approach proposed for the fractographic reconstitution of the fatigue crack growth provides complementary information to that obtained from classical LCF tests, reducing the costs directly related to the specimens preparation and to the realization of extensive FCG test campaigns.

V Conclusion

In the preliminary part of this chapter, attention is given to the cyclic behaviour of Inconel 718 under various LCF test conditions. A cyclic behaviour model is proposed in order to predict the stress-strain response typical of extrusion dies. The considered model is a strain rate independent version of the non-linear kinematic hardening model proposed by Chaboche **[Chaboche et al.,1994]**. The constitutive equations are integrated in a FEA code to simulate the evolution of the stress-strain state in an experimental extrusion die. The good agreement between the simulations and the experimental data, obtained by direct measurements on production presses, indicates that the Dynamic Modelling provides satisfactory estimates of the evolution of the loading state (stress-strain) in the tool

Attempts were made to compare the simulated results using the material dynamic model used by Hydro. Comparisons show that the dynamic model is able to predict the evolution of loading state cycle by cycle, taking into consideration the different transient phenomena (such as softening) which are not assess by the traditional method. In such a way, the so called "Dynamic Material Modelling" may represent an interesting alternative to high risk and cost trial and error approach for design of Ni-base superalloy dies.

In the second part of the chapter, the fatigue life assessment of Inconel 718 at elevated temperature (550°C) is presented. Two LCF fatigue signals are considered. A cyclic symmetric waveform (1 Hz) is considered as a preliminary approach to the fatigue life behaviour, then, a trapezoidal signal (150_20 s), characterised by holding times in tension and compression, is used to reproduce the die loading state during the extrusion cycle. Fatigue life curves are plotted using the so-called Manson-Coffin relationship, identifying the relation between inelastic strain and fatigue life.

In both cases, a similar cyclic behaviour is detected: material exhibits a continuous softening from the very first cycles. This mechanism results in a continuous stress decrease coupled to an inelastic strain enhancement.

Comparisons between Inconel 718 and the traditional Hot Work tool steels are proposed, for similar LCF tests conditions, assessing the better performances of the superalloy. Differences in terms of stress-strain response are identified: after a preliminary stress decrease, steels show a continuous linear softening regime, while Inconel 718 exhibits an apparent stability of the stress amplitude (pseudo-stabilized stage). It can be concluded that as a better cyclic behaviour is obtained, the life time of an extrusion die, using Inconel 718 as a bulk material, will be longer that that of traditional steel dies.

The effects of different mechanical parameters on the fatigue life behaviour of Inconel 718 are investigated in details. The following conclusions can be derived:

- ***Effect of Holding Time***

The application of a holding time at maximal and minimal stress provokes an average

decrease of the fatigue life by 33% as compared to that obtained with a cyclic signal (1 Hz). This effect may be explained by the increase of the plastic strain amplitude at half life due to the stress relaxation during holding time Investigating effect of holding time at maximum strain is corresponding to the influence of extrusion cycle length. The die will be submitted to maximum loading as soon as the pressure ramp-up starts and will be until billet extrusion is completed. Among parameters affecting cycle duration, we especially shall consider the actual billet length, the ramp-up time (time to reach max press force) and deceleration time (extrusion speed decrease to cycle stop). These parameters are prone to fluctuate for process control reasons and it is commonly accepted that overall cycles are spanning from 45s and 300s. Being aware of cycle length effect on die life may be critical and selecting both die design parameters and extrusion process control. Three different wave-forms were considered to cover the 45-300 s interval (holding time 45 s, 150 s and 300 s). The increase of the exposure time at maximal strain does not further decrease the fatigue life. As a matter of fact, material exhibits a rapid stress decrease during the first 40 seconds of the steady time, followed by a linear relaxation which has limited effects on the inelastic strain. It is then understood that over 40s of extrusion cycle and within 300s. no large die life difference should observed which allow to conclude that Inconel 718 die may not need design changes due to selected cycle duration selected by press team.

- ***Strain rate***

At 550°C, low cycle fatigue behaviour is strongly influenced by the strain rate. A strain rate of $5 \cdot 10^{-3} s^{-1}$, defined as the average die loading rate assessed at the press, has been adopted as the reference value for the extrusion cycle simulation. LCF tests carried out at this strain rate ($5 \cdot 10^{-3} s^{-1}$) exhibit, on stable hysteresis stress-strain loops, stress instabilities associated to the Portevin-Le Chatelier effects (PLC). In other words, changes in fatigue behaviour are due to the interaction of cyclic deformation and time dependent processes that act concomitantly on the stress-strain response, on the heterogeneity of the deformation mechanisms and on the resistance to oxidation-assisted intergranular cracking. In terms of microstructural evolution, the reduction in fatigue life, at low strain rate, is attributed to the acceleration of fatigue initiation, associated to the increased density of planar slips, and to the change of crack propagation from a transgranular to a mixed mode type.

Following these assumptions, it can be concluded that strain rate and holding time have a significant impact on fatigue life, although any effects are detected on the cyclic behaviour at 550°C. Generally speaking, we can interpret these effects as *time-dependent phenomena*: the application of a holding time or the variation of strain rate act on the frequency of the fatigue cycle. Slow cycles enhance the interaction between mechanical loading and environmental effects producing mixed or intergranular brittle fractures. In such a way, the total cyclic time affects the deformation mechanisms, which have a direct impact on the fatigue behaviour. Results reported in this chapter

demonstrate that the total cycle time, as well as the loading frequency, can influence the fatigue life of Inconel 718, contributing to its final fracture mode. These assumption are confirmed by previous studies **[Ghonem et al.,1993]** focused on crack growth rate, as reported in Figure IV. 53. At frequencies below 0.01 Hz the fracture behaviour becomes "Time–dependent" and the fatigue crack growth rate increases as cyclic frequencies decrease. On the other hand, for frequencies above 10 Hz, the material becomes totally "Cycle-dependent" leading to crack growth rates that are independent of frequency. Different mechanisms of crack growth are associated to each regime. Transgranular propagation, with striation formation, is generally observed in the cycle-dependent regime, whereas intergranular crack growth is the predominant mechanism observed in the time-dependent regime.

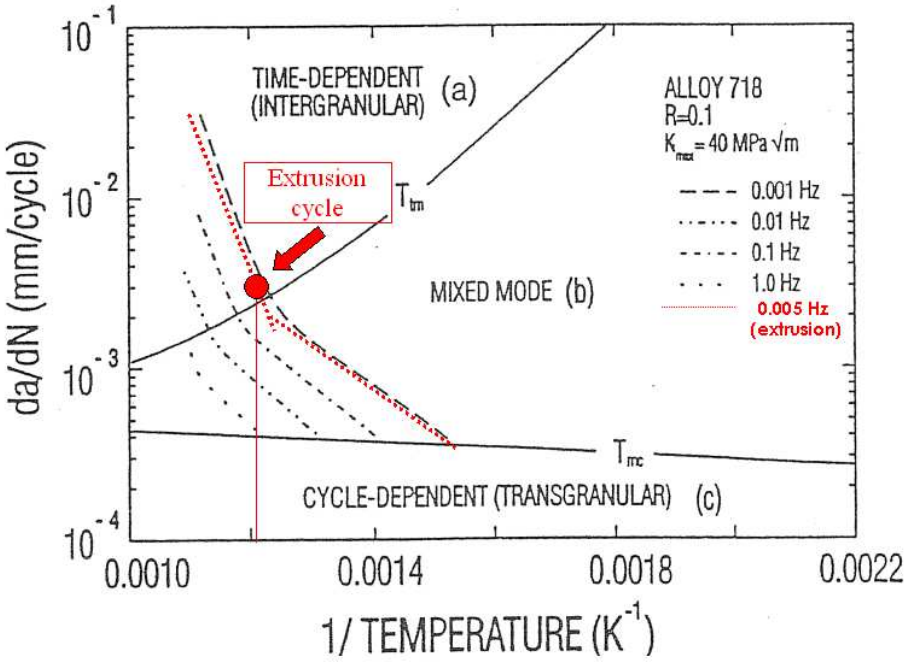

Figure IV. 53 : Effects of cyclic frequency on alloy 718 tested at high temperature [Ghonem et al.,1993].

The reference extrusion cycle, determined by a holding time of 150 seconds at 550°C (1/T=0.0012 K^{-1}), could be defined as an equivalent frequency of 0.005 Hz. These data, opportunely associated to the diagram reported in figure, defines the aluminium extrusion as a process affected by an interaction between a mixed and a time dependent damaging mode. Holding time and strain rate are two mechanical parameters that increase the risks associated to these time dependent phenomena. In particular, the strain rate which corresponds to the die loading rate has an important influence on the mechanical performances of the tools. Results suggest that an increase of the loading rate may improve the extrusion die life limiting the material softening and delaying the fatigue crack nucleation.

Practically at the press, this would mean that it could be of interest to discuss the possibility for the hydraulic piloted ram to have a higher loading rate capacity. Clearly some press construction limitations are expected to be met. On the other hand, a

reduction of this loading rate (excessive reduction of die loading from $5 \cdot 10^{-3} s^{-1}$ to $5 \cdot 10^{-4} s^{-1}$) may lead to negative change of die life (die life reduction by a factor of 3) and shall consequently brought to attention to extrusion managers using Inconel 718 dies.

- ***Fatigue crack growth***

A fractographic reconstitution of the fatigue crack growth is proposed in the last part of the chapter. The fracture surface examination based on the classical fatigue striation counting method is used to determine the crack growth rate as a function of the crack length. This approach supports the applicability of the empiric relationship between macroscopic crack growth rate and striations spacing, as established by previous experiments **[Levaillant et al.,1982; Oudin,2001; de Matos et al.,2005]**.

The crack growth rate assessment is achieved by the use of the cyclic J-integral that takes into consideration the elastic and inelastic effects at crack tip. The obtained crack growth curves are compared to data for Inconel 718 data extracted from the literature. The fractographic reconstitution method is proved to be efficient for the reconstitution of the crack kinetics history providing growth laws similar to that proposed by Paris.

Finally, the life of a LCF sample or an extrusion die is composed of a crack initiation and a crack propagation time. The above method is used to estimate the extension of the two regimes. Comparable results are observed for different strain amplitudes, showing that crack initiation governs the fatigue life of Inconel 718, ranging between 75-80% of the total life.

This alternative approach provides complementary information to that obtained from classical fatigue tests, reducing the costs directly related to the CT specimens preparation and to the realization of extensive FCG test campaigns.

All these assumptions represent a support for the design of alternative Inconel 718 thermal treatments, as it will be described in Chapter V. The optimisation of the material microstructure must be carried out in order to contain the time dependent damage associated to the extrusion cycle (such as the material relaxation during the holding time at maximal strain). Finally, the prevalence of the crack initiation time over the crack propagation requires a tailored microstructure able to further delay the risks of crack initiation associated to the localisation of the plastic strain in specific areas, as well as in the hot spots of an extrusion die.

VI References

[Bathias,1979] Bathias, C. "Endommagement par sollicitation cyclique". Dislocations et déformation plastique. Ed.Diffusion**:** 375-382 (1979).

[Bergstrom et al.,2006] Bergstrom, J. and Rézaï-Aria, F. "*High temperature fatigue of tool steels*". TOOL 06 - 7th International tooling conference, Torino (Italy)**:** 545-554 (2006).

[Branco et al.,2008] Branco, R. and Antunes, F. V. "Finite element modelling and analysis of crack shape evolution in mode-I fatigue Middle Cracked Tension specimens." *Engineering Fracture Mechanics* 75(10): pp. 3020-3037, (2008).

[Cai et al.,2001] Cai, H. and McEvily, A. J. "On striations and fatigue crack growth in 1018 steel." *Materials Science and Engineering A* 314(1-2): pp. 86-89, (2001).

[Chaboche et al.,1994] Chaboche, J.-L. and Lemaitre, J. "Mechanics of solid materials", Cambridge University Press, p., (1994).

[Chermant et al.,1979] Chermant, J. L. and Coster, M. "Quantitative fractography." *Journal of Materials Science* 14(3): pp. 509-534, (1979).

[Chihab,2004] Chihab, K. "On the apparent strain rate sensitivity of Portevin - Le Chatelier effect." *Annales De Chimie-Science Des Materiaux* 29(5): pp. 15-23, (2004).

[Clavel et al.,1975] Clavel, M., Fournier, D. and Pineau, A. "Plastic zone sizes in fatigued specimens of Inco 718." *Metallurgical Transactions a-Physical Metallurgy and Materials Science* 6(12): pp. 2305-2307, (1975).

[Clavel et al.,1982] Clavel, M. and Pineau, A. "Fatigue behaviour of two Nickel base alloys I: Experimental results on Low-Cycle fatigue crack propagation and substructures." *Materials Science and Engineering* 55(2): pp. 157-171, (1982).

[Connors,1994] Connors, W. C. "Fatigue striation spacing analysis." *Materials Characterization* 33(3): pp. 245-253, (1994).

[de Matos et al.,2005] de Matos, P. F. P., Moreira, P. M. G. P., Nedbal, I. and de Castro, P. M. S. T. "Reconstitution of fatigue crack growth in Al-alloy 2024-T3 open-hole specimens using microfractographic techniques." *Engineering Fracture Mechanics* 72(14): pp. 2232-2246, (2005).

[Delagnes,1998] Delagnes, D. "*Comportement et tenue en fatigue isotherme d'aciers à outils Z 38 CDV5 autour de la transition fatigue oligocyclique endurance*". PhD Thesis, Ecole des Mines de Paris (1998).

[Dowling et al.,1976] Dowling, N. E. and Begley, N. A. "Fatigue crack growth during gross plasticity and J- integral". Mechanics of Crack Growth. ASTM**:** 82-103 (1976).

[Fiétier et al.,2009] Fiétier, N., Krähenbühl, Y. and Vialard, M. "New methods for the fast simulations of the extrusion process of hot metals." *Journal of Materials Processing Technology* 209(5): pp. 2244-2259, (2009).

[Fournier et al.,1977] Fournier, D. and Pineau, A. "Low fatigue cycle behaviour of Inconel 718 at 293 K and 823 K." *Metallurgical Transactions a-Physical Metallurgy and Materials Science* 8(7): pp. 1095-1105, (1977).

[Fournier et al.,2001] Fournier, L., Delafosse, D. and Magnin, T. "Oxidation induced intergranular cracking and Portevin-Le Chatelier effect in nickel base superalloy 718." *Materials Science and Engineering A* 316(1-2): pp. 166-173, (2001).

[Garat et al.,2008] Garat, V., Cloue, J. M., Poquillon, D. and Andrieu, E. "Influence of Portevin-Le Chatelier effect on rupture mode of alloy 718 specimens." *Journal of Nuclear Materials* 375(1): pp. 95-101, (2008).

[Ghonem et al.,1993] Ghonem, H., Nicholas, T. and Pineau, A. "Elevated-Temperature

fatigue -crack growth in alloy 718-Part 1: effects of mechanical variables." *Fatigue & Fracture of Engineering Materials & Structures* 16(5): pp. 565-576, (1993).

[Hong et al.,2005] Hong, S. G. and Lee, S. "Mechanism of dynamic strain aging and characterization of its effect on the low-cycle fatigue behavior in type 316L stainless steel." *Journal of Nuclear Materials* 340(2-3): pp. 307-314, (2005).

[Jacquelin,1983] Jacquelin, B. "*Amorçage des fissures en fatigue oligocyclique sous chargement multiaxial*". PhD Thesis, Ecoles des Mines de Paris (1983).

[James,1986] James, L. A. "The effect of grain size upon the fatigue-crack propagation behaviour of alloy 718 under hold-time cycling at elevated temperature." *Engineering Fracture Mechanics* 25(3): pp. 305-314, (1986).

[Kalluri et al.,2004] Kalluri, S., Rao, K. B. S., Halford, G. and McGaw, M. A. "*Deformation and damage mechanisms in Inconel 718 superalloy*". Superalloys 718, 625, 706 and Various Derivatives, E.A Loria (2004).

[Kirman et al.,1970] Kirman, I. and Warrington, D. "The precipitation of Ni3Nb phases in a Ni−Fe−Cr−Nb alloy." *Metallurgical and Materials Transactions B* 1(10): pp. 2667-2675, (1970).

[Krumphals et al.,2010] Krumphals, F., Wlanis, T., Sievert, R., Wieser, V. and Sommitsch, C. "Damage analysis of extrusion tools made from the austenitic hot work tool steel Böhler W750." *Computational Materials Science* In Press, Corrected Proof: pp., (2010).

[Lemaitre et al.,1987] Lemaitre, J., Benallal, A., Ben Cheikh, A., Billardon, R., Dufailly, J., Feng, L., Florez, J., Gautherin, M. T., Geymonat, G., Lienard, C., Marquis, D., Mertz, D. and Moret-Bailly, L. "*Formulaire de caractéristiques mécaniques de matériaux/ Handbooklet of mechanical characteristics of materials*". C. N. d. l. R. Scientifique (1987).

[Levaillant et al.,1982] Levaillant, C. and Pineau, A. "Assessment of high-temperature low cycle fatigue life of austenitic stainless steels by using intergranular damage as a correlating parameter." *Low cycle fatigue and life prediction* ASTM STP 770: pp. 169-183, (1982).

[Liu et al.] Liu, J., Yuan, H. and Liao, R. "Prediction of fatigue crack growth and residual stress relaxations in shot-peened material." *Materials Science and Engineering: A* In Press, Accepted Manuscript: pp.,

[Mannan,1993] Mannan, S. L. "Role of dynamic strain-aging in low-cycle fatigue." *Bulletin of Materials Science* 16(6): pp. 561-582, (1993).

[McEvily et al.,2010] McEvily, A. J. and Matsunaga, H. "On fatigue striations." *Transaction B: Mechanical Engineering* 17(1): pp. 75-82, (2010).

[Mebarki,2003] Mebarki, N. "*Relation microstructure - propriétés mécaniques d'aciers martensitiques revenus destinés aux outillages de mise en forme d'alliages légers.*". PhD Thesis, Ecole des Mines de Paris (2003).

[Mowbray et al.,1976] Mowbray and D, F. "Derivation of a low-cycle fatigue relationship employing the J-integral approach to crack growth", American Society for Testing and Materials, p. 14, (1976).

[Nedbal et al.,2008] Nedbal, I., Lauschmann, H., Siegl, J. and Kunz, J. "Fractographic reconstitution of fatigue crack history - Part II." *Fatigue & Fracture of Engineering Materials & Structures* 31(2): pp. 177-183, (2008).

[Neumann,1974] Neumann, P. "New experiments concerning the slip process at propagating fatigue cracks." *Acta Metallurgica* 22: pp. 1155-1165, (1974).

[Oudin,2001] Oudin, A. "*Thermo-Mechanical Fatigue of Hot Work Tool Steels* ". PhD Thesis, Ecole Nationale Superieure des Mines de Paris (2001).

[Pasqualon,2010] Pasqualon, M. "*Extrusion dies material and surface treatment*

developments". Unpublished Work, Hydro Aluminium PTTC (2010).

[Pelloux,1970] Pelloux, R. M. N. "Crack extension by alternating shear." *Engineering Fracture Mechanics* 1: pp. 697-704, (1970).

[Ponnelle,2001] Ponnelle, S. "*Propagation des fissures par fatigue à haute température dans l'Inconel 718: effets de microstructure et de chargements complexes*". PhD Thesis, Ecole des Mines de Paris (2001).

[Rice,1968] Rice, J. R. "A path independent integral and the approximate analysis of strain concentration by notches and cracks." *Journal of Applied Mechanics* 35: pp. 379-386, (1968).

[Sadananda,1984] Sadananda, K. "Crack propagation under creep and fatigue." *Nuclear Engineering and Design* 83(3): pp. 303-323, (1984).

[Ter-Ovanessian et al.,2008] Ter-Ovanessian, B., Deleume, J., Cloue, J. M. and Andrieu, E. "Influence of interstitials content on the sensitivity of alloy 718 to oxidation assisted intergranular fracture." *High Temperature Corrosion and Protection of Materials 7, Pts 1 and 2* 595-598: pp. 951-958, (2008).

[Underwood,1979] Underwood, E. E. "Quantification of microstructures by stereological analysis." *Journal of Histochemistry & Cytochemistry* 27(11): pp. 1536-1537, (1979).

[Valsan et al.,1994] Valsan, M., Sastry, D. H., Rao, K. B. S. and Mannan, S. L. "Effect of strain rate on the High-Temperature Low-Cycle Fatigue properties of a Nimonic PE-16 Superalloy." *Metallurgical and Materials Transactions a-Physical Metallurgy and Materials Science* 25(1): pp. 159-171, (1994).

[Velay,2003] Velay, V. "*Modélisation du comportement cyclique et de la durée de vie d'aciers à outils martensitiques*". PhD Thesis, Ecole des Mines de Paris (2003).

[Woodford,2006] Woodford, D. A. "Gas phase embrittlement and time dependent cracking of nickel based superalloys." *Energy Materials: Materials Science and Engineering for Energy Systems* 1: pp. 59-79, (2006).

[Xie et al.,1997] Xie, J. Z., Shen, Z. M. and Hou, J. Y. "*Fatigue Crack growth behaviours in alloy 718 at high temperature*". Superalloys 718, 625, 706 and Various derivatives (1997).

[Yang et al.,2006] Yang, F., Kuang, Z. and Shlyannikov, V. N. "Fatigue crack growth for straight-fronted edge crack in a round bar." *International Journal of Fatigue* 28(4): pp. 431-437, (2006).

Chapter V

Relationships between tailored microstructure and fatigue life of Inconel 718

‘’ Les sentiments sont des métaux. Il importe d'en connaître la densité. Il importe également d'en connaître la température de fusion ‘’

Francis Dannemark

Chapter V – Relationships between tailored microstructure and fatigue life

I Introduction

"The heat treatment of nickel base alloys is an art" **[Sims et al.,1972]**

Alternative heat treatments, in addition to the standard procedure, have been proposed in chapter III where their mechanical properties have been assessed by tensile tests. Each modified thermal treatment is defined by a series of parameters (time, temperature, cooling rates), associated to the various steps included in the process (solution annealing, quenching and ageing). The choice of these parameters is related to a detailed study of the correlation between microstructure and mechanical properties. This investigation is based on the understanding and modelling of the various steps of the heat treatment process, taking into account the evolution of the so-called material-intrinsic parameters that are the grain structure and the morphology and content of precipitates (δ, γ' and γ"). This approach may lead to a better control of the heat treatment in order to optimize the alloy microstructure and adapt Inconel 718 to the specific conditions imposed by the extrusion process.

Finally, the microstructure and fatigue properties, resulting from the modified heat treatments, will be discussed providing specific recommendations for the service conditions.

I Structural characterization of heat treated Inconel 718

I.1 Cooling rate effects

Solution treatment is generally followed by quenching prone to maintain, at room temperature, the super-saturated solid solution. Different cooling methods may be used Minimum hardness is obtained by cooling rapidly from the annealing temperature in order to avoid the precipitation of strengthening phases. Loier **[Loier et al.,1984]** studied the effects of the cooling rate on the microstructural and mechanical effects of Inconel 718. The authors showed that each cooling method may be characterized by an instantaneous cooling rate, defined as V_{700} ($V_{700} = \frac{T_a - 700}{\Delta t}$) which typically varies from 50 to 10^5 °C/h.

Figure V. 1 shows the impact of the cooling rate on the material hardness after quenching at 950°C. It is noticeable that harness, in the aged condition, does not exhibit a variation as a function of the adopted quenching method. In general, when V_{700} is higher than 0.5 °C/s^{-1},

the material is not affected by the cooling rate. The same assumptions could be made for the mechanical performances at room temperature (Figure V. 2). The tensile properties of Inconel 718 are insensitive to the cooling rate, after annealing, when V_{700} is higher or equal to 0.25 °C s^{-1}.

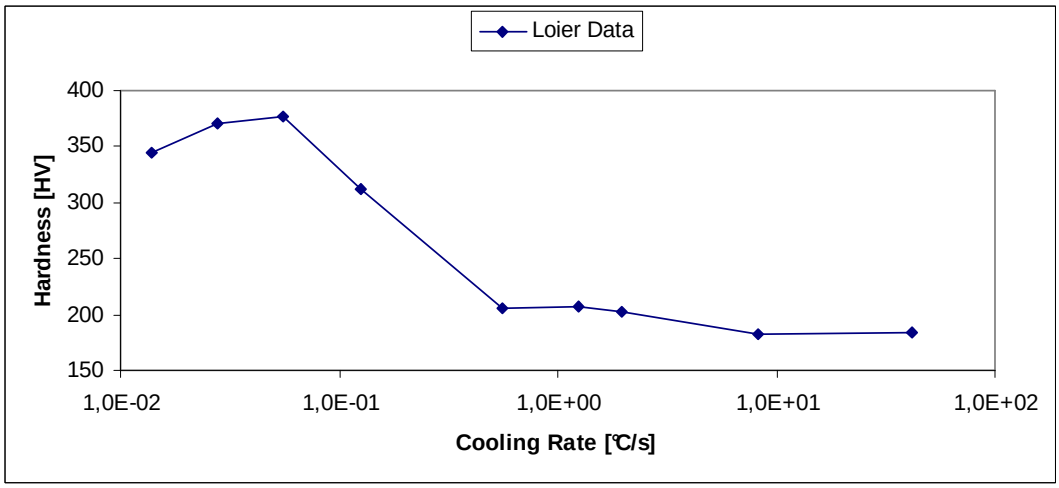

Figure V. 1 : Variation in Vickers hardness with quenching rate for Inconel 718, annealed at 950°C, based on Loier [Loier et al.,1984] data.

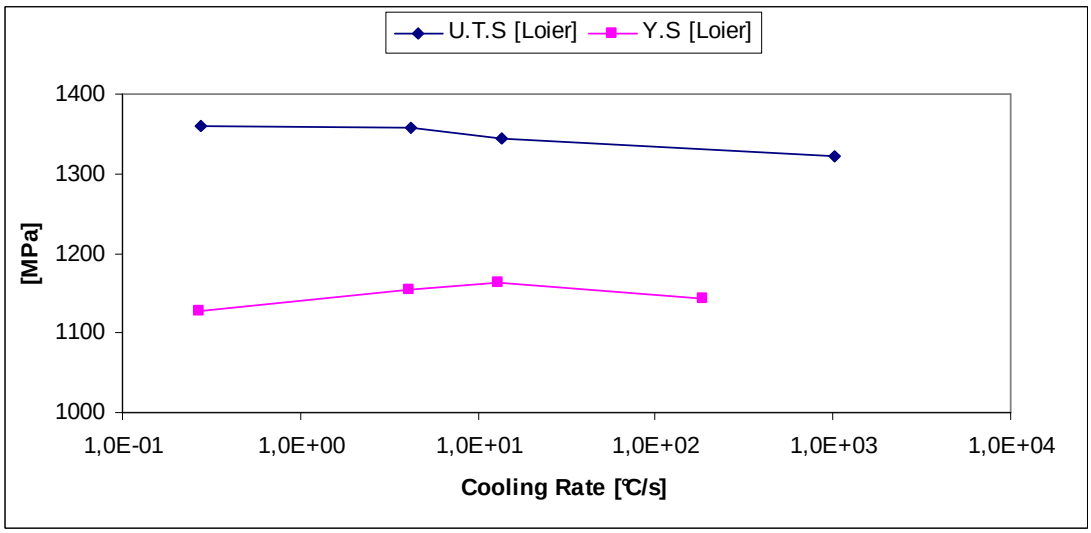

Figure V. 2 : Variation in the mechanical properties four double aged Inconel 718 with the initial quenching rate, based on Loier [Loier et al.,1984] data.

The experimental results reported by Slama **[Slama et al.,1997]**, associated to the continuous cooling rate diagram reported in Figure V. 3, complete the study on the effect of the cooling rate in Inconel 718, with a particular attention to the structural transformations. At first sight, we can deduce that for cooling rate higher than 100°C/s^{-1} the alloy retains an austenitic microstructure.

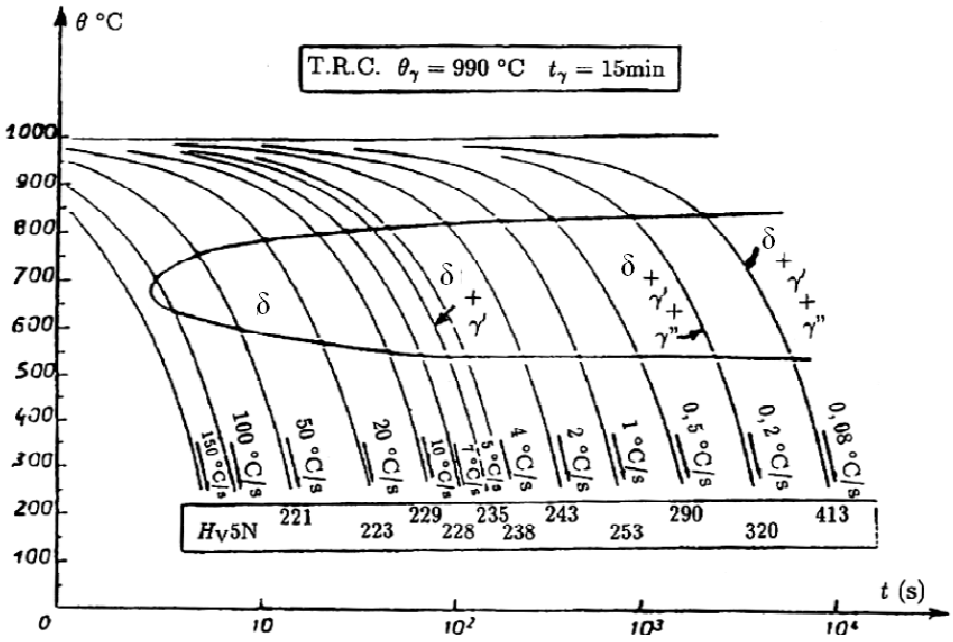

Figure V. 3 : Continuous Cooling (C.C.T) diagram for Inconel 718 [Slama et al.,1997].

However, for $5 \leq V_{700} < 100°C/s^{-1}$, the delta (δ) phase precipitation is identified. In these conditions the hardness of the quenched material is constant. Finally when the cooling rate is slowest than 5 $°C/s^{-1}$ an additional precipitation of the strengthening phases (γ'/γ") takes place leading to a progressive hardening effect.

The quenching rate could be experimentally optimised using a wide range of technological equipments. However, for heavy sections, the cooling rate can change along the profile as a function of the shape and the local thickness. For these reasons, it is recommended to use limited quenching rate so as to reduce the residual stresses which induce early fatigue crack initiations.

The common cooling conditions, for Inconel 718, include:

- **water quenching** with $V_{700} > 28$ °C s^{-1};
- **oil quenching** with $V_{700} \sim 8$ °C s^{-1};
- **air cooling** with $V_{700} \sim 1.25$ °C s^{-1}.

To conclude, the common quenching methods offer cooling rates which induce similar structural transformations in the material and equal resulting mechanical properties. As a result, the cooling rate will not be considered in the study of thermal treatment procedure and no further test will be performed to complete literature results.

I.2 Structural evolution of Inconel 718 during heating process

The microstructural optimisation of the alloy and the desired high temperature properties require multi-stage heat treatments that lead to the nucleation or dissolution of secondary phases. Differential thermal analyse (DTA) has been used as an indirect method for examining the characteristic temperatures and the nature of phase transformations in Inconel 718. A heating rate of 10°C/min has been applied in order to ensure thermodynamic equilibrium so that the observed temperature is as close as possible to the "true" reaction temperature. Figure V. 4 reports the DTA thermogram established for Inconel 718 in the "as received" conditions (rolled at 980°C). The onset of any reaction may be defined at the temperature at which the DTA curve deviates from the base line (dotted line). The general profile of this thermogram is in agreement with those reported in literature **[Cao W.D Kennedy R.L,1991; Slama,1993]**.

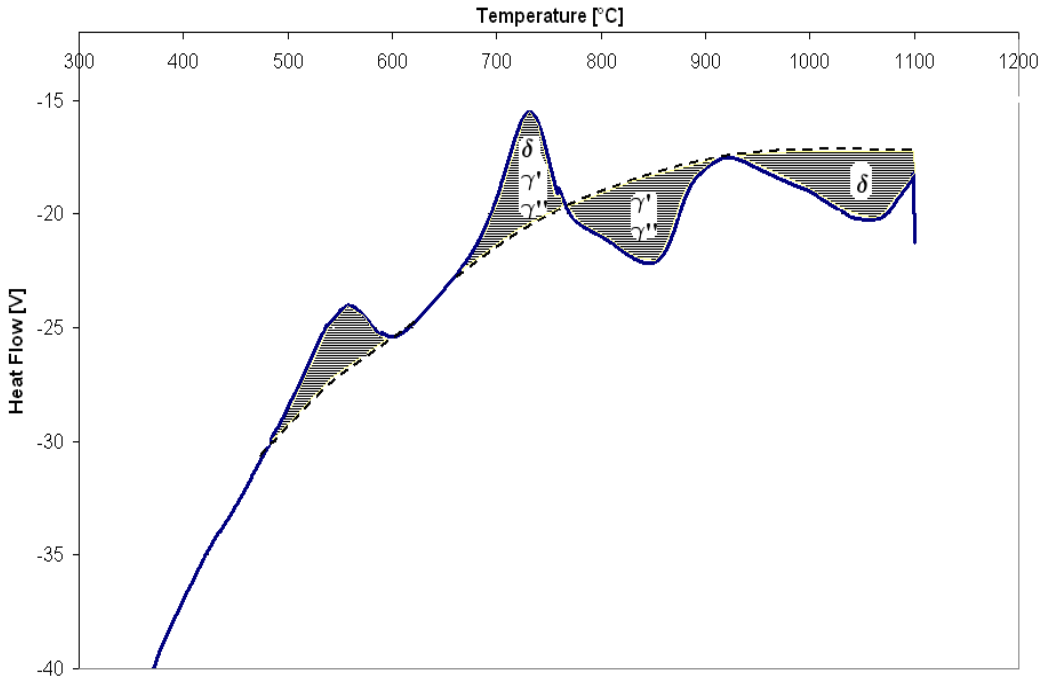

Figure V. 4 : D.T.A analyse on continuous heating of the "as received" Inconel 718.

A preliminary exothermic peak is noticed for temperature ranging between 650°C and 740°C and is associated to a simultaneous precipitation of δ, γ' and γ" phases. However, it is difficult to separate the domains of precipitation of the three different phases. In general, at 700°C the coherent precipitation of γ", coupled with the formation of a small amount of γ', prevails.

An endothermic peak is detected in the range between 760-910°C corresponding to the solvus of the coherent γ' and γ" phases.

A second endothermic peak in the range 920-1060°C is related to the dissolution of the delta precipitates. Beyond, the FCC solid solution is free of precipitates. In agreement with

these assumptions, two types of thermal treatments generally used for Inconel 718, can be defined as a function of the solution annealing process:

- ***Sub-solvus solution annealing***: performed at a temperature below the delta solvus.
- ***Super-solvus solution annealing***: performed at a temperature above the delta solvus.

The sub-solvus treatment retains the small grain size (10-12 ASTM) provided by the thermo-mechanical processing of the alloy, holding a certain amount of delta phase within the microstructure. Conversely, the super-solvus treatment may induce an over-growth of the grains. This microstructural evolution depends on the chemical homogeneity of the alloy and on the energy stored through out the entire thermo-mechanical processing. In this case, the enhanced dissolution of delta phase further promotes the precipitation of the strengthening phases γ' and γ" due to the high availability of Nb within the matrix. Conversely, the largest grain size decreases the strength and fatigue resistance of the alloy. The application of the super-solvus treatment to wrought nickel based alloys requires a detailed understanding of the thermo-mechanical and metallurgical history of the alloy in order to avoid localised grain growth and heterogeneities in mechanical properties.

The effects of the solution annealing on the microstructural features of the alloy (delta phase and grain structure evolution) will be discussed in the next section.

I.3 Delta phase and grain structure evolution

The δ precipitates play an important role in controlling the grain size of Inconel 718. However, a high volume content of this phase, capturing niobium, causes a lower Nb content within the matrix and limits γ" precipitation. As a consequence, the microstructure and the mechanical properties could be significantly affected by the variation of the δ phase volume fractions. Desvallées **[Desvallées et al.,1994]** showed that an increased presence of delta phase has a detrimental effect on yield strength (10% of reduction as compared to a standard Inconel 718 grade) because it induces a lack of γ".

Considering these assumptions, the study of the dissolution kinetics of δ precipitates as function of time and temperature, is extremely important to evaluate the microstructure development during the heat treatment process. In such a way, various solution annealing experiments have been carried out on specimens cut and machined to 15 mm diameter and 10 mm height. After annealing for 1 h, all specimens have been air quenched and prepared for SEM investigations. Figure V. 5 exhibits the microstructural evolution in Inconel 718 after solution treatment at 924, 955, 990, 1010 and 1030°C. It is important to point out that these temperatures are in the range defined by the ASTM B637 specification.

The change of the volume fraction of stable phases, as a function of the temperature, could be addressed by a specific 2D image analyse. Figure V. 6 shows the calculated surface fraction of delta phase for different annealing temperatures. Significant δ phase precipitation results from the lower solution temperatures of 924°C and 955°C because of the high equilibrium content of δ

phase at these temperatures. Limited changes in δ phase structure are noticed at 975°C , whereas at 990°C a partial precipitates dissolution occurs. A certain amount of delta phase still exists at 1010°C, while the dissolution process finishes at 1050°C giving an austenitic microstructure free of precipitates.

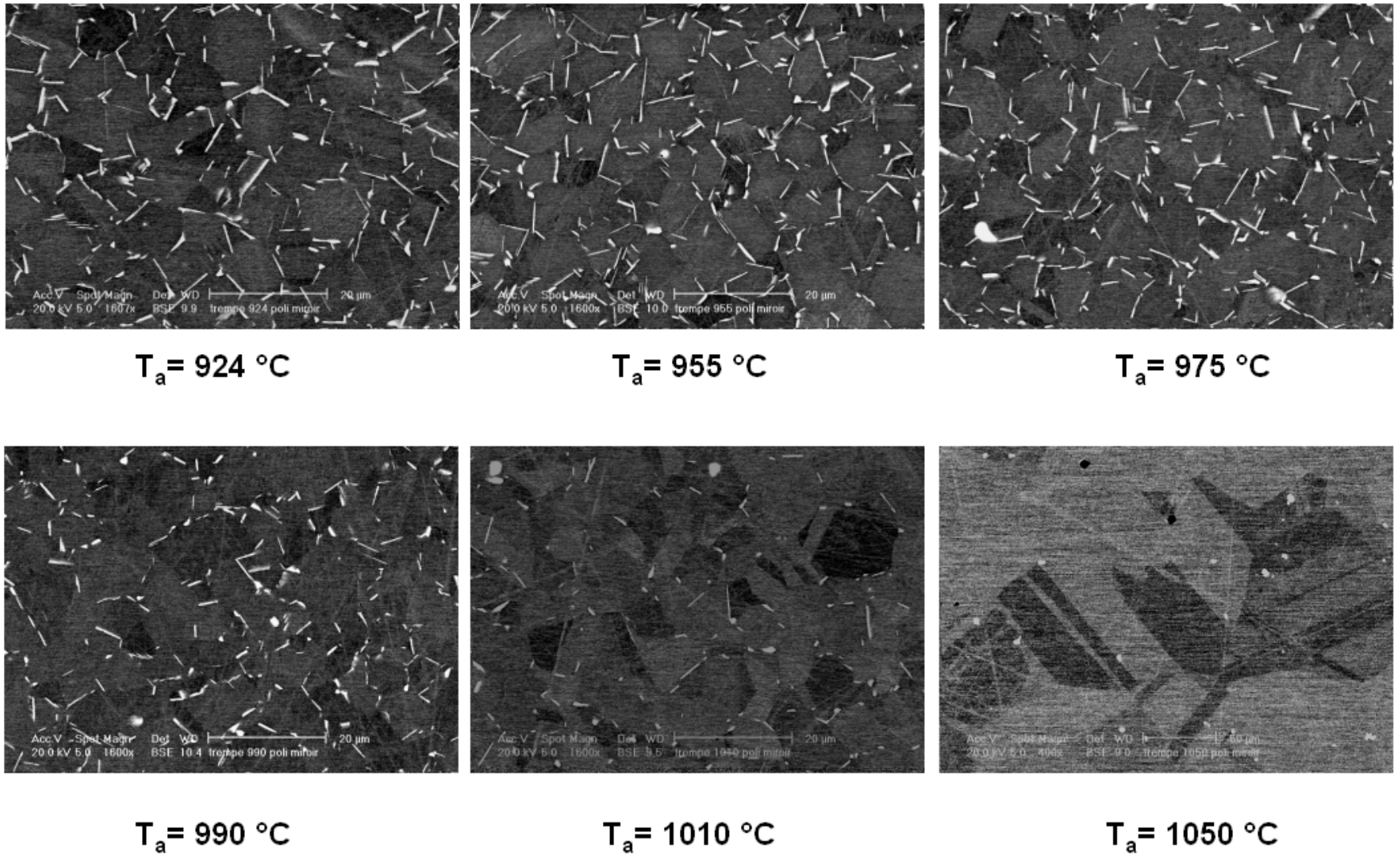

Figure V. 5 : Effect of the solution treatment temperature on the microstructure of Inconel 718.

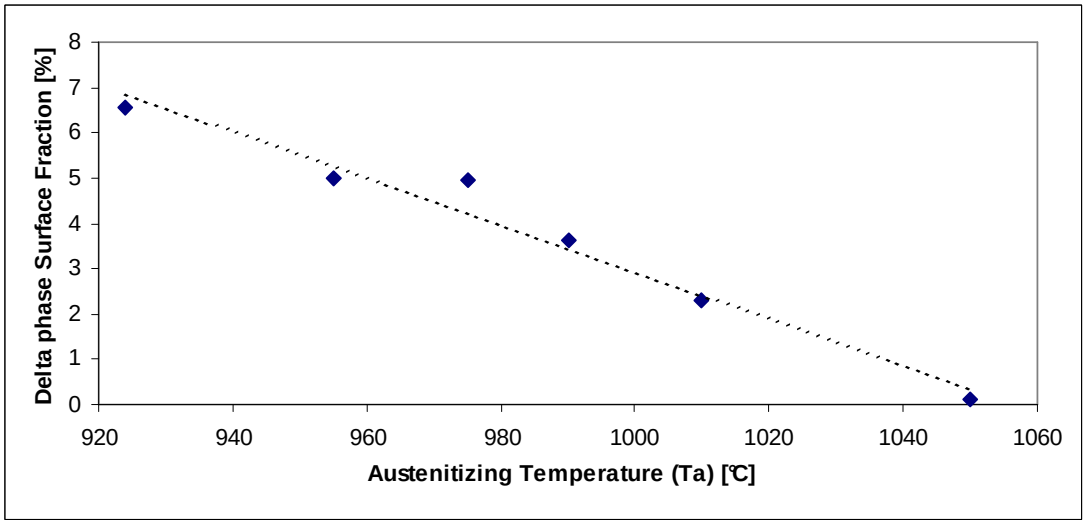

Figure V. 6 : Evolution of the delta phase surface fraction as a function of the solution annealing temperature (t= 1h).

The dissolution process in Inconel 718 is controlled by the diffusion of Nb atoms within the matrix that is influenced by temperature and concentration gradients. This latter parameter decreases gradually with the evolution of the dissolution process. Temperature has also a strong effect on the diffusion process. As listed above, the dissolution rate increases with the increase of the temperature, due to the high solubility of Nb atoms in matrix. The high delta phase dissolution is associated to a rapid grain size growth.

In general, two morphologies of delta precipitates may be detected: spheroidal and plate-like particles. Figure V. 7 shows the effects of the solution annealing temperature on the δ phase shape, as a function of the circularity factor, that ranges between 0 (irregular and long particle) and 1 (perfect round particle).

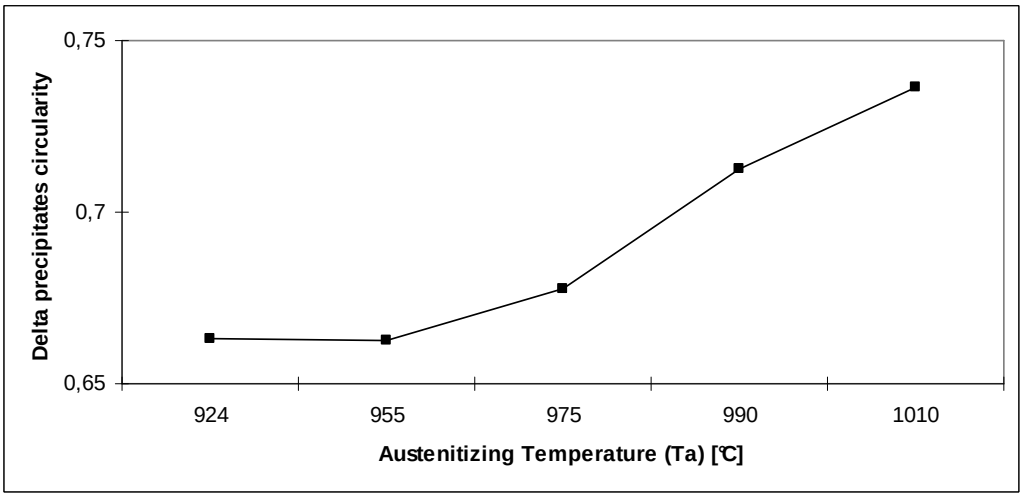

Figure V. 7 : Morphology evolution of the delta phase as function of the solution annealing temperature.

At low annealing temperatures, 924-975°C, Inconel 718 exhibits plate-like delta phase that plays an important role for limiting grain growth. However, spherical delta particles are formed as the temperature increases.

The factors controlling the morphology of the δ phase are multiple and complex. Previous works **[Cai et al.,2007; Huang et al.,2007]** proposed a relationship between the solubility of the secondary phases and their shape. Plate-like delta phases have a larger surface energy than the globular particles and tends to transform into a more blocky morphology prone to attain a lower surface energy. Focusing on the long needle-like delta particles, the solubility at the tip is higher than on the other faces. Thus, the diffusional process alters the equilibrium state of Nb atoms within the phase interface, causing a further dissolution of δ phase. A second explanation is related to the presence of subgrain boundaries or high dislocation density zones through δ precipitates which enhance the dissolution process (Figure V. 8). As a consequence, particles dissolve gradually and fracture along their defect zones, losing their orientation relationship with the matrix. In such a way, the plate-like δ phase transforms into a blocky/globular morphology.

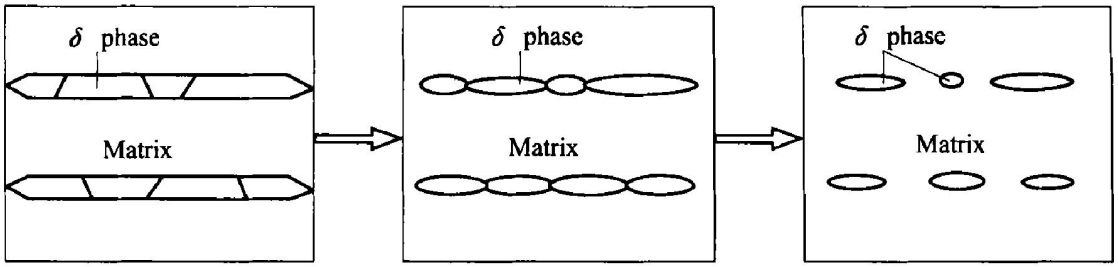

Figure V. 8 : Schematic representation of dissolution and fracture process of δ phase in Inconel 718 [Cai et al.,2007].

The effects of 1-h annealing at various temperatures on the grain size is reported in Figure V. 9 and investigated by image analysis (Figure V. 10).

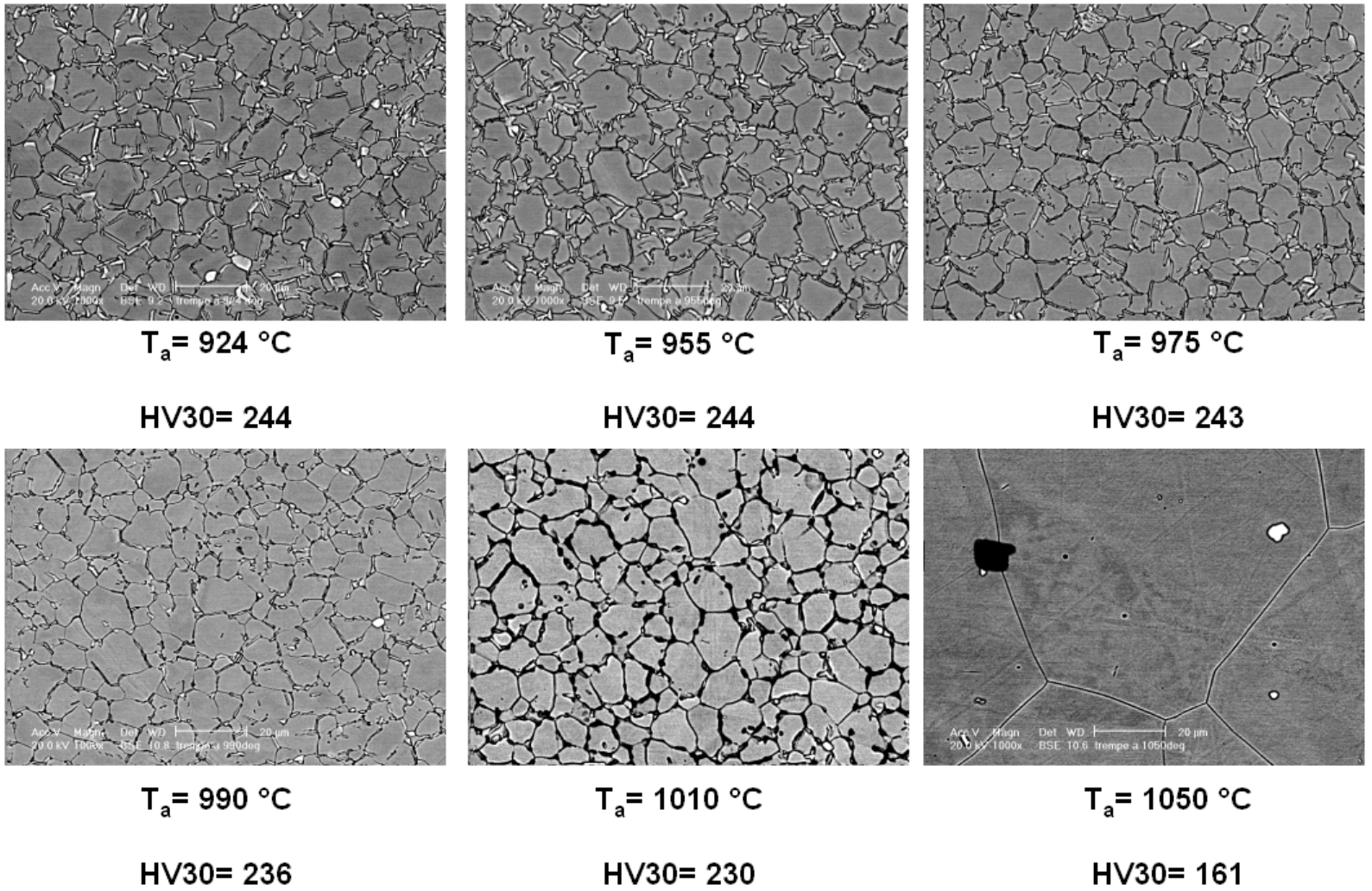

Figure V. 9 : Effect of the solution treatment temperature on the grain size of Inconel 718.

The grain size exhibits a strong increase between 1000 and 1050°C due to the progressive dissolution of the δ phase. The grain growth is accelerated by the evolution and loss of these secondary particles at the grain boundaries, pointing out that needle plate δ phase is more efficient to prevent grain growth than spheroids **[Desvallées et al.,1994]**.

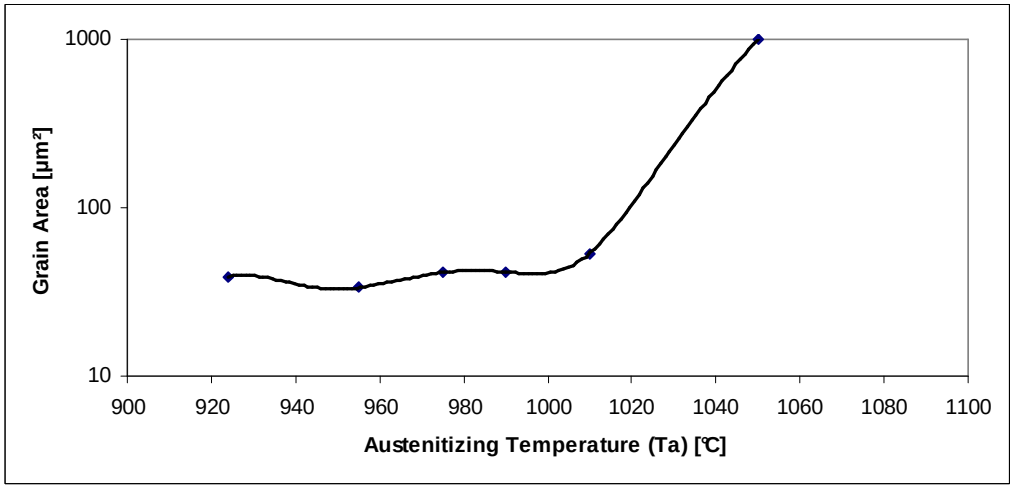

Figure V. 10 : Evolution of the grain area as a function of the solution annealing temperature.

Figure V. 11 compares the microstructures obtained after solution annealing at different times and temperatures. These pictures allow a quantitative measurement of the delta phase content and morphology, as reported in Figure V. 12.

Focusing on the particles morphology, Figure V. 13 reports the evolution of the precipitates circularity as a function of time and temperature. In general, for a given annealing time, the mean circularity increases with temperature, whereas for a given temperature it remains nearly constant with time. In some cases, notably after 4h at 955 and 980°C, the particle shape tends to be similar. The absence of a clear delta phase evolution within the investigated range of time is due to the low nucleation and coalescence rate at these temperatures.

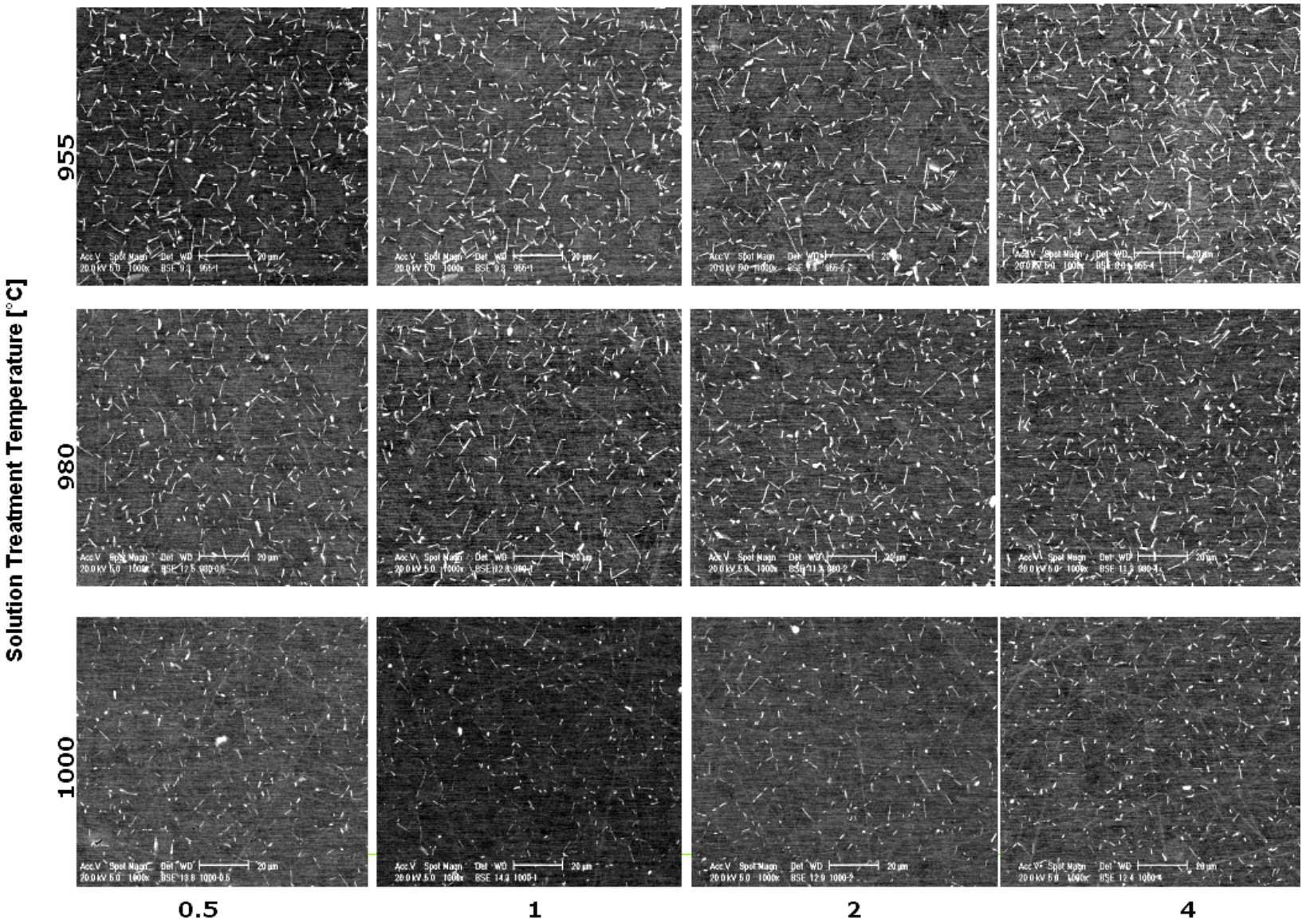

Figure V. 11 : Effect of the solution treatment temperature and time on the microstructure of Inconel 718.

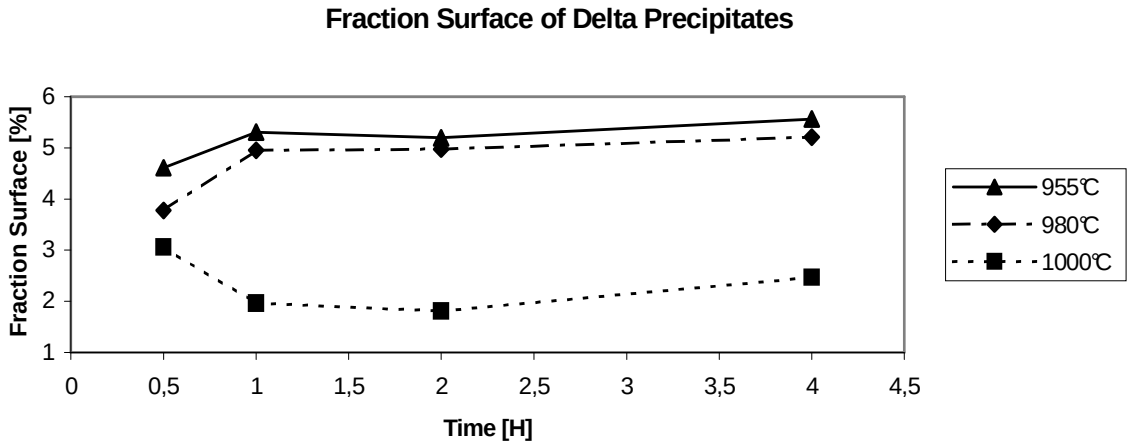

Figure V. 12 : Evolution of the delta phase fraction surface as function of the solution annealing temperature and time.

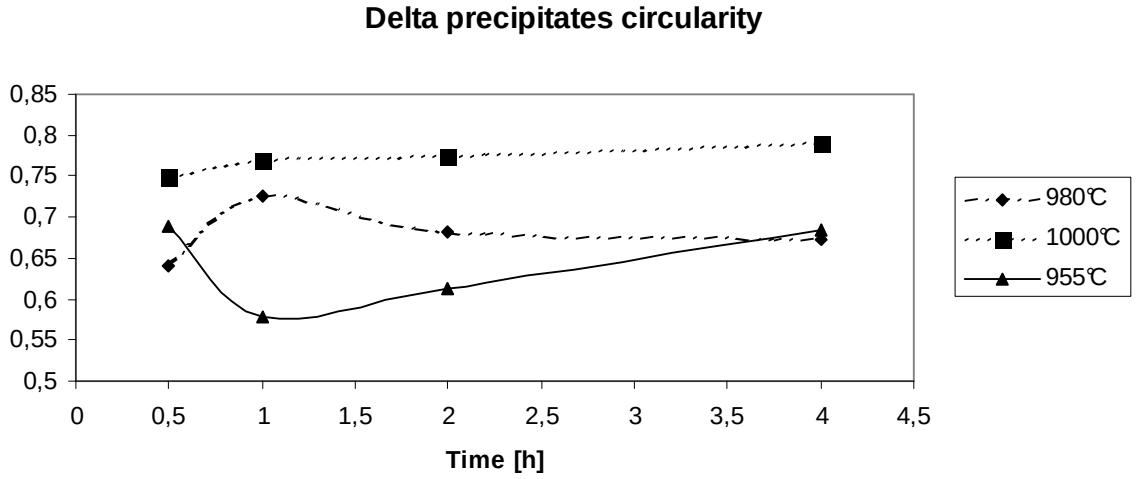

Figure V. 13 : Evolution of delta phase morphology as a function of the solution annealing time and temperature.

I.4 Aging effects on the structural evolution

In the optimisation of the alloy, a pertinent approach is to develop a tailored microstructure based on a specific dispersion of particles (γ' and γ") prone to act as efficient obstacles to the dislocation motion. The finer the dispersion, for the same amount of particles, the stronger the material. A particular heat treatment procedure should be developed to give this required distribution and quantity of precipitates within the matrix. Generally speaking, the precipitation is achieved by aging the alloy at a specific temperature and for a suitable time. The main objective consists in obtaining stable precipitates prone to ensure an extended service at elevated temperature and the targeted mechanical properties. The precipitation temperature determines not only the type but also the size and distribution of precipitates. Donachie **[Donachie,2002]** reports the main factors that influence the selection of the ageing steps and precipitation time-temperature:

- Type and number of precipitating phases;
- Required precipitates size;

- Combination of strength and ductility

This section deals with the study of the phases precipitation resulting from an isothermal aging performed after quenching. Different experimental analyses have been performed using Dilatometry and Differential Thermal Analysis (DTA) techniques prone to point out the microstructural transformations occurring during the heat treatment process. Specimens have been first solution annealed at 955°C for 1 hour, then air cooled and submitted to different isothermal treatments.

In such a way, two reference aging treatments are considered (Figure V. 14): the first one (a) represents the standard ageing process defined by the ASTM B637 specification while, for the second profile (b), a higher ageing temperature of 750°C has been chosen. Both treatments show the same second ageing at 620°C for 8 hours.

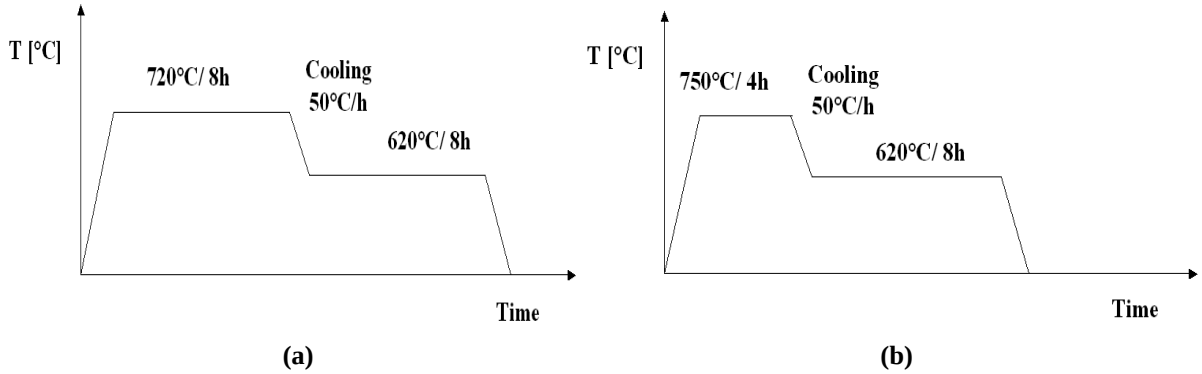

Figure V. 14 : Reference aging treatments considered for analytical investigations.

Figure V. 15 shows the dilatometric analyses carried out for the first ageing. Samples have been heated with a heating ramp of 10°C/min and hold at the ageing temperature. In both cases, the curves exhibit a slight preliminary expansion, occurring during the first 20 minutes, followed by a continuous shrinkage.

As reported by Slama **[Slama,1993]**, this expansion is due to the inertial error of the measurement equipment during the heating process.

Otherwise, the thermal shrinkage is coupled with the precipitation of different phases. The rejection from the austenitic matrix of alloying elements such as Nb, Ti and Al, which interact to form the strengthening phases is the main cause of the dilatometric variation.

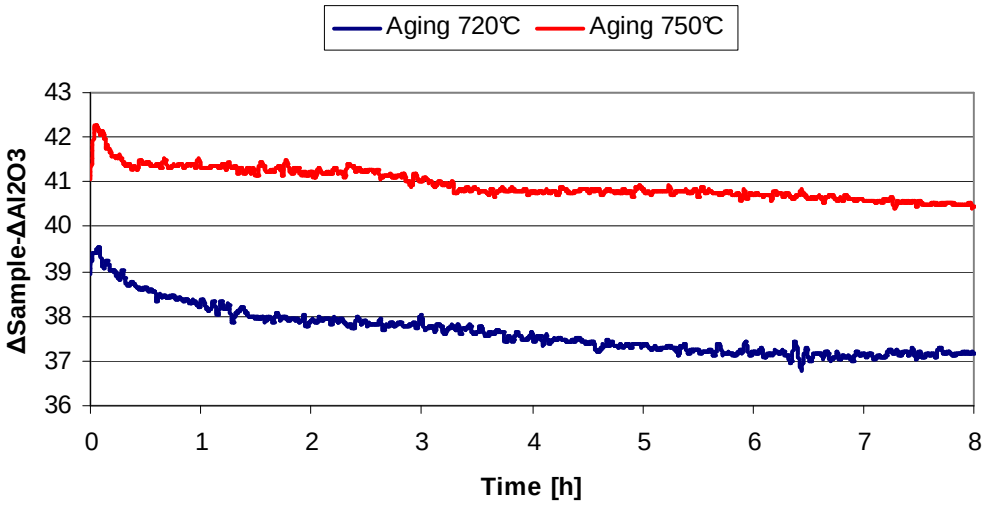

Figure V. 15 : Dilatometric curves for isochronous ageing treatments at different temperature.

The precipitates growth rate is influenced by the diffusion rates of the constitutive elements, which are strongly affected by the temperature. Following these assumptions we can suggest that the preliminary phase of the dilatometric shrinkage (from 0 to 2h aging) is based on a decreasing nucleation rate of the hardening particles, provided by diffusional processes. Conversely, the rest of the structural evolution may be associated to the morphology evolution of the nucleated phases. Previous works **[Han et al.,1982; Devaux et al.,2008]** have pointed out that the size of γ" precipitates increases with increasing aging time during isothermal aging. In such a way the hardening phases change their shape from globular particle, for short aging time, to ellipsoidal disc shaped particles, as shown at the end of the heat treatment process. As it will be described at the end of the chapter, the elastic energy minimization is believed to explain this evolution in particles morphology .

Figure V. 16 exhibits the dilatometric analyses related to the second aging and carried out respectively after a preliminary aging at 750°C or 720°C. The slight difference in terms of dilatometric shrinkage shown between the two curves is associated to the effects of the previous aging process. In general, high temperatures adopted for the first aging enhance the structural evolution associated to the second ageing. The dilatometric variation corresponding to 620°C, independently from the first aging, is then less important, in terms of amplitude, as compared to the first aging step. Recent studies **[Bor et al.,2010]** have reported that the second subsequent 620°C ageing does not alter the morphology of the γ" phase but leads to the growth of the γ' phases, increasing their diameter. In such a way we can conclude that most of the structural transformations take place during the preliminary ageing, whereas the subsequent step has an important impact on the size and morphology refinement of the precipitates.

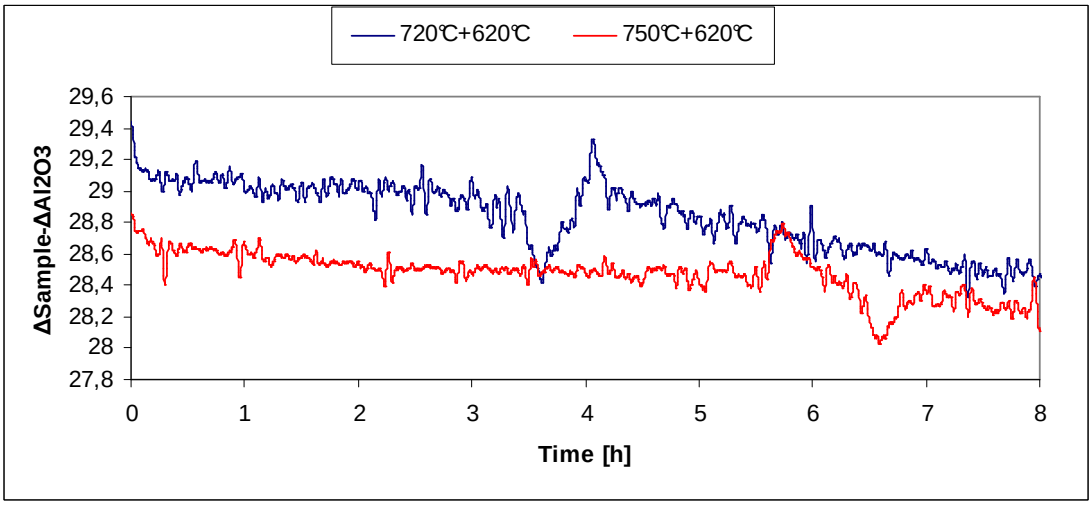

Figure V. 16 : Dilatometric analyses during second aging, subsequent to different preliminary aging steps.

Figure V. 17 shows, the hardness evolution during aging, following the two selected ageing conditions.

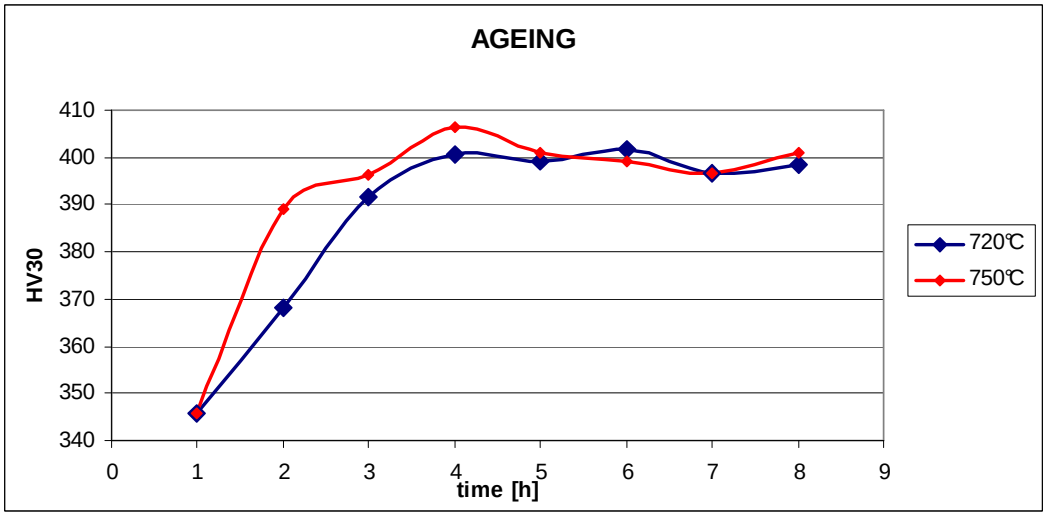

Figure V. 17 : Hardness evolution as a function of the ageing time.

Both curves exhibit a sharp slope, between 0 and 4 h, where hardness progressively increases followed by a plateau, between 4 and 8 h, where hardness remains constant.

Moreover, Kirman and Slama **[Kirman et al.,1970; Slama et al.,2005]** showed that an over-ageing effect, associated to the replacement of γ" by a coarser dispersion of the stable δ particles within the grain , could occur after long aging (100h) leading to a loss of hardness. In such a way, the constant hardness level, exhibited for 720 and 750°C in the range 4-8 hours, may be explained by the high resistance of the alloy to the coalescence of the partially coherent δ laths.

In agreement with the dilatometric results, the ageing at 750°C shows a faster hardening kinetics as compared to that occurring for the standard one (720°C). This is the result of an increased volume fraction of precipitates that enhances the hardening effects.

Finally, the hardness evolution during the second ageing step is reported in Figure V. 18.

Both thermal cycles shows a similar final hardness (445 HV30), obtained after 8 hours ageing. In such a way, the first ageing does not seem to have any effects on the hardness evolution during the second ageing. This last step, however, results in an average increase of the material hardness of 45 HV30 in addition to the hardening ensured by the preliminary ageing.

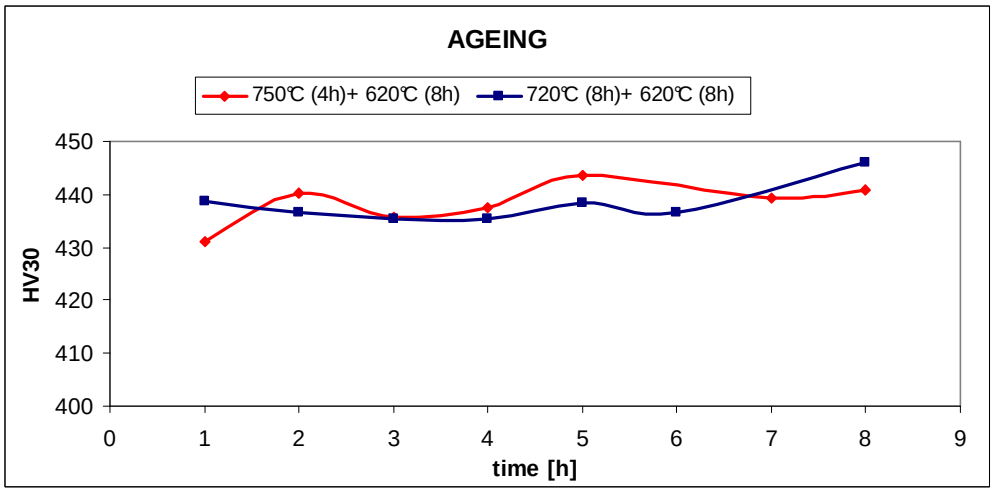

Figure V. 18 : Hardness evolution as a function of the ageing time, for second ageing treatments.

The microstructural investigations, described in this section, provide a valid support for the careful selection of the variables used in the Taguchi plan reported in Chapter III. A wide variety of options are available and many issues must be considered with the aim to improve the mechanical properties of the alloy.

Four different solution annealing temperatures (955, 980, 990 and 1000°C) above the delta solvus, have been considered in order to retain a certain amount of delta precipitates and avoid early grain growth. Considering the ageing procedure, the heat treatment variables chosen in this study are based on data from previous analytical testings (DTA and dilatometer) and on recommendations provided by the literature for the heat treatment of nickel base superalloys. In such a way, two alternative ageing procedures (750°C (4h) and 720°C (8h)) have been performed in order to ensure different distributions and morphologies of the strengthening phases, impacting the fatigue life. In addition, it was assumed that there would be no significant benefit of varying the second ageing step (considering its slight impact on hardening), that has been hold at 620°C for 8 hours.

II Fatigue behaviour of Inconel 718 alternative grades

As previously mentioned, one of the main objective of this PhD work consists in the study of the microstructure influence on the mechanical properties of the alloy under extrusion loading conditions. For this purpose, a series of LCF tests is carried out at 550°C using the reference trapezoidal signal with a strain rate equal to $5x10^{-3}$ s^{-1}.

In the design of the alternative thermal treatments, an important distinction has been made

between the “Intra-specification” and “Extra-specification” Inconel 718 grades. Likewise, the fatigue performances associated to the alternative treatments are discussed in the next sections and directly compared to the data obtained with the standard grade (Chapter IV).

Finally a detailed analysis of the cyclic response of the alloy (stress relaxation under loading, inelastic strain evolution and softening) is reported in order to explain the differences in terms of fatigue behaviour noticed between the various heat treatments.

II.1 Intra-specification thermal treated grades

Following the tensile tests data obtained by the application of the Taguchi method, two alternative thermal treatments (Tr. 990, Tr. 1000) have been chosen to be tested under extrusion conditions. It is important to remind that the selection was conducted considering the static mechanical properties (Y.S and U.T.S) as the discrimining parameters.

Figure V. 19 shows the Manson-coffin relationships of these alternative grades of Inconel 718. The directs comparison with the standard grade emphasizes the better performances shown by Tr.990, especially at high strain amplitudes. Conversely, Tr. 1000, which was selected for its capability to provide tensile properties, exhibits a very slight improvement of the fatigue resistance at high strain amplitudes and it becomes, further on, less efficient at low strain amplitude.

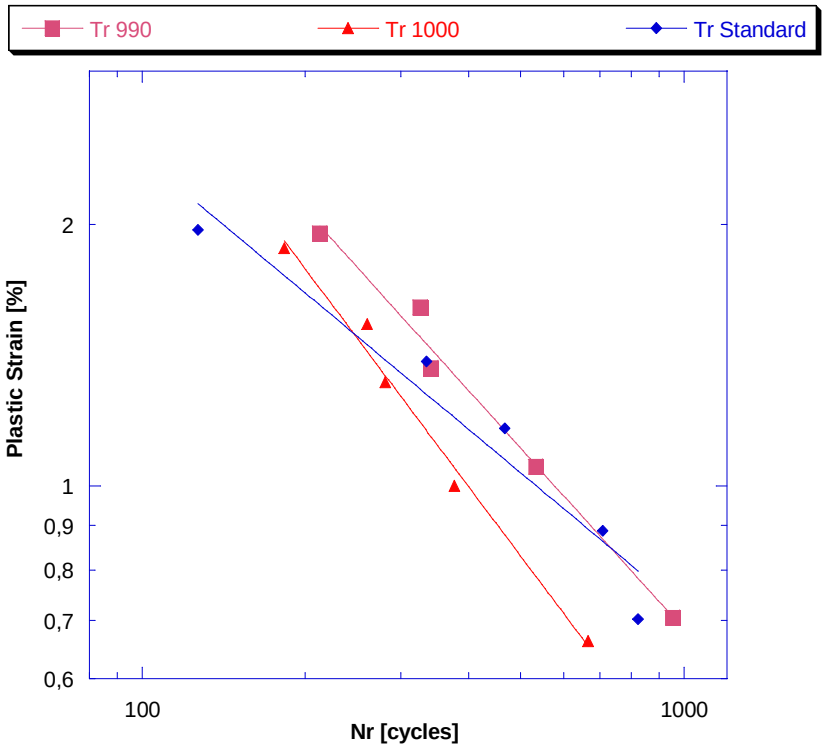

Figure V. 19 : Manson Coffin diagram for intra-specification Inconel 718 thermal treatments.

Similar considerations can be deduced from Figure V. 20 where the number of cycles to failure is plotted as a function of the total strain amplitude.

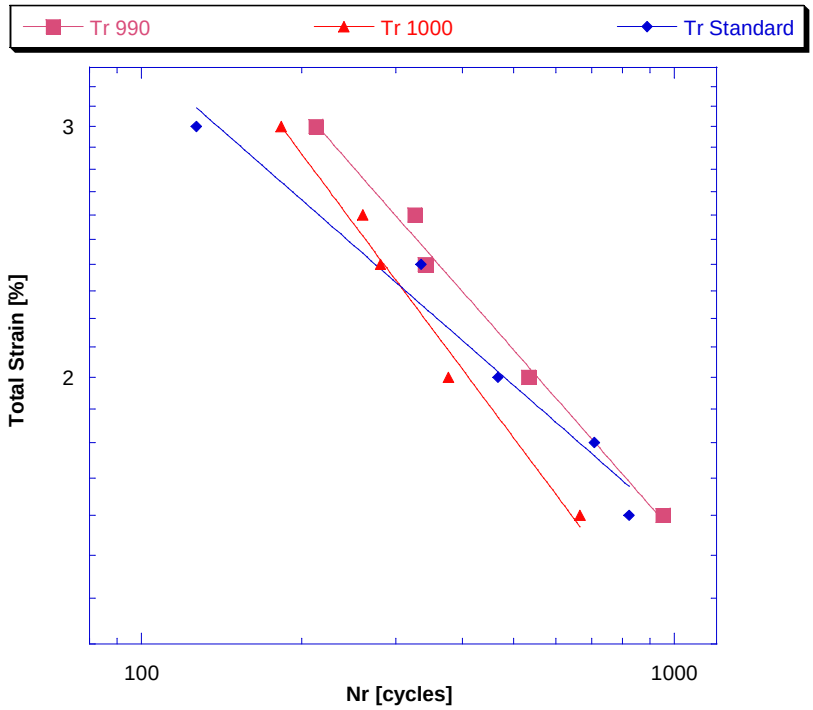

Figure V. 20 : Total strain vs. fatigue life diagram for intra-specification Inconel 718 thermal treatments as a function of the applied total strain.

II.2 Extra-specification thermal treated grade (API 6A)

This alternative grade of Inconel 718 has been chosen, essentially, for its techno-economical advantages, contributing to lower the extrusion die cost. As anticipated in Chapter III, the Oil and Gas (API 6A) treatment improves the alloy toughness but it negatively affects its mechanical properties (Y.S and U.T.S).

The grain size and morphology are shown in Figure V. 21. The Oil and Gas grade exhibits a significant grain growth, as a consequence of the high solution annealing temperature and the absence of delta phases along the grain boundaries. This is the main cause of the decrease of the tensile strength and the increase of the ductility of the alloy.

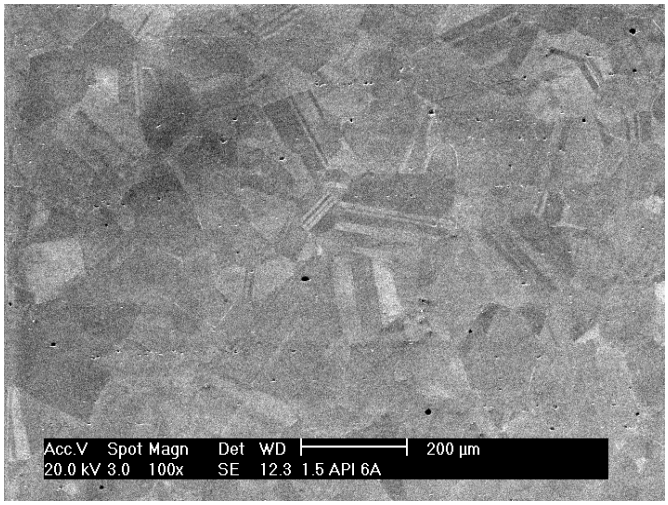

Figure V. 21 : SEM investigation of the microstructure obtained by the API 6A thermal treatment.

The fatigue performances associated to the API 6A treatment are reported in Figure V. 22. The Manson Coffin diagram points out the limited fatigue resistance of this alternative treatment through out the entire range of applied strains.

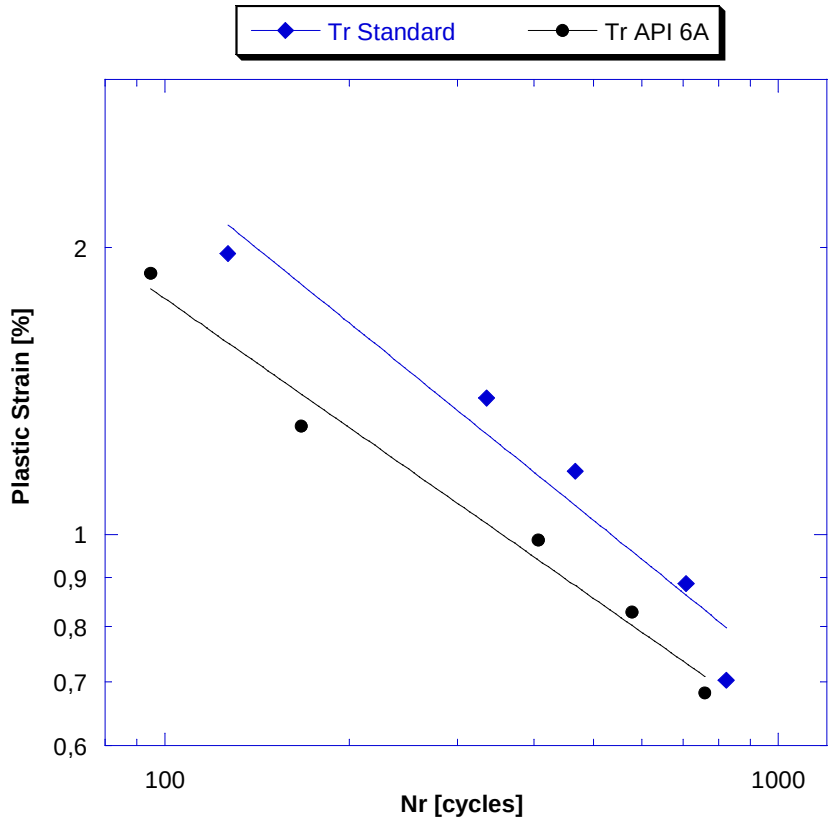

Figure V. 22 : Manson-Coffin diagram for Inconel 718 API 6A grade.

In addition, the cyclic response of Inconel 718 is reported in Figure V. 23, showing the dependence of the stress amplitude on the number of cycles. In this case, the alloy shows a different behaviour as compared to the standard grade. A preliminary hardening is noticed in the first 25 cycles, directly followed by a continuous softening up to the complete fracture of the specimen. This is the consequence of a direct interaction between dislocations and precipitates whose size and inter-particle distances are determined by this specific thermal treatment. However, we can suppose that the over ageing applied to the alloy, is responsible for a significant coarsening of the γ" phases. This has a direct impact on the deformation process: a delayed shearing mechanism can be suggested due to the larger size of the strengthening phases which hinders the dislocations movement.

As described for other alloys **[Jain,1992]**, new dislocations sources are activated, increasing the dislocation density. In such a way the alloy experiences a preliminary hardening until the deformation mechanisms are activated along specific slip systems. Slip is consequently spread over a series of grains enhancing the unlocking of the pinned dislocations which induces a progressive shearing of the γ" phases.

The detailed microstructural investigations reported at the end of this chapter will facilitate the understanding of this particular deformation behaviour

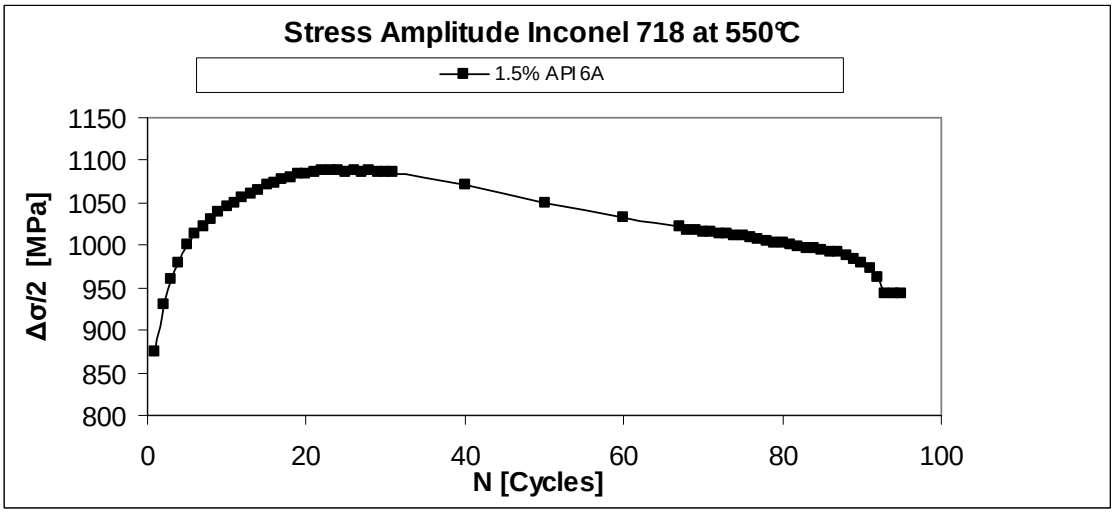

Figure V. 23 : Cyclic stress response for Inconel API 6A grade at 550°C.

II.3 Thermo-mechanical treated grade (DA)

The direct age technique (DA), belonging to the class of the thermo-mechanical treatments, is a way to further exploit the alloy strength ensuring a good combination of tensile, creep and low cycle fatigue properties. This alternative Inconel 718 grade is based on the common idea that a fine grain microstructure, expressly hardened by high forging reductions, provides better LCF resistance .

Before identifying the fatigue performances related to this treatment, it is important to examine the specific forging process and the applied experimental procedure.

Inconel 718 used in this present investigation has been produced by Aubert & Duval as a form of a forged pancake of 300 mm in diameter and 80 mm in height. The chemical composition of the disk is reported in Table V. 1.

Element	***Ni***	***C***	***Cr***	***Fe***	***Nb***	***Ta***	***Mo***	***Ti***	***Al***
[% weight]	53.6	0.027	17.8	18.7	5.23	< 0.01	3.09	0.917	0.503

Table V. 1 : Weight percent analysis of the Inconel 718 Direct Age grade.

The alloy has been forged at a temperature close to 980°C and directly water quenched.

The forged pancake has been divided into two parts (Figure V. 24): a first part has been treated following the “Tr.990” procedure, whereas the second one has been directly aged using the standard duplex ageing. All the fatigue samples used to study the fatigue properties of the Inconel 718 standard grade were obtained from hot rolled bars. Consequently, the idea to consider two different thermal treatments for the forged pancake is based on the interest to define a new reference for the Tr. 990 grade applied to a forged material (Tr.990 forged). In such a way, the fatigue performances of the direct aged material can be directly compared to that of the reference alloy, focusing on the effects of the single heat treatment and excluding the contributions of a different forging process.

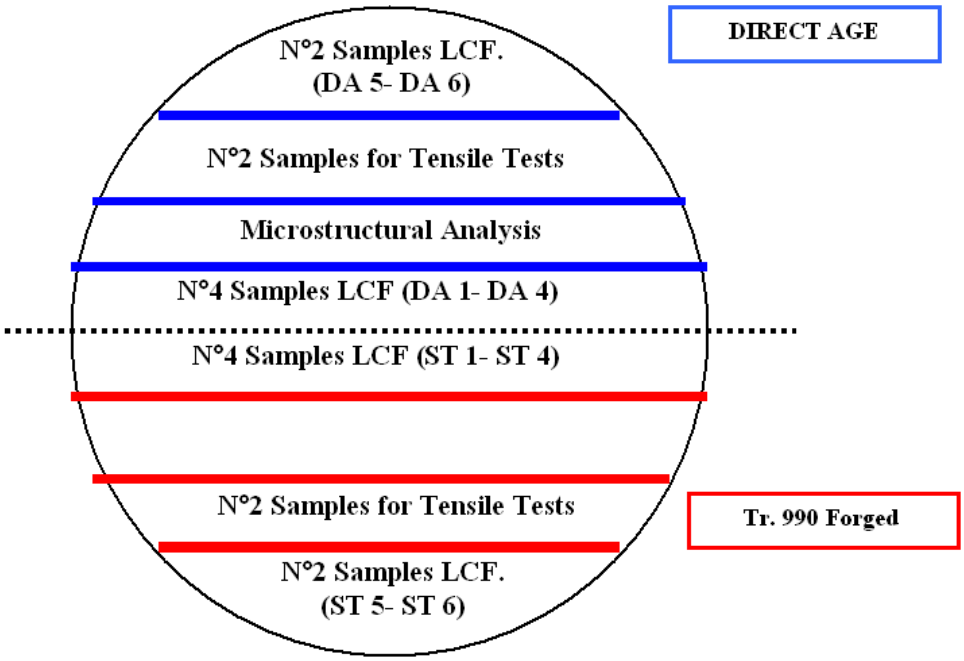

Figure V. 24 : Experimental procedure for the extraction of LCF samples in the forged pancake.

Two tensile samples have been extracted from each part of the pancake: the results of the tensile tests performed at 550°C are reported in Table V. 2.

Heat Treatment		Y.S [MPa]	U.T.S [MPa]	A [%]	Z [%]
Standard	Test 1	1212	984	21	43
	Test 2	1199	981	23	41
	Average	1206	983	22	42
Direct Aged	Test 1	1273	1148	19	43
	Test 2	1287	1118	20	45
	Average	1280	1133	20	44

Table V. 2 : Tensile properties at 550°C of the forged material treated following the "Direct Age" and the "Tr. 990" procedure.

Inconel 718 Direct Age shows a 15% of improvement in the yield strength compared to the reference (Tr.990 Forged), and close values of Y.S and U.T.S, due to the work-hardening effects of the thermo-mechanical process.

The metallographically prepared macro-section, extracted form the D.A part, has been investigated by optical microscopy (Figure V. 25). The pancake exhibits certain heterogeneity of structure, with the presence of "die lock areas" in the top and bottom zones where a low temperature and a reduced strain rate produce a non recrystallized structure with large grains (ASTM 5).

The microstructural investigation of the zone where specimens have been extracted shows

a recrystallized structure, consisting of regular grains, (ASTM 11-12), surrounded by finer grains (ASTM 13).

This is the result of a dynamic recrystallization caused by the generation of subgrains which dictate the size of the recrystallized grains. Previous studies **[Horvath et al.,2001; Guest et al.,2005]** have shown that if the strain rate is low, the deformation taking longer time, gives to the grain boundaries more time to migrate than during deformation at high strain rate. Following these assumptions, it could be suggested that the centre of the forged pancake is subject to a large amount of strain which induces the progression of the dynamic recrystallization.

Figure V. 26 exhibits SEM investigations performed in specific zones of the pancake. The images are used to better characterize the distribution and morphology of the delta phase particles. In “the lock areas” delta phase is uniformly distributed along the grain boundaries in the shape of fine plate like particles. In the regions at the centre of the pancake, precipitates show a more discontinuous distribution, exhibiting a different size and a more globular morphology. This is the result of a different distribution of the strain amplitude within the pancake. Liu and Coste **[Liu et al.,1997; Coste,2003]** studied the effects of the deformation mechanisms on the thermodynamical equilibrium of the delta phase. During deformation, at a sub-solvus temperature, the delta phase precipitates progressively dissolve and tends to re-precipitate in the regions where the dynamic recrystallization progress. However, the strain rate seems to have no influence on the precipitation rate.

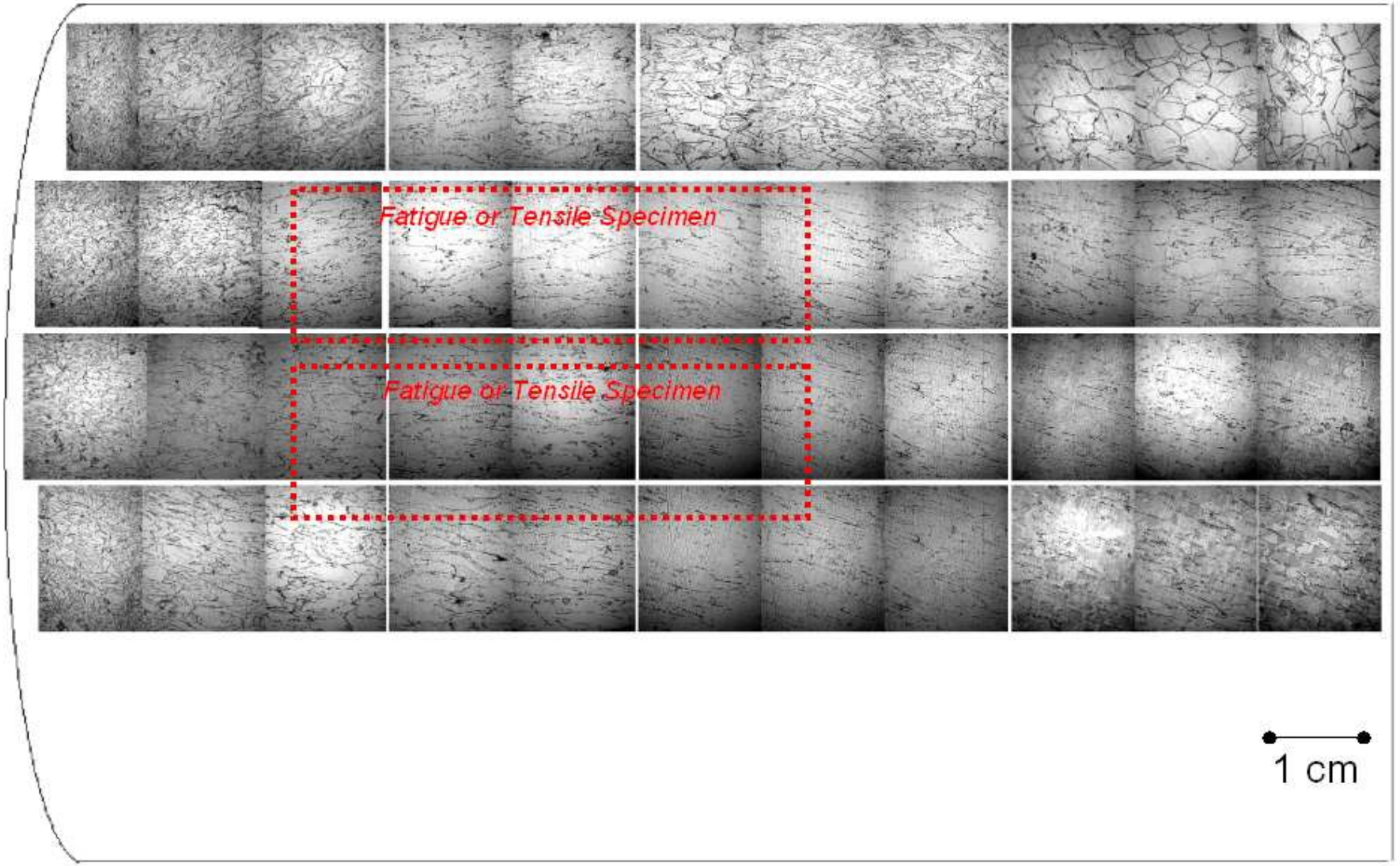

Figure V. 25 : Microstructural investigation of the pancake macro- section treated following the Direct Age process.

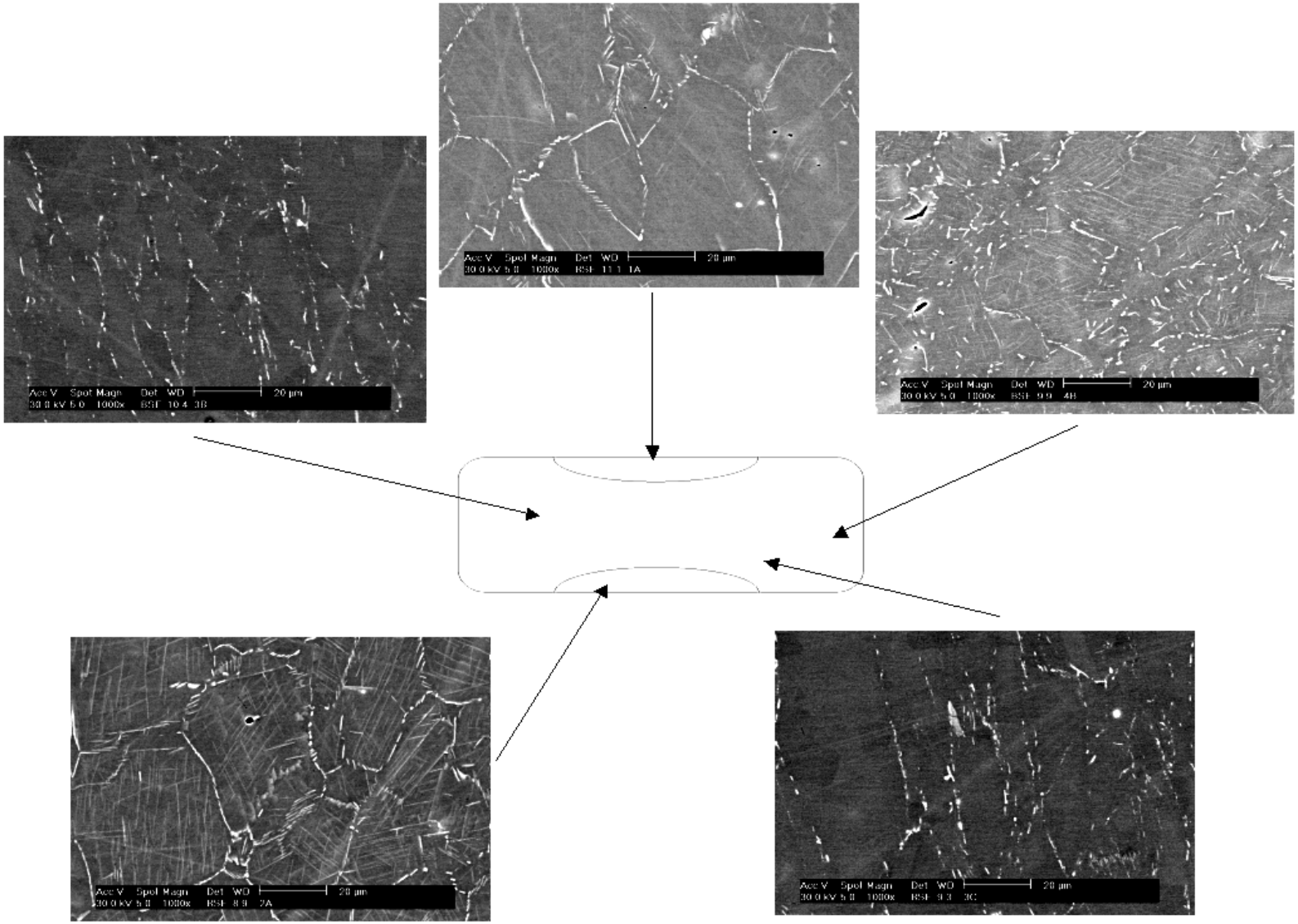

Figure V. 26 : SEM investigations of the delta phase distribution and morphology in the Direct Age pancake.:

The study of the LCF performances associated to the thermo-mechanical treatment have been performed using samples extracted from the centre as well as from the periphery of the pancake in order to evaluate the heterogeneities in fatigue behaviour.

Figure V. 27 shows the SEM micrographs of direct aged specimens (Figure V. 27(a)) and the reference specimens “Tr. 990 forged” (Figure V. 27(b)). However, no clear differences can be detected between a forged and rolled ((Figure V. 27(c)) microstructures treated following the Tr.990 specification. Material exhibits an equiaxe grain structure with a large presence of delta phase laths which act as grain boundaries pinning points.

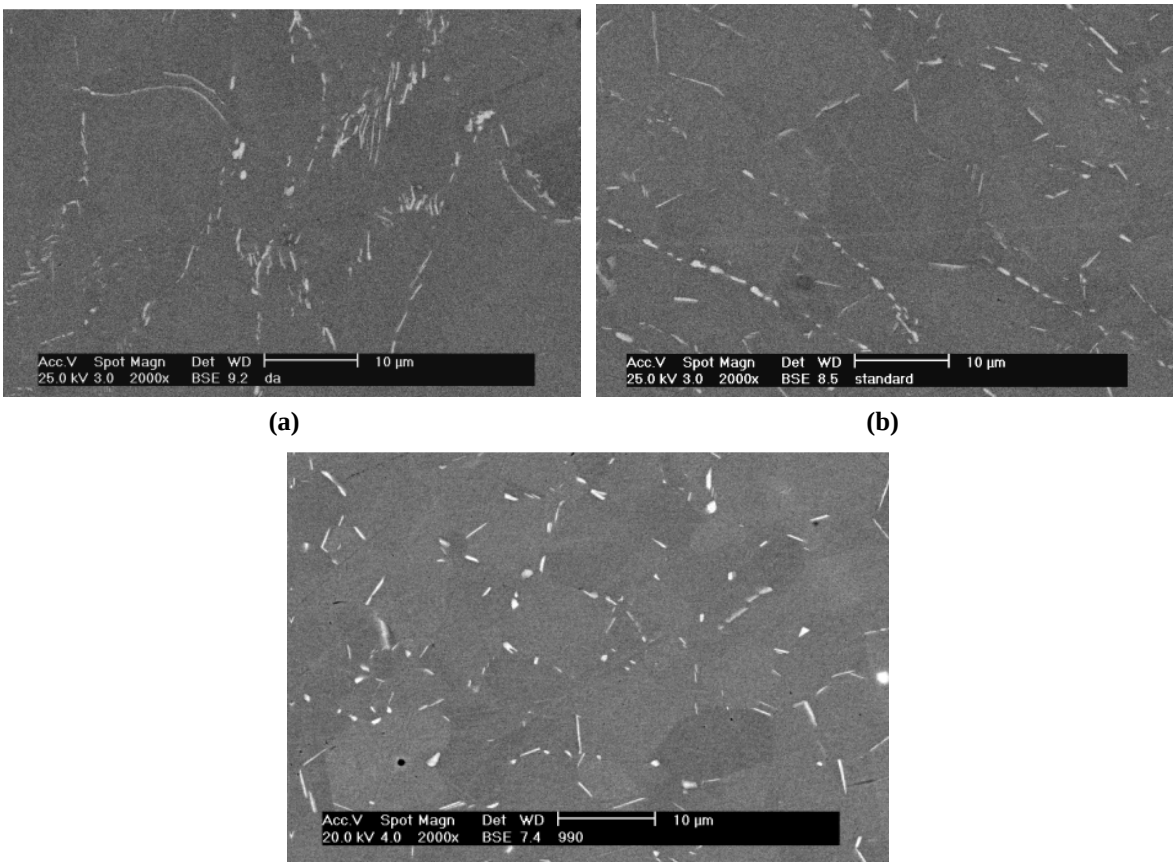

(a) **(b)**

(c)

Figure V. 27 : Typical microstructure of LCF samples, respectively obtained by “Direct Age” (a), “ Tr. 990 forged” (b) and “Tr. 990” (rolled) (c).

The LCF results obtained at 550°C under extrusion conditions are reported in Figure V. 28. The “Manson Coffin” diagram points out the better performances of the forged samples as compared to the rolled ones. Comparing the results of the DA and “Tr 990 forged”, the diagram indicates that the two heat treatments are typically similar except for high plastic strains, where the Direct Age lives become slightly longer. These results are substantially due to the high yield strength associated to the direct age process, which delays and reduces the inelastic effects. Finally, tests have ambiguously shown the limited scatter in fatigue performances between the centre and the edges, indicating a satisfactory degree of process stability and a good isotropy throughout the pancake.

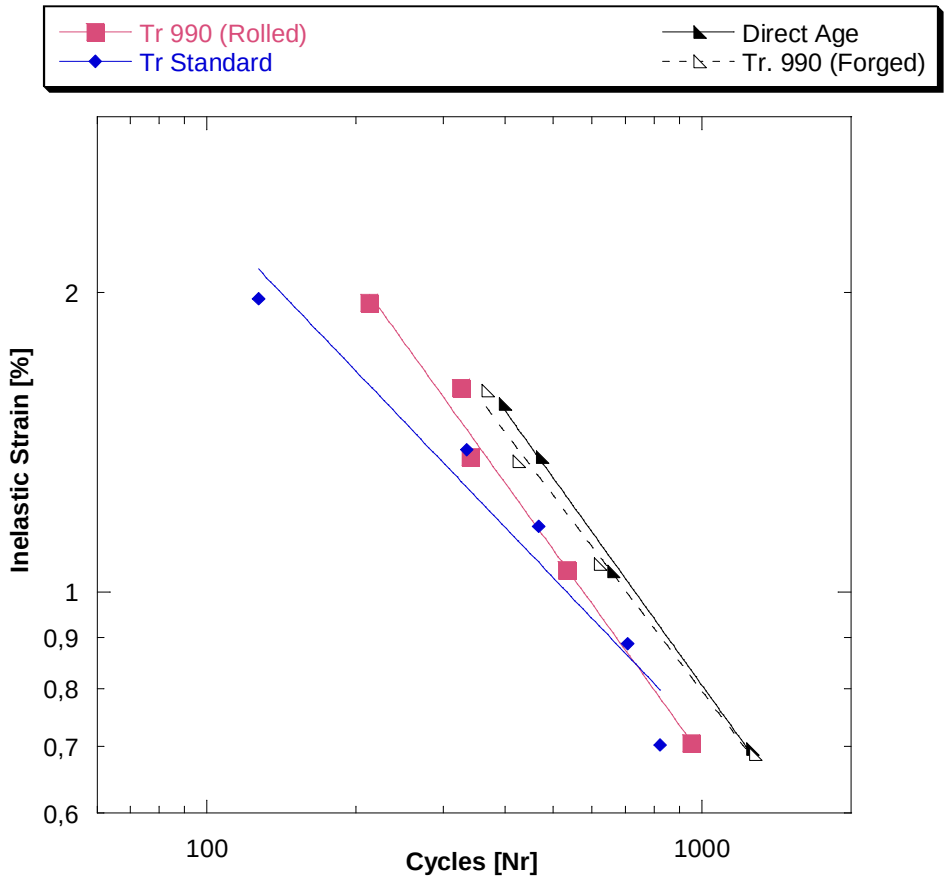

Figure V. 28 : Manson-Coffin diagram of the Direct Age Inconel 718 grade.

III Comparative study of the fatigue life for alternative Inconel 718 grades

The LCF results reported in the previous sections have shown a strong sensitivity of Inconel 718 to the thermal treatment that simultaneously acts on both its microstructure and mechanical behaviour.

Since the fatigue property enhancement is the main objective of this PhD work, it is useful to review the material response under extrusion loading (trapezoidal cycle), with a particular attention to the environment conditions and interactions. A typical list of item, by which the various Inconel 718 grades can be compared includes:

- The Low Cycle Fatigue (LCF) life;
- The fracture surfaces investigation;
- The stress relaxation under load;
- The material softening.

The impact of each parameter on the fatigue life is discussed in details in the following

sections in order to define the most efficient thermal treatment for extrusion die applications.

III.1 Low Cycle Fatigue life

The Manson Coffin diagram, shown in Figure V. 29, reports all the results relative to the LCF tests performed under extrusion conditions for the various investigated Inconel 718 grades.

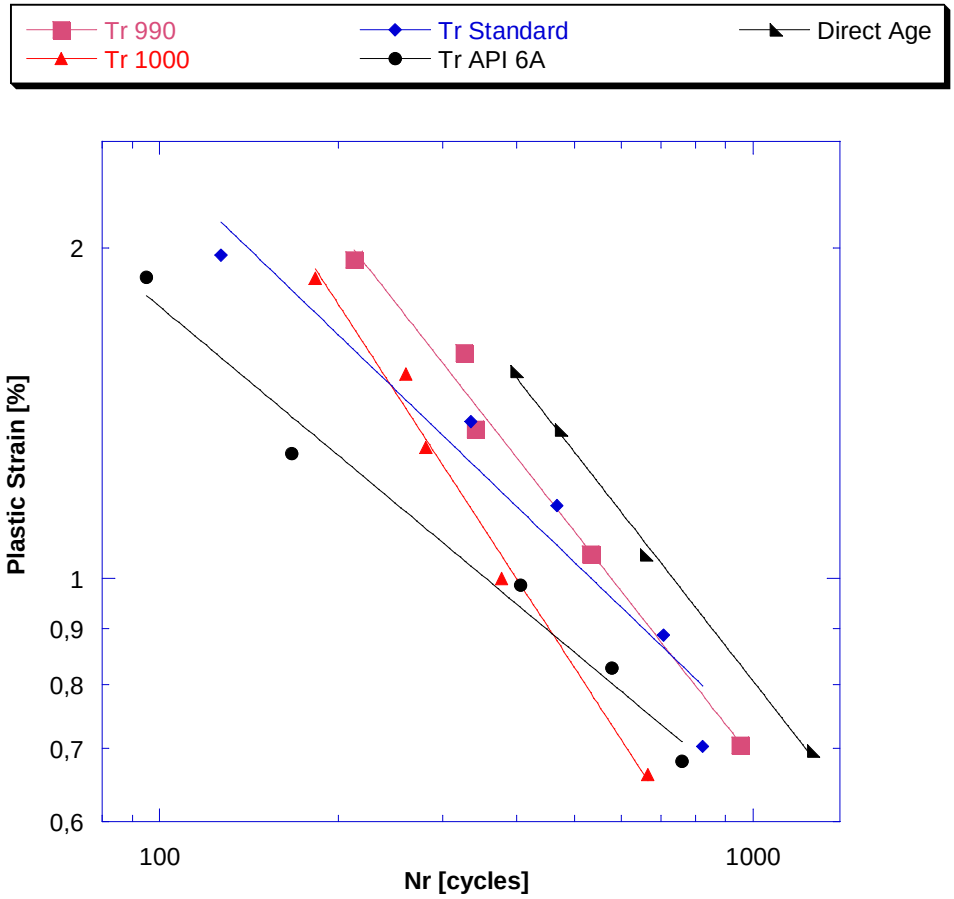

Figure V. 29 : Manson Coffin diagram for the alternative Inconel 718 grades.

Differences in terms of fatigue life can be noticed. Table V. 3 reports a comparison of the fatigue performances considering two different total applied strains. For similar test conditions, it is possible to define a fatigue ratio ($N/N_{Tr.Standard}$) that compares the relative fatigue life of each alternative thermal treatment as compared to that obtained from the Standard Inconel 718 grade.

The Direct Age and Tr.990 process exhibits better performances within the entire range of applied total strains. Conversely, the “API 6A” treatment exhibits low fatigue durability at high strain amplitudes, while it ensures similar performances to that of the standard grade at low strain.

	$N_{(Alternative\ grade)}/N_{(Tr.Standard)}$	
Thermal Treatment	$\Delta\varepsilon_t = \pm 1.2$ %	$\Delta\varepsilon_t = \pm 0.8$ %
Tr.990	1.67	1.15
Tr.1000	1.44	0.81
API 6A	0.75	0.93
Direct Age (DA)	2.12	1.53

Table V. 3 : Effect of the alternative thermal treatments on the fatigue performances of Inconel 718 At 550°C.

III.2 Fracture surfaces

Fractographic observations are conducted on specimen fracture surfaces after low-cycle fatigue at 550°C (Figure V. 30).

The specimens show a similar characteristic in terms of fracture morphologies. Typical fatigue fractures with fatigue striations and signs of plastic deformations are observed in all specimens. However, some traces of intergranular cracks, probably due to the environmental interactions, are noticed.

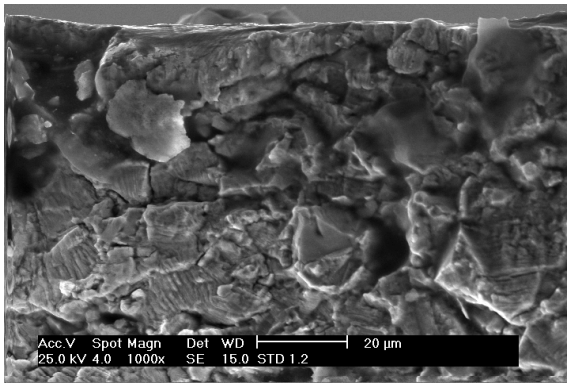

(a)

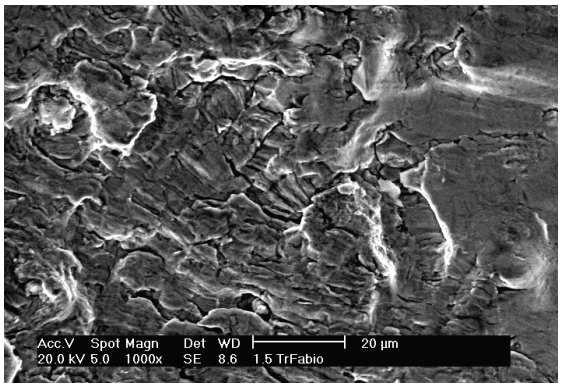

(b)

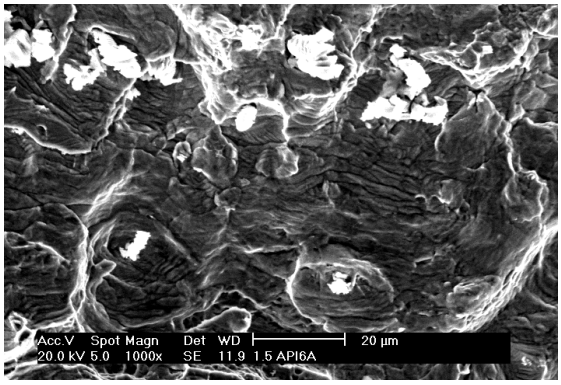

(c)

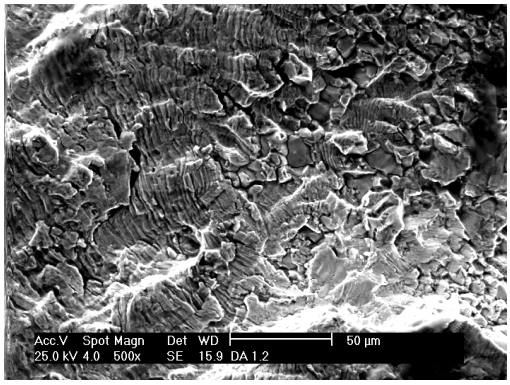

(d)

Figure V. 30 : SEM investigations of the fracture surfaces of LCF samples tested at 550°C for various Inconel 718 grades: Tr.990 (a), Tr.1000 (b), API 6A (c) and Direct Age (d)

III.3 Stress relaxation under high loading strain

Another strategy to compare the macroscopic response of the different Inconel 718 grades is based on the study of the stress relaxation under high strain loading. During the holding time, the application of a constant total strain induces a continuous stress relaxation. Figure V. 31 compares the relaxation behaviour of the various heat treatments under the application of a deformation amplitude of 1.5 % . Stress relaxation is expressed as a dimensionless ratio ($\sigma_i/\sigma_{(t=0)}$) between the current (σ_i) and the initial stress $\sigma_{(t=0)}$.

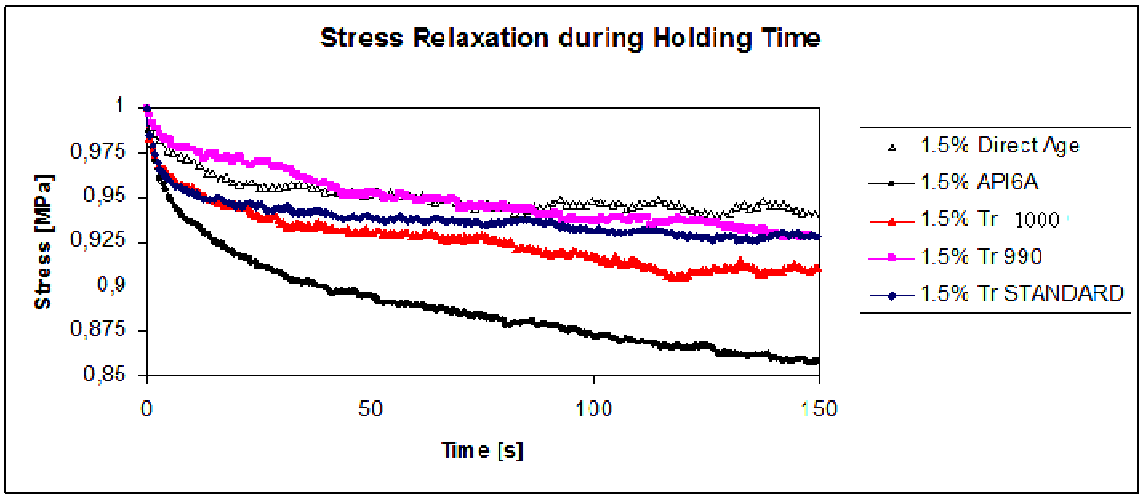

Figure V. 31 : Stress relaxation during loading time at maximal strain for different Inconel 718 grades at 550°C.

The stress relaxation curves point out the resistance of Tr.990, Tr. Standard and Direct Age to stress relaxation.

In addition, during the holding time a conversion of the elastic strain into plastic strain occurs, due to the stress relaxation. Figure V. 32 reports the plastic strain evolution, as function of the holding time, for the various treatments and strain amplitude of ±1.5%. Tr.990 and Direct Age continue show better performances, exhibiting inelastic strain amplitude, at the end of the holding time, similar to the standard grade.

The higher resistance to the plastic deformation under holding time conditions contributes to explain their better fatigue performances under extrusion conditions.

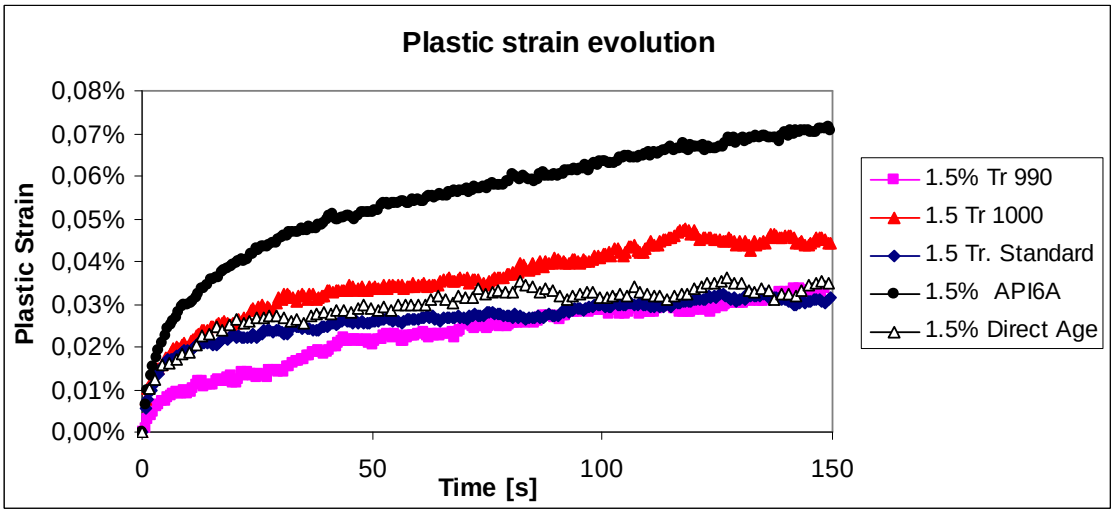

Figure V. 32 : Plastic strain evolution during loading time at maximal strain for different Inconel 718 grades at 550°C.

III.4 Cyclic softening

In addition to the previous results, Figure V. 33 exhibits a similar comparison in terms of cyclic stress repose for a LCF test performed with total amplitude of ±1.2%. Cyclic stress amplitude ($(\sigma_{Max}- \sigma_{min})/2$) is plotted as a function of the number of cycles.

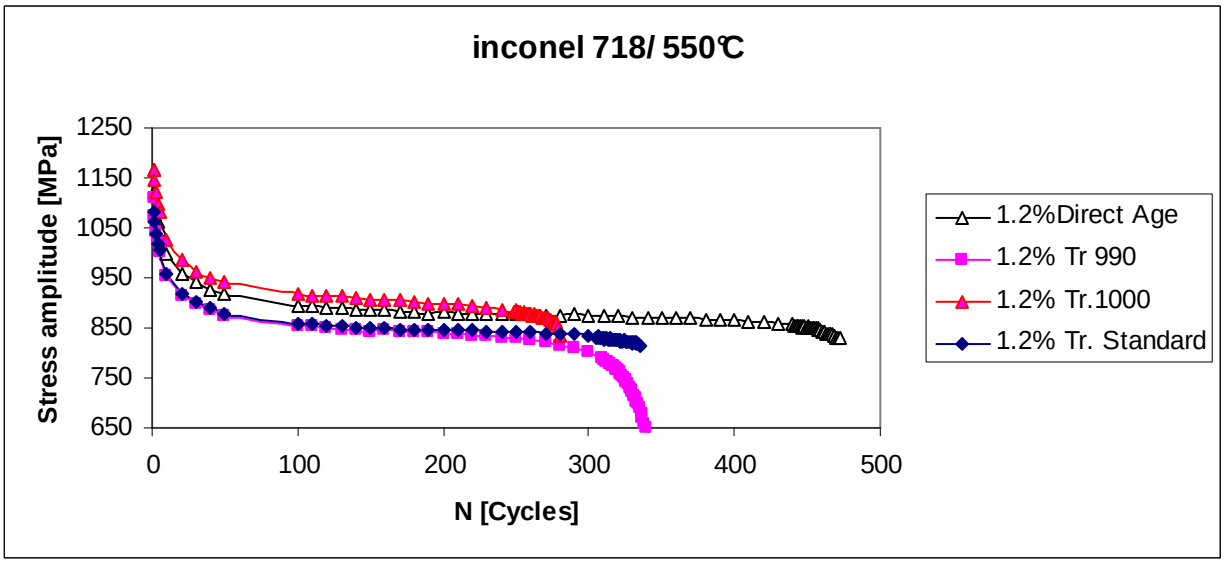

Figure V. 33 : Cyclic stress response at 550°C for different Inconel 718 thermal treatments.

The various thermal treatments result in a different behaviour that is influenced by the Yield Strength (Y.S) associated to each microstructure. In general, a higher Y.S leads to higher stress amplitude along the LCF test.

For these reasons, a dimensionless ratio between the instantaneous stress ratio and the stress amplitude at the first cycle $\Delta\sigma_i / \Delta\sigma_1$ can be plotted as a function of the number of cycles (N) (Figure V. 34).

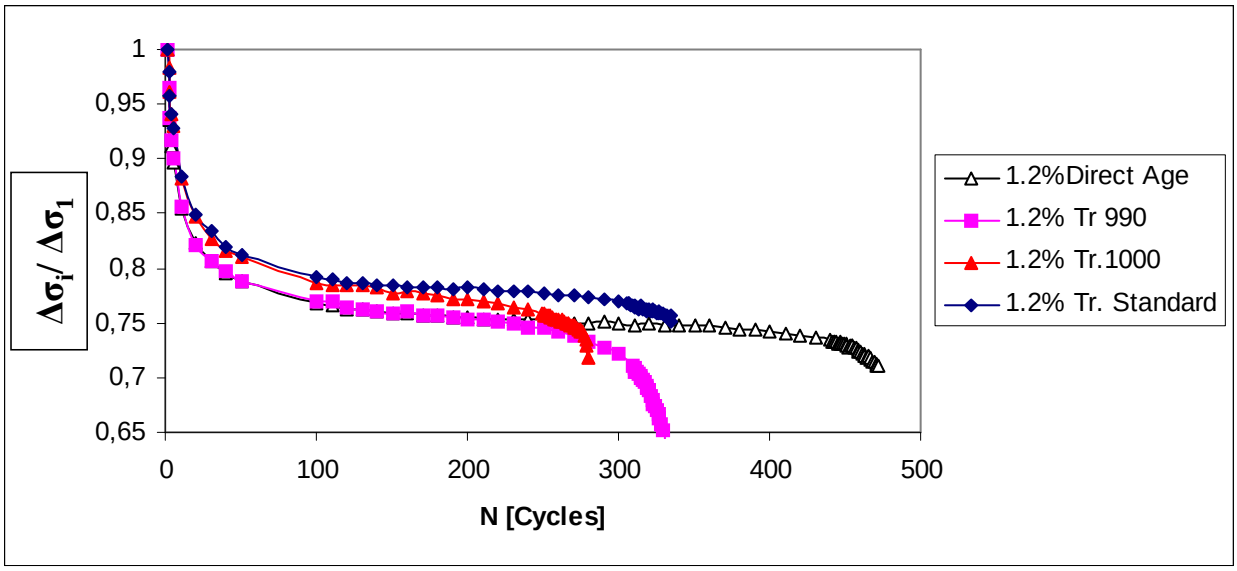

Figure V. 34 : Normalised cyclic stress responses for various Inconel 718 grades under extrusion conditions (trapezoidal signal 150_20) ($\Delta\varepsilon_t$=±1.2%).

In such a way, slight differences in terms of softening can be noticed between the various grades. The microstructural investigations, reported in the next sections, could provide a possible explanation for these specific behaviours.

The cyclic response of the "API 6A" grade has just been considered above due to a different behaviour based on a preliminary hardening followed by a continuous softening.

III.5 Partial conclusions

The purpose of this investigation was to analyse the influence of the heat treatment on the fatigue performances of Inconel 718 under extrusion conditions. The properties of the alloy have been notified and optimized using various heat treatments. The LCF tests have proved a significant influence of the alternative heat treatments on the alloy's fatigue durability at 550°C, the Direct Age grade exhibiting the highest fatigue performances. This results should be related not only to the change of the heat treatment process, no solution annealing, but also to the application of a thermo-mechanical forging that gives to the material residual work hardening. Within the "Intra- specification" designed grades, the Tr.990 variant exhibits superior fatigue properties as compared to both the standard grade and to the alternative Tr.1000 grade whose behaviour, under cyclic loading, does not reflect the high tensile properties measured at 550°C. Finally, the API 6A grade has shown a different cyclic response in which a preliminary hardening process occurs during the very first cycles (20-25 cycles), directly followed by a rapid and continuous softening until the final fracture develops. The reason for lower fatigue durability, under extrusion conditions, of the heat treated specimens in variant Tr.1000 and API 6A can be explained by a different behaviour exhibited under the application of a holding time at maximum strain. The remarkable and rapid stress relaxation exhibited by these Inconel 718 variants, which increase the plastic strain amplitude associated to each cycle, can be considered as a limiting factor under LCF conditions.

However, a detailed investigation of the influence of the thermal treatments on the microstructure, reported in the next section, has been carried out to better understand and compare the mechanical behaviour of the alternative Inconel 718 grades

IV Comparative analysis of the microstructure of alternative IN718 grades

The previous sections have investigated the effects of the alternative thermal treatments on the fatigue life and on the mechanical response of the material under typical extrusion loading. Experiments have shown that changes in microstructure leads to a variability of the mechanical properties of the alloy. As a consequence, the investigation and comparison of the different microstructures provide a detailed overview of the microstructure changes and their correlations with the mechanical properties at high temperatures.

Figure V. 35 shows a SEM investigation of the microstructures corresponding to the alternative thermal treatments. The “Intra-specification” grades (Tr. Standard (a), Tr.990 (b) and Tr 1000 (c)) exhibit very similar microstructural features except for the morphology and content of the delta phase that decreases and tends towards a needle-plate morphology as the annealing temperature increases (Tr.1000 (b)). These results are consistent with the experimental investigations reported in the first sections of this chapter. However, the most significant microstructural changes are associated to the“Extra-specification” procedures. As reported above, the Direct Age (c) treatment is responsible for necklace microstructures with a limited amount of fine and elongated delta particles. Finally, the “API 6A” (d) grade shows a pronounced evolution of the Inconel 718 microstructure, where the absence of the intergranular delta phase particles induces a premature grain growth and an increase of the superalloy ductility.

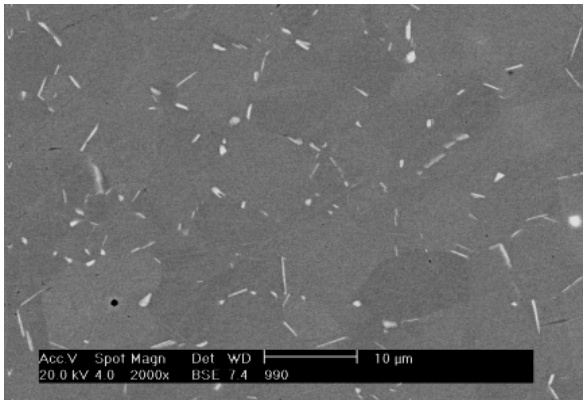

(a)

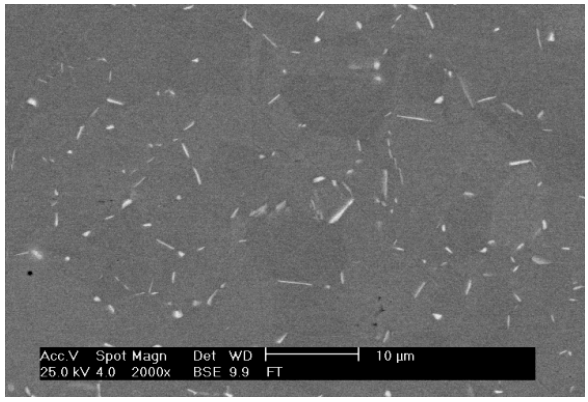

(b)

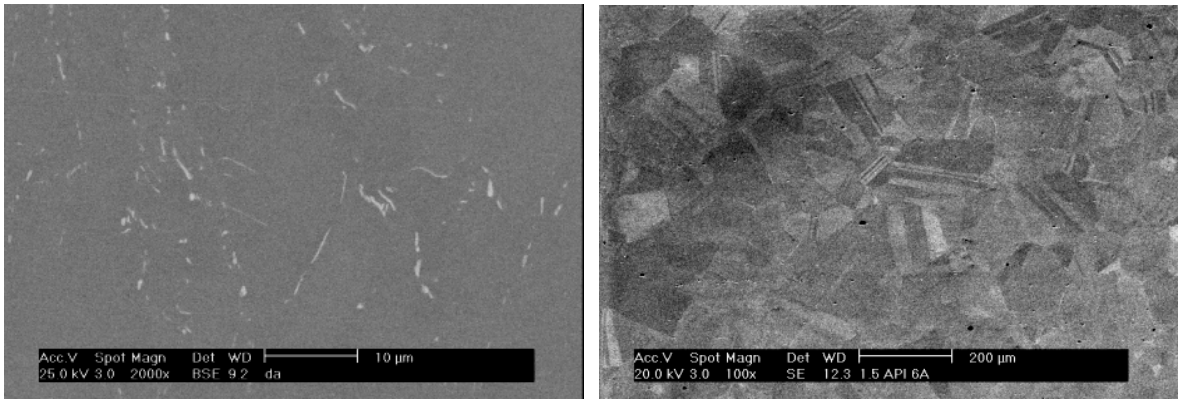

(c) **(d)**

Figure V. 35 : SEM observations of the microstructure of the alternative Inconel 718 grades, respectively: Tr.990 (a), Tr.1000 (b), Direct Age (c) and API 6A (d).

IV.1 Intermetallic phases morphology

As described above, the aging treatments lead to different distributions of γ' and γ" precipitates that evolve through homogeneous nucleation. In such a way, transmission electron microscopy (TEM) observations have been performed in order to characterize the morphology of the intermetallic phases as a function of the specific thermal treatment. Dark field observations of samples have been carried out using diffraction pattern corresponding to the $[001]_\gamma$ zone axis of the γ matrix. The analysed diffraction pattern, reported in Figure V. 36(a), exhibits intense spots associated to the matrix (γ) while the other faint spots corresponds to the strengthening precipitates (γ' and γ"). The indexed pattern **[Niang,2010]** (Figure V. 36(b)) shows the presence of three variants of precipitates in addition to the specific spots of the gamma prime phase as labelled in the figure.

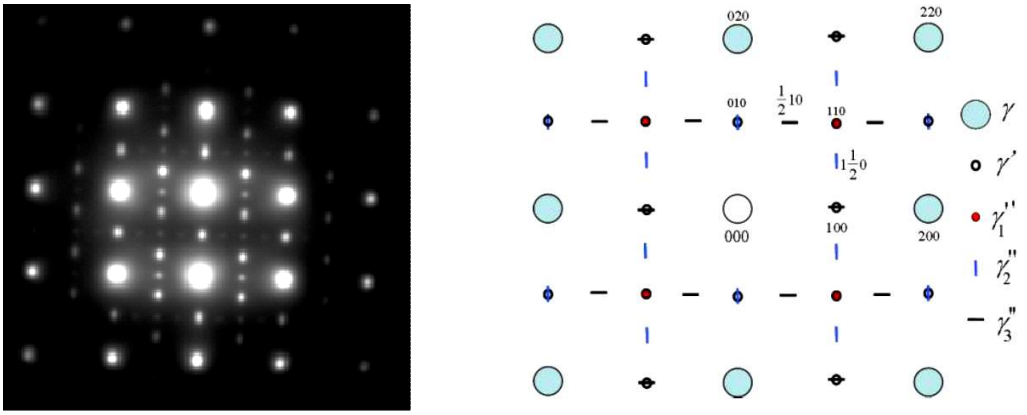

Figure V. 36 : Selected Area Diffraction (SAD) $[001]_\gamma$ zone axis for Inconel 718 (a) and corresponding indexed key pattern [Niang,2010].

The $<001>_\gamma$ zone axis pattern confirms the orientation relationships between the γ matrix and γ" precipitates, previously reported in the literature:

- Variant 1: $[001]_{\gamma"} // [001]_\gamma$
- Variant 2: $[001]_{\gamma"} // [010]_\gamma$
- Variant 3: $[001]_{\gamma"} // [100]_\gamma$

As reported by other authors **[Paulonis et al.,1969; Slama et al.,1997; Niang,2010]**, the adopted experimental approach consists in firstly selecting first the g=100 diffraction spot allowing the simultaneous identification of γ' and γ". Then, the g= ½10 spot is chosen to isolate the γ" variant from the rest of the precipitates. The comparison of the two bright field images leads to the individual analyse of the single phases. However, the γ' particles are too small to be clearly imaged in transmission electron microscopy. For this reason, only the g= 100 selected area diffraction patterns (SADP) will be considered to investigate the precipitates morphology.

Figure V. 37 to Figure V. 40 compare the dark field examination obtained with g=100 for all thermal treatments. Generally speaking, the γ" precipitates are uniformly distributed within the austenite grains showing fairly high density. In particular, the standard treatment (Figure V. 37) shows a significant precipitation of very fine and globular particles, whereas for the other grades, these particles become lens-shaped (Figure V. 38 and Figure V. 39).

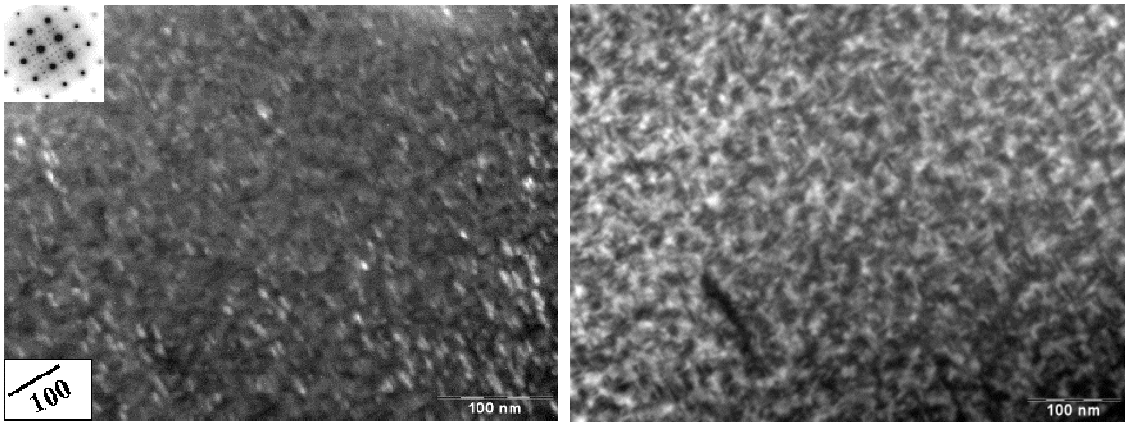

Figure V. 37 : Dark field (a) and bright (b) field TEM micrographs showing the intermetallic precipitates in Inconel 718 Standard grade.

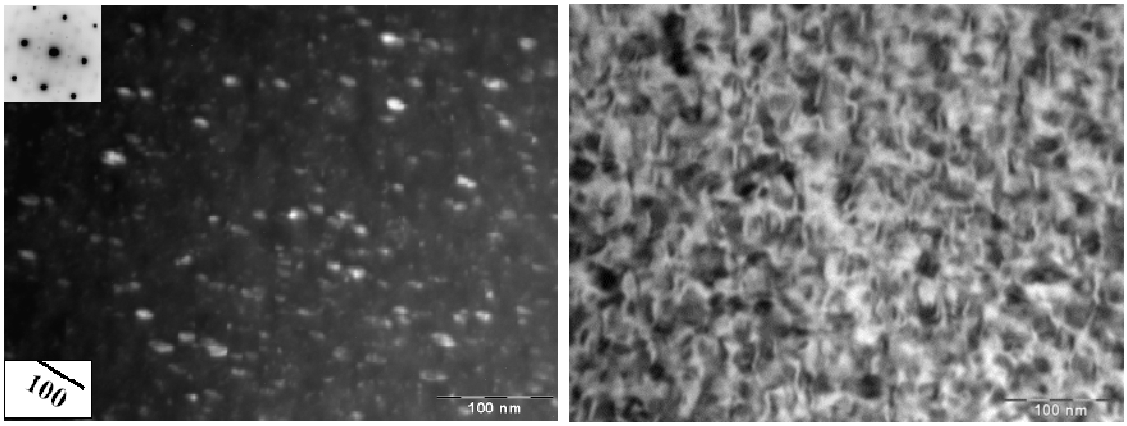

Figure V. 38 : Dark field (a) and bright (b) field TEM micrographs showing the intermetallic precipitates in Inconel 718 Tr.990 grade.

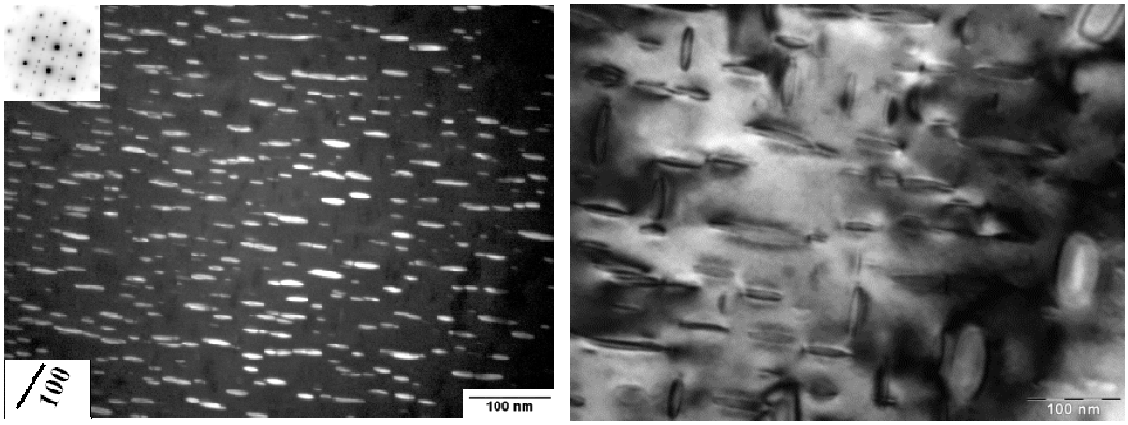

Figure V. 39 : Dark field (a) and bright (b) field TEM micrographs showing the intermetallic precipitates in Inconel 718 API 6A grade.

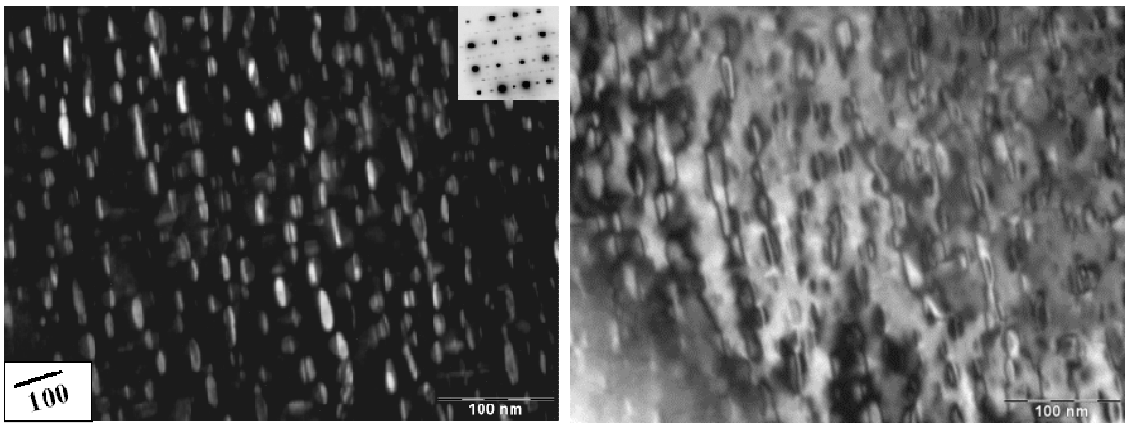

Figure V. 40 : Dark field (a) and bright (b) field TEM micrographs showing the intermetallic precipitates in Inconel 718 Direct Age.

The bright field micrographs show the typical "double-lobe" contrast that reveals the high coherency strain associated to the γ" precipitates. In agreement with Slama **[Slama et al.,1997]**, the length (L), width (e) and the (e/L) ratio of γ" particles may be determined from electron microscopy using the dark field technique. The results, corresponding to the average of measurements carried out on 15 particles, are listed in Table V. 4.

Heat Treatment	L [nm]	e [nm]	e/L
Standard	13 ± 3	5 ± 1	0.38
Tr. 990	14 ± 3	6 ± 1	0.42
API 6A	33 ± 3	7 ± 1	0.21
Direct Age (DA)	23 ± 3	7 ± 1	0.30

Table V. 4 : Intermetallic γ" precipitates morphology (*L* (size) and *e* (width)) corresponding to the average of TEM measurements carried out on 15 particles for each thermal treatment.

Note that the "API 6A" grade exhibits a change in shape of the γ" precipitates that have grown during the over-aging at 785°C for 6.5 hours. As a consequence of this evolution, a more elongated morphology occurs: particles precipitate as long disk-shaped with an average size of 33 nm. Figure V. 41 reports the change in (e/L) ratio as a function of the precipitates

size (L) for the investigated thermal treatments. The experimental data show, for γ" sizes ranging between 10 and 35 nm, a direct (quasi linear) dependence of the (e/L) ratio to the precipitates length (L).

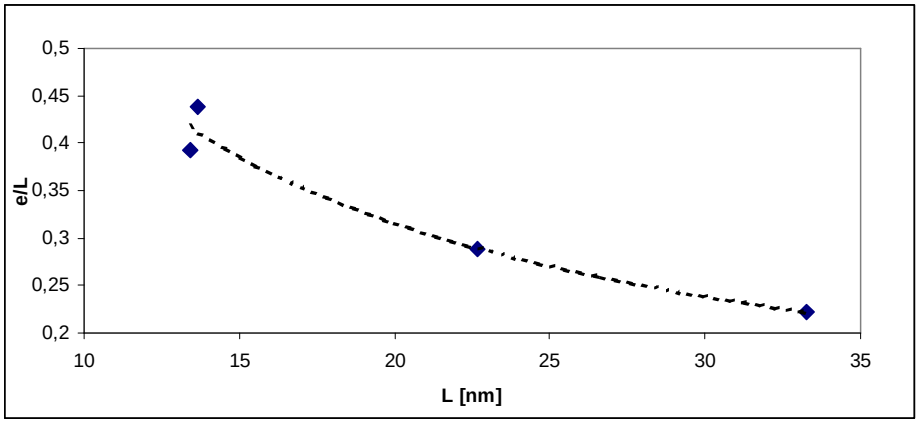

Figure V. 41 : Evolution of the (e/L) ratio, for the γ" precipitates, as a function of the particles size (L).

The growth or coarsening mechanisms observed for the "Tr. API 6A" is associated to a decrease of the density of γ" phases increasing the width of the precipitates-free zones (Figure V. 39). These zones are subject to planar slip bands development occurring during the deformation process. Consequently, preferential paths, showing a lower critical shear stress for dislocation slip, are established during the progressive deformation. As a result, it is suggested that the morphology of the strengthening phases have a direct impact on the deformation mechanisms in Inconel 718.

IV.2 Extraction and analysis of the intermetallic phases

Alternative and complex thermal treatment have been performed on Inconel 718 in order to obtain the required mechanical properties, such yield strength and fatigue resistance. The properties are the result of a through optimisation of the volume fraction, the size and the morphology of the strengthening phases. Previous studies have revealed that the composition of the different phases is largely affected by the thermal treatment. For this purpose, advanced experimental methods are required to determine crystallographic structures, chemical composition of precipitates and matrix as well as the precipitates molar fractions. The approach adopted in this PhD work consists in the identification of the different phases contained in the austenitic matrix using an electrolytic extraction coupled with an X-ray analysis **[Bellot et al.,2011; Carniel et al.,2011]**.

Preliminary electrolytic extractions have been performed in the solution annealed conditions in order to identify the delta phase content right after quenching. Figure V. 42 reports the X ray patterns obtained from the residues. The peaks associated to the delta phases proves that during the electrolysis these phases have totally transferred to the electrolyte. Conversely, no traces of γ' or γ" have been detected after the solution annealing process.

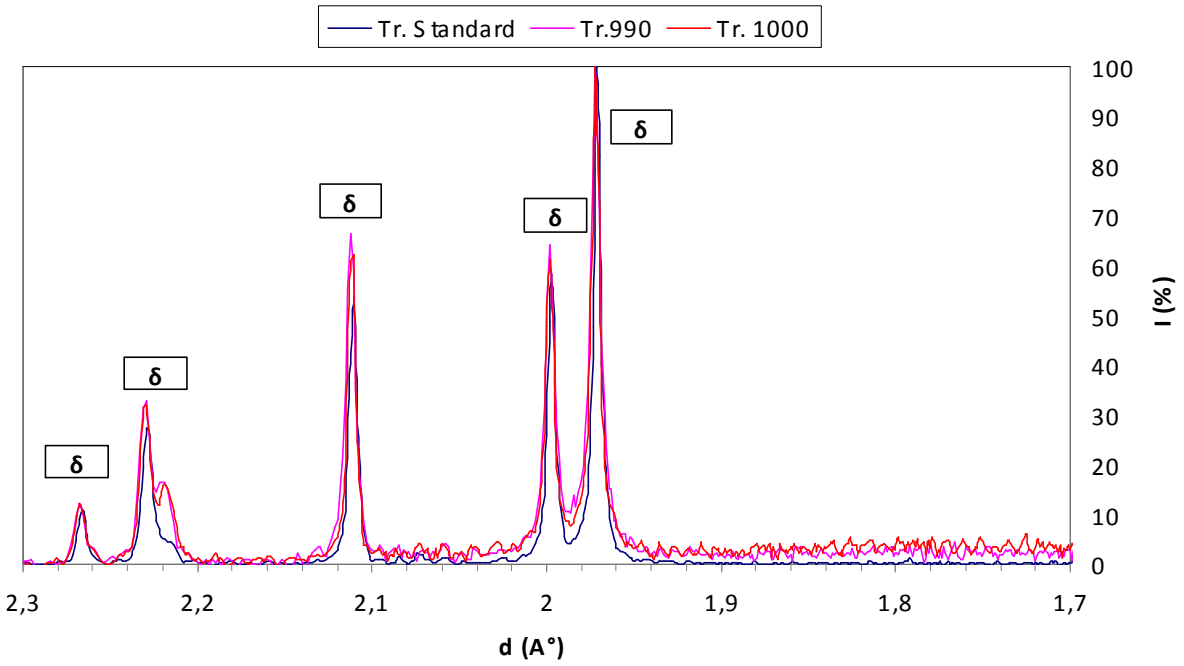

Figure V. 42 : Comparison of X-ray diffraction spectra of the extractive residues obtained, for the alternative IN718 grades, corresponding to the solution annealed conditions.

The investigations have been completed by the electrolytic extractions performed on the aged material as shown Figure V. 43, where, the comparison of various X-ray diffraction spectra of the extractive residues is reported. Results allow a complete identification of the precipitated phases, pointing out the presence of γ" and δ phases. The extraction method has allowed, therefore, the isolation of the γ" and δ particles, that will be analysed in terms of shape and quantity in the following sections. However, it is important to remember that a certain amount of γ' phase is present in all samples, but it has not been extracted by this selective electrolysis. A direct comparison of the intensities of the XRD leads to a qualitative investigation of the phase contents for the different thermal treatments. As a result, Tr. 1000 and Tr. API 6A exhibit a large amount of γ" as compared to the other grades. However, this increase in strengthening phases content is associated to a limited amount of delta precipitates, as described in the first part of the paragraph.

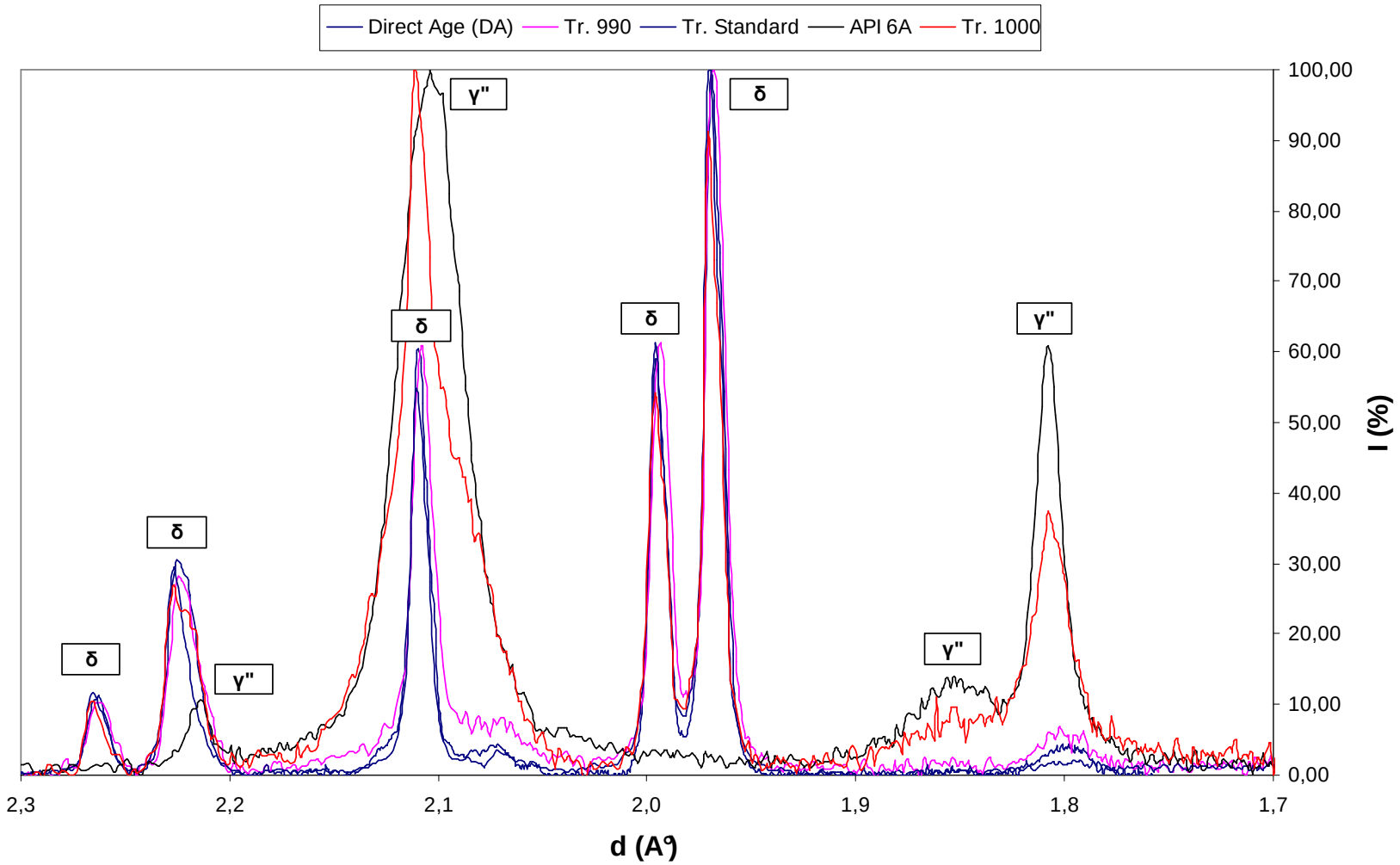

Figure V. 43 : Comparison of various X-ray diffraction spectra of the extractive residues obtained from the alternative IN718 grades.

The observed line broadening associated to the X-ray peaks can be used to estimate the average size of the intermetallic phases. In particular, the γ" size (D) is estimated from the single peak (200) using the Scherrer equation **[Scherrer,1918; Patterson,1939]**:

$$D = \frac{0.9\lambda}{\beta \cos\theta} \qquad \textbf{Eq.V. 1}$$

Where:

λ is the wavelength;

θ is the diffraction angle;

β is the peak width measured at half maximum intensity (FWHM) and expressed in radiants.

The apparent γ" sizes, calculated from the XRD data, are compared to those previously obtained by TEM for all Inconel 718 samples (Table V. 5).

	γ" Sizes	
Thermal Treatment	**XRD Scherrer [nm]**	**TEM [nm]**
Tr. Standard	/	13 ± 3
Tr.990	19 ± 1	13 ± 3
Tr. 1000	27 ± 1	/
API 6A	38 ± 1	33 ± 3
Direct Age	24 ± 1	23 ± 3

Table V. 5 : Comparison between predicted (XRD patterns) and measured (TEM investigations) γ" sizes for various Inconel 718 grades.

Small difference between the results of both experimental approaches is shown.

In such a way, the Scherrer equation allows the prediction of the γ" sizes associate to Tr. 1000 grade that was not assessed by TEM investigations.

Precipitates extraction has allowed the identification of the various intermetallic precipitates, produced by the application of a multistage treatment, and their relative estimated sizes.

The average composition of the γ matrix, as measured by ICP-OES on the solution used for precipitates extraction and containing all the chemical elements remaining in the matrix, is reported in Table V. 6.

	Elements [weight %]								
	Ni	**Cr**	**Mo**	**W**	**Al**	**Co**	**Ti**	**Nb**	**Fe**
Tr. Standard	54,7	19,32	2,91	0	0,57	0,42	0,67	0,87	20,52
Tr. 990	54,04	19,26	3,01	0	0,53	0,33	0,63	1,18	20,98
Tr.1000	54,16	19,4	2,99	0	0,527	0,32	0,603	1	20,97
API 6A	53,99	19,72	2,96	0	0,488	0,33	0,535	0,83	21,14
Direct Age	54,57	19,61	2,98	0	0,529	0,06	0,709	0,943	20,62

Table V. 6 : Average chemical composition of the γ matrix after each thermal treatment determined by ICP-OES.

These results indicate that the composition tends to evolve as a function of the formation of the various precipitates (γ" and δ).

Figure V. 44 reports the evolution of the Al, Ti and Nb contents as a function of the adopted solution annealing temperature. In perfect agreement with previous studies **[Miller et al.,1999; Burke et al.,2000]**, the levels of Al and Ti show a continuous decrease as the solution annealing temperature increases. Conversely, the Nb content does not show a direct dependence from the annealing temperature, but it depends on the whole (annealing + ageing) treatment. In agreement with the qualitative information reflected in Figure V. 44, it is suggested that an increase quantity of γ" precipitates, as mentioned for Tr1000 and API6A grades, is associated to a decrease in Al and Ti content within the matrix. In such a way these elements are expected to enhance the γ' and γ" precipitation during the ageing process.

The other alloying elements (Ni, Al, Co, Cr and Fe) show a constant content whatever the solution annealing is.

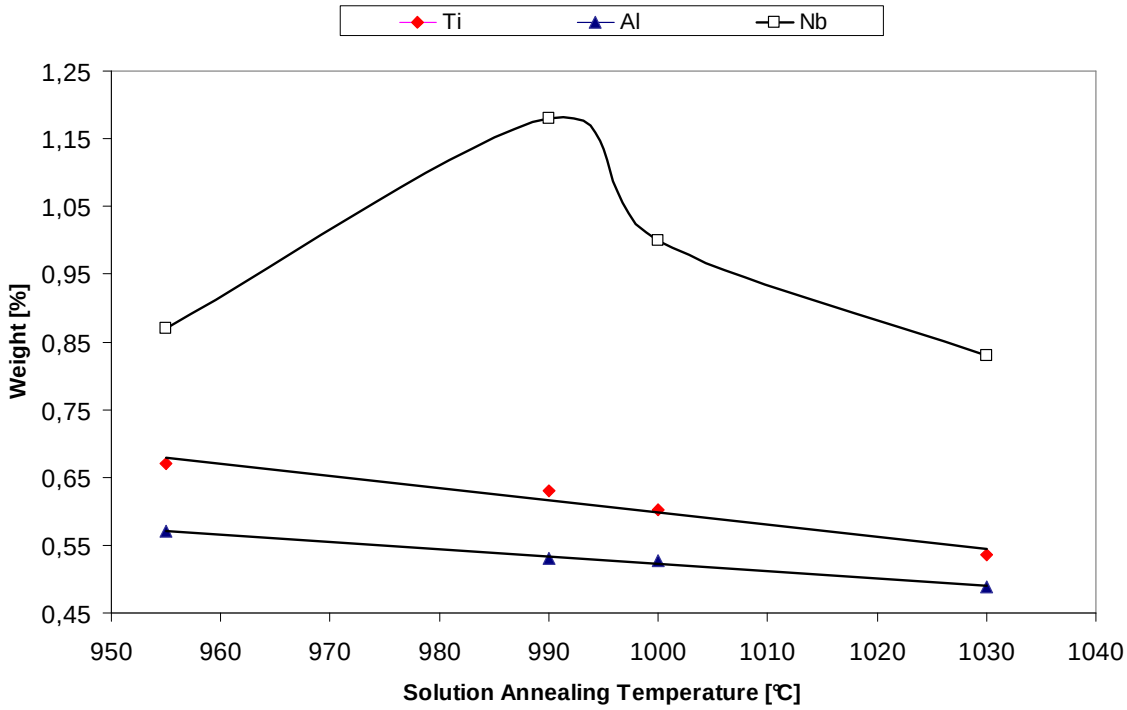

Figure V. 44 : Niobium, Aluminium and Titanium average weight content in the γ matrix as a function of the solution annealing temperature.

Focusing on the extracted precipitates, Table V. 7 reports the experimental weight fractions of the isolated particles, for the various IN718 grades, calculated by the following relationship:

$$F_m = \frac{W^P}{\Delta W^{Tot}} \qquad \textbf{Eq.V. 2}$$

Where W^P corresponds to the weight of the extracted precipitates (δ+γ") and ΔW^{Tot} represents the difference in weight of the sample from the beginning (t=0) and the end of the selective electrolysis. In addition, the surface fraction of delta phase, calculated in the first part of the chapter, is reported in the same table.

Thermal treatment	Dissolved Inconel 718 weight [g] [ΔW^{Tot}]	Extracted precipitates weight [mg] [W^P]	Precipitates (δ+γ") weight fraction [%] [F_m]	Delta phase surface fraction [%]
Tr. Standard	2.58	303	11.7	5
Tr. 990	2.6	209	8	3.8
Tr.1000	2.696	282	10	2.9
API 6A	2.696	341	12	0
Direct Age	3.231	362	11	3.7

Table V. 7 : Molar fractions of (γ"+δ) precipitates for the different Inconel 718 grades.

Figure V. 45 shows the evolution of the experimental molar fraction as a function of the Nb

content in the matrix.

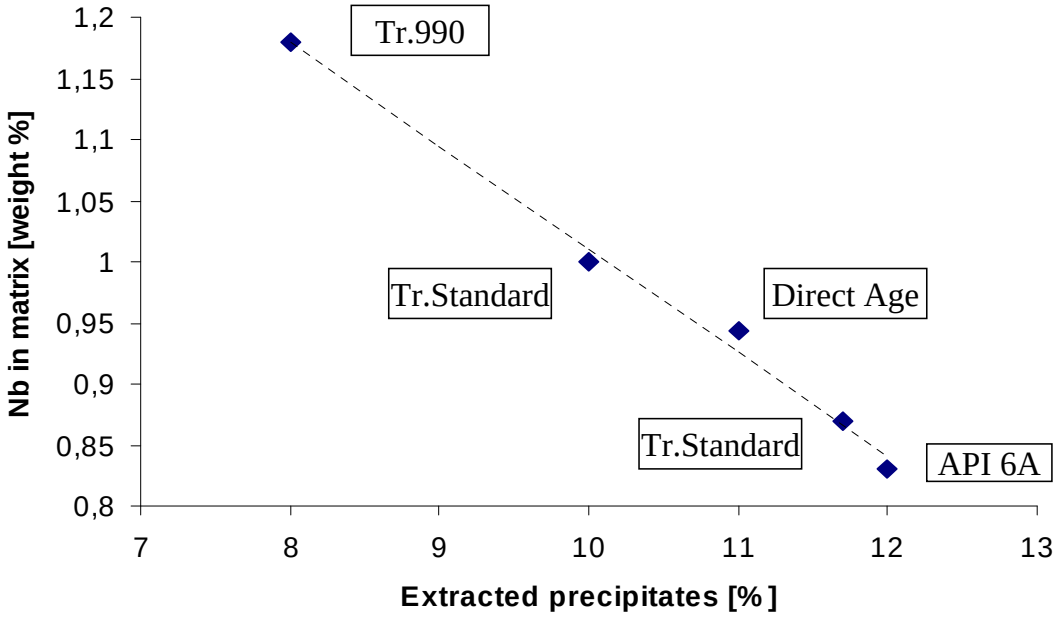

Figure V. 45 : Evolution of the experimental weight fraction of extracted precipitates (δ+γ") for various Inconel 718 grades as a function of the Nb contain retained in matrix.

According to the data reported in Table V. 7, various hypothesis relative to the γ" and δ weight fraction may be formulated. They are detailed, individually for each Inconel 718 grade, as follows:

- **Tr. Standard**: the image analyses carried out on this grade have shown a high content of delta phase due to the application of a low solution annealing temperature (955°C). In addition, the levels of Nb remaining in solution are too low to form high content of γ" phases. The DTA analyses, reported in the preliminary section of this chapter have suggested that γ" forms after the δ precipitates. In such a way it is suggested that a high content of δ, formed after quenching, limits the subsequent precipitation of γ" particles.
- **Tr. 990**: Solution annealing at temperature (990°C) higher than the standard grade limits the volume fraction of delta phase, but enhances the content of Nb remaining in solution. However, the first ageing at 720°C is not able to provide a complete precipitation of γ": this suggestion is confirmed by the high Nb content present in the matrix after the ageing process. Tr.990 grade is then characterized by a moderate content of delta and γ" particles.
- **Tr. 1000**: in accordance to the previous case, it is suggested that solution annealing at 1000°C further increases the Nb level retained in the super-saturated solution. In addition, Tr 1000 exhibits a lower content of delta phase but an increased molar fraction of extracted precipitates as compared to Tr.990. As a consequence, the volume fraction of γ" phase is suggested to be higher than for Tr 990. This is due to the high ageing temperature (750°C) that enhances the γ" precipitation. However, the short ageing time does not maximize the γ"precipitation and limits the molar fraction of intermetallic phases.

- **API 6A**: SEM observations have pointed out the absence of δ particles for this Inconel 718 grade. For this reason, the high content of intermetallic precipitates is exclusively associated to the γ" phases. This is the result of the application of a high solution annealing and ageing temperature: annealing at 1030°C maximizes Nb level remaining in the matrix, while ageing at 785°C produces a widespread distribution of large (33 nm) γ" particles through the matrix.
- **Direct Age (DA):** this grade exhibits a delta phase surface fraction similar to the Tr.990 grade. However the extracted weight fraction is higher. This means that the complementary content of γ" is increased. In this way, the Direct age grade may be classified in an intermediate position between Tr.990 and Tr. 1000

These qualitative considerations provide a microstructural explanation for the different fatigue lives associated to the various Inconel 718 grades. In particular, the γ" volume fraction is assumed as discriminating for the description:

- **Low weight fraction of γ" phases**: this is the case of the standard treatment where the material exhibit good fatigue performances even if they show substantial possible improvement.
- **Moderate weight fraction of γ" phases**: this microstructural arrangement provides the best results in terms of fatigue life. The residual delta particles limits grain growth, while the moderate content of γ" ensures an efficient strengthening of the alloy. This is the case of Tr. 990 grade where fatigue life is optimized. Direct age (D.A) may be classified in this γ" range. However the impact of the precipitates content on the fatigue life is strongly influenced by the work hardening deriving from the thermo-mechanical treatment (in the case of DA grade).
- **High weight fraction of γ" phases**: the excessive precipitation of the strengthening phases reduces, as shown Tr. 1000, the fatigue life as compared to the standard grade. These detrimental effects are not exclusively associated to the γ" volume fraction, but also to the precipitates size that influences the deformation mechanisms as it will be described in the following sections. These aspects are further emphasized in API 6A grade where the absence of delta phase associated to an extensive precipitation of γ" leads to a large reduction of the fatigue life.

In addition to this pertinent information, the study of the relationship between microstructures and fatigue life of Inconel 718 may be integrated by the analysis of the particles shape and their relative effects on the deformation mechanism. This topic is discussed in the following sections.

IV.2.A Shape evolution of the intermetallic phases

Inconel 718 is strengthened by a high volume fraction of intermetallic phases (γ' and γ") whose morphologies, after standard and alternative thermal treatments, have been observed by TEM investigations. These phases causes strengthening through the generation of coherency strains, associated to internal stresses which impact the high temperature mechanical behaviour of the alloy and its microstructural evolution during service. Previous studies have

unambiguously related the mismatch value to the occurrence of precipitate shape changes during precipitation or ageing treatments **[Hazotte,2009]**.

The experimental lattice parameters of the matrix (γ) and the γ" precipitates, measured by the x-ray diffraction presented in chapter III, are reported in Table V. 8. The low intensity peaks relative to the γ" phases associated to the standard treatment do not allow the calculation of the experimental lattice constants.

	Experimental γ lattice parameters	**Experimental γ" lattice parameters**	
Heat Treatment	$a_\gamma = b_\gamma = c_\gamma [\overset{0}{A}]$	$a_{\gamma''} = b_{\gamma''} [\overset{0}{A}]$	$c_{\gamma''} [\overset{0}{A}]$
Standard	3,5981	/	/
Tr. 990	3,6034	3,603	7,406
Tr.1000	3,6024	3,612	7,421
API 6A	3,6034	3,616	7,418
Direct Age	3,6038	3,602	7,397

Table V. 8 : Experimental lattice parameters evaluated by XRD performed on the remaining powder after matrix dissolution for alternative IN718 grades.

The misfit value relative to each thermal treatment, according to the formalism adopted by previous authors **[Cozar et al.,1973; Slama et al.,1997]**, is defined as:

$$\varepsilon^a_{\gamma''} = \varepsilon^b_{\gamma''} = \frac{a_{\gamma''} - a_\gamma}{a_\gamma} \qquad \textbf{Eq.V. 3}$$

$$\varepsilon^c_{\gamma''} = \frac{\left(\frac{c}{2}\right)_{\gamma''} - a_\gamma}{a_\gamma} \qquad \textbf{Eq.V. 4}$$

where a_γ is the lattice constant of the γ matrix and $a_{\gamma''}$ and $c_{\gamma''}$ the lattice parameters of the γ" precipitates.

The resulting coherency strains (misfits), associated to the change from the FCC cell of the matrix to the BCT cell of the γ" precipitates, are listed in Table V. 9. Data are compared to those obtained by XRD synchrotron, performed on solid samples, where precipitates are not isolated but hold within the matrix. A good accordance between the two experimental techniques is shown.

	Dissolution		Synchrotron	
	Misfit γ"/ γ		Misfit γ"/ γ	
Heat Treatment	$\varepsilon^a_{\gamma''}$ [%]	$\varepsilon^c_{\gamma''}$ [%]	$\varepsilon^a_{\gamma''}$ [%]	$\varepsilon^c_{\gamma''}$ [%]
Tr. 990	0,01	2,69	0,05	2,02
Tr.1000	0,26	2,91	0,35	2,58
API 6A	0,35	2,85	0,49	2,37
Direct Age	0,05	2,56	/	/

Table V. 9 : Evaluated lattice mismatch for γ" precipitates corresponding to the various alternative IN718 grades.

The presence of a lattice misfit induces an elastic stress field, often called coherency stress field, which is responsible for the arrangement and morphology of the γ" precipitates. Hazotte **[Hazotte et al.,1996]** pointed out that the final microstructure depends on the minimization of the coherency strain through the precipitate morphologies evolution. In this way, the final shape results in the minimisation of the sum of the interfacial and elastic energy. The spherical shape minimizes the surface energy, but as the mismatch increases, the change to plate-like morphology minimizes the elastic energy.

Considering the TEM investigations, the API 6A grade, where a larger mismatch ($\varepsilon^c_{\gamma''}$=2,85%) with the matrix is shown, exhibits the presence of elongated γ" particles (e/L=0,22) as compared to the Tr.990 where a small misfit ($\varepsilon^c_{\gamma''}$=2,69) leads to more spherical intermetallic particles ((e/L=0,45).

When a second phase particle is introduced into the matrix, different particle-matrix interface configurations can be formed: fully coherent, partially coherent or incoherent. Cozar **[Cozar,1973]** reported that coherent γ" phases have a misfit with the matrix equal or lower than 1%. This is confirmed for all alternative Inconel grades, where the discrepancy in lattice planes is expected to be accommodated by elastic strain. Slip planes can align and interfacial edge dislocations can eventually form at the partially coherent interfaces in order to relieve the elastic strains. As a result, the coherent precipitates provide strengthening through a size misfit and a particle shearing.

However, the Tr.1000 and API 6A grades exhibit a larger mismatch that reflects a reduced coherency between matrix and intermetallic phases. In these conditions, it is suggested that slip can not be easily transferred between matrix and particle due to the misalignment of slip planes.

Figure V. 46 compares the alternative Inconel 718 grade as a function of their relative misfits with the matrix and the fatigue lives associated to an applied total strain amplitude of ±1.2%.

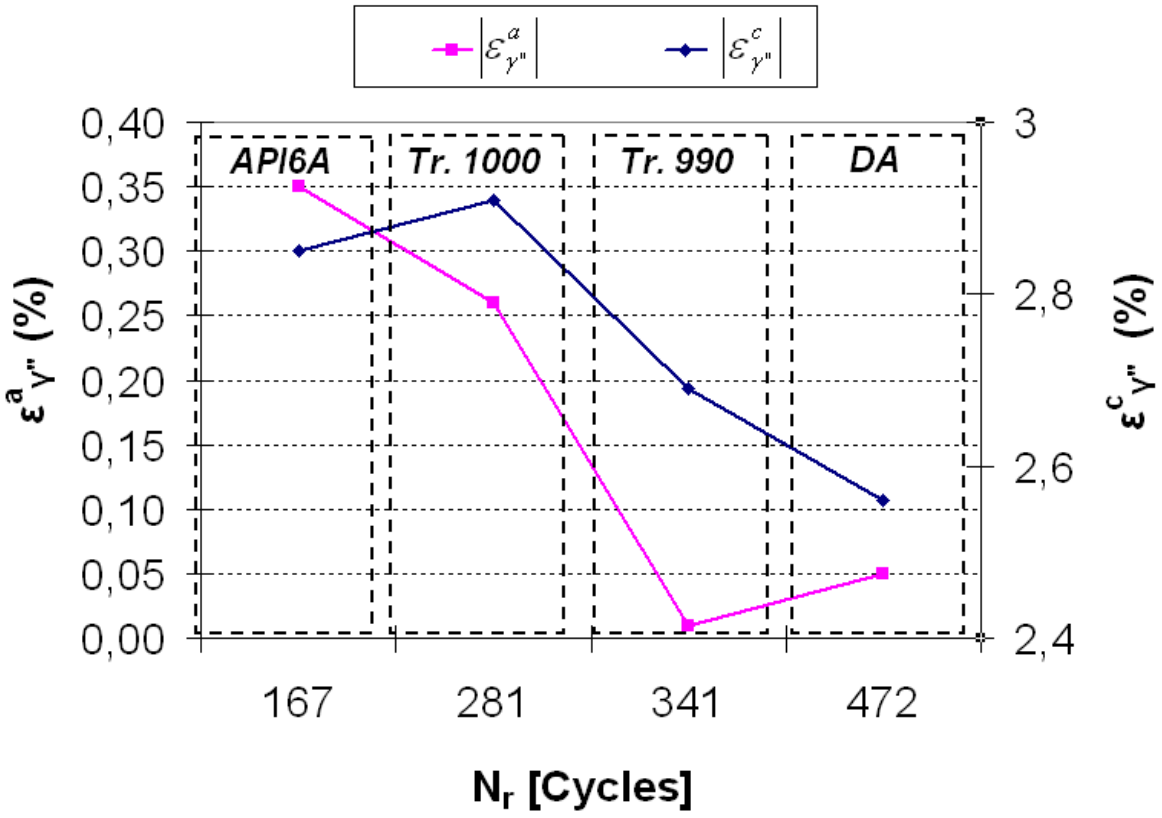

Figure V. 46 : Evolution of the LCF performances under extrusion conditions (trapezoidal signal 150_20 s), (T=550°C and $\Delta\varepsilon_t$=±1.2%), for the alternative IN718 grades as a function of the lattice mismatch between the γ" phases and the matrix.

It is evident, in both cases, that an increase of the lattice mismatch, in the <100>$_{\gamma''}$ direction $\varepsilon^a_{\gamma''}$ and <001>$_{\gamma''}$ direction, leads to a reduction of the fatigue performances of the alloy under extrusion loading (trapezoidal signal 150_20 s).

The reduced coherency exhibited by the γ" phases in the API 6A grade and the increased size of these particles (Figure V. 40) suggest that a dislocations pile-up could occur as a cluster of dislocations unable to shear or cross the strengthening phases.

During the subsequent deformation of the material, the generation of new dislocations occurs, increasing the dislocation density and the resulting flow stress. Consequently, this mechanism could be considered as mainly responsible for the preliminary work hardening exhibited by the API 6A grade during the first cycles under extrusion conditions. At a sufficiently large applied stresses, the barriers to dislocations movement are overcome and the rate of work hardening is reduced.

IV.3 Effect of γ" precipitates size on the deformation mode

The precipitation strengthening is ensured by second phase particles. These particles impede the movement of dislocations throughout the lattice. Physically, this strengthening effect can be attributed to both size and modulus effects and to interfacial or surface energy effects. Within the alloy, consisting in a dispersion of hard precipitates in a fairly soft matrix, two distinct modes of deformation are observed: particles shearing and particle bypassing resulting in the creation of dislocations loops around the particles.

In general, the precipitation hardening mechanism depends on the size of the precipitates bypassing. Cutting is the dominating process for small particles, while for larger size, bypassing is assumed to be the major preliminary deformation mechanism. For this reason, a rough estimation of the required stress to initiate each process can be assessed following the models proposed in the literature **[Sundararaman,1988; Perrut et al.,2011]**.

In such a way, the functional relationship between shear stress and particles size is expressed as:

$$\Delta\tau_{Shear} = \left[\frac{\Gamma}{2b}\right] \cdot \left[\frac{4 \cdot \Gamma \cdot f \cdot L}{\pi \cdot T} \cdot \left(\frac{\sqrt{6}}{3A}\right)^{\frac{1}{2}}\right]^{1/2} \qquad \textbf{Eq.V. 5}$$

[Sundararaman,1988]

Where $\Delta\tau_{Shear}$ is the shear stress increment due to particle shearing, Γ is the antiphase boundary (APB) energy of the ordered precipitate, b is the Burgers vector of the cutting dislocation , f is the precipitate volume fraction and T is the dislocation line tension, which is assumed to be approximately ($T = \frac{1}{2} \cdot \mu \cdot b^2$) where μ is the shear modulus of the matrix. All the calculations are performed considering the γ" precipitates as the primary strengthening phases in Inconel 718. In such a way, the other parameters included in the equation have the following meaning: L corresponds to the length of the major axis of the elliptical γ" precipitates and A is the ratio between the major (L) and minor (e) axes ($A=L/e$). These latter parameters (L and e) have been extracted form the microstructural investigations carried out by TEM as indicated in Figure V. 41 where the evolution of the (e/L) ratio as a function of the precipitates size (L) for the investigated thermal treatments is shown.

Shear stress calculations have been obtained considering the following values (Table V. 10) for the individual parameters:

Parameters [Sundararaman,1988]	**Value**
b [nm]	0.25
T [N]	$2{,}19 \cdot 10^{-9}$
Γ [mJ/m²]	296
f	0.15

Table V. 10 : Input parameters [Sundararaman,1988] for Shear Stress calculation.

The critical residual shear stress (CRSS) calculated by using Eq.V. 5 is plotted in Figure V. 47, as a function of the γ" precipitates size. All results have been assessed considering a constant volume fraction of the γ" particles equal to 0.15, focusing exclusively on the effects of the particles size.

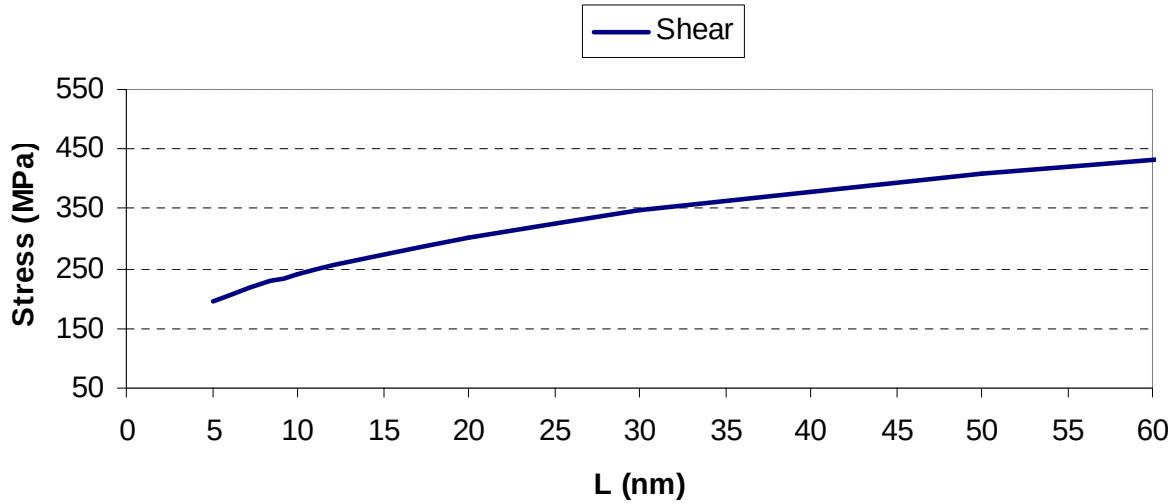

Figure V. 47 : Claculated values of Shear Stress as a function of the γ" particles size.

As previously anticipated, the stress associated to the particles bypassing tends to decrease with increasing particle size. From a microstructural point of view, at a constant volume fraction of γ", an increase in the precipitate size leads to a concomitant increase in the free spacing between the particles. As a result, the stress required for the activation of the bypassing mechanisms may be expressed by the following relation:

$$\Delta\tau_B = \frac{0.85\cdot\mu\cdot b}{2(1-\nu)^{1/2}}\cdot\frac{C}{2L\left[1-\frac{\pi}{2A}C\right]}\cdot\ln\left(\frac{4L}{\pi_0}\right) \qquad \textbf{Eq.V. 6}$$

[Sundararaman,1988]

Where $\Delta\tau_B$ is the stress associated to the bypassing process, ν is the Poisson ratio for the matrix and π_0 is the dislocation core radius that has been considered equal to the Burgers vector ($\pi_0 = b$)

The values assumed for the different parameters figuring in Eq.V. 6 are reported in Table V. 11:

Paramaters [Sundararaman,1988]	**Value**
μ [GN/m²]	70
ν	0.33
π_0 [nm]	0.25

Table V. 11 : Input parameters [Sundararaman,1988] for Bypassing Stress calculation.

In addition, C is expressed as:

$$C = \left[(f\cdot A)^{1/2} + \left(\frac{2}{\pi}-\frac{\pi}{2A}\right)\cdot f\cdot A\right] \qquad \textbf{Eq.V. 7}$$

[Sundararaman,1988]

Focusing on the particles shape, as described for the shearing mechanisms, the aspect ratio (*A*), varies as a function of the γ" particles major (*L*) and minor (*e*) axes. The aspect ratio *A* is assumed to range between 1 (for L= 5 nm) and 7 (for L= 60 nm).

Figure V. 48 reports the evolution of the bypassing stress calculated with Eq.V. 6. The shearing and bypassing plots intercept at a critical size (d_C) equal to 12 nm. For precipitates size larger than d_C the stress required for bypassing is lower that that needed for shearing. Conversely, at smaller particles size the situation is reversed.

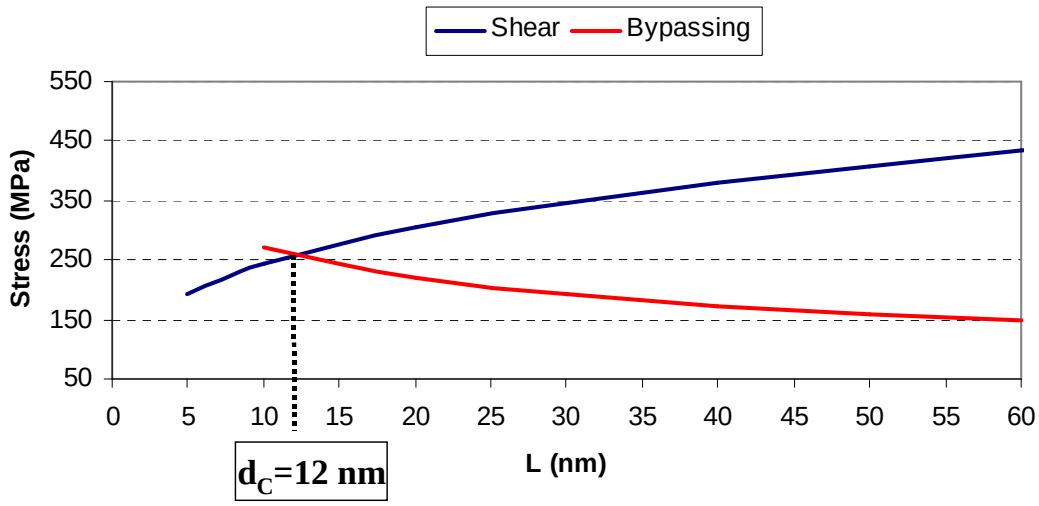

Figure V. 48 : Calculated values of Shear and By-passing stresses. d_C corresponds to the critical particle size at which the deformation mechanism changes from shearing to bypassing.

The experimental value assumed by the critical particle size, ranging between 10 and 15 nm, is in good agreement with the theoretical value calculated with the following expression:

$$d_c = \left(\frac{\mu \cdot b}{\Gamma}\right) \cdot \left(1 + 1.5 \cdot \sqrt{\frac{f}{\pi}}\right) \qquad \textbf{Eq.V. 8}$$

[Sundararaman,1988]

Previous works have pointed out that additional hardening effects (coherency hardening) could be added to the previous precipitates strengthening mechanisms. These coherency hardening processes, due to the lattice misfits between the matrix and the precipitates, are associated to the elastic stresses in the vicinity of the particles. The contribution of coherency strain hardening to the overall yield stress will depend on the number and spacing of the zones or precipitates, and also on the degree of strain produced by each. In general, longer ageing times result in larger, more widely separated precipitates, each having a larger strain field. Coherency strain hardening reaches a maximum when the average zone spacing is similar to the limiting radius of dislocation curvature.

In general the presence of these coherency strain fields tends to increase the slip stress: as a result, the critical particle size (d_C=12 nm) could be further decreased.

The previous calculations have suggested an alternative interpretation of the interactions between the precipitates size and the mechanical properties. This represents a valid support for a further comparison of the alternative Inconel 718 grades, in order to obtain information

about the interaction between the precipitated γ ”particles and the moving dislocations.

The TEM observations, carried out for the “Tr. Standard” and “Tr 990” Inconel 718 grades, have shown mean sizes for γ ”particles closed to 13 nm.

This value corresponds to the critical particles size that has been assessed by the model, described above. However, both the experimental approaches, such as the critical size determination and the TEM image analysis, are subjected to experimental errors due to the different approximations. In such a way, the critical particle size may not be considered as a certain value but it subject to an uncertainty range. In accordance with these assumptions and considering the γ” size associated to these Inconel grades, it is suggested that the deformation process exhibited by these microstructures, under cyclic loading, is based on a shearing mechanism. In addition, the previous studies focused on the lattice misfit between γ” particles and the matrix, have revealed the coherency of the strengthening particles associated to the “Tr.990” grade. These results confirm the hypothesis of the γ” particles shearing, which contributes to the strengthening of the alloy limiting the dislocations motion.

In addition, it has been demonstrated that the application of the “Oil and Gas” treatment to the Inconel 718 alloy has given rise to a strong decrease in the mechanical properties: such as the yield strength at 550°C and the fatigue performances achieved under extrusion conditions. The increased size associated to the γ”particles (33 nm) and the larger free inter-space among them could be associated to a bypassing mechanism. As a result, these changes in mechanical behaviour can be consistently explained on the basis of the variation in the mode of the γ”dislocation interaction. Again, these assumption are confirmed by the previous microstructural investigations that have pointed a reduces of coherency of the γ” particles associated to the API 6A Inconel 718 grade

The effect of microstructure on the deformation mode and fracture behaviour of age-hardened alloys has been largely investigated in the literature **[Pineau,1969; Jiang et al.,2005]**. Pineau showed, on over-aged Waspalloy, a clear change of deformation behaviour due to microstructural variations (large particle sizes). In a similar way, Figure V. 49 shows the SEM investigations of the slip distribution along the longitudinal sections of two deformed fatigue specimens relative to the “Tr. Standard” (a) and “API 6A” (b) grades.

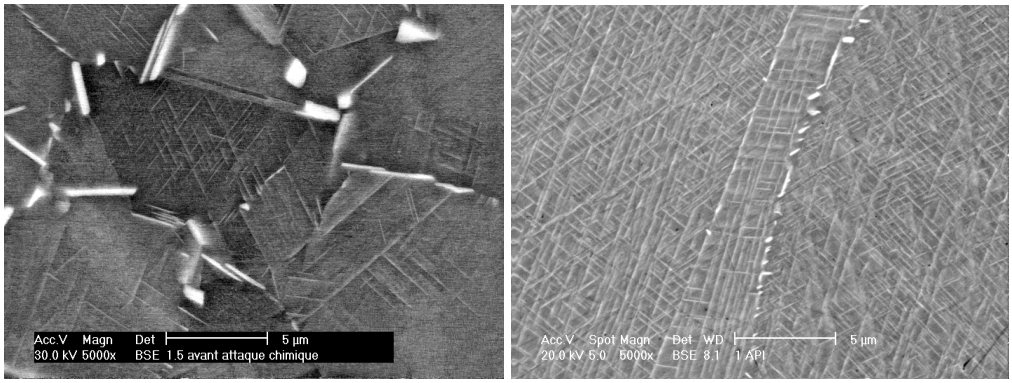

(a) **(b)**

Figure V. 49 : SEM observations of the longitudinal deformed (at 550°C for $\Delta\varepsilon_T$=± 1%) LCF specimens showing different slip distribution : Inhomogeneous slip distribution associated to shearing mechanisms for Inconel 718 “Tr. Standard” grade (a) and homogeneous distribution based on bypassing process for Inconel 718 “API 6A” grade (b).

In the standard Inconel 718 grade, where the under aged conditions are achieved, precipitate shearing gives rise to an inhomogeneous distribution of slip which tends to be localised into shear bands. Conversely, in the overaged conditions, associated to the API 6A grade, the homogeneous slip distribution is associated to the occurrence of precipitates by passing.

This effect, together with changes in microstructural grain size, influences the tensile properties, fatigue properties, and fracture behaviour of the alloy. In particular, the homogeneous distribution of slip, associated to the precipitates bypass, should result in the multiplication of crack initiation sites, localized at the intersection between slip bands and surface. However, additional observations, in transmission electron microscopy, carried out on deformed specimens, are necessary to give more information on the strengthening mechanisms.

All the assumptions, reported in the present section, have emphasized the role of the deformation mechanisms on the fatigue performances of Inconel 718. The alloy have shown a strong microstructural sensibility to the effects of the thermal treatment: as a result, any variation in the heat treatment procedure can alter the interaction between the strengthening phases and the dislocations. These assumptions, added to the effect of the deformation mechanisms on the fatigue performances, have emphasized the importance of the thermal treatment on the optimisation of the mechanical properties of the alloy.

IV.4 Partial Conclusion

The strategy adopted for the optimization of the heat treatment parameters is based on several detailed microstructural investigations and considers the Yield Strenght as the optimization criterion for the material mechanical properties. This approach derives from a specific study of the loading conditions in the extrusion die where the mechanisms of cyclic plasticity are concentrated in specific zones of the tool (hot spots) and lead to a premature failure of the tool. However, the previous investigations under LCF conditions have pointed out the importance of other secondary properties (such as the resistance to the stress relaxation and to the fatigue crack initiation) that have to be optimized as a function of the material workability (forging, weldability, machining…).

Generally speaking, it exists a specific Inconel 718 microstructure, able to provide an optimal combination of the required properties and ensure the best performances under the severe loading conditions imposed by the extrusion process. The aim of this work is not only to point out the contributions of individual parameters, but also to understand the relationships between them.

The microstructural investigations have provided the input data for the design of alternative thermal treatments. In addition, the Taguchi method has been adopted, in Chapter III, in order to reduce the number of tests and investigate the individual parameter contributions.

First, the Yield strength has been adopted as the disciminating parameter for the selection of alternative Inconel 718 grades. Additionally, in accordance with the assumptions reported

by Hornbogen **[Hornbogen,1969]**, a second property was considered to limit the options. In such a way, as a function of the thermomechanical investigations reported in Chapter IV, the fatigue life, under a specific total applied strain, is retained as the secondary property to consider for the material optimisation.

In such a way, the combination between the different properties has to be studied in order to define a specific application domain for each Inconel 718 grade under specific loading conditions (Extrusion loading).

The diagram reported in Figure V. 50 constitutes a reference map prone to range the various Inconel 718 grades as a function of its mechanical properties. The alternative Inconel 718 grades have been classified as a function of their Yield strength at 550°C and their fatigue performances associated to an extrusion loading at a total strain amplitude of ±1.2%.

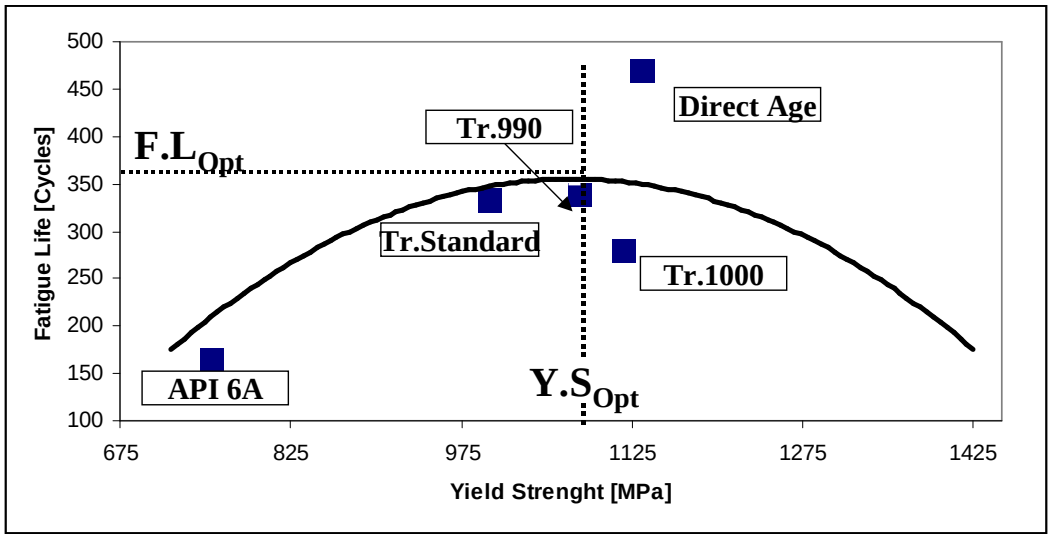

Figure V. 50 : Variation of the fatigue life under experimental extrusion conditions as a function of the Yield Strength at 550°C for various Inconel 718 grades.

A “limit curve” has been plotted in order to delimit a large domain, characterised by different combinations of fatigue resistance and Yield Strength, under which all the alternative tested Inconel 718 grades, obtained from rolled conditions can be situated.

An optimal Yield Strength ($Y.S_{Opt}$), which corresponds to the maximal fatigue life under extrusion conditions ($F.L_{Opt}$), has been defined. The microstructure associated to this reference value ensures a strong resistance to the fatigue crack initiation and a limited stress relaxation under holding time at maximal strain, which corresponds to a limited plastic strain cumulated cycle by cycle.

Finally, a prominent position is occupied by the Direct Age grade which exhibits better properties in terms of static and cyclic loadings due to the application of the thermo-mechanical treatment. This is the result of a specific optimisation of both microstructure and forging process which differentiate this grades from the others reported under the limit curve.

In addition to this diagram, Figure V. 51 proposes a correlation between the specific mechanical properties and the various investigated microstructures.

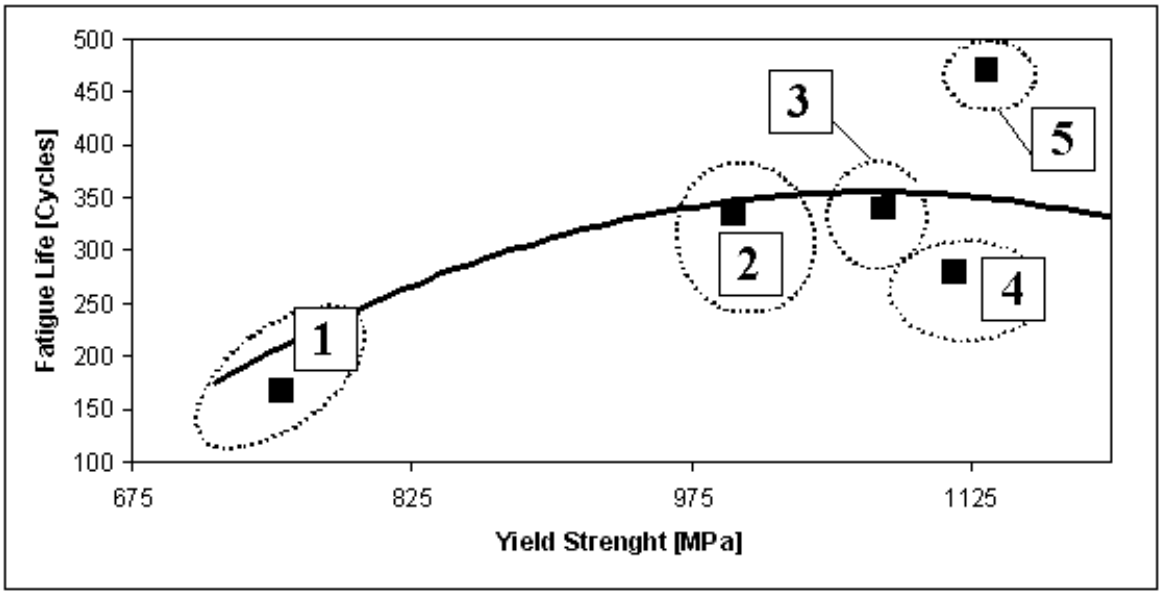

Figure V. 51 : Microstructural reference map showing a correlation between the specific mechanical properties and the various investigated microstructural domains.

This "microstructural map" can be firstly divided into different macro-areas corresponding to the approach adopted for the design of the alternative Inconel 718 grades (intra and extra specification, thermo-mechanical treatment).

Each macro-area can be further divided into specific domains that will be described as follows:

Extra-specification area

1. Region 1 (Extra-specification design) is characterized by low mechanical strength associated to the increase in the material ductility. These properties derive from strong variations of the microstructural features: the quasi total dissolution of the delta phase leads to an excessive grain growth which has a negative impact on the material strengthening. The above described microstructure is obtained by the application of a high solution annealing temperature (T> 1020°C) followed by a rapid quenching (water or oil) and an overaging step. The limited fatigue performances are the direct results of the weak tensile strength and stress relaxation resistance exhibited by these microstructures at 550°C. the This could be explained by the specific microstructure obtained by the over-aged conditions. A wide precipitation of γ" phases, characterized by a lower coherency, occurs limiting their strengthening effects. In addition the increased size of these particles leads to a precipitates bypassing mechanisms which have a detrimental impact on the mechanical properties.

Intra-specification area

2. Region 2 corresponds to the microstructure achieved by the application of the standard thermal treatment. This has been considered as the starting point for the microstructural optimisation of the alloy. A low solution annealing temperature (955° C) limits the dissolution of the delta phase (5% surface fraction) and provides

a good tensile strength. However, the low content of γ" phases does not ensure the maximal strengthening to dislocation slip bands and fatigue life is n already optimised.

3. The microstructure associated to the optimal Yield strength (Region 3) is defined by equiaxial grains whose size is limited by a moderate content of plate-like delta phase (4% surface fraction), as compared to the standard grade. A moderate and coherent precipitation of γ" phases occurs, exhibiting small particles size (13 nm). This microstructure, obtained following the "Tr.990" heat treatment procedure, ensures a limited stress relaxation under holding time at maximal strain, which corresponds to a limited plastic strain cumulated cycle by cycle. As a results, the fatigue performances are optimized.
4. Region 4 is characterised by high values of Yield strength. Similar conditions are achieved adopting solution annealing temperature closed to 1000° C. In this way, the delta phase content is further reduced (3% surface fraction). As a result a large amount of elements (such as Ni, Ti and Nb) are available for the γ' and γ" precipitation during the ageing process. However, the lower fatigue lives than those associated to Region 2 and 3 have been explained as a function of a limited coherency exhibited by the strengthening particles. This is the result of the high aging temperature (750°C) which leads to over-aged conditions, where the γ" weight fraction is too high and the particles size too large.

Thermo-mechanical treatment area

5. Finally, the Region 5 belongs to microstructures provided by the thermo-mechanical treatments, such as the Direct Age process. The better fatigue performances and tensile strength associated to these procedures derive, mainly, from the residual work hardening retained by the alloy. In addition, a necklace structure, where little grains are surrounded by larger one, induces a further strengthening of the alloy.

In conclusion, the diagram proposed in Figure V. 51 allows a detailed interpretation of the mechanical properties as a function of the microstructural features. In this way, a specific thermal treatment procedure, associated to an optimized microstructure, may be chosen in order to satisfy the combination of the required mechanical properties (fatigue life and yield strength) for the extrusion application.

V Conclusions

V.1 Inconel 718 microstructural evolution

The microstructural optimisation of the alloy and the desired high temperature properties require multi-stage heat treatments that lead to the nucleation or dissolution of secondary phases. These particles act as efficient obstacles to the dislocation motion: the finer the dispersion, for the same amount of particles, the stronger the material. As a result, a particular heat treatment procedure is needed to give this required distribution and volume fraction of precipitates within the matrix.

The choice of the thermal treatment parameters (time, temperature, cooling rates), which define the various steps of the process (solution annealing, quenching and ageing) has been assessed by a detailed study of the microstructural evolution that leads to the following conclusions:

Significant δ phase dissolution results from high solution annealing temperatures (T<955°C) , due to the high solubility of Nb atoms in matrix. This dissolution is accompanied by a rapid grain growth accelerated by the evolution and loss of these secondary particles at the grain boundaries.

The second step of the Inconel 718 thermal treatment consists in an isothermal aging right after quenching. Differential thermal analyses have pointed out

The solution annealing has a strong impact on the microstructural evolution of the alloy, especially for the delta phase and grain size evolution. Various solution annealing experiments have been carried out for temperature ranging between 924°C and 1050°C. in order to investigate the microstructural evolution of the alloy. These temperatures are in the range defined by the ASTM B637 specification.

Significant δ phase precipitation results from the lower solution temperatures of 924°C and 955°C because of the high equilibrium content of δ phase at these temperatures. Limited changes in δ phase structure are noticed at 975°C, whereas at 990°C a partial dissolution of precipitates occurs. A certain amount of delta phase still remains at 1010°C, while the dissolution process is completed at 1050°C giving an austenitic microstructure free of precipitates.

Concomitantly, grain strongly grows between 1000 and 1050°C due to the progressive dissolution of the δ phase. The grain growth is accelerated by the evolution and loss of these secondary particles at the grain boundaries, pointing out that needle plate δ phase is more efficient to prevent grain growth than spheroids **[Desvallées et al.,1994]**.

The second step of the Inconel 718 thermal treatment consists in an isothermal aging right after quenching. Experimental analyses have been performed using Dilatometry and Differential Thermal Analysis (DTA) techniques prone to point out the microstructural transformations occurring during the heat treatment process. Two reference ageing treatments have been applied on specimens solution annealed for 1 hour at 955°C. The first one (720°C

for 8h) represents the standard ageing process defined by the ASTM B637 specification while, for the second profile, a higher ageing temperature of 750°C for 8h has been chosen. A similar second ageing at 620°C for 8 hours has been applied for both treatments. All thermal expansion tests have shown a continuous thermal shrinkage due to the precipitation of different phases. The rejection from the austenitic matrix of alloying elements such as Nb, Ti and Al, which interact to form the strengthening intermetallic phases is the main cause of the dilatometric variation. The precipitates growth rate is influenced by the diffusion rates of the constitutive elements, which are strongly affected by the temperature. As a consequence, the preliminary stage of the dilatometric shrinkage (from 0 to 2h aging) is based on a decreasing nucleation rate of the hardening particles, provided by diffusional processes. Conversely, the rest of the structural evolution may be associated to the morphology evolution of the nucleated phases.

Finally, the investigations carried out on the second ageing steps have concluded that most of the structural transformations takes place during the firdt ageing, whereas the subsequent step has an important impact on the size and morphology refinement of the precipitates.

The microstructural investigations, described in the first part of the chapter, provide a valid support for proposing alternative thermal treatments. A wide variety of options are available and many issues must be considered with the aim to improve the mechanical properties of the alloy.

Four different solution annealing temperatures (955, 980, 990 and 1000°C) above the delta solvus, have been considered in order to retain a certain amount of delta precipitates and avoid early grain growth. Considering the ageing procedure, the heat treatment variables chosen in this study are based on data from previous analytical testings (DTA and dilatometer) and on recommendations provided by the literature for the heat treatment of nickel base superalloys. In such a way, two alternative ageing procedures have been performed in order to ensure different distributions and morphologies of the strengthening phases, impacting the fatigue life. In addition, it was assumed that there would be no significant benefit in varying the second ageing step (considering its slight impact on hardening), that has been maintained at 620°C for 8 hours.

V.2 Correlation between microstructural features and mechanical properties

The study of the microstructure influence on the mechanical properties of the alloy, under extrusion loading conditions, represents one the main objective of this PhD work. For this reason, the adopted strategy, reported in Chapter III, is supported by the microstructural results described in the first part of Chapter V.

Two strategies of optimization have been followed:

1. Intra-specification design: the solution treatment temperature are selected in the range recommended by ASTM B 637 (924°C < T < 1010°C).
2. Extra-specification design: high solution treatment temperatures above the

specification range (T> 1010°C).

The alternative Inconel 718 grades, introduced in Chapter III, have been tested under extrusion loading, by a series of LCF tests, carried out at 550°C, using the reference trapezoidal signal (150_20s).

The microstructural sensitivity exhibited by the material under the effect of the heat treatment has been confirmed by the differences in fatigue performances associated to the different thermal treatments.

Focusing on the intra-specification design, two alternative Inconel 718 grades have been selected to be tested under fatigue conditions. The first, labeled “Tr. 1000”, is a particular optimization of the standard process where all the parameters, except those relative to the second ageing, have been refined. The second, defined as “Tr.990“, is another powerful process which is based on the increase of the solution annealing up to 990°C keeping the standard ageing procedure.

The direct comparison of the fatigue performances, with those of the standard grade has emphasized the better performances shown by Tr.990, especially at high strain amplitudes. Conversely, Tr. 1000, that was selected for its capability to provide high tensile properties, has exhibited a slight improvement of the fatigue resistance at high strain amplitudes showing, further on, less efficiency at low strain amplitude.

In the case of extra specification design, a particular practice, based on the NACE standard MR-0175/API 6A specification **[NACE/MR0175]** and largely used for Oil and Gas applications has been adopted. The choice of this alternative thermal treatment has been justified, from an industrial point of view, by technico-economic reasons. This alternative use of Inconel 718 is facilitated by a large availability of stocks opportunely treated in accordance with the API 6A specification. In such a way, the material can be found in large quantity and purchased with an average 30% cost reduction. From a microstructural point of view, The API 6A grade exhibits significant grain growth, as a consequence of the high solution annealing temperature and the absence of delta phases along the grain boundaries. These microstructural features contribute to improve the alloy toughness but they negatively affect its mechanical properties (Y.S and U.T.S). As a consequence, the Manson Coffin diagram associated to this alternative grade has pointed out its limited fatigue resistance in the entire range of applied strains.

Finally, the strategy adopted for the thermo-mechanical treatment consists in the maximization of the cyclic capability and tensile properties through the application of the direct Age (D.A) procedure.

This alternative grade, largely used for the aeronautical applications, is based on the common idea that a fine grain microstructure, expressly hardened by high forging reductions, provides better LCF resistance. The close values of Y.S and U.T.S, due to the work-hardening effects of the thermo-mechanical process, limit the plastic strain mechanisms.

LCF specimens have been extracted form a zone at the heart of forged pancake where a recrystallized structure, consisting of regular grains, (ASTM 11-12) surrounded by finer grains (ASTM 13), is shown. A second part of the pancake has been treated following the “Tr

990" procedure just discussed above. The idea to consider two different thermal treatments for the forged pancake is based on the interest to define a new reference for the Tr. 990 grade applied to a forged material (Tr.990 forged). In such a way, the fatigue performances of the direct aged material can be directly compared to that of the reference alloy, focusing on the effects of the single heat treatment and excluding the contributions of a different forging process. The comparison of the fatigue results of the DA and "Tr 990 forged" indicates that the two heat treatments give similar performances except for high plastic strains, where the Direct Age lives become slightly longer. However, the "Manson Coffin" diagram has pointed out the better performances of the forged grades as compared to the rolled ones (Tr. Standard, Tr 990 and Tr.1000 and API6A).

An additional study the macroscopic response of the different Inconel 718 grades, based on the study of the stress relaxation under high strain loading, has been proposed. Chapter IV has pointed out that during the holding time, the application of a constant total strain induces a continuous stress relaxation that negatively influences the fatigue life.

The reason for lower fatigue durability, under extrusion conditions, of the heat treated specimens in variant Tr.1000 and API 6A can be explained by a different behaviour exhibited under the application of a holding time at maximum strain. The remarkable and rapid stress relaxation exhibited by these Inconel 718 variants, which increase the plastic strain amplitude associated to each cycle, can be considered as a limiting factor under LCF conditions.

The investigations have been completed by the electrolytic extractions performed on the aged materials. The lattice misfit calculated for the precipitates provides further information on the strengthening mechanism associated to the various microstructures. In such a way, the large γ''/γ mismatch shown by the API 6A and "Tr.1000" grade suggests a possible loss of coherency between the matrix and the intermetallic phases. In these conditions, slip can not be easily transferred between matrix and particles due to the misalignment of slip planes. The modified interaction between dislocations and precipitates is considered as the main cause of the decrease of fatigue performances exhibited by these alternative grades.

These comments regarding the microstructural evolution of Inconel 718 and the results of the LCF tests have provided important indications about the microstructure suitable for the severe loading conditions associated to the extrusion cycles. This microstructures consists in a balanced distribution of the different intermetallic phases (δ, γ' and γ'' phases). A moderate presence of delta particles is needed to limit the grain size whereas coherent γ'' phases are required to increase the strength of the alloy. In such a way, the Tr.990 procedure is recommended as the specific thermal treatment for Inconel 718 extrusion dies.

VI References

[Akhtar et al.,2010] Akhtar, S. and Arif, A. "Fatigue Failure of Extrusion Dies: Effect of Process Parameters and Design Features on Die Life." *Journal of Failure Analysis and Prevention* 10(1): pp. 38-49, (2010).

[Alexandre,2004] Alexandre, F. "*Aspects Probabilistes et microstructuraux de l'amorçage des fissures de fatigue dans l'alliage Inco 718*". PhD Thesis, Ecole des Mines de Paris (2004).

[Andrieu,1987] Andrieu, E. "*Influence de l'environnement sur la propagation des fissures dans un superalliage base nickel: l'Inconel 718*". PhD Thesis, Ecole Nationale Superieure des Mines de Paris (1987).

[Andrieu et al.,1992] Andrieu, E., Molins, R., Ghonem, H. and Pineau, A. "Intergranular crack tip oxidation mechanism in a nickel-based superalloy." *Materials Science and Engineering: A* 154(1): pp. 21-28, (1992).

[Arif et al.,2003] Arif, A. F. M., Sheikh, A. K. and Qamar, S. Z. "A study of die failure mechanisms in aluminum extrusion." *Journal of Materials Processing Technology* 134(3): pp. 318-328, (2003).

[ASTMB637] ASTMB637 "*Standard Specification for precipitation-hardening Nickel alloys, bars forgings and forging stock for high temperature Service*"

[Azadian et al.,2004] Azadian, S., Wei, L.-Y. and Warren, R. "Delta phase precipitation in Inconel 718." *Materials Characterization* 53(1): pp. 7-16, (2004).

[Bache et al.,1999] Bache, M. R., Evans, W. J. and Hardy, M. C. "The effects of environment and loading waveform on fatigue crack growth in Inconel 718." *International Journal of Fatigue* 21(1): pp. 69-77, (1999).

[Barbadillo de et al.,2010] Barbadillo de, J. J. and Mannan, S. K. "*Alloy 718 for Oilfiel Applications*". 7th International Symposium on Superalloy 718 and Derivatives (2010).

[Bathias,1979] Bathias, C. "Endommagement par sollicitation cyclique". Dislocations et déformation plastique. Ed.Diffusion**:** 375-382 (1979).

[Bauser et al.,2006] Bauser, M., Sauer, G. and Siegert, K. "Extrusion 2nd Ed.", ASM International, p. 592, (2006).

[Bellot et al.,2011] Bellot, C., Cabrol, E., Lamesle, P. and Delagnes, D. "*New experimental method for the precipitation investigation in steels*". Report Aubert & Duval (2011).

[Bergstrom et al.,2006] Bergstrom, J. and Rézaï-Aria, F. "*High temperature fatigue of tool steels*". TOOL 06 - 7th International tooling conference, Torino (Italy)**:** 545-554 (2006).

[Bhattacharyya et al.,1997] Bhattacharyya, A., Sastry, G. V. S. and Kutumbarao, V. V. "On the dual slope Coffin-Manson relationship during low cycle fatigue of Ni-base alloy in 718." *Scripta Materialia* 36(4): pp. 411-415, (1997).

[Bhowal et al.,2005] Bhowal, P. R. and Wusatowska-Sarnek, A. M. "Carbides and their influence on notched low cycle fatigue behavior of fine-grained IN718 gas turbine disk material." *Superalloys 718, 625, 706 and Derivatives, Proceedings*: pp. 341-349, (2005).

[Björk et al.,2001] Björk, T., Westergård, R. and Hogmark, S. "Wear of surface treated dies for aluminium extrusion -- a case study." *Wear* 249(3-4): pp. 316-323, (2001).

[Bor et al.,2010] Bor, H., Chao-Nan Wei, Huu Tri Nguyen, An-Chou Yeh and Kuo, C.-M. "*Aging effects on γ'and γ" precipitates of Inconel 718 Superalloy*". 7th International Symposium on Superalloy 718 and Derivatives (2010).

[Branco et al.,2008] Branco, R. and Antunes, F. V. "Finite element modelling and analysis of

crack shape evolution in mode-I fatigue Middle Cracked Tension specimens." *Engineering Fracture Mechanics* 75(10): pp. 3020-3037, (2008).

[Burke et al.,2000] Burke, M. G. and Miller, M. K. "The application of AEM and APFIM to the analysis of precipitation behaviour in Alloy 718." *Microbeam Analysis 2000, Proceedings*(165): pp. 161-162, (2000).

[Cai et al.,2007] Cai, D. Y., Zhang, W. H., Nie, P. L., Liu, W. C. and Yao, M. "Dissolution kinetics of delta phase and its influence on the notch sensitivity of Inconel 718." *Materials Characterization* 58(3): pp. 220-225, (2007).

[Cai et al.,2001] Cai, H. and McEvily, A. J. "On striations and fatigue crack growth in 1018 steel." *Materials Science and Engineering A* 314(1-2): pp. 86-89, (2001).

[Cao W.D Kennedy R.L,1991] Cao W.D Kennedy R.L, W. M. P. "*Differential Thermal Analysis (DTA) study of the Homogenization process in Alloy 718*". Superalloys 718, 625 an Various Derivatives**:** 147-159 (1991).

[Carniel et al.,2011] Carniel, C. and Bellot, C. "*Etude des phases intermétalliques dans les superalliages base nickel* ". Confidential Report Aubert & Duval (2011).

[Chaboche et al.,1994] Chaboche, J.-L. and Lemaitre, J. "Mechanics of solid materials", Cambridge University Press, p., (1994).

[Chermant et al.,1979] Chermant, J. L. and Coster, M. "Quantitative fractography." *Journal of Materials Science* 14(3): pp. 509-534, (1979).

[Chihab,2004] Chihab, K. "On the apparent strain rate sensitivity of Portevin - Le Chatelier effect." *Annales De Chimie-Science Des Materiaux* 29(5): pp. 15-23, (2004).

[Clavel,1980] Clavel, M. "*Fatigue plastique et fissuration de deux alliages durcis par des précipités cohérents. Etude comparative des mécanismes*". PhD Thesis, Université de Poitiers (1980).

[Clavel et al.,1975] Clavel, M., Fournier, D. and Pineau, A. "Plastic zone sizes in fatigued specimens of Inco 718." *Metallurgical Transactions a-Physical Metallurgy and Materials Science* 6(12): pp. 2305-2307, (1975).

[Clavel et al.,1978] Clavel, M. and Pineau, A. "Frequency and wave-form effects on the fatigue crack growth behaviour of alloy 718 at 298 K and 823 K." *Metallurgical and Materials Transactions A* 9(4): pp. 471-480, (1978).

[Clavel et al.,1982] Clavel, M. and Pineau, A. "Fatigue behaviour of two Nickel base alloys I: Experimental results on Low-Cycle fatigue crack propagation and substructures." *Materials Science and Engineering* 55(2): pp. 157-171, (1982).

[Coffin,1968] Coffin, L. "Introduction to high-temperature low-cycle fatigue." *Experimental Mechanics* 8(5): pp. 218-224, (1968).

[Connolley et al.,2003] Connolley, T., Reed, P. A. S. and Starink, M. J. "Short crack initiation and growth at 600 °C in notched specimens of Inconel718." *Materials Science and Engineering A* 340(1-2): pp. 139-154, (2003).

[Connolley et al.,2000] Connolley, T., Starink, M. J. and Reed, P. A. S. "Effect of oxidation on high temperature fatigue crack initiation and short crack growth in Inconel 718." *Superalloys 2000*: pp. 435-444, (2000).

[Connors,1994] Connors, W. C. "Fatigue striation spacing analysis." *Materials Characterization* 33(3): pp. 245-253, (1994).

[Coste,2003] Coste, S. "*Détermination des lois d'évolution microstructurale de l'alliage 718 lors du matriçage*". PhD Thesis, INP Toulouse (2003).

[Cottrell,1949] Cottrell, A. H. "Theory of dislocations." *Progress in Metal Physics* 1: pp. 77-96, IN1-IN2, 97-126, (1949).

[Cozar,1973] Cozar, R. "*Etude de la précipitation des phases γ' (L12) et γ" (D022) dans les aciers austenitiques Fe-Ni-(Co)-Ta et des superalliages dérivés de l'Inconel 718*", Université de Nancy 1 (1973).

[Cozar et al.,1973] Cozar, R. and Pineau, A. "Morphology of γ' and γ" precipitates and thermal stability of inconel 718 type alloys." *Metallurgical and Materials Transactions B* 4(1): pp. 47-59, (1973).

[de Matos et al.,2005] de Matos, P. F. P., Moreira, P. M. G. P., Nedbal, I. and de Castro, P. M. S. T. "Reconstitution of fatigue crack growth in Al-alloy 2024-T3 open-hole specimens using microfractographic techniques." *Engineering Fracture Mechanics* 72(14): pp. 2232-2246, (2005).

[Decker,2006] Decker, R. F. "The evolution of wrought age-hardenable superalloys." *Jom* 58(9): pp. 32-36, (2006).

[Delagnes,1998] Delagnes, D. "*Comportement et tenue en fatigue isotherme d'aciers à outils Z 38 CDV5 autour de la transition fatigue oligocyclique endurance*". PhD Thesis, Ecole des Mines de Paris (1998).

[Desvallées et al.,1994] Desvallées, Y., Bouzidi, M., Bois, F. and Beaude, N. "*Delta phase in Inconel 718: mechanical properties and forging process requirements*". Superalloys 718, 625, 706 and Various Derivatives (1994).

[Devaux et al.,2008] Devaux, A., Nazé, L., Molins, R., Pineau, A., Organista, A., Guédou, J. Y., Uginet, J. F. and Héritier, P. "Gamma double prime precipitation kinetic in Alloy 718." *Materials Science and Engineering: A* 486(1-2): pp. 117-122, (2008).

[Donachie,2002] Donachie, M. J. "Superalloys: a technical guide", ASM International, p., (2002).

[Dossin,2010] Dossin, S. "*Stress Anlaysis of Hollow die plate*". Unpublished Work Hydro Aluminium ECC (2010).

[Dowling et al.,1976] Dowling, N. E. and Begley, N. A. "Fatigue crack growth during gross plasticity and J- integral". Mechanics of Crack Growth. ASTM**:** 82-103 (1976).

[Dwight,1999] Dwight, J. "Aluminium design and construction", E & FN Spon, p. 295, (1999).

[Ellyin,1997] Ellyin, F. "Fatigue damage, crack growth, and life prediction", p., (1997).

[Fiétier et al.,2009] Fiétier, N., Krähenbühl, Y. and Vialard, M. "New methods for the fast simulations of the extrusion process of hot metals." *Journal of Materials Processing Technology* 209(5): pp. 2244-2259, (2009).

[Fournier et al.,1977] Fournier, D. and Pineau, A. "Low fatigue cycle behaviour of Inconel 718 at 293 K and 823 K." *Metallurgical Transactions a-Physical Metallurgy and Materials Science* 8(7): pp. 1095-1105, (1977).

[Fournier et al.,2001] Fournier, L., Delafosse, D. and Magnin, T. "Oxidation induced intergranular cracking and Portevin-Le Chatelier effect in nickel base superalloy 718." *Materials Science and Engineering A* 316(1-2): pp. 166-173, (2001).

[Fu et al.,2009] Fu, S. H., Dong, J. X., Zhang, M. C. and Xie, X. S. "Alloy design and development of INCONEL718 type alloy." *Materials Science and Engineering a-Structural Materials Properties Microstructure and Processing* 499(1-2): pp. 215-220, (2009).

[Garat et al.,2008] Garat, V., Cloue, J. M., Poquillon, D. and Andrieu, E. "Influence of Portevin-Le Chatelier effect on rupture mode of alloy 718 specimens." *Journal of Nuclear Materials* 375(1): pp. 95-101, (2008).

[Ghonem et al.,1993] Ghonem, H., Nicholas, T. and Pineau, A. "Elevated-Temperature fatigue -crack growth in alloy 718-Part 1: effects of mechanical variables." *Fatigue & Fracture of Engineering Materials & Structures* 16(5): pp. 565-576, (1993).

[Graff,2006] Graff, S. "*Viscoplastic behaviour of zirconium alloys in the temperatures range 20°C–400°C: characterization and modelling of strain ageing phenomena*". Paris, Ecole Nationale Supérieure des Mines de Paris**:** 319 (2006).

[Guedou,2009] Guedou, J. Y. "Optimisation des traitements thermiques dans les alliages de

titane et de nickel pour pièces structurales de turboréacteurs aéronautiques." *Matériaux et Techniques* 97: pp. 99-108, (2009).

[Guedou et al.,1994] Guedou, J. Y., Simon, G. and Rongvaux, J. M. "Development of damage tolerant INCO 718." *Superalloys 718, 625, 706 1994*: pp., (1994).

[Guest et al.,2005] Guest, R. P. and Tin, S. "*Modelling microstructural transformations of nickel base superalloy IN 718 during hot deformation*". Superalloys 718, 625, 706 and Derivatives, Proceedings (2005).

[Gutovskaya,2003] Gutovskaya, J. "*Material development for Aluminium Hot Extrusion Dies-AISI Premium H13 Tool Steel and Nimonic 90/PK 37 Nickel-Base Superalloys*". Phd Thesis, Norwegian University of Science and Technology (NTNU)**:** 135 (2003).

[Gutovskaya et al.,2004] Gutovskaya, J., Solberg, J. K., Lange, H. I. and Andersen, L. H. "Wear of Inconel 718 die during aluminium extrusion--a case study." *Wear* 256(1-2): pp. 126-132, (2004).

[Hale et al.,2001] Hale, C. L., Rollings, W. S. and Weaver, M. L. "Activation energy calculations for discontinuous yielding in Inconel 718SPF." *Materials Science and Engineering A* 300(1-2): pp. 153-164, (2001).

[Han et al.,1982] Han, Y. F., Deb, P. and Chaturvedi, M. C. "Coarsening behaviour of γ" particles and γ' particles in Inconel Alloy 718." *Metal Science* 16(12): pp. 555-561, (1982).

[Hazotte,2009] Hazotte, A. "Transformations et contraintes de cohérence dans les superalliages et les intermétalliques de base TiAl." *Matériaux & Techniques* 97((Hors serie)): pp. 23-31, (2009).

[Hazotte et al.,1996] Hazotte, A., Racine, A. and Denis, S. "Internal mismatch stresses in nickel-based superalloys: A finite element approach." *Journal De Physique Iv* 6(C1): pp. 119-128, (1996).

[He,1994] He, J. "γ" Precipitate in Inconel 718." *J.Mater.Sci.Technol.* 10: pp. 293-303, (1994).

[He et al.,1998] He, J., Han, G., Fukuyama, S. and Yokogawa, K. "Interfaces in a modified Inconel 718 with compact precipitates." *Acta Materialia* 46(1): pp. 215-223, (1998).

[Hermann et al.,2003] Hermann, W., Neuer, G., Leitner, G., Poeßnecker, W., Quested, P., Richter, F. and Sockel, H. G. "Thermophysical Properties Benchmark Tests on a Monocrystalline Ni-base Alloy." *Advanced Engineering Materials* 5(1-2): pp. 46-51, (2003).

[Hong et al.,2005] Hong, J. K., Park, N. K., Kim, S. J. and Kang, C. Y. "Microstructures of oxidized primary carbides on superalloy Inconel 718." *New Frontiers of Processing and Engineering in Advanced Materials* 502: pp. 249-253, (2005).

[Hong et al.,2005] Hong, S. G. and Lee, S. "Mechanism of dynamic strain aging and characterization of its effect on the low-cycle fatigue behavior in type 316L stainless steel." *Journal of Nuclear Materials* 340(2-3): pp. 307-314, (2005).

[Hornbogen,1969] Hornbogen, E. "Resistance mécaniqueet microstructure". Dislocations et déformation plastique, Diffusion ed.**:** 395-404 (1969).

[Hornbogen et al.,1981] Hornbogen, E., Thumann, M. and Verpoort, C. "Fatigue crack inititation at slip steps." *Journal of Metals* 33(9): pp. A63-A63, (1981).

[Horvath et al.,2001] Horvath, W., Zechner, W., Tockner, J., Berchthaler, M., Weber, G. and Werner, E. A. "*The effectiveness of direct aging on Inconel 718 forgings produced at high strain rates as obtained on a screw press*". Superalloys 718, 625, 706 and Various Derivatives**:** 223-228 (2001).

[Huang et al.,2007] Huang, Y. and Langdon, T. G. "The evolution of delta-phase in a superplastic Inconel 718 alloy." *Journal of Materials Science* 42(2): pp. 421-427, (2007).

[Jacquelin,1983] Jacquelin, B. "*Amorçage des fissures en fatigue oligocyclique sous chargement multiaxial*". PhD Thesis, Ecoles des Mines de Paris (1983).

[Jain,1992] Jain, M. "TEM study of microstructure development during low-cycle fatigue of an overaged Al-Mg-Si alloy." *Journal of Materials Science* 27(2): pp. 399-407, (1992).

[James,1986] James, L. A. "The effect of grain size upon the fatigue-crack propagation behaviour of alloy 718 under hold-time cycling at elevated temperature." *Engineering Fracture Mechanics* 25(3): pp. 305-314, (1986).

[Jiang et al.,2005] Jiang, D. and Wang, L. "Deformation and fracture behavior of an Al–Li alloy 8090." *Journal of Materials Science* 40(9): pp. 2745-2747, (2005).

[Jiang et al.,2007] Jiang, H., Zhang, Q., Chen, X., Chen, Z., Jiang, Z., Wu, X. and Fan, J. "Three types of Portevin-Le Chatelier effects: Experiment and modelling." *Acta Materialia* 55(7): pp. 2219-2228, (2007).

[Kalluri et al.,2004] Kalluri, S., Rao, K. B. S., Halford, G. and McGaw, M. A. "*Deformation and damage mechanisms in Inconel 718 superalloy*". Superalloys 718, 625, 706 and Various Derivatives, E.A Loria (2004).

[Kazanowski,1998] Kazanowski, P. "*Die Performance Optimization through Understanding of the Surface Features of Fatigue Fractures*". ET '08: the Ninth International Aluminum Extrusion Seminar & Exposition (1998).

[Kindlihagen,2008] Kindlihagen, A. "*Modular die concepts: Cost-Benefit analyses*". Unpublished work, Hydro Aluminium ECC (2008).

[Kirman et al.,1970] Kirman, I. and Warrington, D. "The precipitation of Ni3Nb phases in a Ni−Fe−Cr−Nb alloy." *Metallurgical and Materials Transactions B* 1(10): pp. 2667-2675, (1970).

[Klose et al.,2003] Klose, F. B., Ziegenbein, A., Weidenmüller, J., Neuhäuser, H. and Hähner, P. "Portevin-LeChatelier effect in strain and stress controlled tensile tests." *Computational Materials Science* 26: pp. 80-86, (2003).

[Korth,1991] Korth, G. E. "*Effects of various parameters on the Fatigue life of alloy 718*". Superalloys 718, 625, 706 and Derivatives, Proceedings (1991).

[Koul et al.,1988] Koul, A. K., Au P., Bellinger N. and R., T. "Development of a damage tolerant microstructure for Inconel 718 turbine disc material." *Superalloys 1988*: pp. 3-12, (1988).

[Krueger,1989] Krueger "The development of direct age 718 for Gas Turbine Engine disks applications". Superalloy 718-Metallurgy and Applications. M. M. S. The Minerals (1989).

[Krumphals et al.,2010] Krumphals, F., Wlanis, T., Sievert, R., Wieser, V. and Sommitsch, C. "Damage analysis of extrusion tools made from the austenitic hot work tool steel Böhler W750." *Computational Materials Science* In Press, Corrected Proof: pp., (2010).

[Lange,1998] Lange, H. I. "*Low Cycle Fatigue and creep testing of Hot Working Tool Steels at service temperature*". Unpublished Work SINTEF Material Technology (1998).

[Lee et al.,1995] Lee, B. H. and Kim, I. S. "Dynamic Strain Aging in the high temperature Low-Cycle Fatigue of SA508 Cl. 3 forging steel." *Journal of Nuclear Materials* 226(1-2): pp. 216-225, (1995).

[Lemaitre et al.,1987] Lemaitre, J., Benallal, A., Ben Cheikh, A., Billardon, R., Dufailly, J., Feng, L., Florez, J., Gautherin, M. T., Geymonat, G., Lienard, C., Marquis, D., Mertz, D. and Moret-Bailly, L. "*Formulaire de caractéristiques mécaniques de matériaux/ Handbooklet of mechanical characteristics of materials*". C. N. d. l. R. Scientifique (1987).

[Levaillant et al.,1982] Levaillant, C. and Pineau, A. "Assessment of high-temperature low cycle fatigue life of austenitic stainless steels by using intergranular damage as a

correlating parameter." *Low cycle fatigue and life prediction* ASTM STP 770: pp. 169-183, (1982).

[Li et al.,1994] Li, S., Jingyum, Z., Qun, D. and Jinhui, D. "*The effect of delta phase on crack propagation under creep and fatigue conditions in alloy 718*". Superalloys 718, 625, 706 and Various Derivatives (1994).

[Lingenfelter,1989] Lingenfelter, A. "*Welding of Inconel Alloy 718: A Historical Overview*". Superalloy 718, Metallurgy & Applications**:** 673 (1989).

[Liu et al.] Liu, J., Yuan, H. and Liao, R. "Prediction of fatigue crack growth and residual stress relaxations in shot-peened material." *Materials Science and Engineering: A* In Press, Accepted Manuscript: pp.,

[Liu et al.,1997] Liu, W. C., Xiao, F. R., Yao, M., Chen, Z. L., Jiang, Z. Q. and Wang, S. G. "The influence of cold rolling on the precipitation of delta phase in Inconel 718 alloy." *Journal Name: Scripta Materialia; Journal Volume: 37; Journal Issue: 1; Other Information: PBD: 1 Jul 1997*: pp. Medium: X; Size: pp. 53-57, (1997).

[Loier et al.,1984] Loier, C., Ottmann, M. C. and Leymonie, C. "Structural transformations and mechanical-properties of two non-magnetic alloys (Inconel 718 and ASTM A286)." *Materials Science and Engineering* 63(1): pp. 91-100, (1984).

[Lynch et al.,1994] Lynch, S. P., Radtke, T. C., Wicks, B. J. and Byrnes, R. T. "Fatigue crack growth in nickel based superalloys at 500-700°C. Direct Aged alloy 718." *Fatigue & Fracture of Engineering Materials & Structures* 17(3): pp. 313-325, (1994).

[Mannan,1993] Mannan, S. L. "Role of dynamic strain-aging in low-cycle fatigue." *Bulletin of Materials Science* 16(6): pp. 561-582, (1993).

[McEvily et al.,2010] McEvily, A. J. and Matsunaga, H. "On fatigue striations." *Transaction B: Mechanical Engineering* 17(1): pp. 75-82, (2010).

[Mebarki,2003] Mebarki, N. "*Relation microstructure - propriétés mécaniques d'aciers martensitiques revenus destinés aux outillages de mise en forme d'alliages légers.*". PhD Thesis, Ecole des Mines de Paris (2003).

[Mendoza et al.,1989] Mendoza, O. and Feldstein, H. "*Analysis and Elimination of high temperature notch induced microcrack initiation in Inconel 718 Nickel-based alloy*". Report. San Antonio, DTIC Electe (1989).

[Miller et al.,1999] Miller, M. K., Babu, S. S. and Burke, M. G. "Intragranular precipitation in alloy 718." *Materials Science and Engineering A* 270(1): pp. 14-18, (1999).

[Min et al.,1978] Min, B. K. and Raj, R. "Hold Time Effects in High-Temperature Fatigue." *Acta Metallurgica* 26(6): pp. 1007-1022, (1978).

[Molins,1995] Molins, R. "*Oxydation des superalliages à base de Nickel : identification des mécanismes et conséquences sur le mode de propagation des fissures en fatigue à haute température*". PhD Thesis, Ecole Nationale Superieure des Mines de Paris (1995).

[Molins et al.,1997] Molins, R., Hochstetter, G., Chassaigne, J. C. and Andrieu, E. "Oxidation effects on the fatigue crack growth behaviour of alloy 718 at high temperature." *Acta Materialia* 45(2): pp. 663-674, (1997).

[Mowbray et al.,1976] Mowbray and D, F. "Derivation of a low-cycle fatigue relationship employing the J-integral approach to crack growth", American Society for Testing and Materials, p. 14, (1976).

[Mulford et al.,1979] Mulford, R. A. and Kocks, U. F. "New observations on the mechanisms of dynamic strain aging of jerky flow." *Acta Metallurgica* 27(7): pp. 1125-1134, (1979).

[NACE/MR0175] NACE/MR0175 "*NACE MR0175-2003 Impact on API 6A Equipment and Customers*"

[Nedbal et al.,2008] Nedbal, I., Lauschmann, H., Siegl, J. and Kunz, J. "Fractographic

reconstitution of fatigue crack history - Part II." *Fatigue & Fracture of Engineering Materials & Structures* 31(2): pp. 177-183, (2008).

[Neumann,1974] Neumann, P. "New experiments concerning the slip process at propagating fatigue cracks." *Acta Metallurgica* 22: pp. 1155-1165, (1974).

[Niang,2010] Niang, A. "*Contribution à l'étude de la précipitation des phases intermétalliques dans l'alliage 718*". PhD Thesis, INP Toulouse (2010).

[Oftedal,1998] Oftedal, K. O. "*Loads acting on the tools*". Unpublished Work, Hydro Aluminium Extrusion (1998).

[Oudin,2001] Oudin, A. "*Thermo-Mechanical Fatigue of Hot Work Tool Steels* ". PhD Thesis, Ecole Nationale Superieure des Mines de Paris (2001).

[Pasqualon,2010] Pasqualon, M. "*Extrusion dies material and surface treatment developments*". Unpublished Work, Hydro Aluminium PTTC (2010).

[Patterson,1939] Patterson, A. "The Scherrer Formula for X-Ray Particle Size Determination." *Physical Review* 56(10): pp. 978-982, (1939).

[Paulonis et al.,1969] Paulonis, D., Oblak, J. and Duvall, D. "Precipitation in nickel base alloy 718." *ASM* 62: pp. 611-622, (1969).

[Pedron et al.,1982] Pedron, J. P. and Pineau, A. "The effect of microstructure and environment on the crack-growth behaviour of Inconel 718 alloy at 650 °C under fatigue, creep and combined loading." *Materials Science and Engineering* 56(2): pp. 143-156, (1982).

[Pelloux,1970] Pelloux, R. M. N. "Crack extension by alternating shear." *Engineering Fracture Mechanics* 1: pp. 697-704, (1970).

[Perrut et al.,2011] Perrut, M., Mathon, M. H. and Delagnes, D. "Small-Angle Neutron Scattering of Multiphase Secondary Hardening Steels." *Journal of Materials Science* (In Press): pp., (2011).

[Pineau,1969] Pineau, A. "Sollicitation cyclique des alliages durcis par precipites". Dislocations et deformation plastique. Ed.Diffusion**:** 383-394 (1969).

[Ponnelle,2001] Ponnelle, S. "*Propagation des fissures par fatigue à haute température dans l'Inconel 718: effets de microstructure et de chargements complexes*". PhD Thesis, Ecole des Mines de Paris (2001).

[Ponnelle et al.,2001] Ponnelle, S., Brethes, B. and Pineau, A. "Orientational effects and influence of delta phase on fatigue crack growth rates in a forged disc of INCO718 superalloy." *Superalloys 718, 625, 706 and Various Derivatives*: pp. 501-510, (2001).

[Qamar et al.,2008] Qamar, S. Z., Sheikh, A. K., Arif, A. F. M., Younas, M. and Pervez, T. "Monte Carlo simulation of extrusion die life." *Journal of Materials Processing Technology* 202(1-3): pp. 96-106, (2008).

[Radavich et al.,1989] Radavich, J. F. and Couts, W. H. "*Factors affecting delta phase precipitation and growth at hot work temperatures*". Superalloys 718, 625, 706 and Derivatives, Proceedings (1989).

[Reggiani et al.,2010] Reggiani, B., Donati, L., Zhou, J. and Tomesani, L. "The role of creep and fatigue in determining the high-temperature behaviour of AISI H11 tempered steel for aluminium extrusion dies." *Journal of Materials Processing Technology* 210(12): pp. 1613-1623, (2010).

[Rice,1968] Rice, J. R. "A path independent integral and the approximate analysis of strain concentration by notches and cracks." *Journal of Applied Mechanics* 35: pp. 379-386, (1968).

[Rodriguez et al.,1995] Rodriguez, P. and Venkadesan, S. "Serrated Plastic Flow Revisited." *Solid State Phenomena* 42-43: pp. 257-266, (1995).

[Sadananda,1984] Sadananda, K. "Crack propagation under creep and fatigue." *Nuclear Engineering and Design* 83(3): pp. 303-323, (1984).

[Saha,2000] Saha, P. "Aluminum Extrusion technology", ASM International, p. 259, (2000).

[Sanders et al.,1981] Sanders, T., Frishmuth, R. and Embley, G. "Temperature Dependent Deformation Mechanisms of Alloy 718 in Low Cycle Fatigue." *METALLURGICAL AND MATERIALS TRANSACTIONS A* 12(6): pp. 1003-1010, (1981).

[Scherrer,1918] Scherrer, P. "Estimation of the size and internal structure of colloidal particles by means of rontgen." *Nachrichten Gottinger Gesellschaft* 2(98): pp. 96-100, (1918).

[Sims et al.,1972] Sims, C. and Hagel, W. "The Superalloys", A Wiley-Interscience Publication, p. 614, (1972).

[Slama et al.,2005] Slama, C, Abdellaoui and M "Mechanical properties of the inconel 718 aged at 680 and 750 °C." *Physical and Chemical News*(22): pp. 8, (2005).

[Slama,1993] Slama, C. "*Analyse des évolutions structurales et des processus de précipitation intervenant dans l'alliage à base de nickel INCONEL 718 (NC 19Fe Nb). Incidence de la microstructure sur les propriétés mécaniques.*". PhD Thesis, Université de Paris Sud- Centre d'Orsay (1993).

[Slama et al.,2000] Slama, C. and Abdellaoui, M. "Structural characterization of the aged Inconel 718." *Journal of Alloys and Compounds* 306(1-2): pp. 277-284, (2000).

[Slama et al.,1997] Slama, C., Servant, C. and Cizeron, G. "Aging of the Inconel 718 alloy between 500 and 750 degrees C." *Journal of Materials Research* 12(9): pp. 2298-2316, (1997).

[Spath et al.,2001] Spath, N., Zerrouki, V., Poubanne, P. and Guedou, J. Y. "718 superalloy forging simulation : A way to improve process and material potentialities." *Superalloys 718, 625, 706 and Various Derivatives*: pp. 173-183, (2001).

[Special Metals] Special Metals "Inconel Alloy 718" (consulted webpage in March 2011) http://www.specialmetals.com/documents/Inconel%20alloy%20718.pdf.

[Stephens et al.,2001] Stephens, R. I. and Fuchs, H. O. "Metal Fatigue in Engineering (Second Edition)", John Wiley & Sons, p., (2001).

[Strondl et al.,2008] Strondl, A., Fischer, R., Frommeyer, G. and Schneider, A. "Investigations of MX and γ'/γ" precipitates in the nickel-based superalloy 718 produced by electron beam melting." *Materials Science and Engineering: A* 480(1-2): pp. 138-147, (2008).

[Subodh,2004] Subodh, K. "*Technical Solutions for the Aluminum Extrusion Industry*". Eighth International Aluminum Extrusion technology (2004).

[Sundaraman et al.,1993] Sundaraman, M., Singh, J. B. and Mukhopadhyay, P. "Estimation of order strengthening in Inconel 718 type alloys containing all γ” precipitate variants." *Scripta Metallurgica Et Materialia* 29: pp. 557-562, (1993).

[Sundararaman,1988] Sundararaman, M. "Deformation behaviour of γ” strengthened Inconel 718." *Acta Metallurgica* 36(4): pp. 847-864, (1988).

[Sundararaman et al.,1994] Sundararaman, M., Mukhopadhyay, P. and Banerjee, S. "*Precipitation and room temperature deformation behaviour of Inconel 718*". Superalloys 718, 625, 706 &nd Various Derivatives (1994).

[Sundararaman et al.,1997] Sundararaman, M., Mukhopadhyay, P. and Banerjee, S. "*Carbide precipitation in nickel base superalloys 718 and 625 and their effect on mechanical properties*". Superalloys 718, 625, 706 and Various Derivatives (1997).

[Taina et al.,2010] Taina, F., Pasqualon, M., Delagnes, D., Velay, V. and Lours, P. "*Effect of the LCF loading cycle characteristics on the fatigue life of Inconel 718 at high temperature*". 7th International Symposium on Superalloy 718 and Derivatives (2010).

[Tanaka et al.,1981] Tanaka, K. and Mura, T. "A dislocation model for fatigue crack initiation." *Journal of Applied Mechanics* 48: pp. 97-103, (1981).

[Ter-Ovanessian,2011] Ter-Ovanessian, B. "*Etude comparative de différents superalliages*

base Ni pour ressorts de systèmes de maintien". PhD Thesis, INP Toulouse (2011).

[Ter-Ovanessian et al.,2008] Ter-Ovanessian, B., Deleume, J., Cloue, J. M. and Andrieu, E. "Influence of interstitials content on the sensitivity of alloy 718 to oxidation assisted intergranular fracture." *High Temperature Corrosion and Protection of Materials 7, Pts 1 and 2* 595-598: pp. 951-958, (2008).

[Underwood,1979] Underwood, E. E. "Quantification of microstructures by stereological analysis." *Journal of Histochemistry & Cytochemistry* 27(11): pp. 1536-1537, (1979).

[Valsan et al.,1994] Valsan, M., Sastry, D. H., Rao, K. B. S. and Mannan, S. L. "Effect of strain rate on the High-Temperature Low-Cycle Fatigue properties of a Nimonic PE-16 Superalloy." *Metallurgical and Materials Transactions a-Physical Metallurgy and Materials Science* 25(1): pp. 159-171, (1994).

[Velay,2003] Velay, V. "*Modélisation du comportement cyclique et de la durée de vie d'aciers à outils martensitiques*". PhD Thesis, Ecole des Mines de Paris (2003).

[Villechaise et al.,2002] Villechaise, P., Sabatier, L. and Girard, J. C. "On slip band features and crack initiation in fatigued 316L austenitic stainless steel: Part 1: Analysis by electron back-scattered diffraction and atomic force microscopy." *Materials Science and Engineering A* 323(1-2): pp. 377-385, (2002).

[Wang et al.,2009] Wang, Y., Zhen, L., Shao, W. Z., Yang, L. and Zhang, X. M. "Hot working characteristics and dynamic recrystallization of delta-processed superalloy 718." *Journal of Alloys and Compounds* 474(1-2): pp. 341-346, (2009).

[Warren et al.,2006] Warren, J. and Wei, D. Y. "The cyclic fatigue behaviour of direct age 718 at 149, 315, 454 and 538 °C." *Materials Science and Engineering: A* 428(1-2): pp. 106-115, (2006).

[Woodford,2006] Woodford, D. A. "Gas phase embrittlement and time dependent cracking of nickel based superalloys." *Energy Materials: Materials Science and Engineering for Energy Systems* 1: pp. 59-79, (2006).

[Worthem et al.,1990] Worthem, D., Robertson, I., Leckie, F., Socie, D. and Altstetter, C. "Inhomogeneous deformation in INCONEL 718 during monotonic and cyclic loadings." *Metallurgical and Materials Transactions A* 21(12): pp. 3215-3220, (1990).

[Xianghong et al.,2006] Xianghong, W., Guoqun, Z., Yiguo, L. and Xinwu, M. "Numerical simulation and die structure optimization of an aluminum rectangular hollow pipe extrusion process." *Materials Science and Engineering: A* 435-436: pp. 266-274, (2006).

[Xiao et al.,2005] Xiao, L., Chen, D. L. and Chaturvedi, M. C. "Shearing of γ" precipitates and formation of planar slip bands in Inconel 718 during cyclic deformation." *Scripta Materialia* 52(7): pp. 603-607, (2005).

[Xiao et al.,2008] Xiao, L., Chen, D. L. and Chaturvedi, M. C. "Cyclic deformation mechanisms of precipitation-hardened Inconel 718 superalloy." *Materials Science and Engineering: A* 483-484: pp. 369-372, (2008).

[Xie et al.,1997] Xie, J. Z., Shen, Z. M. and Hou, J. Y. "*Fatigue Crack growth behaviours in alloy 718 at high temperature*". Superalloys 718, 625, 706 and Various derivatives (1997).

[Xie et al.,2005] Xie, X. S., Dong, J. X., Wang, G. L. and You, W. "The effect of Nb, Ti, Al on precipitation and strengthening behavior of 718 type superalloys." *Superalloys 718, 625, 706 and Derivatives, Proceedings*: pp. 287-298, (2005).

[Xie et al.,2010] Xie, X. S., Fu, S. H., Zhao, S. Q. and Dong, J. X. "The Precipitation Strengthening Effect of Nb, Ti and Al in Cast/Wrought Ni-Base Superalloys." *Thermec 2009, Pts 1-4* 638-642: pp. 2363-2368, (2010).

[Yang et al.,2006] Yang, F., Kuang, Z. and Shlyannikov, V. N. "Fatigue crack growth for straight-fronted edge crack in a round bar." *International Journal of Fatigue* 28(4): pp. 431-437, (2006).

[Yuan et al.,2005] Yuan, H. and Liu, W. C. "Effect of the [delta] phase on the hot deformation behavior of Inconel 718." *Materials Science and Engineering: A* 408(1-2): pp. 281-289, (2005).

[Zemzemi,2007] Zemzemi, F. "*Caracterisation de modeles de frottement aux interfaces piece-outil-copeau en usinage: application au cas de l'usinage des aciers et de l'Inconel 718*". PhD Thesis, Ecole centrale de Lyon (2007).

[Zhang et al.] Zhang, H. Y., Zhang, S. H., Cheng, M. and Li, Z. X. "Deformation characteristics of [delta] phase in the delta-processed Inconel 718 alloy." *Materials Characterization* 61(1): pp. 49-53,

Conclusions

This present work is a contribution to an extensive development study, promoted by Hydro Aluminium, in the field of the damage mechanisms of extrusion dies from a material selection point of view. In a traditional aluminium extrusion process, the tool is subject to extreme working conditions that strongly influence its service life. The fluctuating stresses (tension/compression) and the continuous contact between the tool and the aluminium enhance the risks of fatigue and wear failures.

In 2004, Hydro Aluminium Automotives Structures proposed a solution to limit the frequent failures of dies used to extrude the 7000 series aluminium alloys. This innovative approach was based on the application of various materials, with specific tailored properties, in different parts of the die. A so-called "**Modular**" extrusion die was designed and worldwide patent application has been submitted in 2010 (patent pending).For this innovative die, **Inconel 718** is adopted as bulk material the zone subjected to the strong thermo-mechanical loading in order to prevent the risks of failure and scrap. This alloy is considered as an alternative material to the conventional hot work tool steels (H13) because of its high mechanical resistance under cyclic loading at the extrusion service temperature (550°C). In addition, for the bearing zone, the insert is manufactured with a wear resistant material (such as high speed tool steel, hot working steel or precipitation hardened steel) specifically optimised by the application of a specific coating. The Modular Extrusion die represents an innovative idea prone to improve die life and simultaneously reduce the directly connected costs. The service life of an extrusion die has a strong impact on the quality, efficiency and cost of a given extruded profile. The number of maintenance interventions (die correction, welding repair, die scrap), caused by tool defections, impact the commercial viability of the production.

Microstructural investigations carried out on a failed extrusion die revealed that **fatigue** is the relevant failure mode for the modular tool. The adoption of the modular concept strongly delays the occurrence of fatigue damage. However, the cyclic mechanical loading is still a limiting factor for the die life. As a consequence, the understanding and the improvement of the mechanical behaviour of the tool bulk material (Inconel 718) is considered as the most efficient way to further increase die life, process stability and later on press productivity. This represents the main objective of this study that has been addressed by a multidisciplinary approach including metallurgical and mechanical experiments as well as behaviour modelling.

The originality of the present work is based on the development of an optimized Inconel 718 alloy for specific applications that is bulk material for extrusion die. A detailed study of the Inconel 718 cyclic behaviour is proposed in the first part of Chapter IV. A cyclic behaviour model is developed in order to predict the stress-strain response typical of extrusion dies. The constitutive equations are integrated in a Finite Elements code to simulate the evolution of the stress-strain state in a base tube extrusion die. The good agreement between the simulations and the experimental data, obtained by direct measurements on production presses, indicates that the so called Dynamic Modelling provides satisfactory estimates of the

evolution of the loading state (stress-strain) through the tool.

In addition the different transient phenomena are taken in consideration. Results are explained as a function of the material cyclic behaviour and its microstructural evolution. The Dynamic Model represents a valid alternative to high risk and high cost trial and error approach for the design of Ni-base superalloy dies.

The fatigue life assessments of Inconel 718 at the extrusion service temperature (550°C) are also investigated. A cyclic symmetric waveform (1 Hz) are considered to compare the fatigue performances of Inconel 718, the new bulk material for extrusion die, with those of the traditionally used Hot Work tool steels, assessing the better performances of the superalloy.

From the scientific point of view, the isothermal Low Cycle Fatigue (LCF) are considered as the most accurate method for testing the thermo-mechanical loading acting on the tool. Various LCF conditions (strain amplitudes and strain rates) are examined in order to address the various damage mechanisms occurring under cyclic loading. Based on the results provided by the Finite Elements Analyses, a trapezoidal waveform, in total strain control mode, are adopted as the reference signal for tests. The symmetric cycle is provided with an holding time (150s) at maximal strain to assess the extrusion loading conditions, and a steady time (20s) at minimal strain to take the unloading into consideration. Some results obtained while simulating the actual thermo-mechanical loadings of extrusion are used to explain the stability to failure exhibited by the new die concept. In general, the application of a holding time at maximal and minimal stress provokes an average decrease of the fatigue life by 33% as compared to that obtained with a cyclic signal (1 Hz). For this reason, a particular attention is given to the influence of the holding time at maximal strain. This parameter allows the experimental simulation of different billet lengths to be extruded. As a matter of fact, material exhibits a rapid stress decrease during the first 40 seconds of the steady time, followed by a linear relaxation which has limited effects on the inelastic strain. It is then understood that over 40s of extrusion cycle and within 300s no significant die life difference should be observed which allow concluding that Inconel 718 die may not need design changes regarding to cycle duration selected at the press.

However, the fatigue life of Nickel based superalloys at elevated temperature is directly affected by the strain rate. The LCF results, supported by microstructural investigations, show that changes in fatigue behaviour are due to the interaction of cyclic deformation and time dependent processes that act concomitantly on the stress-strain response and on the deformation mechanisms. From an industrial point of view, the strain rate corresponds to die loading rate assessed at the press. Results suggest that it could be of interest to discuss the possibility for the hydraulic piloted ram to have a higher loading rate capacity. Clearly some press construction limitations are expected to be met. On the other hand, a reduction of this loading rate (excessive reduction of die loading from $5 \cdot 10^{-3} s^{-1}$ to $5 \cdot 10^{-4} s^{-1}$) may lead to negative change of die life (die life reduction by a factor of 3) and shall consequently bring to attention to extrusion managers using Inconel 718 dies.

Focusing on these results, it can be concluded that strain rate and holding time have a significant impact on fatigue life, although any effects are detected on the cyclic behaviour

(hysteresis loops) at 550°C. These effects are interpretated as *time-dependent phenomena*; where the interaction between mechanical loading and environmental effects produce mixed or intergranular brittle fractures.

The study of the mechanical behaviour of Inconel 718 under extrusion conditions are completed by the introduction of a fractographic method for the reconstitution of the fatigue crack growth. Generally speaking, the life of a LCF sample or an extrusion die is composed of a crack initiation and a crack propagation period. The above method has been used to estimate the extent of the two regimes. Comparable results are observed for different strain amplitudes, showing that crack initiation governs the fatigue life of Inconel 718, ranging between 75-80% of the total life (for fatigue life ranging between 100 and 5500 cycles).

All these considerations, reported in Chapter IV, represent the “Input Data” for the design of an optimized Inconel 718 to provide longer lifetime to extrusion dies. The optimisation of the material microstructure must be carried out in order to limit the time dependent damage associated to the extrusion cycle (such as the material relaxation during the holding time at maximal strain). Finally, the prevalence of the crack initiation time, over the crack propagation, requires a tailored microstructure able to further delay the risks of crack initiation associated to the localisation of the plastic strain.

A specific strategy for the microstructural optimization is first presented in Chapter III. The development of the so called standard Inconel 718 grade, used for all the fatigue tests, is organized considering both industrial and scientific requirements.

Two investigation approaches are considered. The first one consists in the optimization of the heat treatment parameters as a function of the required mechanical properties, while the second is based on the adoption of thermo-mechanical processes where not only the heat treatment, but also the forging procedure is refined. From the macroscopical point of view, the choice and/or design of new heat treatment procedures are made with the aim to contain cyclic plasticity concentrated in specific zones of the tool, considered as the main cause of the fatigue failure of the extrusion dies. The general purpose consists in maximizing the Inconel Yield Strenght in order to reduce plasticity and improve the fatigue behaviour of the alloy. However, the previous investigations under LCF conditions point out the importance of other secondary properties (such as the resistance to the stress relaxation and to the fatigue crack initiation) that have to be optimized as a function of the material workability (forging, weldability, machining…).

The design of an optimized heat treatment procedure has been influenced by the strong sensitivity of the alloy to the thermal profile. The following experimental evidences, about this microstructural evolution, are collected and analyzed:

1. The solution annealing has a strong impact on the microstructure of the alloy, especially for the delta phase precipitation and grain size evolution. Significant δ phase precipitation results from the lower solutionizing temperatures of 924°C and 955°C because of the high equilibrium content of δ phase at these temperatures. Limited changes in δ phase structure are noticed at 975°C, whereas at 990°C partial precipitates

dissolution occurs. A certain amount of delta phase still exists at 1010°C, while the dissolution process is completed at 1050°C giving an austenitic microstructure free of precipitates. As a consequence, the grain size exhibits a strong increase between 1000 and 1050°C due to the progressive dissolution of the δ phase.

2. The adoption of a high solution annealing temperature, which causes partial delta phase dissolution, is associated to the increase of the content of alloying elements, retained within the matrix, such as Nb, Ti and Al that interact to form the strengthening phases. The precipitates growth is influenced by the diffusion rates of the constitutive elements, which are strongly affected by the ageing temperature. A low diffusion (*under aging*), due to short ageing times (t<4h) and/or low ageing temperatures (T< 720°C), induces the formation of too small particles to impede the dislocation motion. Conversely, the application of high ageing temperatures (T>720°C) and/or long ageing times (t>8h) increase the diffusion rate and give rise to *over aging* conditions, where the strengthening particles assume too large sizes (>30 nm) and lose their coherency with the matrix. This microstructural evolution has a negative impact on the fatigue properties of the alloy that cannot block anymore the grain boundaries.

In agreement with these assumptions, various heat treatments are formulated. To validate the efficiency of these procedures, LCF tests, under extrusion conditions, are carried out to compare the cyclic response of the alternative Inconel 718 grades.

These results, added to the microstructural investigations, are a specific Inconel 718 microstructure, able to provide an optimal combination of the required properties and ensure the best performances under the severe loading conditions imposed by the extrusion process. This microstructure consists in a balanced distribution of the different intermetallic phases (δ, γ’ and γ” phases). A moderate presence of delta particles is needed to limit the grain size whereas coherent γ” phases are required to increase the strength of the alloy.

These microstructural features may be provided by an alternative thermal treatment, labeled “Tr.990”, which is the result of our experimental analyses. It consists in choosing an intermediate solution annealing temperature (990°C) and a standard ageing temperature (720°C for 8 hours, furnace cool to 620°C and holding at 620°C for a total ageing-time of 18 hours followed by air-cooling to room temperature)

The “Tr.990” heat treatment is based on an increase of the solution annealing temperature as compared to the reference Inconel 718 grade (Tr. Standard) which was adopted to treat the preliminary Hydro Modular Dies, whereas the ageing conditions remain the same.

The direct comparison of the fatigue performances with the standard grade has emphasized the better results shown by Tr.990, especially at high strain amplitudes where the fatigue life is increased by a factor 1.7.

For this reason the “Tr.990” procedure has been implemented in the Hydro production practice as the new standard procedure for the thermal treatment of the Inconel 718 extrusion dies.

Further work

Although the experimental investigations carried out and described in this PhD work, have provided encouraging results, there are some areas that require further investigations. Three research approaches can be explored. They are briefly summarized as follows:

1. *Investigation of the thermo-mechanical behaviour and prediction of loading state in extrusion dies;*
2. *Quantitative approach for microstructural analysis;*
3. *Industrial approach for technico-economic issues in alternative materials and surface treatments selection.*

The three orientations are described in detail in the following paragraph.

1. Investigation of the thermo-mechanical behaviour and prediction of loading state in extrusion dies:

- The uniaxial Low Cycle Fatigue (LCF) tests have been considered as the most accurate method for testing the thermo-mechanical loading acting on the tool. However, further investigations are needed to better reproduce the cyclic loading of the die. In such a way, particular attention should be paid to the design of multi axial fatigue test to simulate the tri-axial loading acting in the most critical part of the tool (such as sharp corners, section changes or porthole bridges). In addition, considering that the aluminium flow tends to limit the oxygen content retained in the bearing region of the die, these thermo-mechanical experiments should be carried out under controlled atmosphere (vacuum or low oxygen content) in order to better characterize the influence of the environment on the macroscopic response of Inconel 718, such as in the stress relaxation and fatigue damaging.

- The Finite elements simulations carried out by the integration of the Dynamic Modeling have pointed out its efficiency in predicting the evolution of the die loading state cycle by cycle. Despite a good set of results provided by this experimental approach, there exists substantial possible technological improvement. A further development could be achieved for calibrating and validating the model on the results provided by the multi-axial fatigue tests, described above. In addition, in agreement with the results reported by Krumphals **[Krumphals et al.,2010]**, appropriate parameters could be integrated in order to characterize the tool damage evolution (life time consumption) in the zones under high stress tri-axialities and large accumulated inelastic strains (hot spots). Finally specific dynamic models could be defined for all alternative Inconel 718 grades developed by this

PhD work. In such a way the model will represent an efficient support to investigate the effect of the material microstructure on the service response of the extrusion die: especially analyzing the influence of each grade on the cyclic effects (softening, profile eccentricity increase) that are believed to be detrimental for its efficiency. Namely, the influence of each grade on the detrimental and cyclic effect, such as softening and deflection, will be addressed.

2. Quantitative approach for microstructural analysis

- The microstructural optimization has represented the second main objective of this work. Although the experimental investigations have provided important information about the microstructural evolution under the effect of the thermal treatment, further studies are needed to confirm our findings. In particular, a quantitative anlysis of the strengthening phases could be developed. In addition to the results provided by the precipitates extraction, reported in Chapter V, chemical analyses carried out by Inductively Coupled Plasma Optical Emission Spectrometry (ICP-OES) may be used to determine the composition of the matrix and the intermetallic phases. The results provided by this technique will be a valid support for the determination of the molar fraction of the single precipitates. In such a way, the alternative grades could be compared as a function of the strengthening phases' quantity, pointing out the effect of this parameter on the mechanical properties of the alloy. Finally, a possible approach to study the intermetallic phases' evolution (thermal stability, morphology, size) consists in the application of in-situ Synchrotron diffraction technique during the heat treatment processing. This experimental method could give further information, in addition to the results reported in Chapter V, about the evolution of the strengthening phases as a function of thermal profile (time and temperature).

3. Industrial approach for technico-economic issues in alternative materials and surface treatments selection.

- In addition to the microstructural optimization, the adoption of a surface treatment could be suggested as a further improvement of the material fatigue performances. It is considered that industrial processes such as conventional shot peening or Laser shock peening may be used to further improve the mechanical properties of the alloy. In particular, the compressive residual stresses induced at the surface could increase the ratio of initiation life to propagation life in comparison to unpeened specimens. The application of this surface treatment is, anyway, influenced by the complex geometry of the extrusion dies and the process temperature (550°C) that induces the relaxation of the residual stresses. The thermo-mechanical investigations performed on Inconel 718 and the longer lifetime service exhibited by the Hydro Modular dies have confirmed the efficiency of this alloy as bulk material for extrusion dies. However some challenges still exist: manufacturing of Inconel 718 is very difficult and its rough cost is elevated, even if it is minimized by the longer die life. The trend is to select the lowest-cost material to meet

design requirements for the application. The raw material cost is strongly influenced by the Nickel cost, which fluctuates significantly with time. In addition, Differences in working, and other processing costs, which can be substantial, significantly impact product cost. For these reasons, Inconel 706 represents a promising alternative for our specific industrial applications. Compared with Alloy 718, from which it was developed, this material has a chemical composition with no molybdenum, reduced niobium, aluminium, chromium, nickel, carbon and increased titanium and iron. A balanced content of nickel, chromium and aluminum in alloy 706 provides good hardenability and resistance against oxidation and corrosion. As a result the elemental material cost is reduced by a factor 1.5 as compared to Inconel 718. The lower alloying content associated to a more uniform structure lead to a better machining behaviour which can be performed by the application of conventional machining techniques used for iron based alloys. High cutting speed can be adopted, thanks to the absence of work hardening during the machining operations, resulting in an additional cost saving. From the scientific point of view the recommendation of this alloy is not coherent with the strategy adopted for the material optimization: Inconel 706 shows lower yield strength at 550°C that leads one to think that the lifetime of the extrusion die will be shorter than that of the Inconel 718 dies. However, on the industrial side, the adoption of Inconel 706 could further minimize the ratio die cost/kg extruded.

APPENDIXES

Appendix A

Finite Elements Simulations on a batwing extrusion die

Appendix A: Finite Elements Simulations on a batwing extrusion die

I Dynamic Model application : equivalent stress (Von Mises) distribution

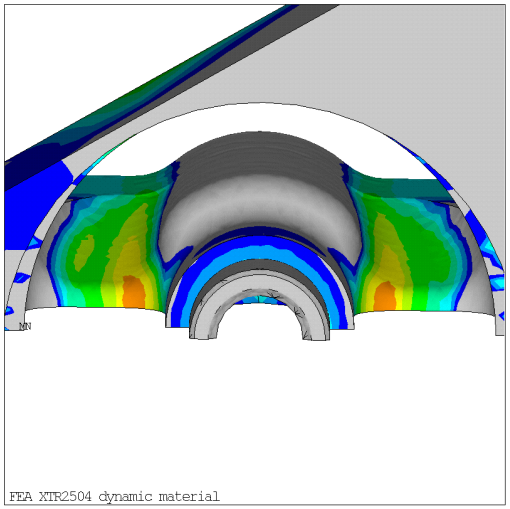

Cycle 1

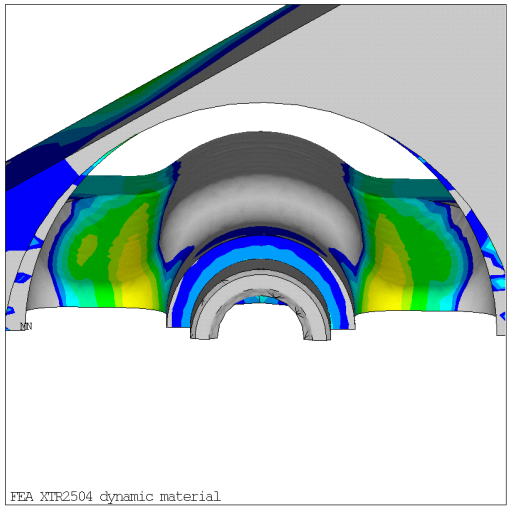

Cycle 2

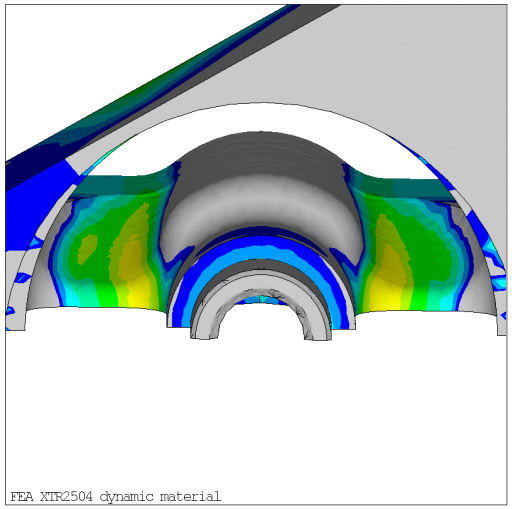

Cycle 3

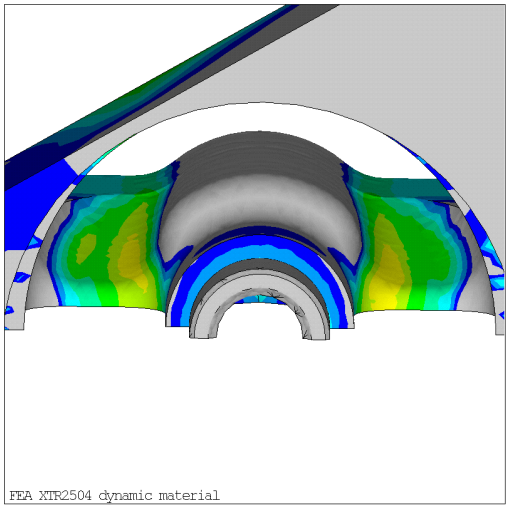

Cycle 4

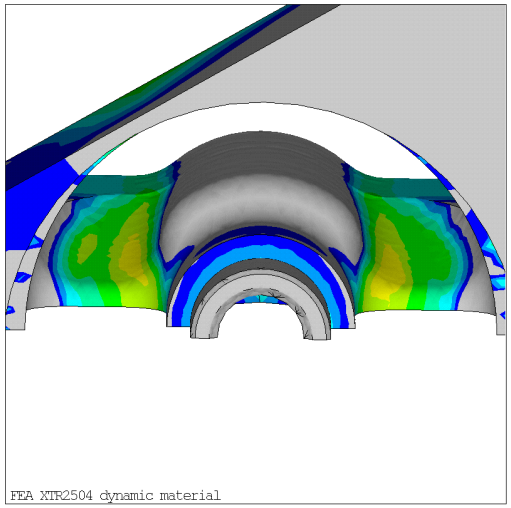

Cycle 5

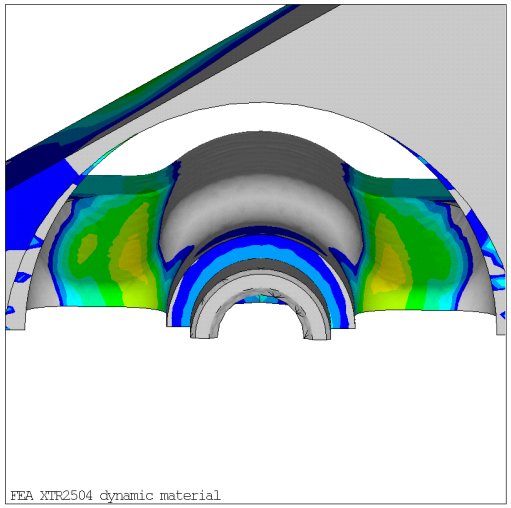

Cycle 6

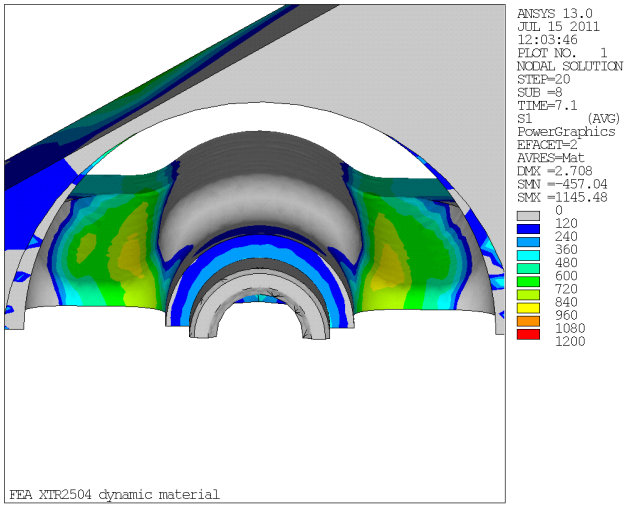

Cycle 7

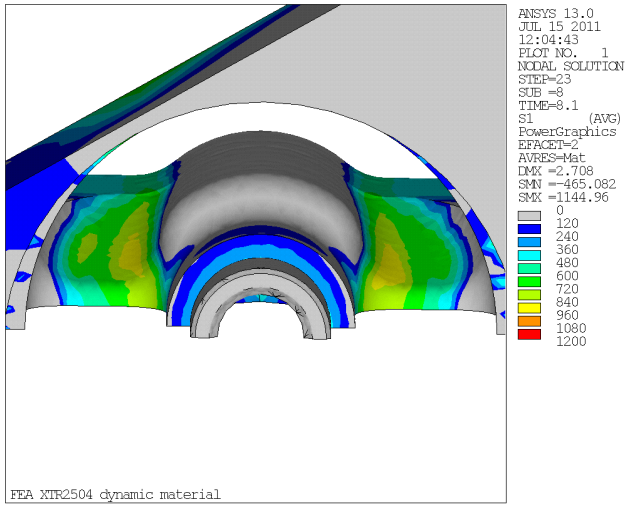

Cycle 8

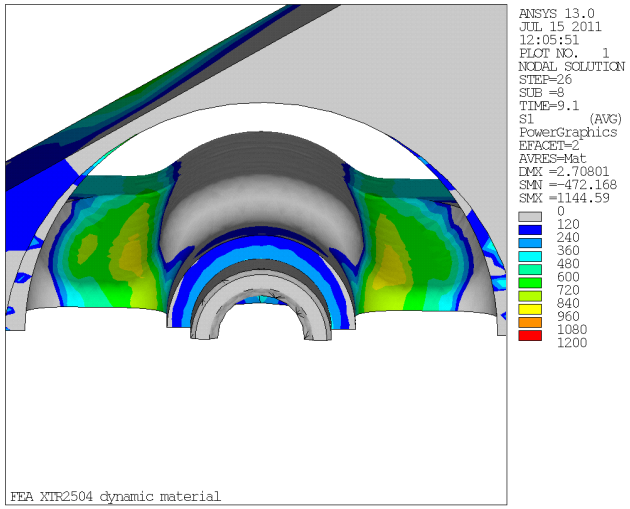

Cycle 9

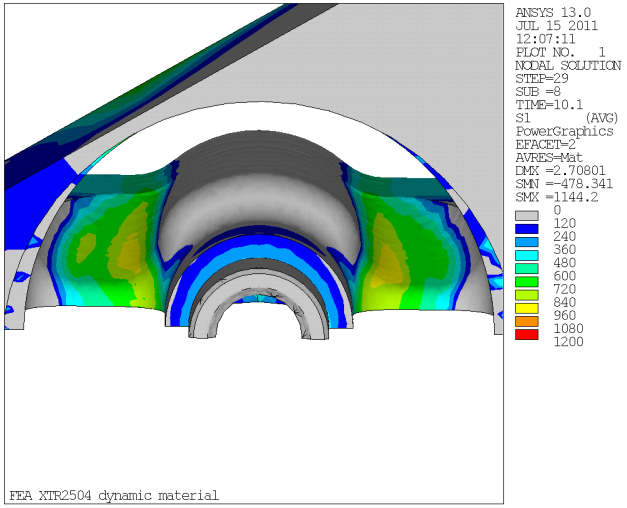

Cycle 10

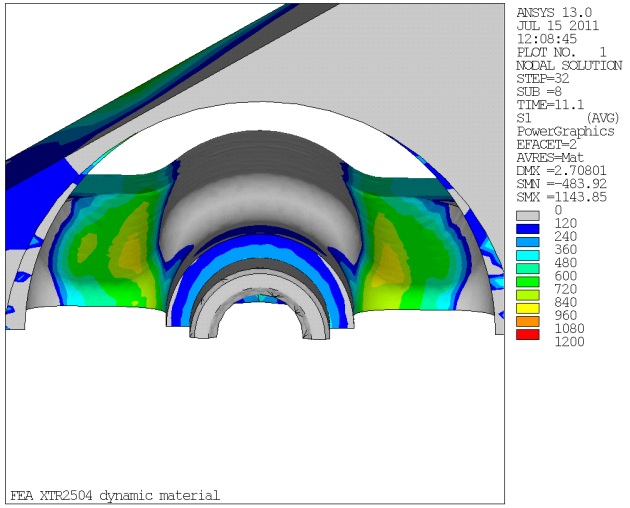

Cycle 11

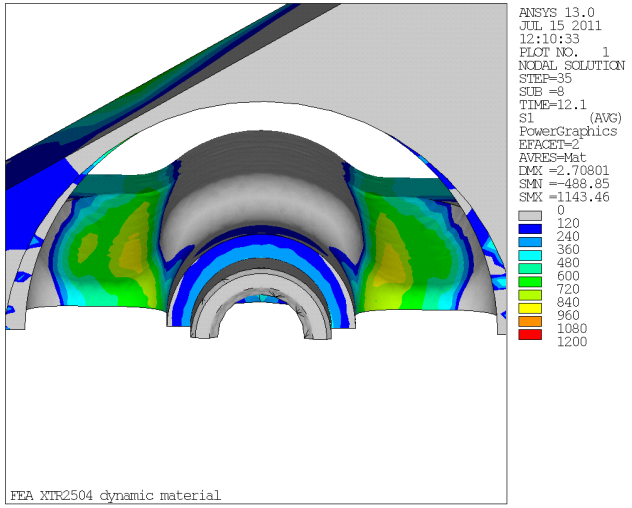

Cycle 12

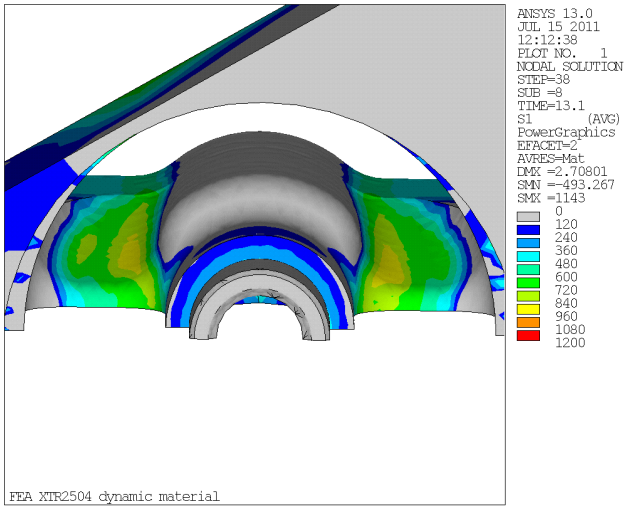

Cycle 13

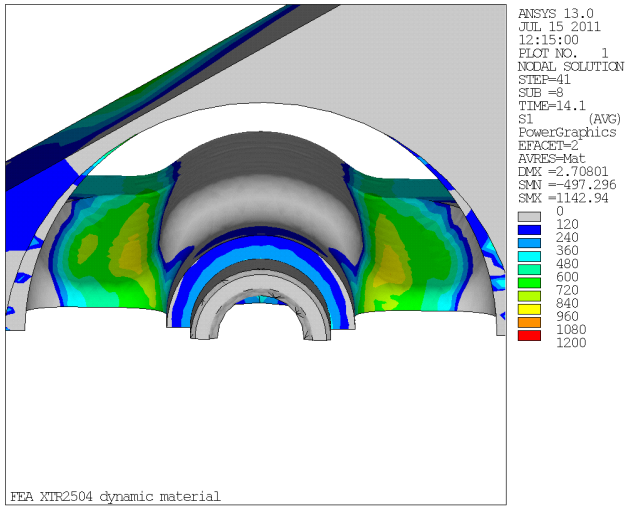

Cycle 14

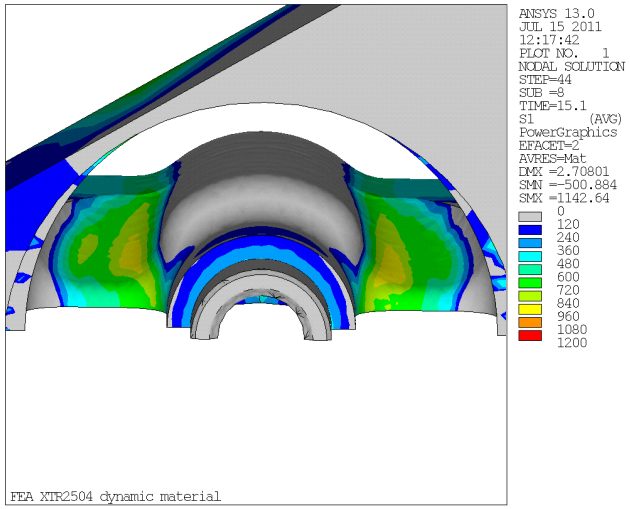

Cycle 15

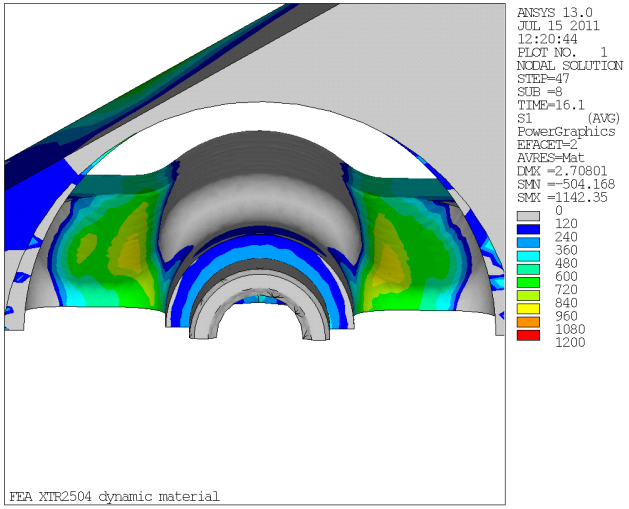

Cycle 16

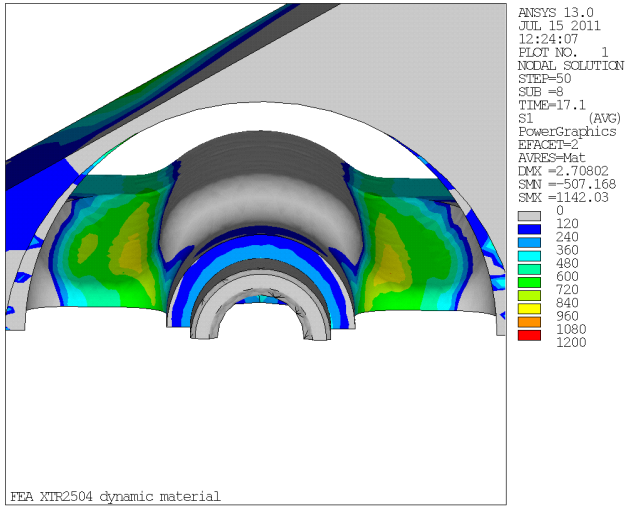

Cycle 17

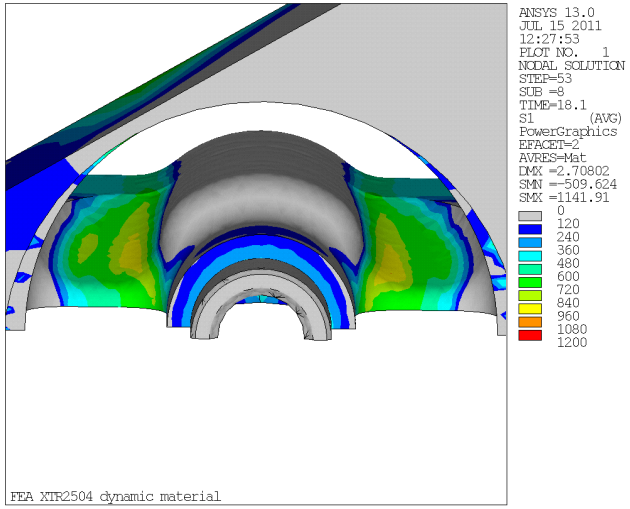

Cycle 18

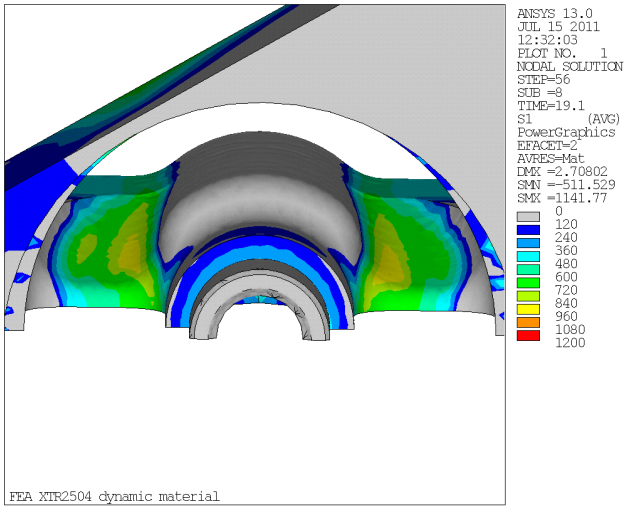

Cycle 19

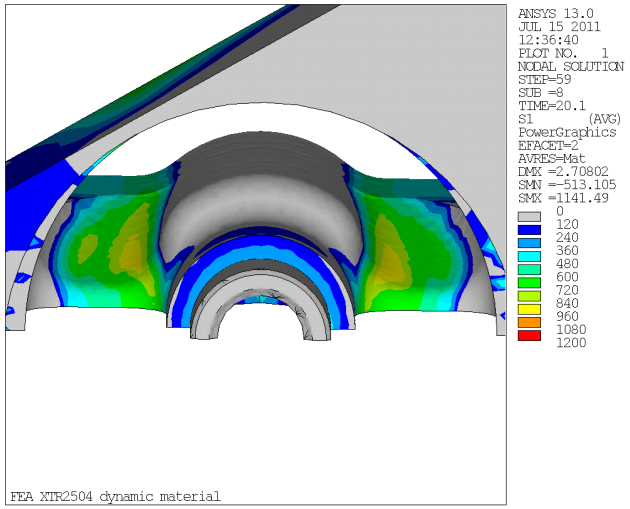

Cycle 20

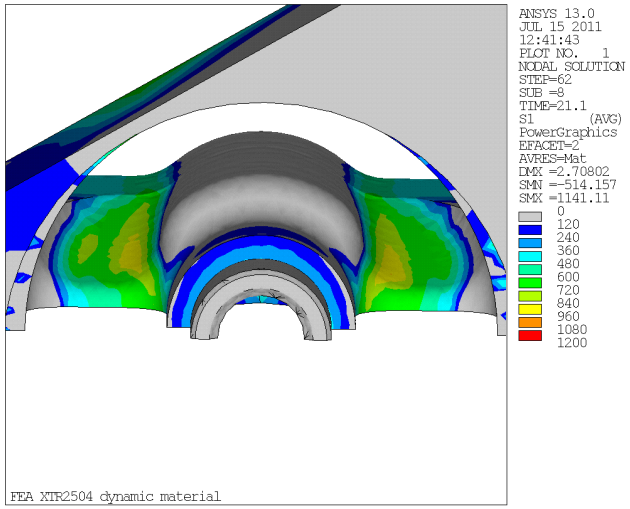

Cycle 21

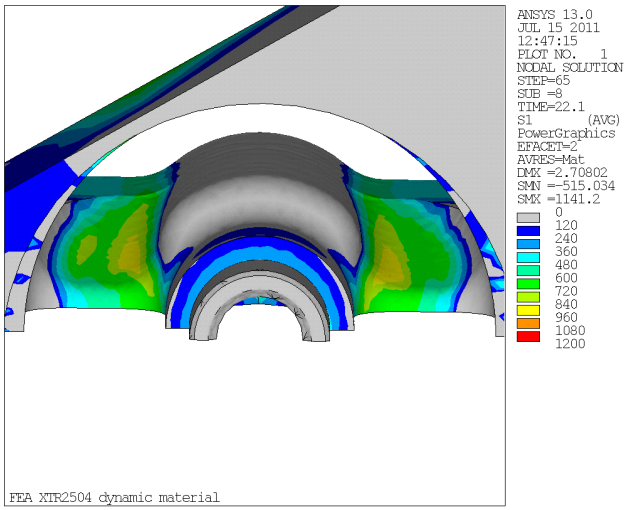

Cycle 22

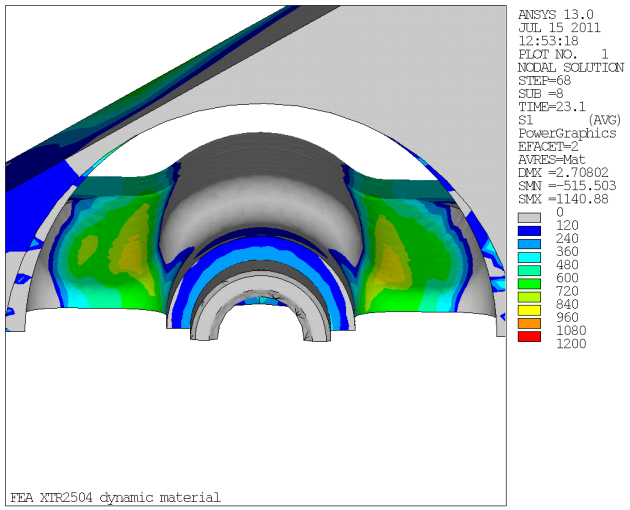

Cycle 23

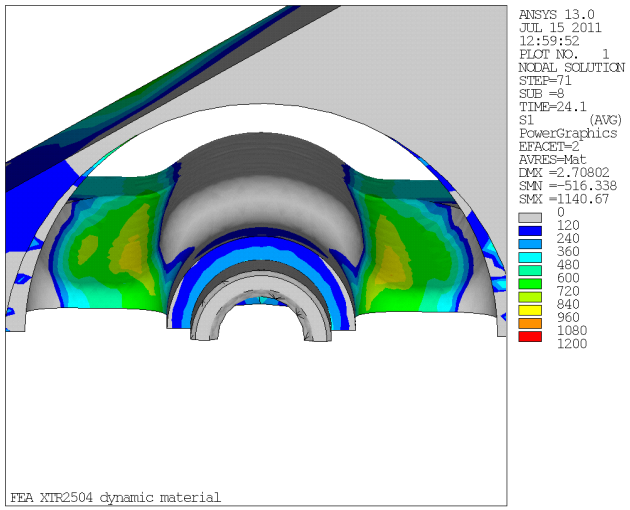

Cycle 24

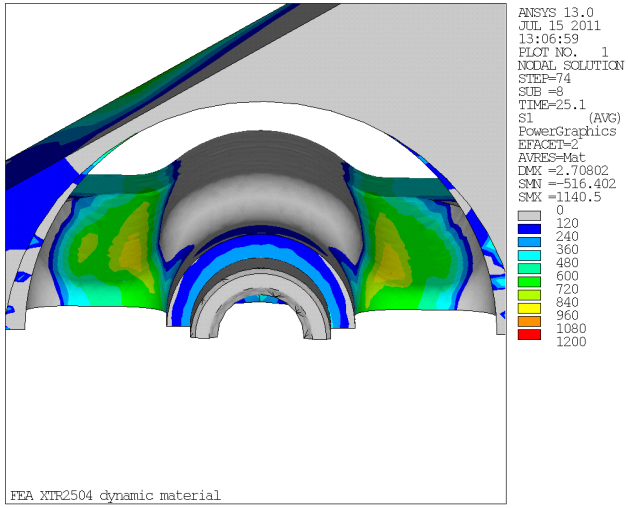

Cycle 25

Figure A. 1 : Equivalent stress (Von Mises) distribution

II Dynamic Model application : inelastic strain distribution

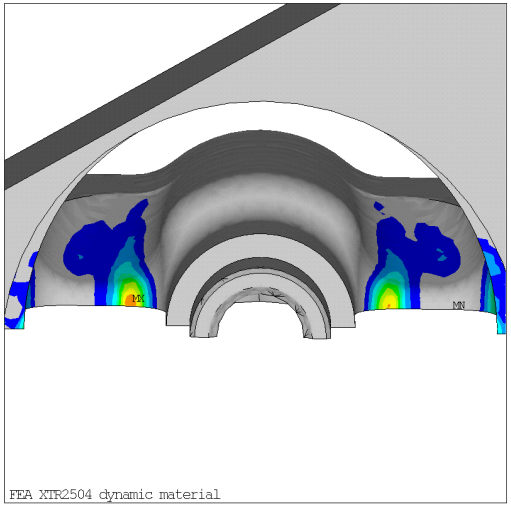

Cycle 1

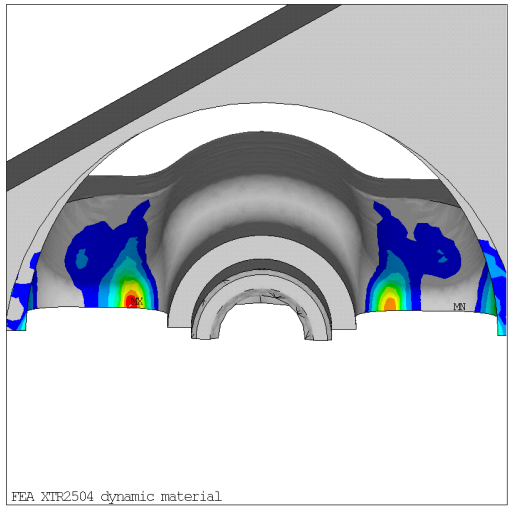

Cycle 2

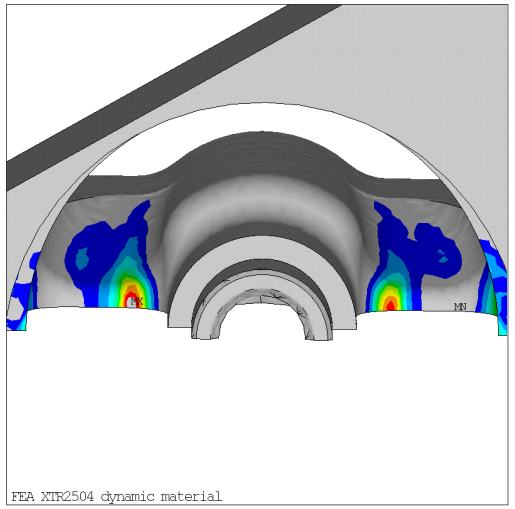

Cycle 3

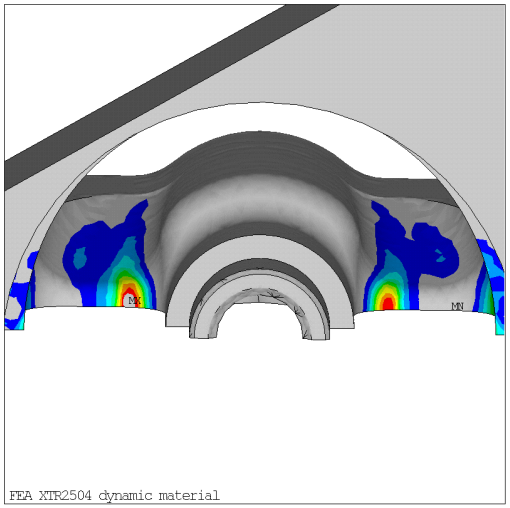

Cycle 4

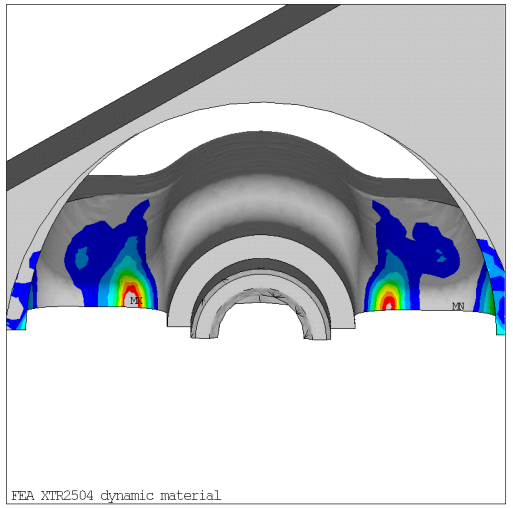

Cycle 5

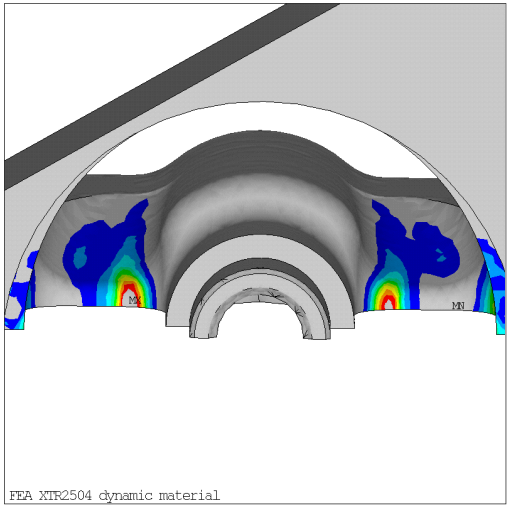

Cycle 6

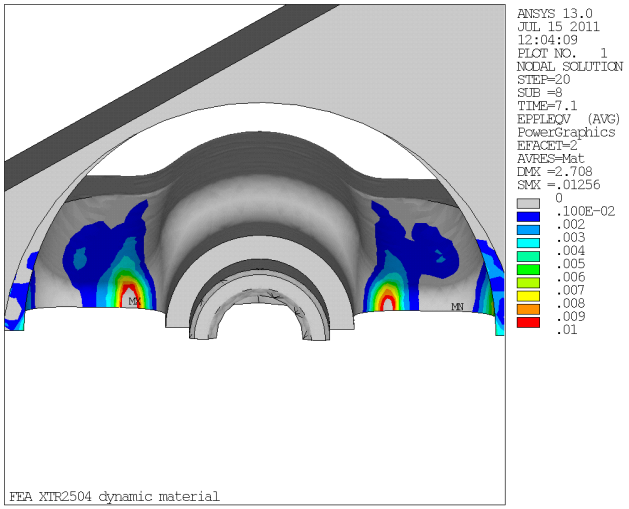

Cycle 7

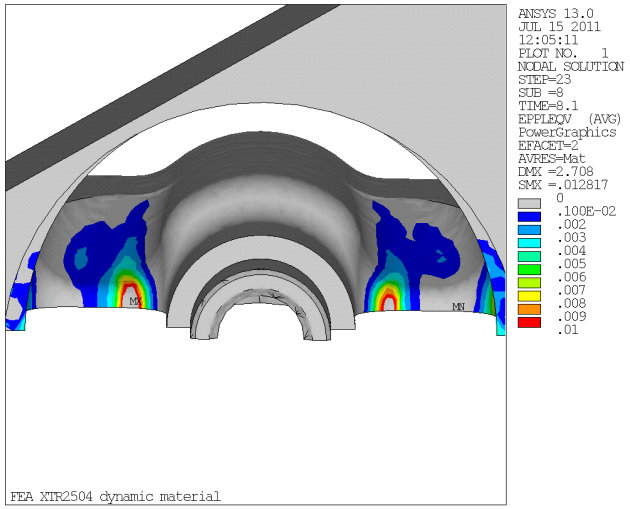

Cycle 8

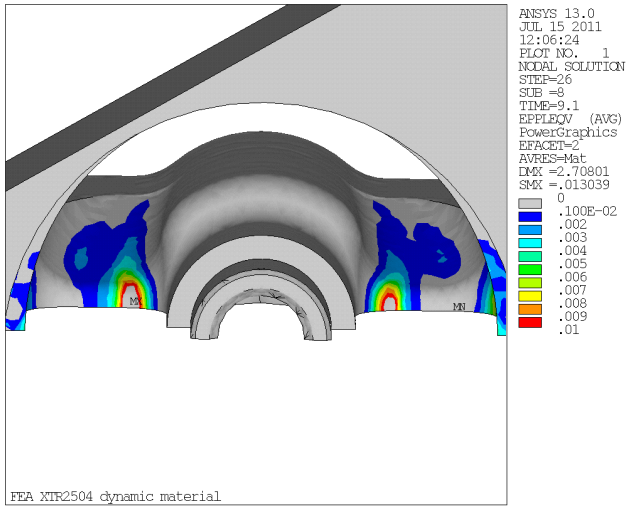

Cycle 9

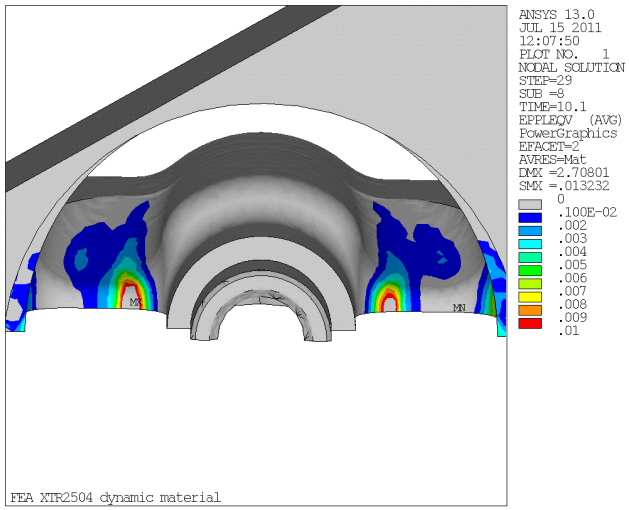

Cycle 10

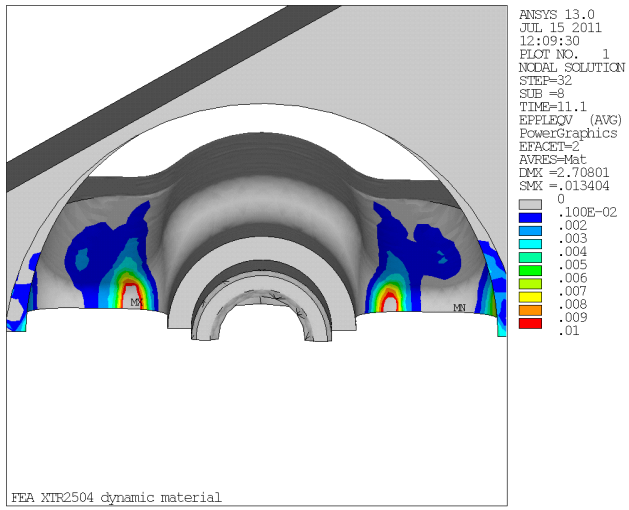

Cycle 11

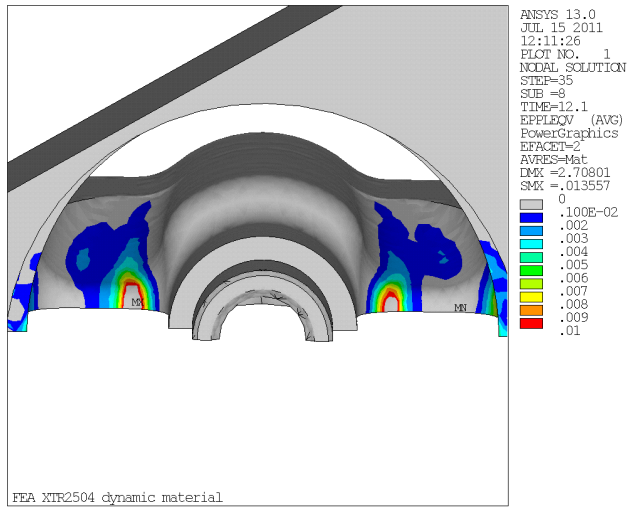

Cycle 12

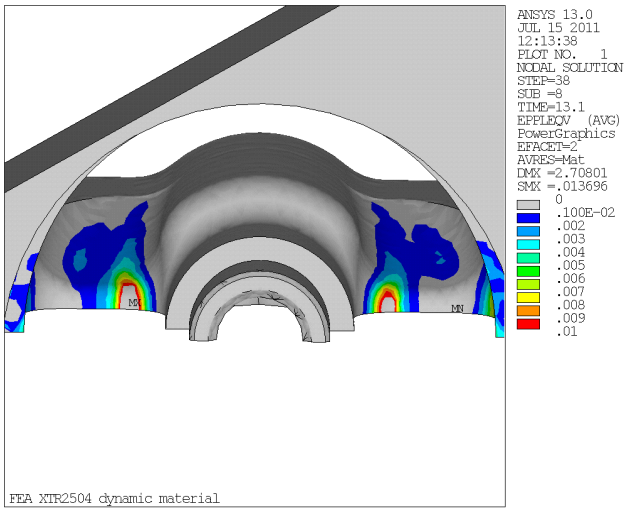

Cycle 13

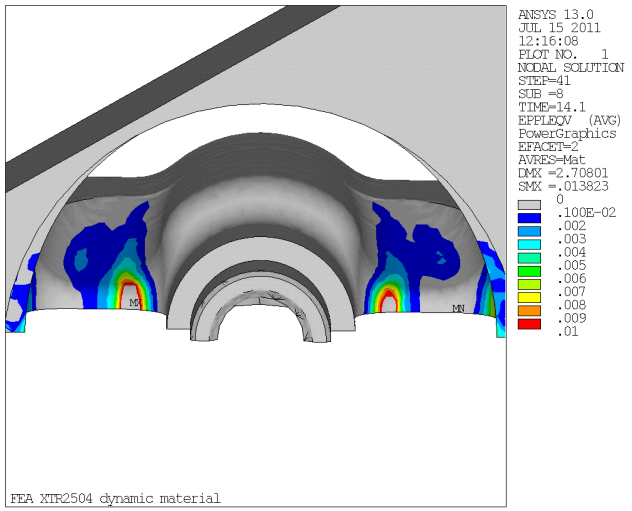

Cycle 14

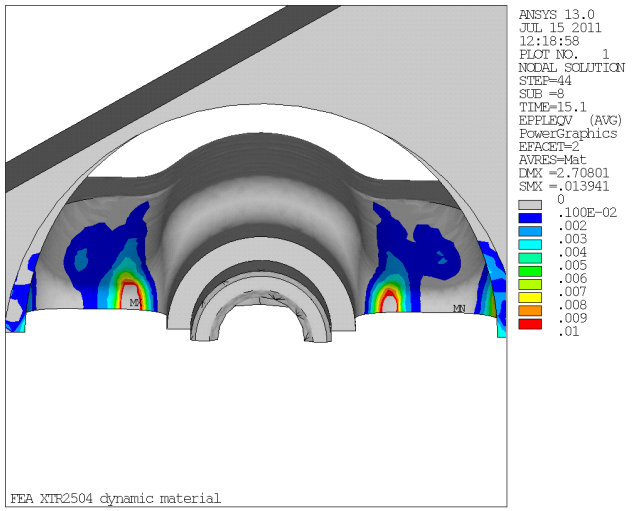

Cycle 15

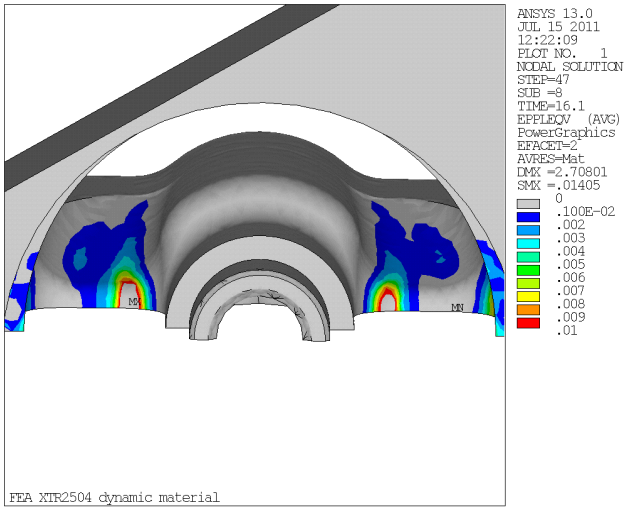

Cycle 16

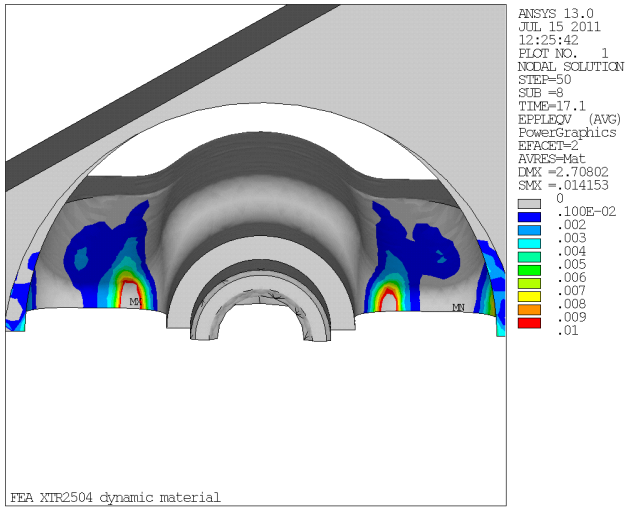

Cycle 17

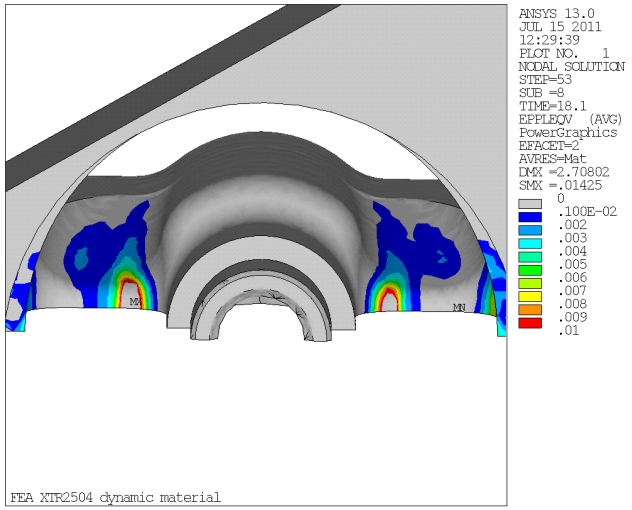

Cycle 18

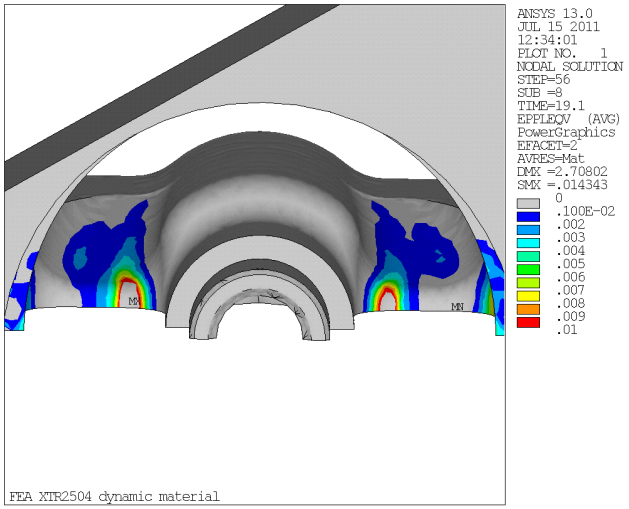

Cycle 19

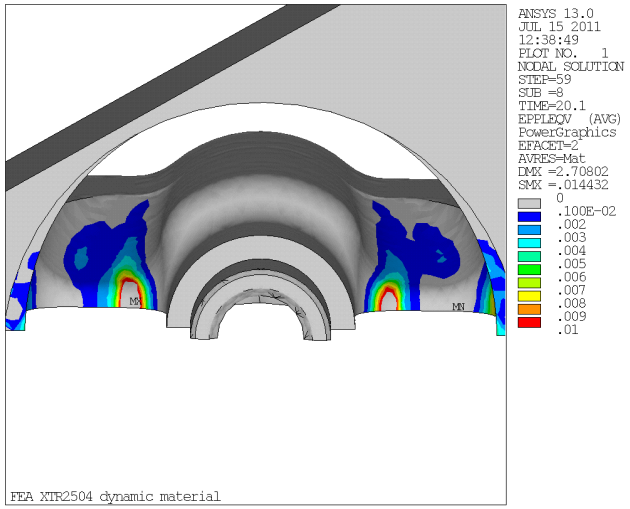

Cycle 20

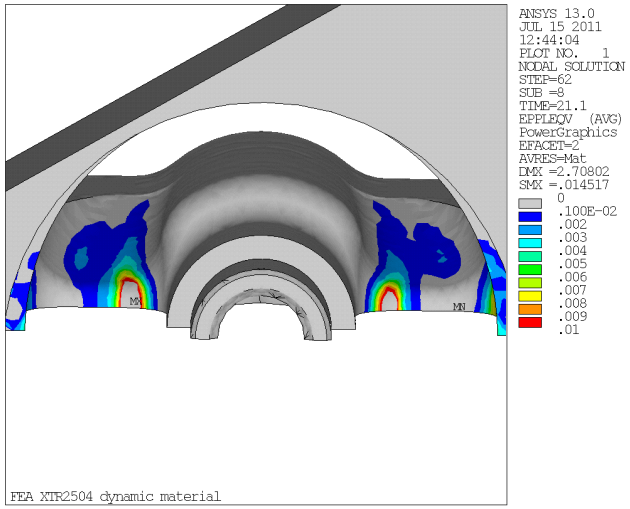

Cycle 21

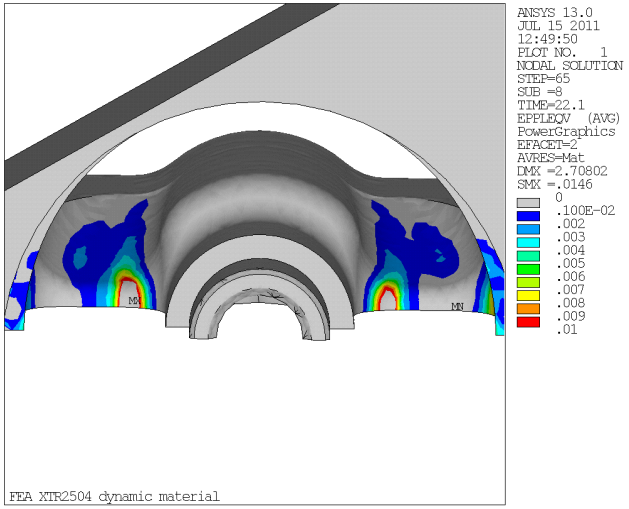

Cycle 22

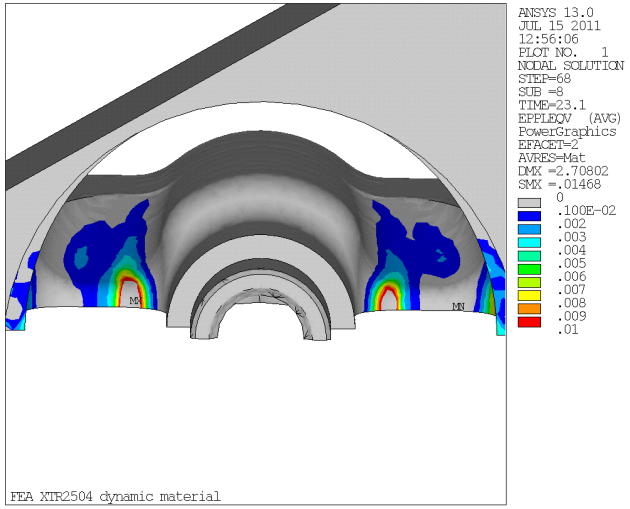

Cycle 23

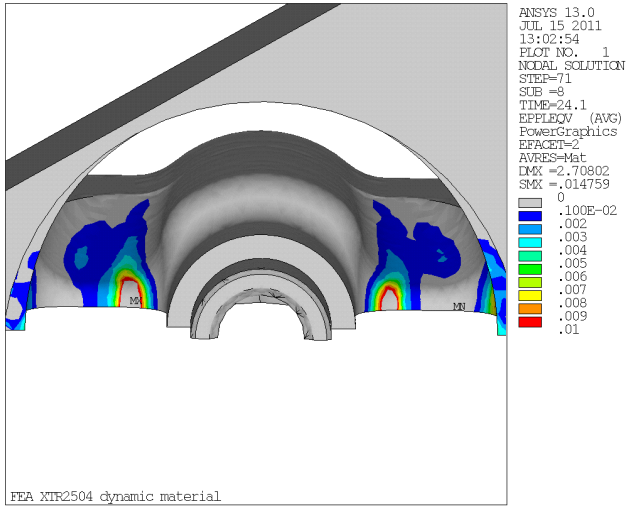

Cycle 24

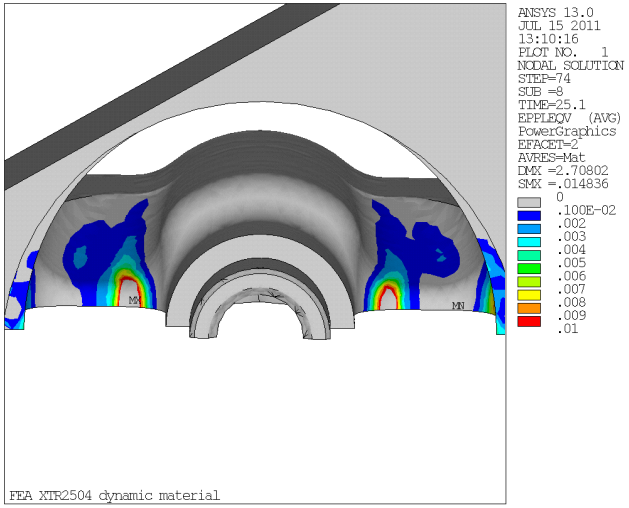

Cycle 25

Figure A. 2 : Inelastic strain distribution

III Traditional experimental approach

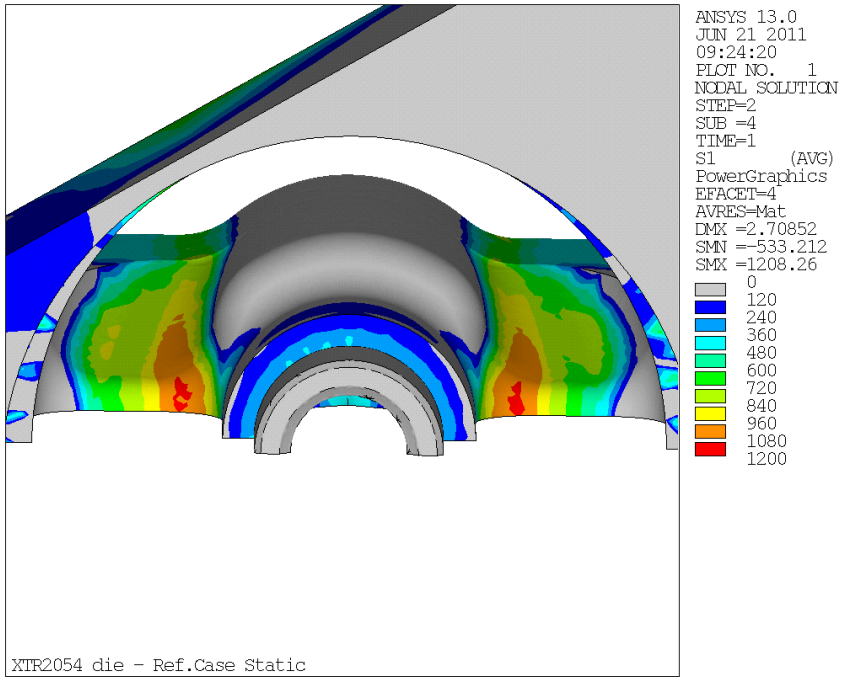

(a)

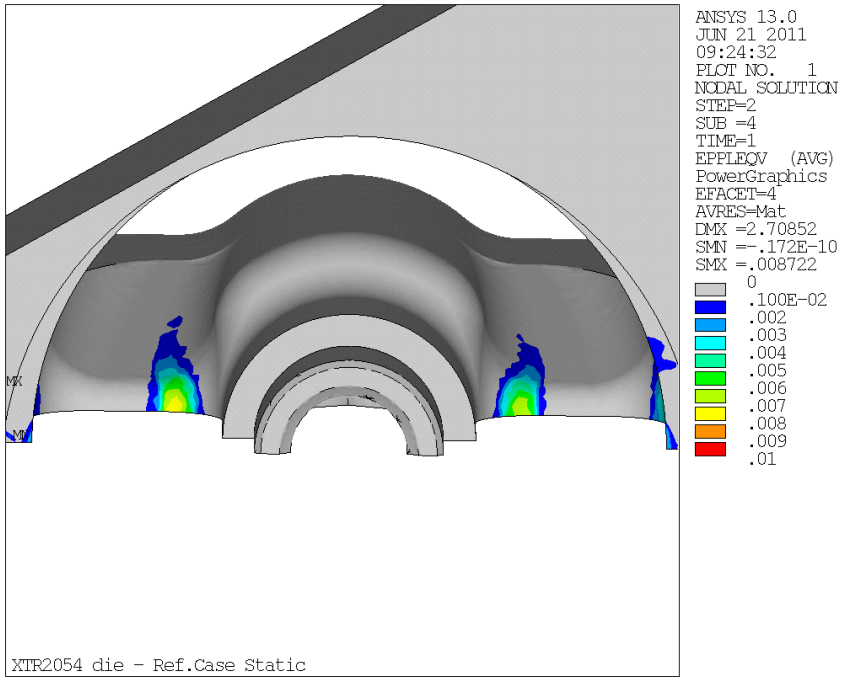

(b)

Figure A. 3 : FE simulation by the traditional experimental approach (linear isotropic hardening): equivalent stress distribution (Von Mises) (a) and inelastic strain distribution (b)

Appendix B

Study of scatter in strain-life Manson Coffin laws

Appendix B: Study of scatter in strain-life Manson Coffin laws

Fatigue testing is considered as the main basis of the relationship between the fatigue resistance of a given material and the application of a cyclic loading.

The results of these cyclic tests have been plotted in Chapter IV and Chapter V on graphs relating the applied loading (plastic or total strain) and the number of cycles to failure.

Generally speaking, the LCF results are assessed by the Manson-Coffin law:

$$\frac{\Delta\varepsilon_p}{2} = \varepsilon_f \cdot (2N_R)^c \qquad \textbf{Eq.B. 1}$$

Where:

- $\Delta\varepsilon_p$ is the plastic strain amplitude at half life;
- ε_f' is an empirical constant known as the *fatigue ductility coefficient*;
- N_R is the number of cycles to failure;
- c is an empirical constant known as the *fatigue ductility exponent*, commonly ranging from -0.5 to -0.7 for metals.

In this way, results are traditionally plotted with in a log-log diagram with *log* $(\Delta\varepsilon_{pl})$ as the y-axis and *log N* as the x-axis. The standard approach consists in assuming the parameter plotted on x-axis as the independent variable and that plotted on the y-axis as the dependent variable.

The parameters of the Manson-Coffin law, ε_f and m, are estimated by ordinary linear regression. The method usually used to estimate the slope and the intercept coefficients is called “least squares estimation”. As a result, the values assumed by the coefficients tend to minimize the sum of the squared deviations of the observed values of log N from those predicted by the fitted line. The parameter ε_f and m correspond respectively to the intercept and slope of the so called “mean” line.

When the Manson Coffin law is used to predict the fatigue life, a systematic scatter between experimental and calculated results occurs. As an example, the estimated vs. experimental fatigue life diagram is reported, in Figure B. 1, for a sample of 50 experimental tests. Data are divided in two main classes: the first one is associated to the fatigue tests described in Chapetr IV, focused on the fatigue life investigation of Inconel 718 at 550°C, whereas the second group reflects the results of the experimental tests carried out on the alternative Inconel 718 alloys. As a results, all these fatigue data come from the study of various cases, such as the application of different holding time or strain rate (Chapter IV) or the adoption of alternative microstructure (Chapter V), all performed at 550°C. Fatigue lives ($N_{Calculated}$) may be calculated by using the Manson-Coffin parameterical relationships that

have been determinated for each specific test case.

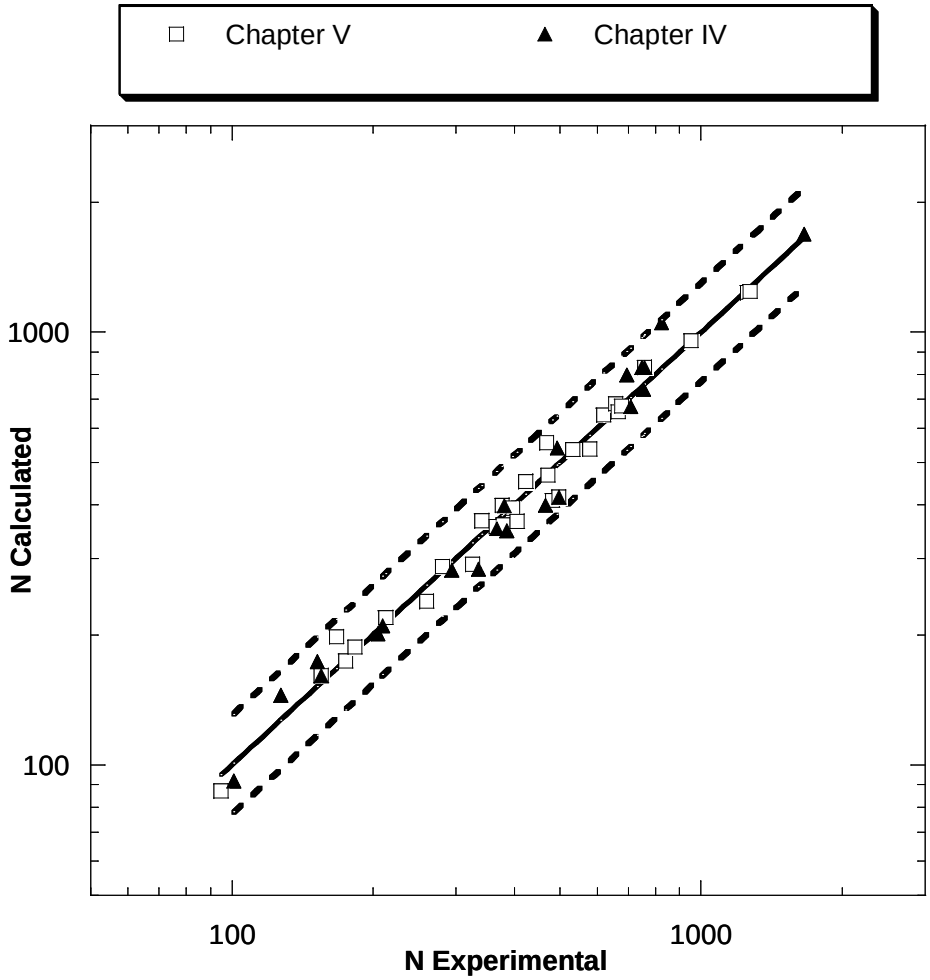

Figure B. 1 : Estimated vs. experimental fatigue life diagram obtained applying the Manson-Coffin relationship for Inconel 718 at 550°C.

The diagram shows a general linearity of the relationship between the variables.

It can be observed that predictions fall within an error band of factor 1.3, independently of the experimental fatigue life. This proves the fact that, for Inconel 718 at 550°C, the Manson Coffin law is able of correctly describing the material fatigue behaviour under tension-compression independently of the applied signal, loading amplitude or microstructure.

However, the accuracy of the Manson Coffin model may be reflected via the residual (e_i) calculation, which is obtained by subtracting the *observed response* (N_{Exp}) from the *predicted response* (N_{Calc}) (Eq.B. 2).

$$e_i = N_{Calculated} - N_{Experimental} \qquad \textbf{Eq.B. 2}$$

Residuals are considered as elements of variation unexplained by the fitted model.

The standardized residual of the regressive model is given by the following equation

Eq.B. 3

$$e_i^* = \frac{e_i - \bar{e}}{s}$$

Where $\bar{e}$ is the mean value and s the standard deviation of residuals.

Finally, a *graphical method is suggested* to examine residuals. The histogram, reported in Figure B. 2, is a frequency plot obtained by placing the residuals in regularly spaced cells and plotting each cell frequency versus the center of the cell. A normal density function, defined by the mean value and standard deviation if residuals, has been superimposed on the histogram. As a result, the diagram shows an approximately normal distribution of residuals obtained by using the Manson Coffin law as a prediction model for fatigue life.

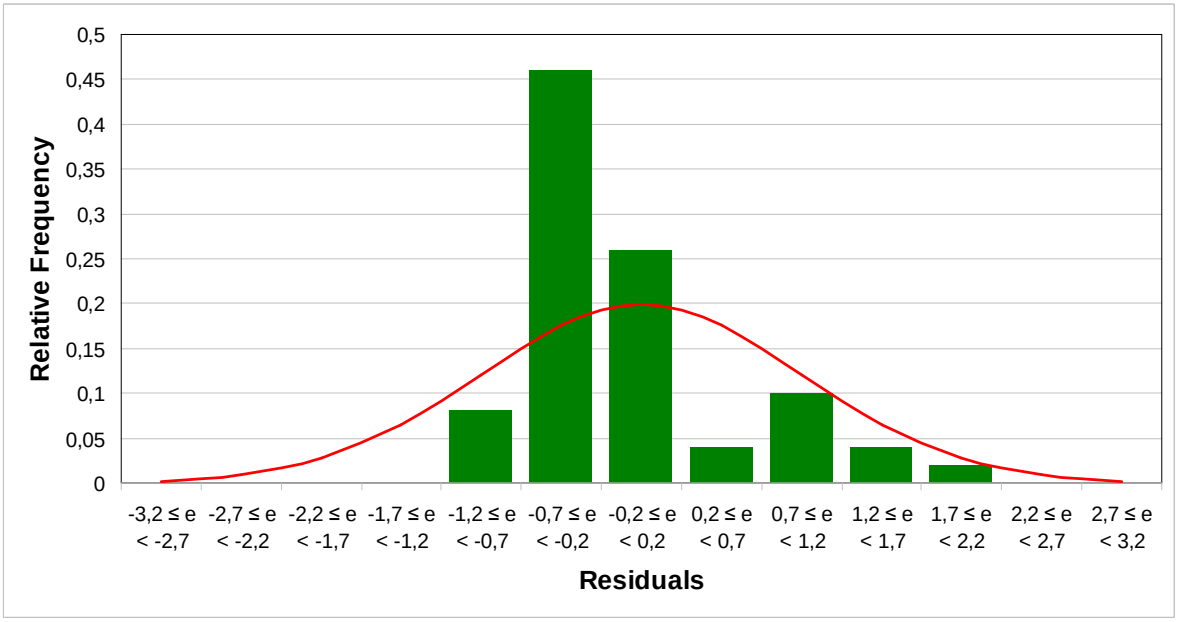

Figure B. 2 : Approximately normal distribution of the residual obtained by using the Manson-Coffin law as a prediction model for fatigue life

Doctorat de l'Université de Toulouse
Délivré par l'Institut National Polytechnique de Toulouse
Ecole doctorale MEGeP – Spécialité Génie Mécanique, Mécanique et Matériaux
Soutenue le 18 Octobre 2011 à Toulouse
Fabio TAINA

Optimisation of micrustructure and fatigue properties of Inconel 718 for extrusion die applications

This present work is a contribution to an extensive development study, promoted by Hydro Aluminium, in the field of the damage mechanisms of extrusion dies. The originality of the present work is based on the development of an optimized Inconel 718 alloy as bulk material for extrusion die., which corresponds to a new application of this alloy in the field of tools: The investigation of the impact of the so called "*Material Extrinsic Parameters*", such as extrusion speed, billet length and thermo-mechanical loading on the mechanical behaviour of the material is proposed. The cyclic tensile and compressive stresses, acting on the die, are simulated by isothermal Low Cycle Fatigue (LCF) tests. Results show that strain rate and holding time have a significant impact on fatigue life. These considerations represent the "Input Data" for the design of an optimized Inconel 718 in order to adapt the material to the specific conditions imposed by the extrusion process. This objective is achieved by modifying the "*Material Intrinsic Parameters*" such as grain size or precipitates morphology through the formulation of alternative thermal treatments. Additional LCF tests, are carried out to compare the cyclic response of the alternative Inconel 718 grades. One of this treatment, elaborated by a multidisciplinary approach including metallurgical, chemical and mechanical experiments ~~that~~ has been implemented in the industrial production practice as the new standard procedure for the thermal treatment of the Inconel 718 extrusion dies.

Keywords : Inconel 718, Extrusion, Die, Thermal treatment, Microstructure, Intermetallic precipitates, LCF fatigue, Thermo-mechanical behaviour

Optimisation de la microstructure et des proprietés en fatigue de l'Inconel 718 pour l'application de filière d'extrusion

Ce travail est une contribution à une étude de recherche et développent, proposée par Hydro Aluminium, dans le domaine des mécanismes d'endommagement de filières d'extrusion ~~et~~. L'originalité du travail de thèse est basée sur le développement d'un alliage Inconel 718 optimisé pour l'application spécifique de filière d'extrusion, ce qui représente un saut technologique dans l'emploi de ce superalliage dans le domaine des outils. L'impact des paramètres du procédé d'extrusion, appelés *paramètres extrinsèques*, - tels que la vitesse d'extrusion, la longueur de billette, le chargement thermo-mécanique - sur le comportement mécanique du matériau a été analysé. Les cycles traction-compression sont simulés à l'aide d'essais isothermes de fatigue oligocyclique (LCF) qui donnent des informations sur les différents mécanismes d'endommagement survenant dans la filière. Du point de vue scientifique, la sollicitation de fatigue oligocyclique isotherme (LCF) est considérée comme la plus représentative des conditions thermomécaniques agissant sur l'outil. Les résultats montrent que la vitesse de déformation et de temps de maintien ont un impact significatif sur la durés de vie en fatigue. Le développent du matériau, enfin, a été atteint en modifiant les *paramètres intrinsèques* au matériau - tels que la taille des grains et la morphologie des précipités intermétalliques. Des traitements thermiques alternatifs, permettant d'adapter le matériau aux conditions spécifiques imposées par le procédé d'extrusion, ont été formulés. Des essais de fatigue LCF supplémentaires, ont permit de comparer la réponse cyclique de ces nouvelles nuances à celle du traitement original. Un de ces traitement, élaboré au travers d'une approche pluridisciplinaire incluant les aspects métallurgie, chimie et mécanique, a été retenu comme la nouvelle procédure standard pour le traitement des matrices d'extrusion en Inconel 718.

Mots-Clés : Inconel 718, Extrusion, Outillage, Traitement thermique, Microstructure, Précipités intermétalliques, fatigue oligocyclique (LCF), Comportement thermomécanique

Institut Clément Ader – Ecole des Mines d'Albi-Carmaux
Campus Jarlard – Route de Teillet
81013 Albi cedex 09